

**THE POTENTIAL ROLE OF *PEPEROMIA PELLUCIDA* (L.)
KUNTH IN AMELIORATING HYPERGLYCAEMIC AND
GLYCATION-INDUCED INFLAMMATION IN HUMAN
RETINAL PIGMENT EPITHELIAL CELL LINE (ARPE-19)**

HO KEAT LAM

**Thesis submitted to the University of Nottingham
for the degree of Doctor of Philosophy**

2024

Table of contents

Section titles	Page
Acknowledgements	VIII
Abstract	XI
List of publications	XIII
List of conference abstracts	XIV
List of abbreviations and symbols	XV
List of tables	XVII
List of figures	XX
List of appendices	XXII
Chapters	
1.0 Introduction	1
1.1 Diabetic retinopathy (DR)	1
1.2 Problem statement	2
1.3 The nature-based therapeutic approach	3
1.4 Research question	4
1.5 Hypotheses	5
1.6 Study aims and objectives	5
2.0 Literature review	7
2.1 Diabetes mellitus (DM)	7
2.2 Diabetic retinopathy (DR)	9
2.2.1 Background	9
2.2.2 Pathophysiology	11
2.2.2.1 Polyol pathway	11
2.2.2.2 Hexosamine pathway	12
2.2.2.3 Protein kinase C (PKC) pathway	14
2.2.2.4 Advanced glycation end product (AGE)	15
2.2.2.5 Oxidative stress	20
2.2.2.6 Inflammation	23
2.2.2.7 Overexpression of angiogenic factors	30
2.2.3 Management of DR	32
2.3 Human retinal pigment epithelial cell line (ARPE-19)	34
2.4 Medicinal plants	35
2.4.1 <i>Peperomia pellucida</i> (L.) Kunth	37
2.4.1.1 Nomenclature and taxonomy	37
2.4.1.2 Botanical description	39
2.4.1.3 Geographical distribution	39
2.4.1.4 Ethnomedicinal uses	40
2.4.1.5 Phytochemistry	43
2.4.1.6 Nutritional and mineral compositions	46
2.4.1.7 Biological activities	50
2.4.1.7.1 Anti-diabetic activity	50
2.4.1.7.2 Anti-inflammatory activity	51
2.4.1.7.3 Antioxidant activity	52
2.4.1.7.4 Anti-angiogenic activity	54

2.4.1.7.5 Anti-microbial activity	54
2.4.1.7.6 Blood pressure lowering activity	55
2.4.1.8 Toxicity studies	56
3.0 Methodology	59
3.1 List of materials and equipment	59
3.2 Plant processing	59
3.2.1 Fresh sample collection	59
3.2.2 Plant sample authentication	60
3.2.3 Sample cleaning and grinding	61
3.2.4 Plant maceration and fractionation	61
3.2.4.1 Extraction yield	63
3.2.5 Sample preparation for analysis	63
3.3 Phase 1: Quantification of biological activities and phytochemicals	64
3.3.1 Phytochemicals	64
3.3.1.1 Total phenolic content (TPC)	64
3.3.1.1.1 Principle	64
3.3.1.1.2 Procedure	64
3.3.1.2 Total flavonoid content (TFC)	65
3.3.1.2.1 Principle	65
3.3.1.2.2 Procedure	65
3.3.1.3 Tannin content	66
3.3.1.3.1 Principle	66
3.3.1.3.2 Procedure	66
3.3.1.4 Saponin content	67
3.3.1.4.1 Principle	67
3.3.1.4.2 Procedure	67
3.3.1.5 Alkaloid content	68
3.3.1.5.1 Principle	68
3.3.1.5.2 Procedure	68
3.3.2 Antioxidant activities	69
3.3.2.1 Ferric-reducing antioxidant power (FRAP)	69
3.3.2.1.1 Principle	69
3.3.2.1.2 Procedure	69
3.3.2.2 DPPH radical scavenging activity	70
3.3.2.2.1 Principle	70
3.3.2.2.2 Procedure	70
3.3.2.3 ABTS radical scavenging activity	71
3.3.2.3.1 Principle	71
3.3.2.3.2 Procedure	71
3.3.2.4 Lipid peroxidation inhibitory activity	72
3.3.2.4.1 Principle	72
3.3.2.4.2 Procedure	73
3.3.2.5 Antioxidant index (AI)	73
3.3.3 Anti-inflammatory activities	74
3.3.3.1 Cyclooxygenase (COX) 1 and 2 inhibitory activities	74
3.3.3.1.1 Principle	74
3.3.3.1.2 Procedure	74
3.3.3.2 5-Lipoxygenase (LOX) inhibitory activity	75
3.3.3.2.1 Principle	75
3.3.3.2.2 Procedure	76
3.3.3.3 Xanthine oxidase (XO) inhibitory activity	76

3.3.3.3.1 Principle	76
3.3.3.3.2 Procedure	77
3.3.3.4 Hyaluronidase inhibitory activity	77
3.3.3.4.1 Principle	77
3.3.3.4.2 Procedure	78
3.3.3.5 Anti-inflammatory index (AII)	79
3.3.4 Anti-glycaemic activities	79
3.3.4.1 α -glucosidase inhibitory activity	79
3.3.4.1.1 Principle	79
3.3.4.1.2 Procedure	80
3.3.4.2 α -amylase inhibitory activity	80
3.3.4.2.1 Principle	80
3.3.4.2.2 Procedure	81
3.3.5 Anti-glycation activities	81
3.3.5.1 AGE formation inhibitory activity	81
3.3.5.2 Total AGE inhibition	82
3.3.5.2.1 Principle	82
3.3.5.2.2 Procedure	82
3.3.5.3 Amadori product inhibition	83
3.3.5.3.1 Principle	83
3.3.5.3.2 Procedure	83
3.3.5.4 Dicarbonyl compound inhibition	84
3.3.5.4.1 Principle	84
3.3.5.4.2 Procedure	84
3.3.5.5 Aldose reductase (AR) inhibitory activity	85
3.3.5.5.1 Principle	85
3.3.5.5.2 Procedure	85
3.3.5.6 Anti-glycation index (AGI)	85
3.3.6 Toxicity evaluation	86
3.3.6.1 Principle	86
3.3.6.2 Procedure	86
3.4 Phase 2: <i>In vitro</i> cellular mechanistic study	87
3.4.1 Preparation of AGE	87
3.4.1.1 Principle	87
3.4.1.2 Procedure	87
3.4.2 Cell culture and sample treatment	87
3.4.3 Plant cytotoxicity evaluation	88
3.4.3.1 3-[4,5-dimethylthiazol-2-yl]-2,5 diphenyl tetrazolium bromide (MTT) cell viability assay	88
3.4.3.1.1 Principle	88
3.4.3.1.2 Procedure	89
3.4.4 Genes expression	90
3.4.4.1 RNA extraction	90
3.4.4.1.1 Principle	90
3.4.4.1.2 Procedure	91
3.4.4.2 Reverse transcription and complementary DNA (cDNA) synthesis	92
3.4.4.2.1 Principle	92
3.4.4.2.2 Procedure	92
3.4.4.3 Reverse transcription real-time polymerase chain reaction (RT-qPCR)	93
3.4.4.3.1 Principle	93
3.4.4.3.2 Procedure	94
3.4.5 Proteins expression	95

3.4.5.1 Cell lysis	96
3.4.5.1.1 Principle	96
3.4.5.1.2 Procedure	96
3.4.5.2 Nuclear and cytoplasmic proteins extraction	97
3.4.5.2.1 Principle	97
3.4.5.2.2 Procedure	97
3.4.5.3 Cell culture supernatant proteins precipitation	98
3.4.5.3.1 Principle	98
3.4.5.3.2 Procedure	98
3.4.5.4 Proteins quantification	99
3.4.5.4.1 Principle	99
3.4.5.4.2 Procedure	99
3.4.5.5 Sodium dodecyl sulfate-polyacrylamide gel electrophoresis (SDS-PAGE)	100
3.4.5.5.1 Principle	100
3.4.5.5.2 Procedure	100
3.4.5.6 Western blot	101
3.4.5.6.1 Principle	101
3.4.5.6.2 Procedure	101
3.4.5.7 Soluble RAGE (sRAGE) quantification	104
3.4.5.7.1 Principle	104
3.4.5.7.2 Procedure	104
3.5 Phase 3: Identification of phytochemicals	106
3.5.1 Purification of phytochemicals	106
3.5.1.1 Thin-layer chromatography (TLC)	106
3.5.1.1.1 Principle	106
3.5.1.1.2 Procedure	106
3.5.1.2 Silica gel column chromatography	107
3.5.1.2.1 Principle	107
3.5.1.2.2 Procedure	108
3.5.1.3 Preparative radial chromatography (PRC)	108
3.5.1.3.1 Principle	108
3.5.1.3.2 Procedure	109
3.5.2 Characterisation of phytochemicals	109
3.5.2.1 Nuclear magnetic resonance (NMR) spectroscopy	109
3.5.2.1.1 Principle	109
3.5.2.1.2 Procedure	110
3.5.2.2 Ultraviolet-visible (UV-Vis) spectroscopy	110
3.5.2.2.1 Principle	110
3.5.2.2.2 Procedure	111
3.5.2.3 Fourier-transform infrared (FTIR) spectroscopy	111
3.5.2.3.1 Principle	111
3.5.2.3.2 Procedure	112
3.5.2.4 Liquid chromatography-mass spectrometry (LC-MS)	112
3.5.2.4.1 Principle	112
3.5.2.4.2 Procedure	113
3.5.2.5 Gas chromatography-mass spectrometry (GC-MS)	114
3.5.2.5.1 Principle	114
3.5.2.5.2 Procedure	115
3.6 Statistical analysis	116
4.0 Results	117

4.1 Phase 1: The biological activities and phytochemicals of <i>P. pellucida</i>	117
4.1.1 Plant extraction yield	117
4.1.2 Phytochemicals	117
4.1.3 Antioxidant activities and indices	120
4.1.4 Anti-inflammatory activities and indices	124
4.1.4.1 COXs inhibitory activity	124
4.1.4.2 LOX inhibitory activity	124
4.1.4.3 XO inhibitory activity	126
4.1.4.4 Hyaluronidase inhibitory activity	126
4.1.5 Anti-glycaemic activities	129
4.1.5.1 α -glucosidase and α -amylase inhibitory activities	129
4.1.6 Anti-glycation activities and indices	131
4.1.6.1 AR inhibitory activity	131
4.1.6.2 Total AGE inhibition analysis	131
4.1.6.3 Dicarbonyl compound analysis	131
4.1.6.4 Amadori product analysis	132
4.1.7 <i>In vivo</i> toxicity assay	134
4.1.8 Correlation analysis	136
4.1.9 Principal component analysis (PCA)	143
4.2 Phase 2: <i>In vitro</i> cellular study	145
4.2.1 Plant cytotoxicity in ARPE-19	145
4.2.1.1 Normal glucose condition	145
4.2.1.2 Hyperglycaemic stress	149
4.2.1.3 AGE-induced stress	152
4.2.2 Gene and protein expression	155
4.2.2.1 NF- κ B p65	155
4.2.2.2 STAT3	159
4.2.2.3 PPAR- γ	162
4.2.2.4 IL-8	164
4.2.2.5 MCP-1	167
4.2.2.6 MMP2	168
4.2.2.7 VEGF	171
4.2.2.8 GPx	172
4.2.2.9 SOCS1	174
4.2.2.10 RAGE	175
4.3 Phase 3: Phytochemicals identification	178
4.3.1 Purification and identification of fraction 1	178
4.3.1.1 Fraction 1	179
4.3.1.2 Chemical characterisation of fraction 1	181
4.3.2 Purification and identification of fraction 2	182
4.3.2.1 Fraction 2	183
4.3.2.2 Chemical characterisation of fraction 2	183
4.3.3 Purification and identification of fraction 3	185
4.3.3.1 Fraction 3	186
4.3.3.2 Chemical characterisation of fraction 3	187
4.3.4 Purification and identification of fraction 4	189
4.3.4.1 Fraction 4	190
4.3.4.2 Chemical characterisation of fraction 4	191
4.3.5 Identification of polar compounds with LC-QToF-MS	195
4.3.6 GC-MS analysis of non-polar volatile compounds	199
4.3.6.1 PPM/A	199
4.3.6.2 PPM/A/1 and PPM/A/2	204

5.0 Discussion	208
5.1 Biological activities and phytochemicals in <i>P. pellucida</i>	208
5.1.1 The influence of extraction parameters on the yield of <i>P. pellucida</i>	208
5.1.2 Phytochemicals	210
5.1.3 Antioxidant effect	217
5.1.4 Anti-inflammatory effect	221
5.1.5 Anti-glycaemic effect	226
5.1.6 Anti-glycation effect	228
5.2 The anti-retinopathy mechanisms of <i>P. pellucida</i> in ARPE-19	232
5.2.1 Regulation on the transcription factors implicated in inflammation and angiogenesis	232
5.2.1.1 Effect of AGE and high glucose-induced oxidative stress on NF- κ B p65 and STAT3 in ARPE-19	233
5.2.1.2 Effect of AGE and high glucose on PPAR- γ in ARPE-19	237
5.2.1.3 Effect of <i>P. pellucida</i> on NF- κ B p65, STAT3 and PPAR- γ transcription factors	239
5.2.2 Regulation on the inflammatory markers	244
5.2.2.1 Effect of AGE and high glucose-induced oxidative stress on pro-inflammatory markers in STAT3 and NF- κ B p65 signalling pathway	244
5.2.2.2 Effect at early phase of inflammation	246
5.2.3 Regulation on the angiogenic markers	248
5.2.3.1 Effect of AGE and high glucose on STAT3 and NF- κ B p65 implicated in angiogenesis	248
5.2.3.2 Effect of <i>P. pellucida</i> on angiogenic response in ARPE-19	249
5.2.4 Regulation on the antioxidant defense and cytokine signalling	251
5.2.4.1 Effect of AGE and high glucose on antioxidant enzyme GPx	252
5.2.4.2 The negative feedback response towards STAT3 activation	253
5.2.4.3 Effect of <i>P. pellucida</i> on antioxidant status and cytokine signalling	254
5.2.5 Regulation on the expression of RAGE and sRAGE	256
5.2.5.1 Effect of AGE and high glucose-induced oxidative stress on RAGE and sRAGE level	256
5.2.5.2 Effect of <i>P. pellucida</i> on RAGE and sRAGE expression in ARPE-19	258
5.3 <i>In vitro</i> and <i>in vivo</i> toxicity of <i>P. pellucida</i>	259
5.3.1 <i>In vitro</i> cytotoxicity	259
5.3.2 <i>In vivo</i> toxicity	260
5.3.3 Cytoprotective effect of <i>P. pellucida</i>	262
5.4 Future study	265
6.0 Conclusion	267
References	269
Appendices	362

Acknowledgements

To begin with, this PhD thesis of mine reflects not only the amount of hard work and years of research, to which I have committed, but also the emotional and financial supports shown by a group of individuals and institutions, to whom I am indebted. As I express my deepest gratitude, I am humbled by the experiences and people that I have come across, which contributed to shaping my postgraduate journey.

First and foremost, I would like to express my profound gratitude to my family and friends, whose unwavering support has laid the foundation to the completion of my studies. Your encouragement and emotional support to me have been the driving force behind my achievements. To my parents, who taught me the values of hard work and perseverance, I owe the foundation of my character. Besides, your relentless mental and financial supports have contributed significantly to my PhD journey.

I hereby extend my deepest appreciation to my supervisors, whose encouragement and guidance have been invaluable throughout my PhD journey. To my main supervisor, Dr. Ng Zhi Xiang, your expertise, patience and wisdom have shaped my studies to its conclusion. I am grateful for your mentorship and for the opportunities provided to help me gain experiences for my future career. I would also like to thank Professor Dr. Festo Massawe for his insightful comments during my PhD journey. His constructive feedback has been invaluable in guiding my research endeavours.

I am sincerely grateful to my co-supervisor, Dr. Yong Phaik Har from MAHSA University for her invaluable guidance in plant extraction, mammalian cell culture and western blotting techniques. I would also like to extend my heartfelt gratitude to Dr. Lim Siew Huah from the University

of Malaya for her exceptional guidance in phytochemical purification and characterisation techniques. Their mentorship has been instrumental in shaping my research journey. I am deeply grateful for their unwavering support and encouragement throughout this process, which has not only enhanced my scientific skills but also fostered my personal and professional growth.

I express my deepest appreciation to Dr. Bavani Arumugam from the University of Malaya for generously donating the ARPE-19 cell line for my PhD study. Her contribution has been indispensable to the progress of my research, enabling critical experiments and advancing scientific inquiry. I am sincerely grateful for her support and commitment in fostering collaborative research efforts.

I am thankful to my peers, who have enriched my academic experiences with your insights. Our cooperation and support to each other have fostered the research laboratory into a conducive environment for intellectual growth. The exchange of ideas and discussions among us have also expanded my knowledge, which is critical in my research journey. I am grateful for the opportunities to work together and learn from each other.

I extend my gratitude to the laboratory personnel who also work very hard behind the scenes to ensure the smooth operation of our workplace. Your invaluable efforts have created a stimulating environment for learning, research and personal development, for which I am grateful.

I would also like to acknowledge the institutions and funding bodies, including University of Nottingham Malaysia School of Biosciences, University of Malaya, Fundamental Research Grant Scheme (FRGS) and Malaysia Toray Science Foundation (MTSF), which have supported my

academic pursuits. The facilities and financial assistance provided by these organizations have eased the burden of my educational and research expenses, which enabled me to focus on completing my research.

Finally, I am grateful to the researchers and scholars whose work has been a source of inspiration for my research. Your contributions to the field have paved the way for innovative thinking and discoveries. I am thankful for the knowledge and insights that I am able to gain from your research, which have contributed significantly to the novel discoveries in my research.

Abstract

Diabetic retinopathy (DR) is a microvascular complication that causes blindness. DR management is costly and accompanied with adverse effects. *Peperomia pellucida* (L.) Kunth is traditionally used for inflammation, but its effects on DR remain unexplored. This study aimed to elucidate the regulatory mechanism of *P. pellucida* against high glucose and glycation induced stress in human retinal pigment epithelial cell line (ARPE-19). *P. pellucida* was macerated with methanol, and fractionated with hexane, chloroform, ethyl acetate, n-butanol and water. Semi-quantitative colorimetric assays indicated that the ethyl acetate plant fraction demonstrated potent antioxidant, anti-inflammatory and anti-glycation activities, alongside significant ($p < 0.05$) higher α -amylase and α -glucosidase inhibitory activities when compared to the standard anti-diabetic drug, acarbose. Both ethyl acetate fraction and crude methanolic plant extract significantly ($p < 0.05$) restored the ARPE-19 cell viability under high glucose and glycation stress. High glucose and glycation induced the nuclear factor kappa B (NF- κ B) p65 and signal transducer and activator of transcription 3 (STAT3) signalling pathways with significant ($p < 0.05$) increase of gene (1.22-31.30 folds) and protein (1.39-7.79 folds) expression for angiogenic and inflammatory markers, including interleukin 8 (IL-8), matrix metalloproteinase 2, monocyte chemoattractant protein 1, receptor for AGE, and vascular endothelial growth factor in ARPE-19, as determined via reverse transcription real-time polymerase chain reaction and western blot. Conversely, the gene and protein (0.12-0.56 folds) expression of glutathione peroxidase were significantly reduced due to the suppression of peroxisome proliferator-activated receptor gamma (PPAR- γ). *P. pellucida* did not alter the biomarkers' gene and protein expression under normal glucose condition except for IL-8 (0.75-0.89 folds). Although *in vivo* brine shrimp toxicity analysis revealed that crude methanolic

extract and ethyl acetate fraction were mildly toxic, *in vitro* cell viability findings showed that they were non-cytotoxic towards ARPE-19. Dillapiole, 2,4,5-trimethoxystyrene, β -caryophyllene, β -santalene, methyl 9-octadecenoic acid and methyl pheophorbide-a were among the predominant phytochemicals identified in the crude methanolic extract via spectroscopic and spectrometric techniques. Notably, methyl pheophorbide-a was identified for the first time in *P. pellucida*. The current findings support *P. pellucida* as an alternative therapeutic source to mitigate high glucose and glycation-induced stress in DR by regulating the NF- κ B p65, PPAR- γ and STAT3 signalling pathways.

List of publications

- 1) Ho, K.L., Yong, P.H., Lim, S.H., Ng, Z.X., 2024. *Peperomia pellucida* (L.) Kunth suppresses glycation-induced inflammatory response in human retinal pigment epithelial cell line ARPE-19 via JAK-STAT3 signalling. *Archiv der Pharmazie*. 2024, e2400299. <https://doi.org/10.1002/ardp.202400299>
- 2) Ho, K.L., Yong, P.H., Wang, C.W., Kuppusamy, U.R., Ngo, C.T., Massawe, F. and Ng, Z.X., 2022. *Peperomia pellucida* (L.) Kunth and eye diseases: A review on phytochemistry, pharmacology and toxicology. *Journal of Integrative Medicine*, 20(4), 292-304. <https://doi.org/10.1016/j.joim.2022.02.002>
- 3) Ho, K.L., Tan, C.G., Yong, P.H., Wang, C.W., Lim, S.H., Kuppusamy, U.R., Ngo, C.T., Massawe, F. and Ng, Z.X., 2022. Extraction of phytochemicals with health benefit from *Peperomia pellucida* (L.) Kunth through liquid-liquid partitioning. *Journal of Applied Research on Medicinal and Aromatic Plants*, 30(2), 100392. <https://doi.org/10.1016/j.jarmap.2022.10039>

List of conference abstracts

- 1) Ho, K.L., Yong, P.H. and Ng, Z.X., 2023. *Evaluating the anti-inflammatory role of Peperomia pellucida (L.) Kunth on human retinal pigment epithelium through JAK-STAT3 signaling pathway.* 2023 Malaysia Toray Science Foundation Grant Research Symposium, University of Malaya, Kuala Lumpur, 23 October 2023.
- 2) Ho, K.L., Tan, C.G., Yong, P.H., Wang, C.W., Kuppusamy, U.R., Ngo, C.T., Massawe, F. and Ng, Z.X., 2021. *The anti-glycation and antioxidant potential of phytochemicals extracted from Peperomia pellucida (L.) Kunth.* 5th International Symposium on Phytochemicals in Medicine and Food, Nanchang University, Nanchang, 25-30 August 2021.

List of abbreviations and symbols

Abbreviations and symbols	Full forms
°C	Degree celsius
¹ H	Hydrogen-1
¹³ C	Carbon-13
AA	Arachidonic acid
ABTS	2,2'-azino-bis(3-ethylbenzothiazoline-6-sulfonic acid
AGE	Advanced glycation end product
AGI	Anti-glycation index
AI	Antioxidant index
AII	Anti-inflammatory index
AR	Aldose reductase
ARPE-19	Human retinal pigment epithelial cell line
BCA	Bicinchoninic acid
BCE	Berberine chloride equivalent
BRB	Blood-retinal barrier
CDCl ₃	Deuterated chloroform
cDNA	Complementary deoxyribonucleic acid
COX	Cyclooxygenase
DM	Diabetes mellitus
DME	Diabetic macular edema
DMSO	Dimethyl sulfoxide
DNA	Deoxyribonucleic acid
DPPH	2,2-diphenyl-1-picrylhydrazyl
DR	Diabetic retinopathy
ESI	Electrospray ionization
ETOH	Ethanol
Fe ²⁺	Ferrous ion
FRAP	Ferric-reducing antioxidant power
FTIR	Fourier-transform infrared
g	Gram
GAE	Gallic acid equivalent
GAPDH	Glyceraldehyde-3-phosphate dehydrogenase
GC	Gas chromatography
GPx	Glutathione peroxidase
HA	Hyaluronic acid
IC ₅₀	Half-maximal inhibitory concentration
IκB	Inhibitor of nuclear factor kappa B
IKK	Inhibitor of nuclear factor kappa B kinase
IL-8	Interleukin 8
JAK	Janus kinase
kg	Kilogram
l	Liter
LC-MS	Liquid chromatography-mass spectrometry
LOX	5-Lipoxygenase
m	Meter
m/z	Mass to charge
MIC	Minimum inhibitory concentration
MCP-1	Monocyte chemoattractant protein-1
MS	Mass spectrometry
μg	Microgram

μl	Microliter
μm	Micrometer
μM	Micromolar
mg	Miligram
MH ⁺	Molecular ion
MHz	Megahertz
ml	Mililiter
mm	Milimeter
mM	Milimolar
MMP2	Matrix metalloproteinase 2
mRNA	Messenger ribonucleic acid
MTT	3-(4,5-Dimethylthiazol-2-yl)-2,5-diphenyl tetrazolium bromide
NAD ⁺	Nicotinamide adenosine dinucleotide
NADH	Reduced nicotinamide adenosine dinucleotide
NADPH	Reduced nicotinamide adenosine dinucleotide phosphate
NBT	Nitroblue tetrazolium chloride
NF-κB	Nuclear factor kappa B
nm	Nanometer
NMR	Nuclear magnetic resonance
PAGE	Polyacrylamide gel electrophoresis
PCA	Principal component analysis
PKC	Protein kinase C
PPAR-γ	Peroxisome proliferator-activated receptor gamma
PRC	Preparative radial chromatography
PVDF	Polyvinylidene difluoride
Qct	Quercetin equivalent
QqQ	Triple quadrupole
QSE	Quillaja saponin equivalent
QToF	Quadrupole time-of-flight
RAGE	Receptor for advanced glycation end products
Rf	Retention factor
RNA	Ribonucleic acid
ROS	Reactive oxygen species
RPE	Retinal pigment epithelium
rpm	Revolutions per minute
SDS	Sodium dodecyl sulfate
SET	Single electron transfer
SOCS1	Suppressor of cytokine signalling 1
sRAGE	Soluble receptor for advanced glycation end product
STAT3	Signal transducer and activator of transcription 3
TAE	Tannic acid equivalent
TFC	Total flavonoid content
TLC	Thin layer chromatography
TPC	Total phenolic content
Trolox	6-Hydroxy-2,5,7,8-tetramethylchroman-2-carboxylic acid
U	Enzyme unit
UV-Vis	Ultraviolet-visible
VEGF	Vascular endothelial growth factor
XO	Xanthine oxidase

List of tables

Table 2.1	The different parts of <i>P. pellucida</i> used in different countries for medicinal and non-medicinal purposes.
Table 2.2	The phytochemicals present in different parts of <i>P. pellucida</i> .
Table 2.3	The nutritional and mineral compositions of <i>P. pellucida</i> .
Table 3.1	The list of locations where <i>P. pellucida</i> was collected.
Table 3.2	The forward and reverse primer sequences for the genes of interest.
Table 3.3	The primary antibodies targeting the proteins of interest.
Table 4.1	The extraction yield, total phenolic, flavonoid, tannin, saponin and alkaloid content of <i>P. pellucida</i> crude methanolic extract and fractions.
Table 4.2	The antioxidant activity of <i>P. pellucida</i> crude methanolic extract and fractions.
Table 4.3	The antioxidant index of <i>P. pellucida</i> crude methanolic extract and fractions.
Table 4.4	The anti-inflammatory activity of <i>P. pellucida</i> crude methanolic extract and fractions.
Table 4.5	The anti-inflammatory index of <i>P. pellucida</i> crude methanolic extract and fractions.
Table 4.6	The anti-glycaemic and anti-glycation activities of <i>P. pellucida</i> crude methanolic extract and fractions.
Table 4.7	The anti-glycation index of <i>P. pellucida</i> crude methanolic extract and fractions.

Table 4.8	The <i>in vivo</i> toxicity of <i>P. pellucida</i> crude methanolic extract and fractions.
Table 4.9	Linear correlation and regression of biological activities in <i>P. pellucida</i> .
Table 4.10	The relative protein expression of STAT3 and phosphorylated STAT3 in ARPE-19 treated with <i>P. pellucida</i> crude methanolic extract and ethyl acetate fraction under normal glucose (17 mM), high glucose (34 mM, 68 mM) and AGE-treated conditions.
Table 4.11	The relative gene and protein expression of PPAR- γ in ARPE-19 treated with <i>P. pellucida</i> crude methanolic extract and ethyl acetate fraction under normal glucose (17 mM), high glucose (34 mM, 68 mM) and AGE-treated conditions.
Table 4.12	The relative gene and protein expression of IL-8 and MCP-1 in ARPE-19 treated with <i>P. pellucida</i> crude methanolic extract and ethyl acetate fraction under normal glucose (17 mM), high glucose (34 mM, 68 mM) and AGE-treated conditions.
Table 4.13	The relative gene and protein expression of MMP2 and VEGF in ARPE-19 treated with <i>P. pellucida</i> crude methanolic extract and ethyl acetate fraction under normal glucose (17 mM), high glucose (34 mM, 68 mM) and AGE-treated conditions.
Table 4.14	The relative gene and protein expression of GPx and SOCS1 in ARPE-19 treated with <i>P. pellucida</i> crude methanolic extract and ethyl acetate fraction under normal glucose (17 mM), high glucose (34 mM, 68 mM) and AGE-treated conditions.
Table 4.15	The relative gene and protein expression of RAGE and sRAGE

	in ARPE-19 treated with <i>P. pellucida</i> crude methanolic extract and ethyl acetate fraction under normal glucose (17 mM), high glucose (34 mM, 68 mM) and AGE-treated conditions.
Table 4.16	The polar compounds detected in PPM/B/16-18/2, PPM/E/8 and PPM/E/11 with liquid chromatography-mass spectrometry quadrupole time-of-flight.
Table 4.17	The non-polar volatile compounds detected in PPM/A with gas chromatography-mass spectrometry.
Table 4.18	The non-polar volatile compounds detected in PPM/A/1 and PPM/A/2 with gas chromatography-mass spectrometry.

List of figures

Figure 2.1	The physical form of <i>Peperomia pellucida</i> (L.) Kunth.
Figure 2.2	The geographical distribution of <i>P. pellucida</i> in the tropical and subtropical regions of the world.
Figure 2.3	The Fischer projections of some common phytochemicals detected in <i>P. pellucida</i> . (A) Terpenes. (B) Peperomins.
Figure 2.4	The Fischer projections of some common phytochemicals detected in <i>P. pellucida</i> . (A) Phenylpropanoids. (B) Polyphenols. (C) Fatty acids. (D) Sterol. (E) Naphthalenes. (F) Glycosides.
Figure 3.1	Procedure of plant sample processing.
Figure 4.1	The PCA biplot of biological activities in <i>P. pellucida</i> crude methanolic extract and solvent fractions.
Figure 4.2	The morphology of ARPE-19. (A) negative control group. (B) 0.5 % DMSO vehicle control group. (C) Crude methanolic extract (4 mg/ml onwards). (D) Ethyl acetate fraction (5 mg/ml onwards).
Figure 4.3	The cell viability (%) of ARPE-19 treated with <i>P. pellucida</i> crude methanolic extract and ethyl acetate fraction under normal glucose condition after 24 hours.
Figure 4.4	The cell viability (%) of ARPE-19 treated with <i>P. pellucida</i> crude methanolic extract and ethyl acetate fraction under normal glucose (17 mM) and the high glucose (34 mM, 68 mM) conditions.
Figure 4.5	The cell viability (%) of ARPE-19 treated with <i>P. pellucida</i> crude methanolic extract and ethyl acetate fraction under normal glucose (17 mM) and the high glucose (34 mM, 68 mM) AGE-treated conditions.

Figure 4.6	The relative gene expression of NF-κB p65 in ARPE-19 treated with <i>P. pellucida</i> crude methanolic extract and ethyl acetate fraction under normal glucose (17 mM), high glucose (34 mM, 68 mM) and AGE-treated conditions.
Figure 4.7	The relative protein expression of NF-κB p65 in ARPE-19 treated with <i>P. pellucida</i> crude methanolic extract and ethyl acetate fraction under normal glucose (17 mM), high glucose (34 mM, 68 mM) and AGE-treated conditions.
Figure 4.8	The relative protein expression of phosphorylated NF-κB p65 in ARPE-19 treated with <i>P. pellucida</i> crude methanolic extract and ethyl acetate fraction under normal glucose (17 mM), high glucose (34 mM, 68 mM) and AGE-treated conditions.
Figure 4.9	The relative gene expression of STAT3 in ARPE-19 treated with <i>P. pellucida</i> crude methanolic extract and ethyl acetate fraction under normal glucose (17 mM), high glucose (34 mM, 68 mM) and AGE-treated conditions.
Figure 4.10	The TLC profiles of PPM/A/5-7 (A) and PPM/B/2-4 (B).
Figure 4.11	The TLC profile of PPM/B/5-6.
Figure 4.12	The chemical structure of dillapiole.
Figure 4.13	The chemical structure of 2,4,5-trimethoxystyrene.
Figure 4.14	The TLC profile of PPM/B/7-9.
Figure 4.15	The chemical structure of methyl 9-octadecenoic acid
Figure 4.16	The TLC profile of PPM/B/13-15
Figure 4.17	The chemical structure of methyl pheophorbide-a
Figure 4.18	The schematic diagram of the purification of fraction 1, fraction 2, fraction 3 and fraction 4 from <i>P. pellucida</i> crude methanolic extract.
Figure 4.19	The TLC profile of PPM/A/1 and PPM/A/2.

List of appendices

A1	Materials and reagents.
A2	List of equipment.
B1	The expression of transcription factors in ARPE-19. (a) STAT3 protein. (b) Phosphorylated STAT3 protein. (c) PPAR- γ gene. (d) PPAR- γ protein. (e) Phosphorylated PPAR- γ protein.
B2	The relative gene expression of antioxidant, pro-inflammatory and angiogenic markers in ARPE-19. (a) IL-8. (b) MCP-1. (c) MMP2. (d) VEGF. (e) GPx.
B3	The relative protein expression of antioxidant, pro-inflammatory and angiogenic markers in ARPE-19. (a) IL-8. (b) MCP-1. (c) MMP2. (d) VEGF. (e) GPx.
B4	The expression of pro-inflammatory and anti-inflammatory markers involved in cytokine signalling in ARPE-19. (a) SOCS1 gene. (b) SOCS1 protein. (c) RAGE gene. (d) RAGE protein. (e) sRAGE protein.
B5	The western blot bands of antioxidant, anti-inflammatory and pro-inflammatory biomarkers in ARPE-19 under normal glucose (17 mM) and moderately high glucose (34 mM) conditions.
B6	The western blot bands of antioxidant, anti-inflammatory and pro-inflammatory biomarkers in ARPE-19 under high glucose (68 mM) condition and normal glucose (17 mM) AGE-treated condition.
B7	The western blot bands of antioxidant, anti-inflammatory and pro-inflammatory biomarkers in ARPE-19 under moderately high glucose (34 mM) and high glucose (68 mM) AGE-treated conditions.
C1	TLC profiles of <i>P. pellucida</i> crude methanolic extract and solvent fractions.

C2	¹ H NMR spectrum (CDCl ₃ , 400 MHz) of fraction PPM/A.
C3	¹ H NMR spectrum (CDCl ₃ , 400 MHz) of fraction PPM/B.
C4	¹ H NMR spectrum (CDCl ₃ , 400 MHz) of fraction PPM/A/5-7/2-4.
C5	¹ H NMR spectrum (CDCl ₃ , 400 MHz) of fraction PPM/B/2-4/7.
D1	¹ H NMR spectrum (CDCl ₃ , 400 MHz) of fraction 1.
D2	¹³ C NMR spectrum (CDCl ₃ , 100 MHz) of fraction 1.
D3	UV-Vis spectrum of fraction 1.
D4	FTIR spectrum of fraction 1.
D5	ESIMS spectrum of fraction 1.
E1	¹ H NMR spectrum (CDCl ₃ , 400 MHz) of fraction 2.
E2	¹³ C NMR spectrum (CDCl ₃ , 100 MHz) of fraction 2.
E3	UV-Vis spectrum of fraction 2.
E4	FTIR spectrum of fraction 2.
E5	ESIMS spectrum of fraction 2.
F1	¹ H NMR spectrum (CDCl ₃ , 400 MHz) of fraction 3.
F2	¹³ C NMR spectrum (CDCl ₃ , 100 MHz) of fraction 3.
F3	UV-Vis spectrum of fraction 3.
F4	FTIR spectrum of fraction 3.
F5	ESIMS spectrum of fraction 3.
G1	¹ H NMR spectrum (CDCl ₃ , 400 MHz) of fraction 4.
G2	¹³ C NMR spectrum (CDCl ₃ , 100 MHz) of fraction 4.
G3	UV-Vis spectrum of fraction 4.
G4	FTIR spectrum of fraction 4.
G5	ESIMS spectrum of fraction 4.

Chapter I

Introduction

Diabetes mellitus (DM) is a metabolic syndrome characterised by chronic high blood glucose level due to the impairment of insulin production, secretion or action (Kharroubi and Darwish, 2015). DM is generally classified into type 1 and type 2 DM, in addition to specific types such as gestational DM (American Diabetes Association, 2022; Kharroubi and Darwish, 2015). If the symptoms of DM persist over a long time, it could affect other vital organs and lead to the development of microvascular complications such as nephropathy, neuropathy and retinopathy (Kharroubi and Darwish, 2015; Papatheodorou *et al.*, 2018). The risk of developing microvascular complication increases with the duration of DM (Papatheodorou *et al.*, 2018). Most importantly, microvascular complications are associated with high morbidity and mortality among the patients suffering from DM (Papatheodorou *et al.*, 2018). This is largely due to the significant loss of function in the blood circulatory system, excretory system, nervous system and vision (Kharroubi and Darwish, 2015).

1.1 Diabetic retinopathy (DR)

Diabetic retinopathy (DR) is the most common diabetic microvascular complications in both developing and developed countries (Nentwich and Ulbig, 2015). From year 2021 to the period between 2030 and 2045, the number of patients suffering from DM is expected to rise by 16 % to 30 % (International Diabetes Federation, 2022). In Malaysia, the prevalence of DM is projected to increase from 18.3 % in 2019 to 31.3 % by 2025 (Akhtar *et al.*, 2022). A rise in diabetic microvascular complication

cases including DR is inevitable following the rise in DM prevalence. As vision is one of the most important senses that occupies a great proportion of cognitive function, its deterioration would significantly impact the patient's quality of life (Ho *et al.*, 2022b). When compared to other diabetic microvascular complications, DR is more likely to cause severe cognitive decline among the DM patients (Floch *et al.*, 2013). Considering the challenges for the management of DR, more attention should be devoted to discovering alternative medical solution for DR.

1.2 Problem statement

The management of DR requires a long-term commitment, and this may pose emotional and financial burdens on the affected individuals (Coney, 2019). According to Goldhaber-Fiebert *et al.* (2010), the expenses incurred on patients with DR are three times higher than those without developing the complication. Besides, there is currently no effective treatment for DR. Apart from the high cost, the current management of DR using anti-vascular endothelial growth factor (VEGF) agent fails to produce promising therapeutic response, not to mention the need for periodic administration of the drug (Wang and Lo, 2018). Current treatment via laser photocoagulation produces undesired side effects due to its destructive nature (Maniadakis and Konstantakopoulou, 2019). The use of laser photocoagulation is only effective when used with other treatment approaches, which are usually accompanied with adverse effects (Maniadakis and Konstantakopoulou, 2019).

1.3 The nature-based therapeutic approach

The application of natural resources such as medicinal plants in the management of DR could be a safer and cost-effective approach due to their origin and abundance in the nature (Sofowora *et al.*, 2013). Among the medicinal plants, *Peperomia pellucida* (L.) Kunth has been demonstrated to exhibit different biological activities including anti-diabetes, anti-cancer, anti-inflammatory, antioxidant and blood pressure reducing effects (Alves *et al.* 2019). More importantly, *P. pellucida* has been recently reported to inhibit glycation, a biochemical process implicated in the development of DR (Ho *et al.*, 2022a). The herbal plant has long been part of the diet for local communities and a traditional remedy for inflammatory-related illnesses such as conjunctivitis, gastrointestinal disorders, respiratory tract disorders and kidney infections (Ho *et al.*, 2022b). Previous scientific evidence has collectively suggested that *P. pellucida* could be a potential therapeutic ingredient for inflammatory diseases (Alves *et al.*, 2019). To date, there is a lack of effective nature-based therapeutic method to manage DR. Although the plant has been traditionally used to treat many inflammation-related complications (Amarathunga and Kankanamge, 2017), there is no report on its usage in alleviating DR. Based on a series of past evidence on the plant's anti-inflammatory effect, *P. pellucida* is considered a potential therapeutic source for the management of DR (Ho *et al.*, 2022b). Whether *P. pellucida* could be utilised as an anti-retinopathy agent remains to be elucidated.

1.4 Research question

Although *P. pellucida* has been used traditionally for the treatment of inflammatory-related illnesses, it remains unclear about its underlying mechanism in regulating the inflammatory and angiogenic processes involved in the development of DR. Such therapeutic effect could be stemmed from the biological activities of the plant, in which the presence of bioactive compounds assumes a major role (Yahia *et al.*, 2020). Several phytochemicals have been recently discovered in *P. pellucida* but their roles in human health have not been determined (Alves *et al.*, 2019). There is currently no effective strategy to manage DR as laser photocoagulation therapy merely slows down the progression of DR while most patients show poor compliancy towards anti-VEGF agents (Boyd *et al.*, 2013; Yang *et al.*, 2016). All the above unsolved issues have led to the following research questions:

- i. Does *P. pellucida* display anti-retinopathy effect such as anti-glycaemic, anti-glycation, anti-inflammatory and antioxidant activities with low toxicity?
- ii. Could *P. pellucida* ameliorate high glucose-induced oxidative-glycation damage in human retinal pigment epithelial cell line (ARPE-19) by modulating the expression of genes and proteins involved in nuclear factor kappa B (NF- κ B) p65, peroxisome proliferator activated-receptor gamma (PPAR- γ) and signal transducer and activator of transcription 3 (STAT3) signalling pathways?
- iii. What are the phytochemicals present in *P. pellucida* that contribute to the aforementioned functional activities listed in i and ii?

1.5 Hypotheses

This study hypothesises that:

- i. *P. pellucida* exhibits potent anti-glycaemic, anti-glycation, anti-inflammatory and antioxidant activities with low toxicity.
- ii. *P. pellucida* could ameliorate high glucose-induced oxidative-glycation damage in ARPE-19 by modulating the mediators involved in NF- κ B p65, PPAR- γ and STAT3 signalling pathways.
- iii. *P. pellucida* contains different classes of phytochemicals that contribute to the different functional activities listed in (i) and (ii).

1.6. Study aims and objectives

This study aims to investigate the underlying regulatory mechanism of *P. pellucida* extract against high glucose-induced oxidative-glycation cellular damage in APRE-19 model. The following three objectives are formatted to achieve the study aim:

- i. To identify the solvent fraction of *P. pellucida* crude methanolic extract that yields phytochemical content with low toxicity and potent anti-glycaemic, anti-glycation, anti-inflammatory and antioxidant activities.
- ii. To elucidate the underlying modulatory mechanism of the *P. pellucida* solvent fraction on the expression of genes and proteins within NF- κ B p65, PPAR- γ and STAT3 signalling pathways via an *in vitro* ARPE-19 model.

iii. To identify and characterise the phytochemicals in *P. pellucida* extract, which contribute to the functional activities listed in (i) and (ii).

Chapter II

Literature review

2.1 Diabetes mellitus (DM)

DM is one of the largest global health emergencies in the 21st century (Fan, 2017). The prevalence of DM has increased worldwide over the past few decades (Fan, 2017). It is also the ninth major cause of morbidity worldwide with an approximate 10 percent of the working adults living with DM (International Diabetes Federation, 2022). It is estimated that 537 million adults aged from 20 to 79 years old are suffering from DM, of which 90 % of the cases belong to type 2 DM (International Diabetes Federation, 2022). In low- and middle-income countries, more than 75 % of adults are living with DM (International Diabetes Federation, 2022). In Malaysia, DM is one of the most prevalent chronic metabolic syndromes affecting an approximate 20 % of total working adult population (International Diabetes Federation, 2022; Ministry of Health Malaysia, 2017). As of 2021, it was worth noting that there are approximately 2 million undiagnosed DM cases in Malaysia (International Diabetes Federation, 2022).

The widespread of DM and its complications has contributed tremendously to the disability and mortality worldwide and this has posed a major threat to the global health (International Diabetes Federation, 2022). In 2021, DM alone has resulted in an estimated 6.7 million deaths, which is equivalent to 1 death in every 5 seconds (International Diabetes Federation, 2022). According to Punthakee *et al.* (2018), DM is defined as a heterogeneous metabolic disease characterised by the manifestation of hyperglycaemia due to the impairment of insulin secretion, defective insulin action or both. Hyperglycaemia is the most common indicator of the disease, which arises due to insulin deficiency in both type 1 and type 2 DM.

Hyperglycaemia is also commonly accompanied with weight loss, blurred vision as well as increased thirst and urination (American Diabetes Association, 2022). Insulin deficiency in type 1 DM occurs as a result of the autoimmune destruction of pancreatic beta cells (Canadian Diabetes Association, 2018). In rare cases, type 1 DM can occur in an idiopathic manner when there is insulin deficiency but an absence of autoimmune response, whereby such cases are mostly inherited (American Diabetes Association, 2022). On the other hand, type 2 DM is characterised by either predominant insulin resistance with relative insulin deficiency or predominant insulin deficiency with relative insulin resistance (Canadian Diabetes Association, 2018).

The other specific types of DM can be induced by drugs, genetic anomalies or as a secondary manifestation to viral infections and pathological conditions such as endocrinopathies (American Diabetes Association, 2022). Besides, they are characterised by the abnormal production of hormones that antagonise the action of insulin (American Diabetes Association, 2022). Gestational DM refers to glucose intolerance that develops during the period between 24th and 28th week of pregnancy (American Diabetes Association, 2022). Typically, gestational DM is resolved after labour (American Diabetes Association, 2022). However, the term can also be applied to DM that persists after pregnancy (American Diabetes Association, 2022). There is also other specific form of DM that has been suggested, which can be accompanied by certain underlying health condition. According to de la Monte and Wands (2008), the term type 3 DM is used to refer to the abnormal glucose utilisation in the cerebrum of individuals with Alzheimer's disease. Similar features of type 1 and type 2 DM are observed in type 3 DM, but they are only confined in the brain (de la Monte and Wands, 2008). This could serve as a causative

mechanism of neurodegeneration and potentially contributing to the development of the neurodegenerative condition (de la Monte and Wands, 2008). Regardless of the types of DM, genetic and environmental predispositions play an important role in the pathogenesis of DM. Furthermore, the classification of DM based on age-groups is obsolete as both type 1 and type 2 DM can occur in adults and children (American Diabetes Association, 2022). In DM, chronic hyperglycaemia is positively correlated with specific long-term microvascular complications affecting the retina, kidneys, nervous system, in addition to an increased risk for cardiovascular diseases.

2.2 Diabetic Retinopathy (DR)

2.2.1 Background

DR is a major diabetic microvascular complication and a common cause of vision loss among the working-age population (Lee *et al.*, 2015a). Globally, an approximate one-third of patients suffering from DM are affected by the vision-threatening DR (Lee *et al.*, 2015a). DR also affects more than 45 % of type 2 DM patients worldwide (Calderon *et al.*, 2017; Papatheodorou *et al.*, 2018) while in Malaysia, the prevalence of developing DR among type 1 and type 2 DM patients were 12.3 % and 22.3 %, respectively (Ali *et al.*, 2016). In Malaysia, as much as 7.1% of the diabetic population is impacted by the advanced stage of proliferative DR (PDR). (Ali *et al.*, 2016). The incidence of developing DR between 5 years and 25 years after the diagnosis of DM ranges from 25 % to 90 % (Cecilia *et al.*, 2019).

DR is characterised by progressive damage to the retinal vasculature (Nentwich and Ulbig, 2015). Based on the International Clinical

Disease Severity for DR, DR can be classified into non-proliferative DR (NPDR) and PDR (Ting *et al.*, 2016). NPDR is the early asymptomatic stage of the disease, and it features increased vascular permeability and capillary occlusion in the retinal vasculature (Wang and Lo, 2018). NPDR can be further subcategorised into mild, moderate and severe cases based on the presence of diabetic macular edema (DME) (Tarr *et al.*, 2013). In NPDR, fundus photography is applied to detect haemorrhages, microaneurysms as well as hard exudates in the retina (Wang and Lo, 2018). On the contrary, neovascularisation is the hallmark feature of the advanced stage PDR that may progress to vision impairment due to vitreous haemorrhage and retinal detachment (Stitt *et al.*, 2016; Wang and Lo, 2018).

DME is a condition caused by the accumulation of fluid at the macula region of retina due to the breakdown of blood-retinal barrier (BRB), in which the retinal pigment epithelium (RPE) has an essential role (Wang and Lo, 2018). RPE is a monolayer of pigmented cells found between the photoreceptor layer and choroidal vasculature (Senanayake *et al.*, 2020). It possesses a vital role in the maintenance of photoreceptors as well as supporting the functional integrity of the choroidal vasculature (Zhou *et al.*, 2020a). Besides, RPE is involved in filtering excess light to mitigate photo-oxidative stress, immune regulation and nutritional supplementation in the retina (Kang *et al.*, 2019). The RPE is also an integral part of the BRB due to its tight cell junction (Kang *et al.*, 2019). In DR, the leaky and fragile newly-formed blood vessels in microaneurysms fail to constitute an efficient BRB, leading to the breakdown of BRB (Abcouwer and Gardner, 2014). This is followed by the distortion of visual images and deterioration of visual acuity, a result of the accumulation of fluid at the macula (Wang and Lo, 2018).

2.2.2 Pathophysiology

The classic pathophysiological mechanisms leading to the development of DR involve the dysregulation of biochemical pathways (Safi *et al.*, 2014). This includes the polyol pathway, protein kinase C (PKC) pathway and hexosamine pathway (Safi *et al.*, 2014). Besides, the non-enzymatic formation and interaction of advanced glycation end product (AGE) with the receptor for AGE (RAGE) also contributes to the progression of DR (Tarr *et al.*, 2013). These abnormalities in biochemical processes collectively give rise to the occurrence of oxidative stress in the retina (Li *et al.*, 2017). Subsequently, oxidative stress triggers cellular inflammatory responses through the activation of transcription factors and inflammatory signalling pathways that induce the gene and protein expression of pro-inflammatory and angiogenic mediators (Al-Kharashi, 2018).

2.2.2.1 Polyol pathway

One of the theories associated with the development of DR is the polyol pathway (Lorenzi, 2007). The physiologic function of polyol pathway is to maintain the level of circulating glucose (Yan, 2018). In DM, excess glucose is converted to sorbitol by aldose reductase (AR), a rate-limiting enzyme in the pathway (Yan, 2018). AR is expressed in human retina, in which glucose homeostasis takes place (Lorenzi, 2007). The enzyme utilises the reduced nicotinamide adenosine diphosphate (NADPH) as a cofactor (Safi *et al.*, 2014). Under high glucose environment, this process is accelerated and eventually results in the depletion of NADPH (Yan, 2018). Under normal physiological condition, NADPH is required by the glutathione reductase to convert glutathione into reduced glutathione, an antioxidant that counters oxidative stress (Yan, 2018). As a result, the depletion of

NADPH could contribute to the imbalance of redox homeostasis in human retina (Yan, 2018).

In addition, the excessive production of sorbitol may impart osmotic damage to the retina (Tarr *et al.*, 2013). Hence, this precedes the second reaction in the polyol pathway, which involves the conversion of sorbitol to fructose by the enzyme sorbitol dehydrogenase (Mathebula, 2015). The process is accompanied by the conversion of co-factor nicotinamide adenosine dinucleotide (NAD⁺) into reduced nicotinamide adenosine dinucleotide (NADH) (Mathebula, 2015), resulting in an increased NADH/NAD⁺ ratio (Yan, 2018). The accumulation of NADH has been implicated in the development of DM due to the inhibition of insulin release from pancreatic β -cells (Lamson and Plaza, 2002). Besides, the overproduction of NADH could impair the mitochondria as the organelle is responsible to recycle NADH and mitigate the pseudohypoxic condition (Yan, 2018). Subsequently, this triggers the formation of reactive oxygen species (ROS) in the mitochondrial electron transport chain when NADH is being oxidised to form NAD⁺ by the enzyme NADH oxidase (Yan, 2014). The final product of polyol pathway, fructose would undergo phosphorylation to form fructose-3-phosphate, which is further degraded into 3-deoxyglucosone (Yan, 2018). These two products have high glycation potential that are capable of producing more AGEs (Tarr *et al.*, 2013). Besides, fructose could undergo structural modification in a process known as Heyns reaction to produce additional AGEs (Cecilia *et al.*, 2019). Ultimately, AGE induces oxidative stress and pro-inflammatory response in the retina, leading to the development of DR (Safi *et al.*, 2014).

2.2.2.2 Hexosamine pathway

The hexosamine pathway is derived from the glycolytic pathway, in which glucose is utilised for energy production during cellular respiration (Queiroz *et al.*, 2019). The activation of hexosamine pathway results in the production of uridine diphosphate N-acetylglucosamine, which is a substrate and vital component for the post-translational modification of transcription factors through protein glycosylation (Kowluru and Mishra, 2015; Queiroz *et al.*, 2019). In DM, ROS inhibits a key enzyme, glyceraldehyde-3-phosphate dehydrogenase (GAPDH) in the pathway (Li *et al.*, 2017). The inhibition of GAPDH causes diversion of a glycolytic metabolite, fructose-6-phosphate to the hexosamine pathway (Kowluru and Chan, 2007). Upon activating hexosamine pathway, the other enzyme glutamine fructose-6-phosphate amidotransferase converts fructose-6-phosphate into glucosamine-6-phosphate and subsequently forms glucosamine-1-phosphate (Buse, 2006). Finally, through the addition of uridine, uridine diphosphate N-acetylgalactosamine and cytidine-5'-monophospho-N-acetylneuraminic acid are the final products that form part of the components of glycoproteins, glycolipids and gangliosides (Buse, 2006). The glycosylation process is induced by the substrate, uridine diphosphate N-acetylglucosamine via the modification of serine threonine residues with O-linked β -N-acetylglucosamine (Buse, 2006). The hexosamine pathway may lead to the glycosylation and activation of the NF- κ B p65 transcription factor, which assume a major role in initiating inflammation and apoptosis in the retina (Li *et al.*, 2017). The post-translational modification of stimulating proteins by the substrate could initiate the transcription of angiopoietin 2 through the binding of gene promoter (Yao *et al.*, 2007). The increased production of this protein is associated with the loss of pericytes, which contribute to the development of DR (Yao *et al.*, 2007). In addition, the inhibition of GAPDH by ROS could

result in the accumulation of glyceraldehyde-3-phosphate, thereby leading to the accumulation of AGE precursors and synthesis of AGE (Beisswenger *et al.*, 2003).

2.2.2.3 Protein kinase C (PKC) pathway

The PKC is an enzyme that falls under the serine/threonine family of kinase enzymes (Prakash *et al.*, 2008). It is present in various body tissues except the brain and peripheral nerve tissues (Prakash *et al.*, 2008). The β 1, β 2 and delta isoforms of PKC are specifically linked to the development of DR (Prakash *et al.*, 2008; Tarr *et al.*, 2013). PKC catalyses the phosphorylation of proteins involved in signal transduction, such as NF- κ B p65 and signal transducer and activator of transcription 3 (STAT3) (Tarr *et al.*, 2013). The phosphorylation of these transcription factors give rise to pathological features, including angiogenesis and inflammation (Tarr *et al.*, 2013). The overactivation of the PKC pathway is associated with disruption in the retinal haemodynamics, which may subsequently lead to the development of DR (Prakash *et al.*, 2008). In DM, hyperglycaemia promotes glucose flux through the glycolytic pathway and increases the *de novo* synthesis of diacylglycerol, the activator of PKC (Tarr *et al.*, 2013). Subsequently, it triggers the activation of downstream signal transduction pathway. For instance, the activation of NF- κ B p65 and STAT3 signalling pathways induces the expression of pro-inflammatory genes, such as interleukin 8 (IL-8) and monocyte chemoattractant protein 1 (MCP-1) that cause detrimental effects in the retinal vasculature through angiogenesis, leukostasis, increased vascular permeability and alteration of extracellular matrix in the retinal endothelium (Prakash *et al.*, 2008; Tarr *et al.*, 2013). Angiogenesis occurs as a result of an increased production of angiogenic

factors, such as matrix metalloproteinase 2 (MMP2) and VEGF and this eventually leads to neovascularisation, a main feature of PDR (Prakash *et al.*, 2008; Tarr *et al.*, 2013). Leukostasis and alteration of basement membranes in the retinal endothelium may affect the retinal blood flow and cause capillary occlusion, which increases the likelihood of vascular leakage (Fu *et al.*, 2016; Tarr *et al.*, 2013). Furthermore, the regulatory domain of PKC is made up of zinc fingers that are susceptible to oxidation (Kowluru and Chan, 2007). The zinc fingers are composed of two zinc atoms and six cysteine residues, which activate PKC when modified by ROS (Cosentino-Gomes *et al.*, 2012). Hence, DM-induced oxidative stress could activate PKC pathway due to oxidative modification of PKC by ROS (Cosentino-Gomes *et al.*, 2012; Kowluru and Chan, 2007). The above evidences collectively describe how DM-induced PKC pathway could affect the retinal vasculature.

2.2.2.4 Advanced glycation end product (AGE)

Glycation is a post-translational modification process during which sugar is covalently bonded to proteins present in the human body (Fournet *et al.*, 2018). This structural modification could alter the biological role of proteins on various important metabolic processes (Fournet *et al.*, 2018). Unlike the glycosylation process, which synthesises glycoproteins, glycation is both a physiological and pathological process (Fournet *et al.*, 2018). The formation of AGE during glycation is strongly associated with the development of DR (Fournet *et al.*, 2018).

Glycation can occur both exogenously in the extracellular matrix as well as endogenously in the cytoplasm or even organelles (Fournet *et al.*, 2018). The final product of the process, AGE is formed via the non-

enzymatic reaction of reducing sugars with proteins (Tarr *et al.*, 2013). This chemical reaction is a common manifestation in DM as persistent high blood glucose level accelerates the glycation process (Fournet *et al.*, 2018). Generally, the formation of AGE can be divided into initial, propagation and advanced phases (Yeh *et al.*, 2017).

In the initial phase, covalent bond is formed between the carbonyl group of reducing sugar and a free amino group of the protein (Fournet *et al.*, 2018). Schiff base, Amadori products and Heyns-Carson products are the precursors of AGE that are initially formed (Tarr *et al.*, 2013). The precursors of AGE could alter the protein structure and promote the glycation process (Tarr *et al.*, 2013). Schiff base is formed through a reversible process that involves the release of a water molecule (Fournet *et al.*, 2018). Schiff base will then undergo irreversible isomerisation (Fournet *et al.*, 2018). Subsequently, this gives rise to the formation of Amadori product and Heyns-Carson product, which are formed from aldoses and ketoses, respectively. An example for such product is the fructosamine (Fournet *et al.*, 2018).

In the propagation phase, Amadori product and Heyns-Carson product are involved in the retro-aldol reaction, during which the precursors undergo fragmentation to form aldehydes and dicarbonyl compounds (Fournet *et al.*, 2018). These compounds, which include glyoxal, methylglyoxal and 3-deoxyglucosone (Yeh *et al.*, 2017) would undergo further fragmentation to form glycation intermediaries that eventually react with other proteins to produce AGEs in the advanced stage (Fournet *et al.*, 2018). They also promote glycation by reacting with other amino groups (Fournet *et al.*, 2018). Furthermore, AGEs have fluorescence properties; pentosidine is a common example of fluorescent cross-linking AGE that is formed irreversibly from glycooxidation (Yeh *et al.*, 2017). Imidazolium

dilysine is an example of minor non-fluorescent cross-linking AGE (Yeh *et al.*, 2017). Other non-fluorescent and non-crosslinking AGEs includes N- ϵ -carboxymethyl-lysine and N- ϵ -carboxyethyl-lysine (Gkogkolou and Böhm, 2012).

Just like any other bioactive mediators, AGEs exert its effect via the ligand-receptor interaction, which initiates a cascade of downstream signal transduction pathways that results in the generation of pathological responses (Ramasamy *et al.*, 2011). The interaction of AGE with RAGE is the key reaction that leads to pathological events through the activation of pro-inflammatory signalling pathways (Logan and Storey, 2018). For instance, this could lead to retinal dysfunction through angiogenesis, inflammation and the breakdown of BRB (Xu *et al.*, 2018). RAGE is an immunoglobulin superfamily of transmembrane receptor that is expressed in many cell types including RPE (Jensen *et al.*, 2015). It is composed of three protein domains: extracellular domain, hydrophobic transmembrane-spanning domain and a highly charged cytoplasmic domain (Chuah *et al.*, 2013). The cytoplasmic domain is the part of the receptor that are responsible for intracellular signalling (Chuah *et al.*, 2013). The extracellular domain is composed of a variable-type domain and two constant-type domains. The binding of ligands such as AGEs to the variable-type domain of the extracellular domain activates RAGE and induce subsequent oxidative stress and pro-inflammatory responses (Jensen *et al.*, 2015). Genetic polymorphism in RAGE could influence the development of DR by altering the expression of RAGE (Ng *et al.*, 2012). According to Ng *et al.* (2013a), the 2245G/A RAGE polymorphism, in which nucleotide variation occurs at the intron 8 region, is associated with the development of DR. In addition, the progression of DR can be influenced by the increased activity of pro-inflammatory mediators, reduced sRAGE level

and deteriorating antioxidant status due to the characteristic low plasma GPx activity in different RAGE polymorphisms (Ng *et al.*, 2013a).

The expression of RAGE is found to positively correlate with the level of pro-inflammatory response (Chuah *et al.*, 2013). According to Chuah *et al.* (2013), there are numerous ways that the interaction of RAGE and its ligands can contribute to pro-inflammatory response. Firstly, RAGE is commonly expressed in epithelial cells including RPE as well as immune cells such as neutrophils and macrophages (Wang *et al.*, 2016). Hence, the ligands that bind to RAGE are known to be associated with the production of pro-inflammatory mediators involved in acute and chronic immune responses (Orlova *et al.*, 2007). Methylglyoxal, a major AGE precursor, is down-regulated by the enzyme glyoxalase. Interestingly, the expression of the enzyme is suppressed by the expression of RAGE (Reiniger *et al.*, 2010). Therefore, a forward feedback loop is formed as the overproduction of AGEs could up-regulate the expression of RAGE, which subsequently down-regulate the expression of glyoxalase, leading to the continuous generation of pro-inflammatory response (Schmidt, 2015).

RAGE could also function as an adhesion receptor for leukocytes by interacting with leukocyte β 2 integrin macrophage-1 antigen (Chuah *et al.*, 2013). Pro-inflammatory responses induced by AGE-RAGE interaction mostly depends on the activation of NF- κ B p65 transcription factor and its subsequent downstream pro-inflammatory genes, which may induce the innate and adaptive immune responses (Safi *et al.*, 2014). For instance, the activation of NF- κ B p65 signalling pathway induces the secretion of pro-inflammatory (IL-8, MCP-1) and angiogenic (MMP2, VEGF) mediators (Liu *et al.*, 2017; Martin *et al.*, 2009). The subsequent binding of pro-inflammatory and angiogenic mediators to their receptors may induce apoptosis and amplification of inflammatory and angiogenic responses via

the production of mediators (Liu *et al.*, 2017). Zong *et al.* (2010) had demonstrated that the hyperglycaemic-induced up-regulation of RAGE could lead to the generation of pro-inflammatory responses in retinal Müller glial cells involved in the progression of DR. The accumulation of AGEs and advanced lipoxidation end products are associated with Müller glial dysfunction in rat model of DR (Curtis *et al.*, 2011).

On the other hand, sRAGE is the C-terminal truncated form of RAGE that lacks the transmembrane domain (Juraneck *et al.*, 2016). There are two distinct forms of sRAGE. The first form is the endogenous secretory RAGE, which is mainly synthesised as a splice variant from a truncated RAGE messenger ribonucleic acid (mRNA) (Miranda *et al.*, 2018). The second form, cleaved RAGE is mainly produced from the proteolytic cleavage of RAGE via MMPs and A Disintegrin and Metalloprotease (Jensen *et al.*, 2015; Schmidt, 2015). The sRAGE acts as a competitive inhibitor to prevent the binding of ligands to RAGE (Juraneck *et al.*, 2016). The production of sRAGE acts as a feedback regulation of RAGE signalling (Koyama *et al.*, 2007). In other words, sRAGE serves as a decoy by preventing the binding of AGE to RAGE, thereby minimising the activity of RAGE (Schmidt, 2015). In addition, the production of sRAGE could be a good prognosis to DM complications. A study conducted by Miranda *et al.* (2018) showed that an increase production of sRAGE attenuated the AGE-RAGE mediated DM complications through the sequestration of AGEs. Besides, sRAGE level was reported to increase with the duration of DM as a counterbalance response to the formation of RAGE (Ng *et al.*, 2013b). Interestingly, patients suffering from DM and proliferative DR also demonstrated higher sRAGE/pentosidine ratio than NPDR, which makes sRAGE/pentosidine an ideal measure of risk factor for DR (Ng *et al.*, 2013b). Nevertheless, other studies have found low sRAGE level in patients

suffering from type 2 DM (Nadali *et al.*, 2021; Wang *et al.*, 2018). This may also suggest an increased susceptibility to inflammation and vascular complications (Nadali *et al.*, 2021).

2.2.2.5 Oxidative stress

Oxidative stress is a condition in which the production of ROS exceeds the free radicals-neutralising capacity of antioxidants (Velasquez, 2015). The production of ROS is an inevitable process in the midst of maintaining the normal physiological function of the cell (Birben *et al.*, 2012). Under normal physiological condition, ROS such as superoxide anions and hydrogen peroxides are inevitably generated from cellular respiration via the electron transport chain (Kowluru and Chan, 2007; Li *et al.*, 2017). ROS are highly reactive radicals containing at least an oxygen atom and they are capable of independent existence with one or more unpaired electrons (Patel *et al.*, 2018). ROS could interact with other molecules in redox reactions in order to achieve a stable state (Calderon *et al.*, 2017). This in turn induces oxidation of the target molecules (Calderon *et al.*, 2017).

Oxidative stress affects the functionality of biomolecules such as carbohydrates, proteins, lipids and deoxyribonucleic acid (DNA), which subsequently alters the body's homeostatic process and resulting in pathological outcomes (Cutler, 2005). Oxidative stress is another classical pathological mechanisms that lead to the occurrence of DR, and it could occur as a result of the activation of polyol pathway, PKC pathway, hexosamine pathway and RAGE signalling (Li *et al.*, 2017). Oxidative stress is also associated with the disruption of retinal tight junctions that form the BRB, leading to increased retinal permeability (Kang *et al.*, 2019).

Additionally, oxidative stress plays a significant role in RPE injury by decreasing the mitochondrial function of the cells (Baek *et al.*, 2016).

The retina is highly susceptible to oxidative stress due to abundance of polyunsaturated fatty acids and its high demand for oxygen (Kowluru and Chan, 2007). This criteria also gives rise to increased rate of glucose oxidation, which further accelerates oxidative stress (Kowluru and Chan, 2007). Oxidative stress is associated with increased apoptotic events in the retina due to the activation of pro-apoptotic mediators by ROS (Mohammad *et al.*, 2015). A previous study has shown that the suppression of ROS in the retinal capillary by antioxidants could revert apoptosis as well as mitochondrial dysfunction in the retina of DM animal models (Coucha *et al.*, 2015). Furthermore, ROS may also activate redox kinases and NF- κ B p65 transcription factor that induce the expression of pro-inflammatory genes and proteins implicated in the development of DR (Liu *et al.*, 2017).

On the other hand, eukaryotic cells are equipped with antioxidant defense system that protects the cells against the adverse effect of ROS (Jo *et al.*, 2020). Excessive ROS are neutralised by the antioxidant defense system to maintain the normal physiological functions (Kowluru and Chan, 2007). In addition to non-enzymatic antioxidants obtained solely from the diet, intracellular antioxidant enzymes form the enzymatic antioxidant defense system within cells, aimed at mitigating the impact of oxidative stress on the body (Birben *et al.*, 2012). GPx is an important antioxidant enzyme that is produced as part of the cellular enzymatic defense system (Birben *et al.*, 2012). This may highlight the importance of GPx as a first-line antioxidant defense to protect ARPE-19 against oxidative stress caused by high glucose and glycation (Ighodaro and Akinloye, 2018). Under physiological condition, harmful hydrogen peroxides and lipid peroxy radicals were rendered harmless by converting them into water via GPx

(Ighodaro and Akinloye, 2018). The activity of GPx in the retina was significantly lowered under the influence of high glucose and AGE (Cepas *et al.*, 2020; Shi *et al.*, 2019). Besides, the levels of GPx were significantly lower in DM and DR patients when compared to healthy control, implying the connection of GPx and oxidative stress to the development of DR (Ng *et al.*, 2013b).

Lipid peroxidation is the generation of lipid peroxyl radicals due to the attack of free radicals on cellular lipids whereby high peroxidation rate causes significant damage to cell membranes and disrupt cellular function (Nam, 2011). Lipid peroxidation generates products that are capable of forming adducts with DNA and proteins, thereby disrupting the physiological functions of these biomolecules (Nam, 2011). Subsequently, the dysfunctional biomolecules may lead to pathological consequences (Nam, 2011). Some products of lipid peroxidation are mainly reactive aldehydes such as γ -ketoaldehydes, 4-hydroxy-2-alkanal and malondialdehyde (Nam, 2011). Cell apoptosis is also induced when the rate of radicals production overwhelms the cellular repair capacity (Velasquez, 2015). In addition, the mitochondrial transcription factor A responsible for the transcription of mitochondrial DNA, may undergo ubiquitinylation under oxidative stress (Calderon *et al.*, 2017). This eventually down-regulates the transcription of mitochondrial DNA, causing mitochondrial dysfunction in RPE (Calderon *et al.*, 2017). Interestingly, GPx serves as a first line antioxidant defence against lipid peroxidation (Ighodaro and Akinloye, 2018). This may underscore the therapeutic significance of restoring GPx levels. Interestingly, the enzyme GPx plays a crucial role as the primary defense mechanism against lipid peroxidation (Ighodaro and Akinloye, 2018). By neutralising ROS and reducing lipid peroxides, GPx helps maintain the integrity of cell membranes and protects against oxidative

damage (Ighodaro and Akinloye, 2018). Therefore, restoring GPx levels could be therapeutically significant in mitigating the harmful effects of oxidative stress and preserving cellular health.

Excessive oxidative stress can disrupt the balance of pro-inflammatory signalling pathways, leading to aberrant activation and the generation of inflammatory responses (Mittal *et al.*, 2014). In hyperglycaemia, ROS is generated as a result of PKC-induced activation of the enzyme NADPH oxidase (Mittal *et al.*, 2014). The enzyme participates in the oxidative reaction, which involves the transfer of electrons to oxygen atoms, producing ROS (Mittal *et al.*, 2014). ROS may activate the NF- κ B signalling pathway, which induces cellular inflammatory response and further exaggerates oxidative stress through the production of ROS (Prakash *et al.*, 2008; Tarr *et al.*, 2013). The excessive generation of ROS could cause localised oxidative stress in the retina, thereby resulting in inflammation and tissue injury (Prakash *et al.*, 2008; Tarr *et al.*, 2013).

2.2.2.6 Inflammation

Inflammation is widely acknowledged for its association with the development of retinal abnormalities, which is usually accompanied by disrupted retinal permeability (Al-Kharashi, 2018). Retinal inflammation is an indirect result of the production of pro-inflammatory mediators (Tarr *et al.*, 2013). Pro-inflammatory mediators, such as cytokines and chemokines, can induce a state known as leukostasis (Deshmane *et al.*, 2009). In leukostasis, circulating leukocytes adhere to the retinal endothelial cells and become trapped within the retina vasculature (Wang and Lo, 2018). Leukocyte adhesion may increase the permeability of retinal vasculature and lead to the breakdown of BRB (Adamis and Berman, 2008; Jousseaume *et al.*, 2008).

et al., 2004). The accumulation of leukocytes in the vasculature could impair blood flow and disrupt tissue perfusion, thereby leading to tissue damage and retinal inflammation (Al-Kharashi, 2018). Apart from being an important clinical manifestation, retinal inflammation plays a substantial role in the progression of DR and may ultimately lead to visual impairment (Rübsam *et al.*, 2018).

The synthesis of pro-inflammatory mediators is an indirect cause for inflammatory response. Inflammation can result from the catalytic action of pro-inflammatory enzymes such as cyclooxygenases (COXs), xanthine oxidase (XO), lipoxygenases and hyaluronidase. For instance, COX-1 and COX-2 catalyse the production of pro-inflammatory prostaglandins during acute inflammation (Ricciotti and Fitzgerald, 2011). These prostaglandins modulate vascular permeability and recruitment of immune cells to the site of injury (Ricciotti and Fitzgerald, 2011). COX-1 is constitutively expressed in most tissues and involved in homeostatic functions, while COX-2 is inducible and is upregulated in response to inflammatory stimuli (Gacche *et al.*, 2011). On the other hand, xanthine oxidase (XO), the enzyme involved in the metabolism of purine bases and subsequent synthesis of uric acid (Abu Bakar *et al.*, 2018). Excessive uric acid levels can lead to the formation of urate crystals, which can accumulate in the joints, causing features like inflammation and pain as observed in gout (Abu Bakar *et al.*, 2018). XO could also promote the expression of inflammatory cytokines through the production of ROS (Abu Bakar *et al.*, 2018).

Lipoxygenases catalyse the production of pro-inflammatory mediators, such as leukotrienes (Wisastra and Dekker, 2014). Leukotrienes are potent chemoattractants for leukocytes and contribute to the recruitment of immune cells to sites of inflammation (Wisastra and Dekker, 2014). Additionally, these mediators can induce hyperpermeability of blood

vessels, leading to the leakage of fluid and proteins into surrounding tissues, which further amplifies the inflammatory response (Wisastra and Dekker, 2014). Furthermore, The enzyme hyaluronidase facilitates the degradation of hyaluronic acid (HA), a key component of the extracellular matrix (Buhren *et al.*, 2016). The enzymatic breakdown of HA disrupts the structural integrity of tissues and promotes inflammation by releasing inflammatory mediators and increasing vascular permeability (Buhren *et al.*, 2016). Moreover, the degradation of HA by hyaluronidase has been associated with the induction of angiogenesis (Buhren *et al.*, 2016).

Besides, transcription factors are important elements in the cell that control cell growth, proliferation, differentiation (Al-Kharashi, 2018). The generation of inflammatory response is also controlled by transcription factors, which function as master regulator for the gene and protein expression of pro-inflammatory and angiogenic factors (Al-Kharashi, 2018). Through the intricate regulatory network of transcription factors, they exert tight control over the expression of inflammatory mediators (Al-Kharashi, 2018). Dysregulated transcription factor activity can lead to aberrant inflammatory signalling and contribute to the pathogenesis of inflammatory diseases (Tarr *et al.*, 2013). Several important transcription factors have been linked to the development of DR (Tarr *et al.*, 2013). The NF- κ B p65, PPAR- γ and STAT3 were some notable transcription factors that regulate inflammatory response.

NF- κ B is a family of structurally related transcription factors that are sequestered by the inhibitor of NF- κ B (I κ B) family of inhibitory proteins with ankyrin repeats, rendering them in an inactive state in the cytoplasm (Sun *et al.*, 2013). The NF- κ B family consists of five members, namely the NF- κ B1 (p50), NF- κ B2 (p52), RelA (p65), RelB and c-Rel (Sun *et al.*, 2013). The activation of NF- κ B p65 is commonly associated with the transcription

of wide range of genes and proteins participated in inflammation (Liu *et al.*, 2017). This can be achieved through a cascade of reactions mediated by various signalling molecules in a process known as a signalling pathway (Liu *et al.*, 2017). The NF- κ B signalling pathway can be subdivided into canonical and non-canonical (Lawrence, 2009; Sun *et al.*, 2013). The canonical pathway is initiated by a broad class of receptors such as IL receptors, toll-like receptors and RAGE (Liu *et al.*, 2017). The binding of ligands to these receptors would result in the degradation of I κ B through phosphorylation by the I κ B kinase (IKK) (Lawrence, 2009). Subsequently, this leads to the phosphorylation and activation of NF- κ B p65 (Lawrence, 2009). The activated NF- κ B p65 proteins form dimers and translocate into the nucleus, where it binds to specific DNA elements and activates the transcription of target genes involved in inflammation (Liu *et al.*, 2017). Unlike canonical pathway, the non-canonical pathway responds to specific ligands for TNF receptor such as lymphotoxin β (Lawrence, 2009). Besides, the activation of non-canonical pathway depends the degradation of p100, the precursor protein of p52 (Liu *et al.*, 2017). In this pathway, the NF- κ B inducing kinase and IKK phosphorylate p100 for further ubiquitinylation and degradation (Liu *et al.*, 2017). The process ultimately leads to the nuclear translocation of activated NF- κ B proteins with mature p52 and RelB components (Lawrence, 2009).

Regardless of the canonical and non-canonical pathways, binding of the transcription factor to the DNA element κ B enhancer in the nucleus may lead to the gene and protein expression of pro-inflammatory (IL-8, MCP-1) and angiogenic (VEGF, MMP2) mediators (Liu *et al.*, 2017). IL-8, a member of the C-X-C chemokine family, is a soluble protein that plays a crucial role in initiating pro-inflammatory responses (Singh *et al.*, 2013). The C-X-C family of cytokines are structurally characterised by a single

amino acid sandwiched between two cysteine amino acids, hence the term, 'C-X-C' (Matsushima *et al.*, 2022). IL-8 is commonly secreted by epithelial cells, endothelial cells, lymphocytes and neutrophils during inflammation (Singh *et al.*, 2013). IL-8 assumes a critical role in the early phase of inflammation by promoting the activation and recruitment of neutrophils and basophils to the injured tissue (Silva, 2010). During retinal injury, neutrophils are among the frontline of immune responders (Deliyanti *et al.*, 2022). The accumulation of neutrophils in the retina could further aggravate inflammation by recruiting more leukocytes (Deliyanti *et al.*, 2022). Besides, depleting neutrophil count is associated with reduced incidence of vascular leakage and neovascularisation in the retina (Deliyanti *et al.*, 2022). Hence, IL-8 could serve as an important biomarker in the management of DR.

On the other hand, MCP-1 is another chemotactic cytokine that belongs to the C-C cytokine family (Deshmane *et al.*, 2009). Unlike IL-8, the structure of MCP-1 is characterised by two adjacent cysteine amino acids (Deshmane *et al.*, 2009). MCP-1 plays a crucial role during inflammation by promoting the recruitment and infiltration of monocytes and macrophages (Singh *et al.*, 2021). In the early and late phases of inflammation, MCP-1 contributes by directing the migration of monocytes to the site of injury (Deshmane *et al.*, 2009). In the immune system, monocyte is an important leukocyte that conducts regular monitoring of body tissues for pathological matters (Deshmane *et al.*, 2009). Upon activation, monocytes are differentiated into macrophages that infiltrate the body tissues to scavenge the disease-causing agents (Yang *et al.*, 2014). Besides, monocytes also activate the T-lymphocytes for sustained immune defense (Yang *et al.*, 2014). Hence, monocyte plays a pivotal role in the innate and adaptive immune systems (Kratofil *et al.*, 2017). Both IL-

8 and MCP-1 serve as an important indicator for early and late phases of inflammatory responses (Kratofil *et al.*, 2017).

The STAT3 signalling pathway is also widely known for its implication in inflammation via the expression of pro-inflammatory mediators such as IL-8 and MCP-1 as well as the angiogenic mediators, VEGF and MMP2 (Fan *et al.*, 2013; Zegeye *et al.*, 2018). Similar to the NF- κ B p65 signalling pathway, the STAT3 signalling pathway can also be subdivided into canonical and non-canonical pathways (Bharadwaj *et al.*, 2020). The canonical pathway of STAT3 is activated upon the binding of ligands such as cytokines or hormones to their receptor (Sethi *et al.*, 2014). Subsequently, this leads to the phosphorylation of tyrosine residues in the cytoplasmic portion of the receptor by Janus kinase (JAK) (Bharadwaj *et al.*, 2020). This process eventually recruits and activates cytoplasmic STAT3 proteins (Sethi *et al.*, 2014). The activated STAT3 proteins dimerise and translocate to the nuclear region, where the transcription of target genes is initiated upon binding to the promoter region (Bharadwaj *et al.*, 2020). The non-canonical pathway of STAT3 is characterised by its activation at the endoplasmic reticulum and mitochondria (Bharadwaj *et al.*, 2020). The activation of NF- κ B p65 and STAT3 signalling pathways was recognised for signalling the up-regulation of angiogenic and pro-inflammatory mediators in DR (Tarr *et al.*, 2013). Interestingly, both NF- κ B p65 and STAT3 could also interact together to amplify the mutual inflammatory response (Bharadwaj *et al.*, 2020). Nevertheless, STAT3 signalling pathway can be antagonised by the SOCS protein in a negative feedback loop to hinder further STAT3 activation (Chen *et al.*, 2016).

Among the SOCS family of proteins, SOCS1 demonstrates the highest potency as a regulatory protein (Liau *et al.*, 2018). This was achieved by the binding of SOCS1 protein to the tyrosine domains of

STAT3, which obstructs the phosphorylation of JAK (Bharadwaj *et al.*, 2020). In ARPE-19, the expression of SOCS1 can be induced in high glucose environment through the JAK-STAT3 signalling pathway (Chen *et al.*, 2016). It was previously demonstrated that SOCS1 plays a fundamental part in regulating inflammation in DR (Chen *et al.*, 2016). Likewise, the PPAR- γ nuclear receptor has been known to elicit anti-inflammatory response in ocular tissues (Zhang *et al.*, 2015a). Hence, PPAR- γ gene expression could serve as a potential anti-inflammatory marker when investigating the modulatory effects of plant extract on inflammation in the retina.

PPAR- γ represents the superfamily of PPAR nuclear receptors along with other two isoforms, PPAR- α and PPAR- β (Heming *et al.*, 2018). Among the PPAR nuclear receptors, the modulatory role of PPAR- γ is not only limited to glucose homeostasis, insulin sensitivity and lipogenesis (Zhang *et al.*, 2015a). PPAR- γ is also involved in the regulation of immune system as evident by the gene and protein expression of PPAR- γ in inflammatory cells (Heming *et al.*, 2018). In recent studies, PPAR- γ has even been linked to eliciting anti-inflammatory response by suppressing the production of angiogenic and pro-inflammatory mediators (Heming *et al.*, 2018; Zhang *et al.*, 2015a). Furthermore, the activation of PPAR- γ has been associated with reduced incidence of angiogenesis and retinal dysfunction (Gui *et al.*, 2020), suggesting its potential role in the management of DR (Gui *et al.*, 2020). Interestingly, the nuclear receptor could operate in the absence of a ligand apart from the classical activation of transcription factors that requires the binding of ligands such as 15-hydroxyeicosatetraenoic acid (Zhang *et al.*, 2015a). Upon the activation of PPAR- γ , PPAR-RXR heterodimers react with specific PPAR response element in the nucleus to trigger anti-inflammatory responses (Heming *et al.*, 2018). For instance,

the activation of PPAR- γ competes with NF- κ B p65 for the promoter regions, thereby resulting in diminished expression of pro-inflammatory and angiogenic mediators. However, phosphorylation of the ligand binding domain by protein kinase C may interfere with the activation of PPAR- γ (Brunmeir and Xu, 2018). Efforts in mitigating inflammatory response by targeting the phosphorylation of PPAR- γ remain a potential approach for the management of DR (Frkic *et al.*, 2021).

2.2.2.7 Overexpression of angiogenic factors

Neovascularisation is both a physiological and pathological process that could facilitate the development of DR (Tarr *et al.*, 2013). It is also the key attribute in the advanced stage PDR (Wang and Lo, 2018). According to Johnson and Wilgus (2014), neovascularisation encompasses both the *de novo* formation of new blood vessel (vascularigenesis) and formation of blood vessel from preceding blood vessels (angiogenesis). In DR, inflammation promotes neovascularisation in the retina (Rezzola *et al.*, 2020). The new blood vessels that formed in this process is usually dysfunctional and leaky, which subsequently leads to the breakdown of BRB (Abcouwer and Gardner, 2014). Ultimately, visual impairment occurs as a result of the accumulation of fluid in the macula region of the retina (Wang and Lo, 2018). Besides, angiogenesis is a critical process in inflammation, as it provides oxygen and nutrients to inflamed tissues and facilitates the recruitment of immune cells to the site of injury (Johnson and Wilgus, 2014).

The role of angiogenic factors such as VEGF and MMP2 is well-documented in the development of DR (Tarr *et al.*, 2013). The expression of angiogenic factors promotes neovascularisation and vascular

permeability, which causes haemodynamic changes in the retina (Tarr *et al.*, 2013). Furthermore, increased leukocyte adhesion has been reported in patients suffering from DR due to the overproduction of angiogenic factors in the retina (Ismail *et al.*, 2012; Wang and Lo, 2018). The angiogenic factors are capable of interacting with leukocyte integrins and thus they are important mediators secreted for leukocyte adhesion and transmigration in the retinal vasculature (Al-Kharashi, 2018; Kong *et al.*, 2018). As a result, they are associated with vascular leakage in the retina of patients suffering from DR (Wang *et al.*, 2010).

VEGF is a family of growth factor proteins consisting of VEGF-A, VEGF-B, VEGF-C, VEGF-D, VEGF-E and placental growth factor (Apte *et al.*, 2019). Apart from the virally encoded VEGF-E, VEGF-A predominates over the remaining four VEGF proteins in the regulation of angiogenesis in human (Apte *et al.*, 2019). Angiogenesis is induced by the binding of VEGF to its main receptor, the VEGF receptor 2 (Apte *et al.*, 2019). VEGF undertakes a vital role on vascular development by promoting the proliferation of endothelial cells following the degradation of vascular matrix proteins by MMP2 (Hazzaa *et al.*, 2020; Quintero-Fabián *et al.*, 2019). Dysregulated angiogenesis is often associated with the development of fragile and leaky blood vessels in DR (Apte *et al.*, 2019). There were numerous studies surrounding the involvement of VEGF in the development of DR (Tarr *et al.*, 2013). In DR, the expression of VEGF is up-regulated by the activation of PKC due to an increased glucose flux (Tarr *et al.*, 2013). The administration of anti-VEGF also remains the standard of care for DR patients to prevent vision loss (Wang and Lo, 2018). By targeting VEGF, anti-VEGF drugs can inhibit the growth of abnormal blood vessels in the retina and reduce vascular leakage, thereby preserving vision and preventing further deterioration of visual acuity in DR patients (Wang and

Lo, 2018). However, the administration of anti-VEGF therapy is accompanied by side effects (Wang and Lo, 2018).

On the other hand, MMPs are a family of zinc-dependent metalloproteinases and angiogenic factors that play an integral part in angiogenesis (Hazzaa *et al.*, 2020). Among the MMPs, the MMP2 is involved in the degradation of collagens in the retinal vascular matrix to facilitate the development of new blood vessels (Nikolov and Popovski, 2021). The subsequent process is then regulated by VEGF (Quintero-Fabián *et al.*, 2019). In DR, MMP2 has been demonstrated to induce mitochondrial dysfunction and destruction of blood vessels in the retina (Mohammad and Kowluru, 2010). Besides, the expression of MMP2 is also regulated by the transcription factors NF- κ B p65 and STAT3 (Lan *et al.*, 2009; Xie *et al.*, 2004). Thus MMP2 serves as one of the significant angiogenic indicators in the progression of DR. According to Bandyopadhyay and Rohrer (2012), the up-regulation of MMP2 is positively correlated with the expression of VEGF, which collectively contribute to neovascularisation in DR. The sustained formation of AGE and subsequent AGE-RAGE interaction in DM promotes the activation of transcription factor NF- κ B p65, and ultimately increases the expression of angiogenic mediators, VEGF and MMP2 (Kong *et al.*, 2018; Safi *et al.*, 2014).

2.2.3 Management of DR

The current management of DR relies on laser treatment and pharmacological approach that mitigates angiogenesis and inflammation. According to Wang and Lo (2018), the intravitreal injection of anti-VEGF is the gold standard for managing DR as it provides better visual outcomes compared to other approaches. However, the anti-VEGF therapy is only

partially effective towards DME (Duh *et al.*, 2017). The visual improvement benefitted by the majority patients from this approach is not clinically significant (Wang and Lo, 2018). Furthermore, the administration of anti-VEGF therapy is not without potential side effects. Common side effects include transient ocular discomfort, intraocular inflammation, and increased intraocular pressure (Wang and Lo, 2018). Additionally, long-term use of anti-VEGF agents may lead to adverse effects such as retinal atrophy and macular atrophy (Wang and Lo, 2018). Due to the short half-life, frequent intravitreal injection of anti-VEGF agent is required and this could lead to endophthalmitis and retinal detachment (Wang and Lo, 2018).

The laser photocoagulation precedes the anti-VEGF therapy as the mainstay treatment for DR (Fong *et al.*, 2007). Laser photocoagulation works by promoting the oxygen uptake of retinal epithelium (Fong *et al.*, 2007). By reducing retinal hypoxia, laser photocoagulation helps to stabilize and regress abnormal blood vessels in the retina, thereby preventing further vision loss (Fong *et al.*, 2007). Due to the destructive nature of high energy laser, this can cause collateral damage to surrounding retinal tissue, leading to potential complications such as permanent vision loss, night blindness and reduced peripheral vision (Fong *et al.*, 2007). Additionally, laser therapy may not be suitable for all patients, particularly those with DME or PDR (Wang and Lo, 2018).

Corticosteroid is another pharmacological agent administered intravitreally to treat DME, owing to its potent anti-inflammatory and anti-angiogenic properties (Cunningham *et al.*, 2008). When administered intravitreally, corticosteroid can effectively suppress angiogenesis, reduce retinal edema and alleviate inflammation, thereby improving visual outcomes in patients suffering from DME (Cunningham *et al.*, 2008). The usage of intravitreal steroid is also associated with adverse effects such as

retinal detachment, vitreous haemorrhage and endophthalmitis (Cunningham *et al.*, 2008). Due to the associating side effects, which are similar to the symptoms of PDR, the advent of anti-VEGF agent and laser treatment has gradually replaced corticosteroid for the treatment of DME (Cunningham *et al.*, 2008).

2.3 Human retinal pigment epithelial cell line (ARPE-19)

Retina is the main target tissue that is susceptible to the damaging effect of inflammation in DR (Juel *et al.*, 2012). In the retina, RPE is responsible for regulating the human eye immune system for overall visual health (Juel *et al.*, 2012). Specifically, RPE plays a pivotal role in safeguarding other ocular tissues against pathological events while forming an effective BRB (Juel *et al.*, 2012). The ARPE-19 is commonly employed as a cellular model of RPE in *in vitro* experimental studies (Hellinen *et al.*, 2019). ARPE-19 is a spontaneously arising cell line, which is derived from the primary RPE cell culture (Hellinen *et al.*, 2019). Under normal physiological condition, ARPE-19 cell culture displays hallmark stable monolayer of cobblestone morphology with microvilli and tight cell junctions (Hellinen *et al.*, 2019). Among the cellular models of RPE, ARPE-19 is the most preferable for experiments due in part to its superiority in reproducibility and broad cell passage range (Hellinen *et al.*, 2019). Most importantly, ARPE-19 mimics the genotypic and phenotypic characteristics of the human primary RPE cells in such a way that the similar experimental outcomes are reproducible with *in vitro* studies (Dunn *et al.*, 1996).

Gene expression study shows that differentiated ARPE-19 expresses RPE-specific genes that are involved in the regulation of visual cycle such as the RPE-specific 65 kDa protein, cellular retinaldehyde-binding protein,

lecithin retinol acyltransferase and retinol dehydrogenases (Samuel *et al.*, 2017). The cell line also expresses various inflammatory cytokines, chemokines and receptors in response to inflammatory stress (Mateos *et al.*, 2015). For instance, cytokine-stimulated ARPE-19 could promote the expression of IL-8 and MCP-1 via the activation of NF- κ B p65 and STAT3 signalling pathways (Mateos *et al.*, 2015; Patel *et al.*, 2012a). Besides, the secretion of the angiogenic factors, VEGF and MMP2 by ARPE-19 could explain the increased vascular permeability and neovascularisation in the retina during PDR (Hellinen *et al.*, 2019; Mateos *et al.*, 2015). According to Puddu *et al.* (2012), the expression of RAGE and VEGF in ARPE-19 can be induced by the presence of high glucose and AGE. Furthermore, the expression of PPAR- γ in ARPE-19 may partake in mitigating the inflammatory response in ocular tissues (Mateos *et al.*, 2015). As a result, studies using ARPE-19 could provide valuable insights into the pathophysiology of DR and facilitate the development of novel therapeutic strategy.

2.4 Medicinal plants

In Malaysia, medicinal plants are traditionally used by rural community to treat various ailments (Milow *et al.*, 2017). This practice is rooted in the belief in the therapeutic properties of these plants (Milow *et al.*, 2017). The therapeutic properties of medicinal plants are related to their biological activities, encompassing effects like anti-aging, anti-diabetic, anti-cancer, anti-inflammatory and anti-microbial actions (Xu *et al.*, 2017). The biological activities of medicinal plants can be attributed to the natural occurrence of specific types of phytochemicals, each exerting distinct biological effect (Xu *et al.*, 2017). Phytochemicals are a diverse group of

secondary metabolites produced by plants primarily for defence against biological and environmental stressors (Müller and Junker, 2022). Beyond their defensive role, they may also mediate plant growth, reproduction, and interaction with other organisms in their ecological niche (Müller and Junker, 2022). These compounds can influence seed germination, root development, flower pigmentation and even serve as signalling molecules in communication and defence mechanisms (Müller and Junker, 2022). The major classes of phytochemicals encompass a wide array of chemical structures and biological activities, including alkaloids, naphthalenes, phenolic compounds, phenylpropanoids, and terpenoids, each contributing to the diverse biological action of plants and their adaptation to diverse environmental conditions (Do *et al.*, 2014).

According to Eddouks *et al.* (2014), the modern therapeutic drugs used in current medical practice are derived from 7000 natural compounds that can be found in natural products such as plants and microorganisms. The presence of antioxidative phytochemical constituents in medicinal plants could protect human body against the harmful effect of oxidative stress and prevent the development of metabolic diseases (Do *et al.*, 2014). These compounds have served as valuable sources of inspiration for drug discovery and contributed significantly to the pharmaceutical industry (Eddouks *et al.*, 2014). Hence, it is evident that the natural compounds found in medicinal plants are capable of treating various illnesses. For instances, the *in vitro* and *in vivo* anti-diabetic activities of *Orthosiphon aristatus* were linked to its therapeutic use in diabetes management (Abdullah *et al.*, 2020). Additionally, *Ficus deltoidei*, a flowering plant native to Southeast Asia, displayed anti-glycation properties in a study conducted in Malaysia (Dom *et al.*, 2020). Furthermore, the decline in drug efficacy and increasing likelihood of contraindications from the use of

synthetic drugs has led to the increasing usage of herbal medicine over the years (Eddouks *et al.*, 2014). Herbal medicines offer a promising alternative, as they are often perceived as safer and more tolerable due to their natural origin and complex chemical compositions (Eddouks *et al.*, 2014). The holistic approach of herbal medicine, which emphasizes the synergy among multiple bioactive compounds within plant extracts, may provide enhanced therapeutic benefits and reduced risk of adverse effects compared to single-target synthetic drugs (Eddouks *et al.*, 2014).

2.4.1 *Peperomia pellucida* (L.) Kunth

2.4.1.1 Nomenclature and taxonomy

Peperomia pellucida (L.) Kunth, a medicinal plant classified under the Piperaceae family, is widely distributed in the tropical and subtropical regions (Ooi *et al.*, 2012). As the plant is native to Americas, it is commonly known as pepper elder and shiny bush (Amarathunga and Kankanamge, 2017). The binomial nomenclature of *P. pellucida* is followed by the abbreviations 'L.' and 'Kunth'. The former, 'L' is used to specify Carl Linnaeus as the naming authority while the latter 'Kunth' indicates Carl Sigismund Kunth as the first person who published the plant's name (Mathieu and Posada, 2006). Another scientific name, *Peperomia pellucida* (L.) H. B. K., can be seen in numerous publications in South America. The abbreviation 'H. B. K.' was used to indicate Humboldt, Bonpland and Kunth as the authors who published the taxonomic information of the plant in the book "Nova Genera et Species Plantarum" in year 1816 (Alves *et al.*, 2019). Figure 2.1A and 2.1B depict the respective aerial part and whole plant of *P. pellucida*.

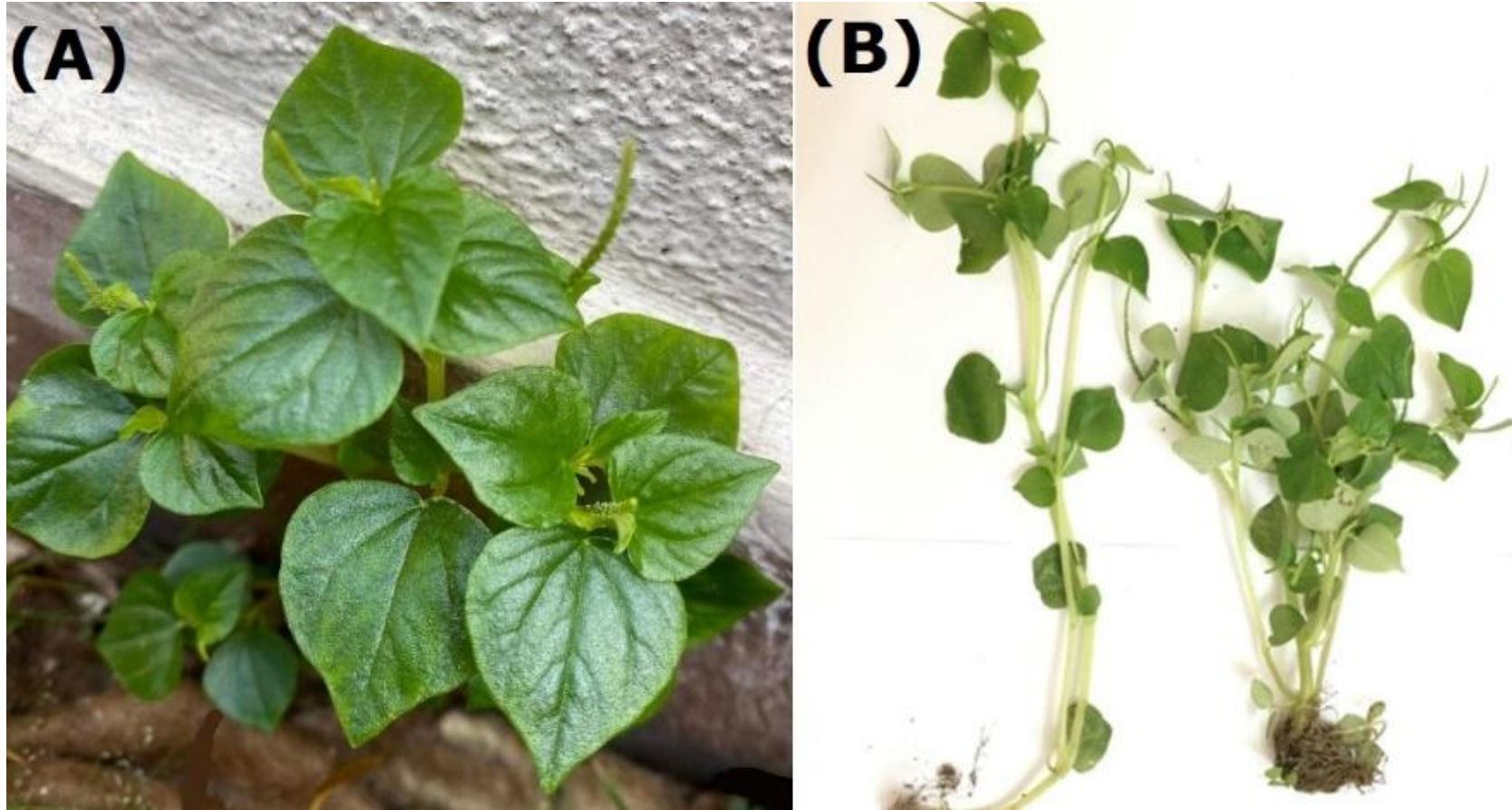


Figure 2.1. The physical form of *Peperomia pellucida* (L.) Kunth. (A) the aerial part; (B) the whole plant.

2.4.1.2 Botanical description

P. pellucida is a slender and annular herb, which is usually grown in clump (Roslida and Aini, 2009). The plant could grow up to about 50 centimetres in length (Roslida and Aini, 2009). The plant is succulent and light green in colour (Amarathunga and Kankanamge, 2017). They either appear as erected, ascending, decumbent or freely branched stems to which the petioles that connect the leaves are usually 2 cm long (Amarathunga and Kankanamge, 2017). *P. pellucida* is characterised by smooth, heart-shaped, ovoid or triangular-shaped leaves, which grow to around 3 cm in length (Melo *et al.*, 2016). The upper surface of the leaves is medium green in colour while the lower surface is comparatively lighter in colour (Majumder *et al.*, 2012). Besides, the plant also features dot-like seeds that are attached to the fruiting spikes, which arise from the leaf axils. The spikes are slender, solitary, terminal or leaf-opposed and they could be up to 6 cm long and 2 mm in diameter when they reach full maturity (Flora of North America, 2020). The fruiting spikes emit a mustard-like scent if pulverised (Ibe-Diala *et al.*, 2021). *P. pellucida* also has suborbicular-shaped flowers, which are short-stalked and loosely arranged whereby the flowers normally possess two stamens where the ovary is ellipsoid and the stigmas are pubescent (Amarathunga and Kankanamge, 2017). In addition, the fruits are minute, round to oblong in shape, reticulate and appear dark brown in colour when mature (Amarathunga and Kankanamge, 2017).

2.4.1.3 Geographical distribution

P. pellucida is native to tropical North and South America (Amarathunga and Kankanamge, 2017). It is now widely cultivated and naturalised throughout the tropical regions of other continents such as Africa

and Asia (Bayma *et al.*, 2000). The plant flourishes during rainy periods as well as in loose and humid loamy soil in nurseries and under the shade of trees (Roslida and Aini, 2009). Besides, *P. pellucida* is usually a terrestrial and epiphyte but it can occasionally be a lithophyte, which blooms throughout the year (Amarathunga and Kankanamge, 2017). *P. pellucida* can also be found along the coast of Asia and the Americas at a sea level of about 200 to 2000 meters (Flora of North America, 2020). Figure 2.2 shows the geographical distribution of *P. pellucida* in the tropical and subtropical regions of the world.

2.4.1.4 Ethnomedicinal uses

As a traditional medicinal plant, the aerial parts of *P. pellucida* can be converted into decoction to treat various inflammatory complications such as conjunctivitis and diabetes (Alves *et al.*, 2019). The decoction could serve as a remedy for snake bites due to its anti-microbial properties (Felix-Silva *et al.*, 2017). *P. pellucida* is also used to treat fever due to its anti-pyretic characteristic, which is comparable to aspirin (Khan *et al.*, 2008). The essential oil from this plant demonstrates anti-fungal and anti-helminthic activities, enhancing its therapeutic potential in combating fungal infections and parasitic infestations (Kenedi *et al.*, 2019; Verma *et al.*, 2014). Commercial plant powder derived from *P. pellucida* is also available for maintaining general well-being (Ebay, 2024). These diverse medicinal properties underscore the value of *P. pellucida* as a natural remedy for addressing various health ailments across different regions. Despite being widely used as a traditional medicine, the scientific evidence surrounding its therapeutic properties remains scarce. Table 2.1 shows the application of *P. pellucida* for medicinal and non-medicinal purposes in different parts of the world.

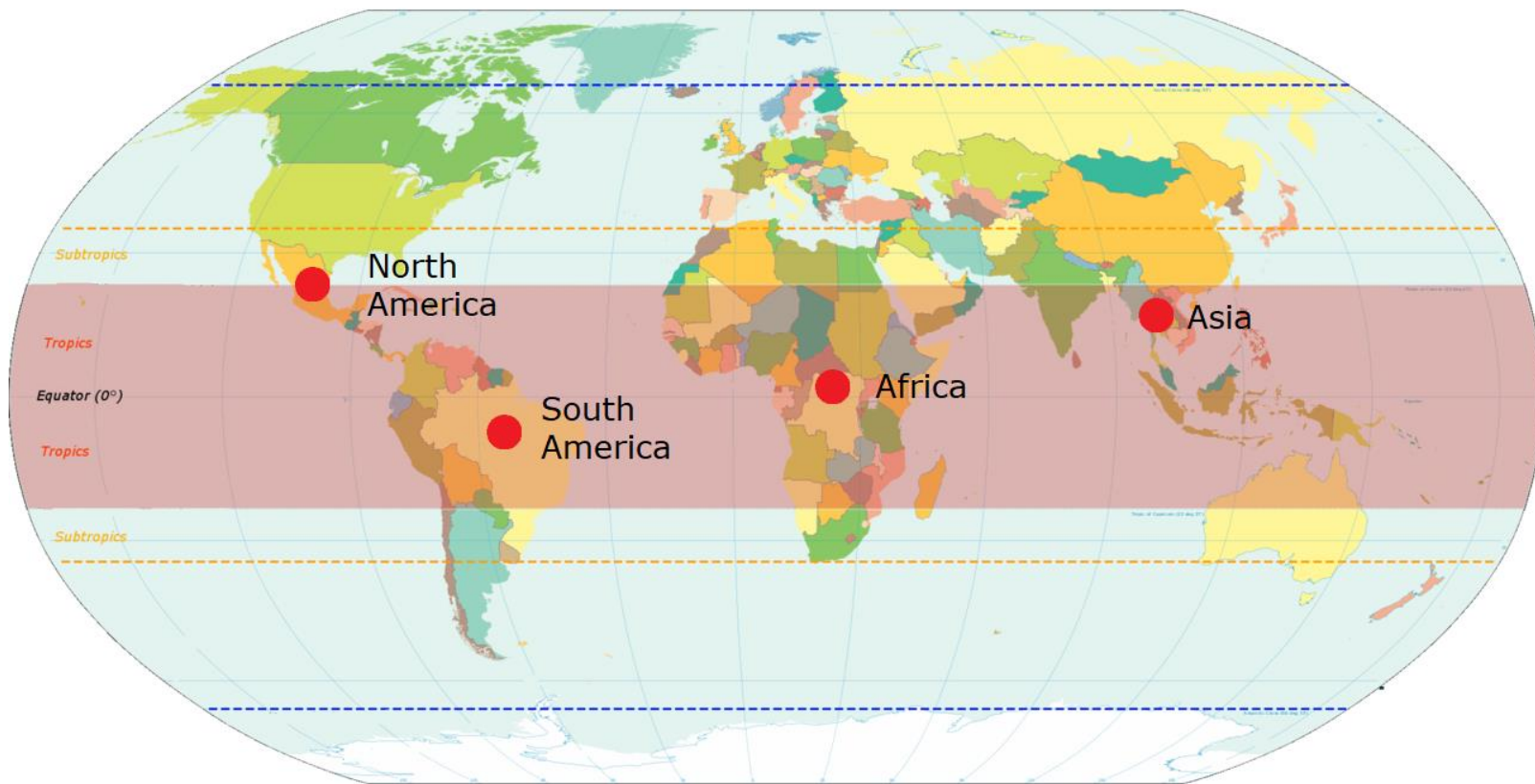


Figure 2.2. The geographical distribution of *P. pellucida* in the tropical and subtropical regions of the world.

Table 2.1: The different parts of *P. pellucida* used in different countries for medicinal and non-medicinal purposes.

Country	Part	Purposes	Reference
Malaysia	Whole plant	Decoction is used as a treatment for rheumatism.	Ibrahim and Hamzah (1999)
		Whole plant is used to reduce blood glucose level.	Hamzah <i>et al.</i> (2012)
India	Whole plant	Plant juice is used to treat digestive problems.	Kalita <i>et al.</i> (2015)
		Decoction is used as a treatment for rheumatism.	Chithra and Geetha, (2016)
		Paste is used for burns relief.	Bose (2011); Buragohain <i>et al.</i> (2011)
	Leaves	Paste is used for skin cuts and wounds.	Kalita <i>et al.</i> (2015)
	Aerial parts	To relieve stomach ache, joint pain and headache.	Bordoloi <i>et al.</i> (2017)
	Leaves and stem	To treat urinary disorder and fever.	Gogoi and Zaman (2011)
	Young shoots	Flavouring agents.	Bharali <i>et al.</i> (2017)
Indonesia	Aerial parts	To relieve dizziness, headache, fever, stomachache.	Waty <i>et al.</i> (2017)
Bangladesh	Whole plant	To treat diarrhea.	Rahmatullah <i>et al.</i> (2010)
	Leaves	Paste made from the whole plant is used to relieve snake, insect or reptile bites as well as fever.	Das <i>et al.</i> (2013)
Dominican Republic and New York City	Aerial parts, leaves	Aerial parts are used as flu relief. Leaves are used for the treatment of vaginal infections and asthma.	Vandebroek <i>et al.</i> (2010)
DR Congo	Leaves	Consumed as part of diet.	Termote <i>et al.</i> (2010)
Papua New Guinea	Leaves, whole plant	Leaves have antidepressant properties acne relief. Whole plant is used to treat fever and headache.	Koch <i>et al.</i> (2015)
Suriname	Whole plant	Use as herbal bath for general well-being.	Ruysschaert <i>et al.</i> (2009)
	Leaves and stem	Made into juice for the treatment of conjunctivitis.	Kartika <i>et al.</i> (2016)
Nigeria	Leaves	Athletes' foot.	Uzodimma (2013)
Trinidad	Whole plant	Infusion or decoction is used to provide relief to cold and cough.	Clement <i>et al.</i> (2015)

2.4.1.5 Phytochemistry

Phytochemicals that contribute to the functional activities of *P. pellucida* have been reported to be found in different parts of the plant (Table 2.2), including the leaves, roots and stems (Alves *et al.*, 2019). The leaves and stems collectively constitute the aerial part of the plant. The type of phytochemicals is essential to determine the possible therapeutic properties of each plant part (Ho *et al.*, 2022b). For instance, the phytochemicals with significant functional activities of *P. pellucida* are concentrated in the aerial part of *P. pellucida*, including anti-angiogenic, anti-hyperglycaemic, anti-inflammatory, anti-microbial and blood pressure lowering properties (Alves *et al.*, 2019). The phytochemical composition of *P. pellucida* can also be classified based on their volatility (Alves *et al.*, 2019). Most of the predominating compounds found in the plant fall under the phenylpropanoid and terpenoid categories of non-polar volatile compounds. For terpenes, monoterpenes and sesquiterpenes are found abundantly in the leaves and stem of the plant (Okoh *et al.*, 2017). The leaf is mainly composed of d-limonene and β -caryophyllene whereas linalool, d-limonene, α -terpineol and β -caryophyllene are the major terpenoid constituents of essential oil in the stem of *P. pellucida* (Okoh *et al.*, 2017). According to Verma *et al.* (2014), the major predominant phytochemicals found in the whole plant of *P. pellucida* are constituted of dillapiole, a phenylpropanoid with a mixture of sesquiterpenes such as β -caryophyllene and carotol.

Table 2.2. The phytochemicals present in different parts of *P. pellucida*.

Part of plant	Compounds	Reference
Leaves	D-limonene and β -caryophyllene,	Okoh <i>et al.</i> (2017)
	Carotol, dillapiole and β -caryophyllene	Verma <i>et al.</i> (2014)
	γ -gurjunene, 1,10-di-epi-cubenol, (E)-caryophyllene and dillapiole	Oliveira <i>et al.</i> (2017)
	Apiol, phytol, n-hexadecanoic acid and E-2-tetradecen-1-ol	Narayanamoorthi <i>et al.</i> (2015)
	Phytol, 2-naphthalenol, hexadecanoic acid, 9,12-octadecadienoic acid and patuloside A	Khan <i>et al.</i> (2010); Wei <i>et al.</i> (2011)
Stem	Linalool, d-limonene, α -terpineol and β -caryophyllene	Okoh <i>et al.</i> (2017)
	Carotol, dillapiole, trans- β -guaiene and (E)-caryophyllene	Oliveira <i>et al.</i> (2017)
Aerial part	3',4', dihydroxy-3-5-dimethoxy flavone-7-O- β -rhamnose, β -caryophyllene, germacrene D, dillapiole and pellucidin A	Bayma <i>et al.</i> (2000); François <i>et al.</i> (2013); Kurniawan <i>et al.</i> (2016)
Roots	Dillapiole, apiole, and β -caryophyllene	Verma <i>et al.</i> (2014)
Whole plant	Carotol, dillapiole, pygmaein and β -caryophyllene	Verma <i>et al.</i> (2014)
	Dillapiole, carotol and (E)-caryophyllene	De Lira <i>et al.</i> (2009)
	Stigmasterol, analogue pheophytin, β -sitosterol-D-glucopyranoside, piperidine-based alkaloid, vitexin, isoswertisin sesamin peperomins A, B, C and E	Fachriyah <i>et al.</i> (2018); Hartati <i>et al.</i> (2015); Pappachen (2013); Xu <i>et al.</i> (2006)

Along with dillapiole, the apiole is another volatile constituent detected in the essential oil from the root part of *P. pellucida* (Verma *et al.*, 2014). De Lira *et al.* (2009) has reported that the essential oil of *P. pellucida* was mainly composed of dillapiole, carotol and (E)-caryophyllene. β -caryophyllene was also found to be the major phytochemicals along with germacrene D and dillapiole in the aerial part of the plant (François *et al.*, 2013). Oliveira *et al.* (2017) has reported the presence of γ -gurjunene, 1,10-di-epi-cubenol, (E)-caryophyllene and dillapiole in the leaves as well as carotol, dillapiole, trans- β -guaiene and (E)-caryophyllene in the stem of *P. pellucida*. According to Narayanamoorthi *et al.* (2015), the leaves of *P. pellucida* consisted of apiole, phytol, n-hexadecanoic acid and E-2-tetradecen-1-ol. The non-volatile compounds identified in *P. pellucida* were mainly polar due to their strong intermolecular forces (Alves *et al.*, 2020; Dračinský, 2017). For instance, pellucidin A is a non-volatile, argon dimeric carbon compound that was first discovered in the aerial part of the plant (Bayma *et al.*, 2000). Recent study has discovered that 2,4,5-trimethoxystyrene, another phenylpropene is the precursor of pellucidin A and it was isolated along with dillapiole from the leaves of *P. pellucida* (de Moraes and Kato, 2021). Besides, a xanthone glycoside called patuloside A has been found to exhibit significant anti-bacterial activity in the leaves of *P. pellucida* (Khan *et al.*, 2010).

Vitexin, a flavones glycoside isolated from the whole plant of *P. pellucida*, displayed blood pressure lowering properties (Ho *et al.*, 2022b). Another flavonoid compound, 3', 4', dihydroxy-3-5-dimethoxy flavone-7-O- β -rhamnose, which is known to exhibit anti-angiotensin converting enzyme activity, has been isolated from the aerial part of the plant (Kurniawan *et al.*, 2016). The flavones, isoswertisin, was isolated together with methylenedioxy lignans sesamin along with peperomins A, B, C, E and five

other novel compounds which include two secolignans, two tetrahydrofuran lignans and dihydronaphthalenone from the whole plant (Xu *et al.*, 2006). Furthermore, Hartati *et al.* (2015) had isolated pheophytin, a derivative of the chlorophyll pigment from the whole plant of *P. pellucida*. Moreover, an alkaloid with a piperidine-based structure was isolated from the entire part of *P. pellucida* by Fachriyah *et al.* (2018). The alkaloid extract possessed anti-xanthine oxidase activity even higher than that of *P. pellucida* ethanol (EtOH) extract. Figures 2.3 and 2.4 illustrate some common phytochemicals in Fischer projections that were previously discovered in *P. pellucida*.

2.4.1.6 Nutritional and mineral compositions

Apart from the phytochemical constituents, *P. pellucida* is also rich in nutrients especially lipids (Alves *et al.*, 2019). Both saturated and unsaturated fatty acids are examples of lipids found extensively in the leaves of *P. pellucida* (Ho *et al.*, 2022b). According to Teoh *et al.* (2021), the 9-octadecenoic acid is the major unsaturated fatty acid reported in the aerial part of the plant whereas the saturated fatty acid n-hexadecanoic acid was identified in the leaf plant extract of *P. pellucida* (Wei *et al.*, 2011). Besides, phytosterol is a class of cholesterol-like lipid commonly found in plants (Hartati *et al.*, 2015). For instance, the stigmasterol and β -sitosterol-D-glucopyranoside are some phytosterols isolated from the EtOH extract of *P. pellucida* along with pheophytin (Hartati *et al.*, 2015). The presence of both lipids and chlorophyll derivatives may underscore *P. pellucida* as a promising candidate for the management of inflammatory conditions.

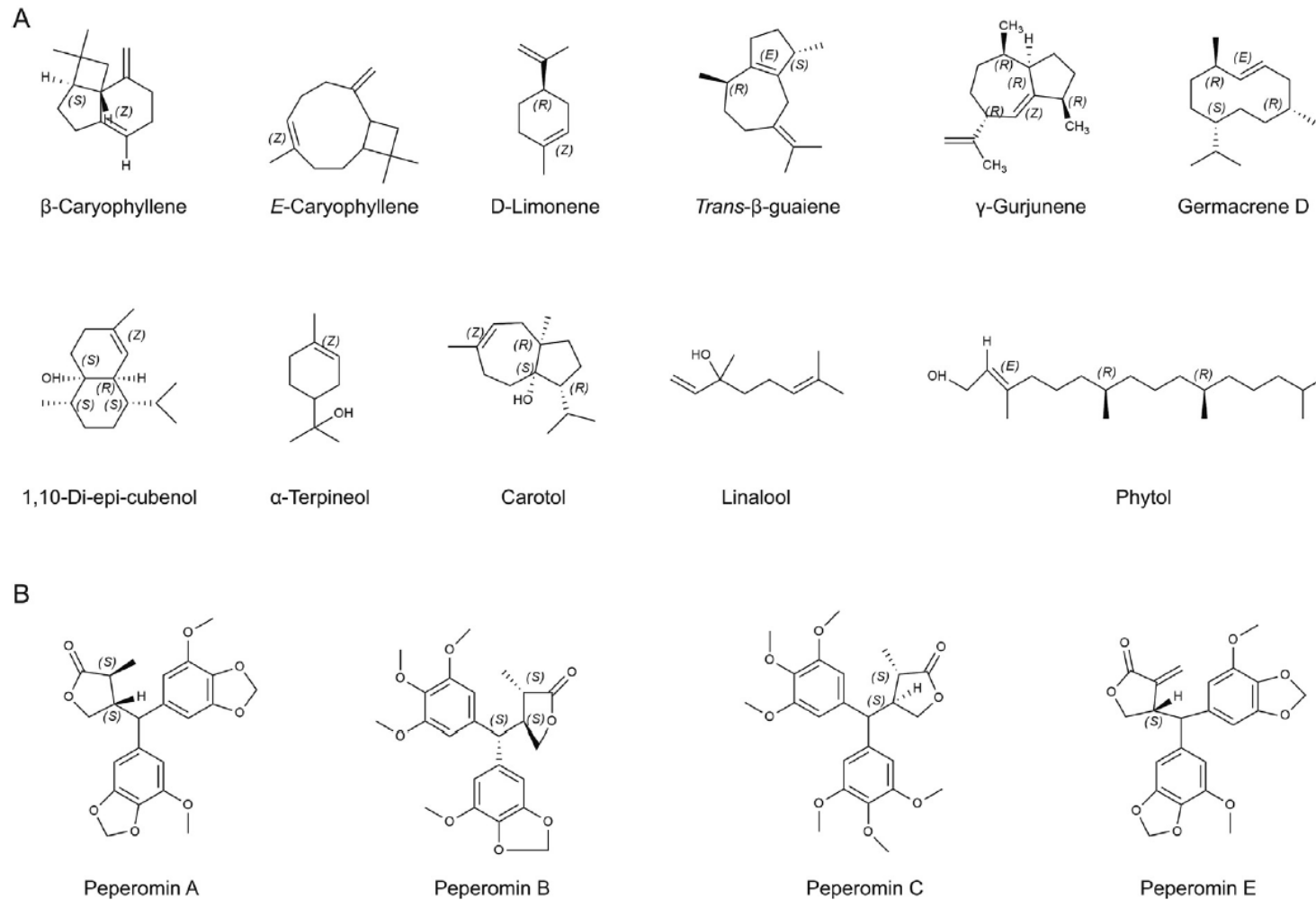


Figure 2.3. The Fischer projections of some common phytochemicals detected in *P. pellucida*. (A) Terpenes. (B) Peperomins.

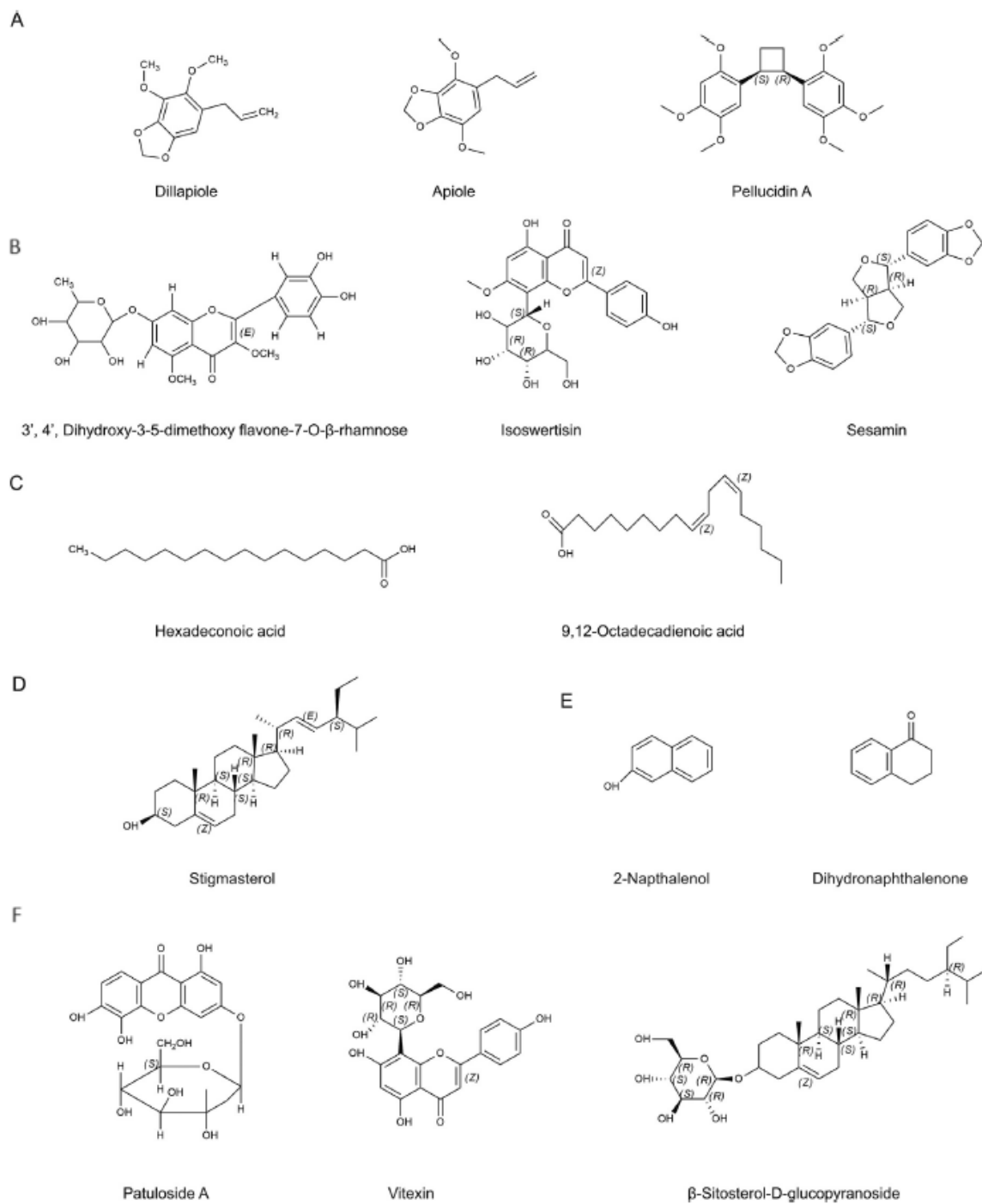


Figure 2.4. The Fischer projections of some common phytochemicals detected in *P. pellucida*. (A) Phenylpropanoids. (B) Polyphenols. (C) Fatty acids. (D) Sterol. (E) Naphthalenes. (F) Glycosides.

On the other hand, the succulent characteristic of *P. pellucida* also imparts high moisture content to the plant (Ooi *et al.*, 2012). The high level of ash content could be attributed to the significant amount of mineral content in *P. pellucida* (Ooi *et al.*, 2012). Potassium is the richest source of mineral in the plant, followed by calcium, iron, sodium, zinc and copper (Ooi *et al.*, 2012). Besides, Egwuiche *et al.* (2011) also reported minute amount of magnesium and manganese in *P. pellucida*. The low sodium to potassium ratio may suggest *P. pellucida* as an ideal dietary source for hypertensive patients while the high calcium and iron content of the plant is suitable for calcium and iron supplementation, respectively (Park *et al.*, 2016). In addition, the low zinc to copper ratio in *P. pellucida* could potentially lower the risk for cardiovascular disorders (Ooi *et al.*, 2012). The phytochemical, nutritional and mineral profiles collectively suggest that the consumption of *P. pellucida* is beneficial in the pharmacological and nutritional aspects. Table 2.3 has summarised the nutritional and mineral compositions of *P. pellucida*.

Table 2.3. The nutritional and mineral compositions of *P. pellucida*.

Category	Nutritional and mineral contents	Reference
Saturated fatty acid	9-octadecenoic acid	Teoh <i>et al.</i> (2021)
Unsaturated fatty acid	N-hexadecanoic acid	Wei <i>et al.</i> (2011)
Phytosterols	Stigmasterol	Hartati <i>et al.</i> (2015)
	β -sitosterol-D-glucopyranoside	
Minerals	Calcium	Ooi <i>et al.</i> (2012)
	Copper	
	Iron	
	Potassium	
	Sodium	
	Zinc	
	Magnesium	Egwuche <i>et al.</i> (2011)
	Manganese	

2.4.1.7 Biological activities

2.4.1.7.1 Anti-diabetic activity

To date, several papers have highlighted the potential anti-diabetic effect of *P. pellucida*. A study conducted by Hamzah *et al.* (2012) has demonstrated a reduction of blood glucose in alloxan-induced hyperglycaemic mice fed on diet supplemented with *P. pellucida*. Similarly, Susilawati *et al.* (2017) showed that 8,9-dimethoxy ellagic acid from the leaf extract of *P. pellucida* could lower blood glucose by up to 33.7 % in mice model. Another study conducted by Sheikh *et al.* (2013) also revealed similar hypoglycaemic result in oral glucose tolerance test upon the consumption of *P. pellucida* extract when compared to the control mice group. According to Ho *et al.* (2022a), the ethyl acetate fraction of *P. pellucida* displayed strong inhibitory activities on the carbohydrate-

hydrolysing enzymes, α -amylase and α -glucosidase, even greater than the standard drug acarbose. The inhibition of these enzymes is crucial to reduce the spike in blood glucose level (Ho *et al.*, 2022a).

An experiment conducted on sucrose-induced hyperglycaemic rats showed 58.15 % reduction in blood glucose upon fed with 40 mg/kg of *P. pellucida* EtOH extract (Salma *et al.*, 2013). Another study found that 40 mg/kg of *P. pellucida* EtOH and hexane fractions were able to reduce the blood glucose by 54.57 % and 51.25 %, respectively (Togubu *et al.*, 2013). In India, an interesting docking study by Akhila *et al.* (2016) showed the strong ability of *P. pellucida* extract to inhibit AR when compared to the standards flavonoid and quercetin. AR is a rate-limiting enzyme of polyol pathway which is critical in the development of DM microvascular complications among the DM population (Tarr *et al.*, 2013). In Malaysia, phytochemical screening test conducted by Raman *et al.* (2012) showed that the crude methanolic extract of *P. pellucida* contained phytochemical compounds such as alkaloids, saponin and flavones. These studies have highlighted the potential of *P. pellucida* as a therapeutic agent for managing diabetes.

2.4.1.7.2 Anti-inflammatory activity

The carrageenan-induced oedema test is commonly used to evaluate the *in vivo* anti-inflammatory activity of a compound. It is based on the release of histamine and serotonin from the biological model within three hours after the injection of carrageenan thereby causing an oedematous response (Antônio and Souza Brito, 1998). Prostaglandins, bradykinins and leukotrienes are the mediators involved in the secondary phase of oedematous response after three hours (Antônio and Souza Brito,

1998). In a study conducted by Parise-Filho *et al.* (2011), the phytochemicals, dillapiole and phytol isolated from *P. pellucida* attenuated carrageenan-induced paw oedema within two hours of induction. This indicated that both phytochemicals inhibited histamine and serotonin in the primary phase of inflammation (Antônio and Souza Brito, 1998). Besides, phytol was also shown to suppress the secondary phase of oedematous response (Silva *et al.*, 2019).

In another study, the aqueous extract of the aerial part of *P. pellucida* was reported to display anti-inflammatory activity based on its inhibition against prostaglandin synthesis mechanism in rat and mouse models (Arrigoni-Blank *et al.*, 2004). Significant anti-inflammatory activity was found in the petroleum ether extract of the plant with marked reduction of carrageenan-induced hind paw oedema in rat model after four hours of carrageenan induction (Mutee *et al.*, 2010). This suggested the suppression of prostaglandins in the event of inflammation as well (Mutee *et al.*, 2010). This finding could be beneficial to the management of DR in which inflammation plays a crucial part of the pathogenic process. A study carried out by Parawansah *et al.* (2016) demonstrated that *P. pellucida* EtOH extract inhibited xanthine oxidase activity with IC₅₀ of 19.5 µg/ml. Furthermore, the non-polar hexane fraction of *P. pellucida* strongly inhibited the pro-inflammatory enzymes, lipoxygenase, COX-1 and COX-2. All the above evidence suggested that *P. pellucida* possessed the anti-inflammatory activity against DR.

2.4.1.7.3 Antioxidant activity

The antioxidant activity of *P. pellucida* has been evaluated in numerous studies. 2, 2-diphenyl-1-picrylhydrazyl (DPPH) radicals

scavenging assay is commonly employed to assess the antioxidant activity of a sample (Nagarajan *et al.*, 2017). Based on Wei *et al.* (2011), the methanolic leaf extract of *P. pellucida* displayed significant DPPH radical scavenging activity with an inhibition of 30 % at a concentration of 0.625 µg/ml. The same study also showed the presence of phytol, 2-naphthalenol, hexadecanoic acid and 9, 12-octadecadienoic acid which were responsible for the antioxidant activity of the plant (Wei *et al.*, 2011). In another study conducted by Mutee *et al.* (2010), the concentration of the plant required to scavenge 50 % of the DPPH radicals was even lower at 0.08 µg/ml. According to Okoh *et al.* (2017) and Oloyede *et al.* (2011), the antioxidant properties of *P. pellucida* extend beyond its reactivity towards DPPH, encompassing other free radicals like 2,2'-azino-bis(3-ethylbenzothiazoline-6-sulfonic acid) (ABTS), hydrogen peroxide, and lipid peroxy radicals. Furthermore, an increase in superoxide dismutase and catalase activities and a decrease in thioltransferase and thioredoxin reductase activities observed in the rat liver after treatment of *P. pellucida* methanolic extract suggested a good antioxidant response from *P. pellucida* extract against oxidative stress (Beltran-Benjamin *et al.*, 2013). The extraction of antioxidants with methanol, n-butanol and ethyl acetate using reflux method yielded higher DPPH radical scavenging activity and ferric-reducing power compared to those found in maceration method where the ethyl acetate extract displayed the highest total phenolic content and antioxidant activity (Phongtongpasuk and Poadang, 2014). These findings suggested the potential of *P. pellucida* in mitigating oxidative stress which is linked to the development of DR.

2.4.1.7.4 Anti-angiogenic activity

The anti-angiogenic activity of *P. pellucida* has been previously determined via *ex vivo* chorioallantoic membrane assay in which the crude methanolic plant extract displayed mild inhibition against blood vessel formation (26.81 %) as compared to the standard quercetin (60.24 %). The anti-angiogenic activity of the plant has been associated to alkaloids, phenolic compounds, tannins, carbohydrate derivatives and sterols (Camposano *et al.*, 2016). Another study applying *in vivo* duck embryo chorioallantoic membrane assay reported a reduction in blood vessels branch points in the chorioallantoic membrane of duck embryo after administration of *P. pellucida* EtOH extract (Briones, 2019). According to Buhren *et al.* (2016), the substrate of hyaluronidase, HA, has been shown to possess anti-angiogenic properties, inhibiting blood vessel formation. Therefore, the potential of *P. pellucida* herbal tea to inhibit hyaluronidase enzyme activity, responsible for breaking down HA, suggests a possible anti-angiogenic activity of the plant (Ng *et al.*, 2021). The studies mentioned above collectively offer compelling evidence supporting *P. pellucida* as a potential source of anti-angiogenic compounds. Such findings suggest that the plant could hold promise for managing neovascularization in DR.

2.4.1.7.5 Anti-microbial activity

Past research has provided substantial evidence regarding the antimicrobial properties of *P. pellucida* against Gram-positive, Gram-negative bacteria and fungi. In Malaysia, The methanol leaf extract of *P. pellucida* demonstrated inhibitory effects against *Escherichia coli* and *Pseudomonas aeruginosa*, with a minimum inhibitory concentration (MIC)

of 31.2 µg/ml (Wei *et al.*, 2011). Besides, it inhibited *Klebsiella* sp. and *Salmonella* sp. at concentration of 62.5 µg/ml and 125 µg/ml, respectively (Wei *et al.*, 2011). On the other hand, the EToH extract was assessed against *Staphylococcus aureus*, *Enterococcus faecalis*, *Bacillus cereus*, *Salmonella typhi*, *Proteus mirabilis*, and *E. coli* using the disc diffusion technique (Igwe and Mgbemena, 2014). However, the extract displayed notably high MIC values, suggesting its lack of activity against the tested bacteria. The antifungal activity of *P. pellucida* against *Aspergillus* sp. has also been described previously, attributing to the presence of apiole (Alves *et al.*, 2019). Patuloside A, the xanthone glycoside from *P. pellucida*, exhibited significant activity against the Gram-positive *Staphylococcus aureus* and Gram-negative *Shigella dysenteriae* with MIC values ranging from 8 to 64 µg/ml (Khan *et al.*, 2010).

2.4.1.7.6 Blood pressure lowering activity

The blood pressure reducing effect of *P. pellucida* could be valuable in addressing DR due to a connection between the intraocular pressure and systemic blood pressure. This relationship involves the β -2 receptors, which are responsible for the production of aqueous humour in the eyes (Machiele *et al.*, 2022). For instance, the aqueous extract of *P. pellucida* was found to target the nitric-oxide signalling pathway and exert blood pressure reducing effects such as bradycardia and vasodilation in rodents (Nwokocha *et al.*, 2012). Diet supplemented with methanolic extract of *P. pellucida* consisting of glycosides and alkaloids reduced the overall blood pressure and heart rate by targeting the β -2 receptors in rat models (Fasola and Adeboye, 2015). In another study, 3',4',dihydroxy-3-5-dimethoxy flavone-7-O- β -rhamnose detected in *P. pellucida* exhibited high

angiotensin-converting enzyme inhibitory activity ($IC_{50} = 3.59 \mu\text{g/mL}$) when compared to the standard drug captopril ($IC_{50} = 7.72 \mu\text{g/mL}$) (Kurniawan *et al.*, 2016). Its enzyme inhibitory activity was found to increase ($IC_{50} = 3.44 \mu\text{g/mL}$) in the ethyl acetate plant fraction, possibly due to the synergistic interactions among the phytochemicals (Hajimehdipoor *et al.*, 2014). The presence of 5,6,7-trimethoxy-4-(2,4,5-trimethoxyphenyl)-3,4-dihydronaphthalen-1(2H)-one in *P. pellucida*, which displayed high affinity towards angiotensin-converting enzyme, further supports the blood pressuring lowering activity of the plant (Ahmad *et al.*, 2019). The enzyme binding ability of this compound (-6.78 kcal/mol) was comparable to captopril (-6.36 kcal/mol). Furthermore, a flavone glycoside detected in *P. pellucida* also displayed blood pressure lowering activity, probably due to its inhibitory action on angiotensin-converting enzyme (Pappachen, 2013). The above findings collectively suggest that the blood pressure lowering activity of *P. pellucida* could be crucial in the management of DR.

2.4.1.8 Toxicity studies

The cytotoxicity of *P. pellucida* has been previously evaluated with 3-[4,5-dimethylthiazol-2-yl]-2,5-diphenyl tetrazolium bromide (MTT) assay in malignant tissues, including the breast adenocarcinoma (Pejin *et al.*, 2014), cervical carcinoma (Pappachen and Chacko, 2013; Pejin *et al.*, 2014), colon carcinoma (Narayanamoorthi *et al.*, 2018; Pejin *et al.*, 2014), hepatic carcinoma (Pappachen and Chacko, 2013), promyelocytic leukaemia and prostate cancer-3 cell lines (Li *et al.*, 2019; Pejin *et al.*, 2014). Besides, normal tissues such as embryonic kidney tissues and human foetal lung fibroblast have also been subjected to cytotoxicity test

with *P. pellucida* samples (Pappachen and Chacko, 2013; Pejin *et al.*, 2014). Intriguingly, the methanolic extract of *P. pellucida* was shown to display low cytotoxicity towards the normal embryonic kidney cell line when compared to the other malignant cell lines (Pappachen and Chacko, 2013). The terpene, phytol previously isolated from *P. pellucida*, were toxic towards other malignant tissues but not for normal human foetal lung fibroblast cell line (Pejin *et al.*, 2014). In contrast, cytotoxicity towards colon carcinoma and breast adenocarcinoma was observed for *P. pellucida* extract (François *et al.*, 2013; Narayanamoorthi *et al.*, 2018). Previous *in-vitro* studies have collectively suggested that *P. pellucida* is safe to be applied to ARPE-19 as it was toxic against most cancerous cell lines but non-toxic towards the normal human cell lines.

The toxicity of *P. pellucida* has also been assessed with *in-vivo* biological models. For instance, it was found that the polar aqueous plant fractions did not cause significant death rate among the brine shrimp population (Oloyede *et al.*, 2011). In another study, the EtOH extract of *P. pellucida* also showed significant toxicity towards the brine shrimps (Htun *et al.*, 2018). Despite that, a previous study has suggested that both aqueous and EtOH plant extracts were mildly toxic towards the brine shrimps (Bibanco *et al.*, 2016). In an *in-vivo* toxicity study conducted on mice model, the application of *P. pellucida* methanolic extract did not result in toxicological manifestation (Waty *et al.*, 2017). Likewise, the aqueous extract of *P. pellucida* was also not toxic to the mice up to a dosage of 5000 mg/kg (Sheikh *et al.*, 2013). Furthermore, liver damage was not observed in rats exposed to *P. pellucida* extract, in which the hepatic vein, histopathology and biomarkers such as alanine phosphatase and alkaline phosphatase were monitored (Kartika *et al.*, 2016). However, the rats experienced mild liver fibrosis after a fortnight-long treatment with *P.*

pellucida methanol extract (Kartika *et al.*, 2016). The irritability of *P. pellucida* extract towards ocular tissues has been evaluated with *ex-vivo* hen's egg chorioallantoic membrane test (Mckenzie *et al.*, 2015). It was found that the plant extract could prevent sodium dodecyl sulfate (SDS)-induced haemorrhage in the blood capillary (Bork *et al.*, 1997). In addition, the ethnobotanical use of *P. pellucida* to alleviate ocular inflammation also did not result in serious adverse effects, except for allergy in some rare cases (Ho *et al.*, 2022b). All the above evidence based on *in-vivo* and *ex-vivo* studies confirmed the safety profile of *P. pellucida* in animal models.

Chapter III

Methodology

3.1 List of materials and equipment

The list of materials, chemical reagents and equipment utilised for plant processing and extraction as well as experiments for phase 1, phase 2 and phase 3 studies were provided in Appendix A1 and A2, respectively.

3.2 Plant processing

The plant processing step served as the primary phase in preparing the *P. pellucida* samples for subsequent phases of studies. It consisted of several key stages: fresh sample collection, plant sample authentication, sample cleaning and grinding, plant maceration and fractionation, as well as sample preparation for analysis.

3.2.1 Fresh sample collection

Approximately 10 kilograms of fresh *P. pellucida* were harvested in Selangor and Federal Territory of Kuala Lumpur, Malaysia, between September 2019 and December 2019. The plant samples were gathered specifically from humid loamy soil located at multiple shady and humid areas to reduce the variability of physical and chemical traits that may be resulted from the impact of geographical and environmental factors (Robinson *et al.*, 2022). Among the different types of soil, loamy soil displays the highest level of moisture and nutrient retention while attaining the equilibrium of sandy, clay and silt properties (Vittum, 2009), which makes loamy soil the ideal soil type for maintaining the chemical and

moisture contents of *P. pellucida*. The list of locations where the *P. pellucida* was collected, was shown in Table 3.1.

Table 3.1. The list of locations where *P. pellucida* was collected.

No.	Location	Coordinate
1	Bandar Damai Perdana, Cheras, Federal Territory of Kuala Lumpur	3°02'59.1"N 101°44'06.3"E
2	Jalan Pelanduk, Kuala Lumpur, Federal Territory of Kuala Lumpur	3°08'17.7"N 101°42'52.9"E
3	Rimba Ilmu Botanic Garden, Kuala Lumpur, Federal Territory of Kuala Lumpur	3°07'51.3"N 101°39'28.8"E
4	Taman Rasa Sayang, Cheras, Selangor	3°04'17.1"N 101°45'22.0"E
5	Taman Sri Aman, Cheras, Selangor	3°04'18.7"N 101°45'31.4"E
6	University of Nottingham Malaysia, Semenyih, Selangor	2°56'45.5"N 101°52'26.4"E

3.2.2 Plant sample authentication

A complete whole plant of *P. pellucida*, which consisted of the leaves, fruiting spikes, stem and roots was rinsed with running water and shade dried under well-ventilated condition ($25 \pm 2^\circ\text{C}$). The dried plant sample was embedded on an A4-sized paper and sent to the Rimba Ilmu Botanic Garden of University of Malaya for plant authentication purpose. A voucher

specimen (KLU50130) of *P. pellucida* was deposited at the University of Malaya Herbarium.

3.2.3 Sample cleaning and grinding

Upon sampling, the aerial part of *P. pellucida* was immediately washed with distilled water to remove soil and other impurities. As the presence of water molecules in the plant matrix could prevent the extraction of phytochemicals (Chaves *et al.*, 2020). The plant was then shade-dried under well-ventilated condition ($25 \pm 2^\circ\text{C}$) to eliminate the interference of water in the subsequent extraction process (Chaves *et al.*, 2020). This was followed by grinding of the dried plant sample into coarse powder with a mechanical grinder. The fine powder ($<125 \mu\text{m}$) was separated with a strainer with mesh size of 100 (equivalent to $125 \mu\text{m}$ openings). Grinding increases the surface area by reducing the size of the particles (Rezazi *et al.*, 2017). This would promote the diffusion of phytochemicals into solvents during the extraction process (Rezazi *et al.*, 2017). The powder was stored at -20°C until plant maceration and fractionation.

3.2.4 Plant maceration and fractionation

Approximately 1 kg of coarse plant powders were macerated with absolute methanol in a solid-solvent ratio of 1:10 for 3 days at room temperature on an orbital shaker set to 100 rpm (Ho *et al.*, 2022a). Methanol was selected as the extraction solvent as polar solvents are highly effective for the extraction of phytochemicals (Chaves *et al.*, 2020). According to Abu *et al.* (2017), the plant antioxidants extraction yield of

methanol was greater than EtOH, making it the solvent of choice for plant extraction. Besides, the boiling point of methanol is lesser than EtOH (Helmenstine, 2019). Hence, heat-labile compounds are more likely to be preserved during the extraction process. The methanol extract was filtered with No.1 Whatman filter paper and concentrated under reduced pressure at 40°C to obtain crude methanolic extract. Two grams of crude methanolic extract was dissolved in 60 ml of distilled water and fractionated successively in an increasing order of polarity with equal volume of hexanes, chloroform, ethyl acetate and n-butanol. According to Nawaz *et al.*, (2020), this is also known as serial exhaustive extraction technique. This method served as the preliminary large-scale separation of phytochemical compounds from crude methanolic extract (Nawaz *et al.*, 2020). The solvents were selected based on polarity index with equal difference as solvent polarity could influence the solubility of phytochemicals (Nawaz *et al.*, 2020). Each plant fraction was filtered and concentrated under reduced pressure at 40°C to obtain the dried plant fractions. The solvent-free extracts were stored in air-tight glass containers at -20°C until analysis. Figure 3.1 outlines the overall steps of plant processing.

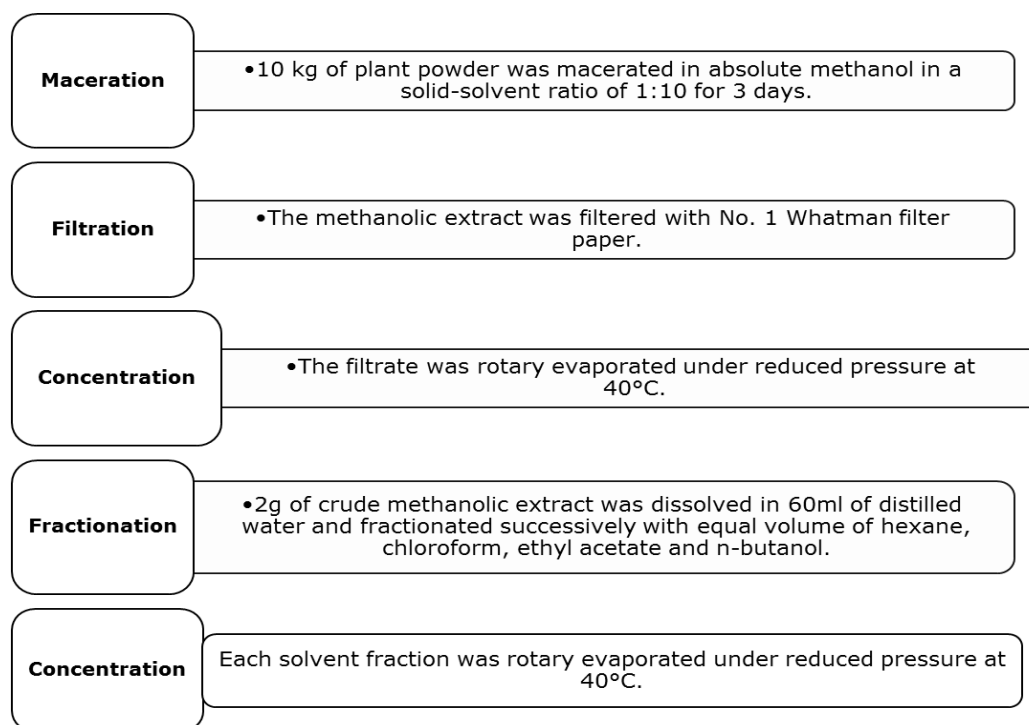


Figure 3.1. Procedure of plant sample processing.

3.2.4.1 Extraction yield

The extraction yield (%) of crude methanolic extract and plant fractions was calculated as follows:

$$\text{Crude methanolic extract (\%)} = \frac{\text{Weight of crude methanolic extract (g)}}{\text{Total dry weight (g)}} \times 100$$

$$\text{Plant fraction (\%)} = \frac{\text{Weight of plant fraction (g)}}{\text{Weight of crude methanolic extract (g)}} \times 100$$

3.2.5 Sample preparation for analysis

The sample stock was prepared by dissolving the solvent-free extracts (10 mg/ml) in 5 % dimethyl sulfoxide (DMSO). For phase 1 analysis, the sample stock was diluted to the desired concentration with distilled water, ensuring that the final concentration of DMSO did not exceed 0.5 %.

3.3 Phase 1: Quantification of biological activities and phytochemicals

3.3.1 Phytochemicals

3.3.1.1 Total phenolic content (TPC)

3.3.1.1.1 Principle

The Folin-Ciocalteu assay is based on the reduction of the heteropolyphosphotungstate–molybdate by the phenolic compounds to form the blue phosphotungsteic-phosphomolybdenum chromophore. This assay is widely used to determine the TPC in biological sample (Jadhav *et al.*, 2012). The sodium carbonate solution imparts the alkalinity required by the phenolic compounds to be dissociated into phenolate anions (Jadhav *et al.*, 2012). The phenolate anions are responsible for the reduction process (Jadhav *et al.*, 2012). The absorbance of the blue chromophore formed will be measured at 750 nm (Singleton and Rossi, 1965).

3.3.1.1.2 Procedure

The determination of TPC was based on the method described by Singleton and Rossi (1965) with slight modifications. The reaction mixture consisted of 10 % Folin-Ciocalteu solution and 1 mg/ml sample. The reaction mixture was incubated for 3 minutes in the dark at room temperature. Following the addition of 10 % sodium carbonate solution, the mixture was incubated for 1 hour in the dark at room temperature and the absorbance was measured at 750 nm against the sample blank with a microplate reader. Gallic acid solution was used as the standard. The TPC

of plant extract was expressed as miligram gallic acid equivalent per gram of sample (mg GAE/g).

$$\text{TPC level (mg GAE/g)} = \left[\frac{\text{Concentration of standard equivalent}}{\text{Concentration of plant extract}} \right]$$

3.3.1.2 Total flavonoid content (TFC)

3.3.1.2.1 Principle

The aluminium chloride method is a common semi-quantitative technique to determine the TFC in biological sample (Pontis *et al.*, 2014). This assay is based on the formation of yellow acid complex from the reaction between aluminium ions and ketone or hydroxyl groups in flavones and flavonols (Bag *et al.*, 2015). The reagent also forms acid complex with the ortho-dihydroxyl groups of flavonoids (Bag *et al.*, 2015). The absorption of the yellow complex formed will be measured at a wavelength of 415 nm (Lee *et al.*, 2011).

3.3.1.2.2 Procedure

The determination of TFC was based on the method described by Lee *et al.* (2011) with minor modifications. The reaction mixture consisted of 1 mg/ml sample, distilled water, 95 % EtOH, 1 M potassium acetate and 10 % aluminum chloride. The reaction mixture was incubated for 30 minutes in the dark at room temperature. The absorbance was measured at 415 nm against the sample blank with a microplate reader. Quercetin solution was used as the standard. The sample and 10 % aluminum chloride solution were replaced by distilled water for negative control and

sample blank, respectively. The TFC of plant extract was expressed as miligram quercetin equivalent per gram of sample (mg Qct/g).

$$\text{TFC level (mg Qct/g)} = \left[\frac{\text{Concentration of standard equivalent}}{\text{Concentration of plantextract}} \right]$$

3.3.1.3 Tannin content

3.3.1.3.1 Principle

Tannins are high molecular weight polyphenols that are present in most plants (Soares *et al.*, 2020). As tannins are classified as phenolic compounds, the method of determining the tannin content involves the application of TPC assay (Siddhuraju and Manian, 2007). The method also takes advantage of the high affinity of PVPP towards tannins (Mahlo and Chauke, 2012). Centrifugation aids in the separation of PVPP-tannin complex from the supernatant, which will be subjected to TPC determination (Siddhuraju and Manian, 2007). The TPC difference between the samples treated with and without PVPP denotes the amount of tannins that are present in the sample (Siddhuraju and Manian, 2007).

3.3.1.3.2 Procedure

The determination of tannin content was carried out according to the method described by Ng *et al.* (2020). Ten milligrams of PVPP were incubated with 1 mg/ml of sample (500 µL) at 4°C for 15 minutes. After the mixture was centrifuged at 15000 x g for 10 minutes, the supernatant was used for the determination of TPC. The difference of TPC between the sample and negative control was equivalent to the amount of tannins that were present in the sample. For negative control, PVPP was replaced with

distilled water. Tannic acid was used as the standard. The tannin content of plant extract was expressed as miligram tannic acid equivalent per gram of sample (mg TAE/g).

$$\text{Tannin content (mg TAE/g)} = \left[\frac{\text{Concentration of standard equivalent}}{\text{Concentration of plantextract}} \right]$$

3.3.1.4 Saponin content

3.3.1.4.1 Principle

The determination of saponin content with vanillin-sulphuric acid method is based on the oxidation of saponins present in the biological sample by sulphuric acid (Le *et al.*, 2018). The reaction between the oxidised saponins and vanillin gives rise to the formation of red-purplish complex that can be measured at 560 nm (Le *et al.*, 2018).

3.3.1.4.2 Procedure

The saponin content of sample was measured using the vanillin-sulphuric acid method described by Le *et al.* (2018). Briefly, twenty-five microliters of sample (1 mg/ml) were incubated with 4 % vanillin dissolved in EtOH and 72 % sulphuric acid at 60°C for 15 minutes. The mixture was then cooled to room temperature for 5 minutes before the absorbance was read at 560 nm against the sample blank with a microplate reader. Quillaja saponin was used as the standard. The saponin content of plant extract was expressed as miligram quillaja saponin equivalent per gram of sample (mg QSE/g).

$$\text{Saponin content (mg QSE/g)} = \left[\frac{\text{Concentration of standard equivalent}}{\text{Concentration of plantextract}} \right]$$

3.3.1.5 Alkaloid content

3.3.1.5.1 Principle

The measurement of alkaloid content with bromocresol green method is based on the formation of yellowish complex from the reaction between bromocresol green and nitrogen-containing alkaloids in the sample (Zhang *et al.*, 2016a). The pH of the reaction is balanced with the use of potassium hydrogen phthalate, an acidic salt (Zhang *et al.*, 2016a). The non-polar yellow complex that forms can be extracted with chloroform, from which the absorbance was measured (Zhang *et al.*, 2016a).

3.3.1.5.2 Procedure

The determination of alkaloid content was performed based on the bromocresol green method described by Zhang *et al.* (2016a) with slight modifications. Briefly, one part of sample (1 mg/ml) was mixed with five parts of citrate buffer solution (pH 5.4). Then the mixture was homogenised with working reagent comprising of 0.5 mg/ml of bromocresol green and 10 mg/ml potassium hydrogen phthalate. After the addition of chloroform, the mixture was shaken vigorously for 30 seconds and incubated at room temperature for 50 minutes. The absorbance of the chloroform layer was read at 416 nm with a microplate reader. Berberine chloride was used as the standard. The alkaloid content of plant extract was expressed as miligram berberine chloride equivalent per gram of sample (mg BCE/g).

$$\text{Alkaloid content (mg BCE/g)} = \left[\frac{\text{Concentration of standard equivalent}}{\text{Concentration of plantextract}} \right]$$

3.3.2 Antioxidant activities

3.3.2.1 Ferric-reducing antioxidant power (FRAP)

3.3.2.1.1 Principle

The FRAP assay measures the ability of an antioxidant to reduce ferric ion into ferrous ion (Fe^{2+}) in the presence of 2,4,6-tripyridyl-s-triazine. This assay is based on the single electron transfer (SET) mechanism (Cerretani and Bendini, 2010). The ionising potential is used to gauge the antioxidant capability in the SET mechanism in which the lower the ionising potential, the easier the electron will be transferred to the radicals (Liang and Kitts, 2014). The reaction is maintained at a low acidic condition to enhance the redox potential (Cerretani and Bendini, 2010). This is accompanied by corresponding reduction in ionization potential that facilitates the transfer of hydrogen atom (Cerretani and Bendini, 2010). The absorption of the Fe^{2+} -coloured product formed from the reduction will be measured at a wavelength of 593 nm to determine the ferric-reducing ability of the antioxidant (Cerretani and Bendini, 2010).

3.3.2.1.2 Procedure

The FRAP assay was performed according to the method described by Benzie and Strain (1996) with minor modifications. The reaction mixture consisted of 1 mg/ml sample and FRAP reagent. The FRAP reagent was prepared from 300 mM sodium acetate buffer (pH 3.6), 10 mM 2,4,6-tripyridyl-s-triazine solution prepared in 40 mM hydrochloric acid and 20 mM ferric chloride hexahydrate in a ratio of 10:1:1. The reaction mixture was incubated at room temperature for 4 minutes and the absorbance was measured at 595 nm with a microplate reader against a sample blank.

Ferrous sulphate heptahydrate was used as the standard. The FRAP value of plant extract was expressed as mmol Fe²⁺ equivalents per gram of sample (mmol Fe²⁺/g).

$$\text{FRAP level (mmol Fe}^{2+}\text{/g)} = \left[\frac{\text{Concentration of standard equivalent}}{\text{Concentration of plant extract}} \right]$$

3.3.2.2 DPPH radical scavenging activity

3.3.2.2.1 Principle

The DPPH radical scavenging assay is an antioxidant assay based on the SET mechanism that measures the capacity of an antioxidant in scavenging the stable free radical, DPPH (Liang and Kitts, 2014). The DPPH radical is characterised by its deep violet colour as a result of delocalization of spare electron over the molecular structure which makes the molecules less likely to dimerise (Kedare and Singh, 2011). In DPPH radical scavenging assay, the nitrogen atoms in the purple DPPH radicals were reduced to form non-radical diphenylpicrylhydrazine upon accepting a hydrogen atom from the sample with antioxidant properties (Kedare and Singh, 2011). Ultimately, this process renders a colourless reaction (Kedare and Singh, 2011).

3.3.2.2.2 Procedure

DPPH radical scavenging assay was performed according to Gerhäuser *et al.* (2003) with minor modifications. The reaction mixture consisted of 1 mg/ml sample and 100 µM DPPH reagent. The reaction mixture was incubated at room temperature in the dark for 15 minutes. The decrease of absorbance was monitored every 15 minutes for 2 hours at

515 nm with a microplate reader. Ascorbic acid was used as the standard. The sample was replaced with distilled water as negative control. The DPPH radical scavenging activity of plant extract was expressed as the half-maximal inhibitory concentration (IC₅₀) in mg/ml, which was derived from the DPPH radical scavenging activity (%) calculated as follows:

$$\text{DPPH radical scavenging activity (\%)} = \left[\frac{A_{\text{control}} - A_{\text{sample}}}{A_{\text{control}}} \right] \times 100\%$$

A_{control} and A_{sample} refer to the respective absorbance of the negative control and sample.

3.3.2.3 ABTS radical scavenging activity

3.3.2.3.1 Principle

The 6-hydroxy-2,5,7,8-tetramethylchroman-2-carboxylic acid (Trolox) equivalent antioxidant capacity assay is based on the hydrogen atom transfer mechanism which measures the scavenging ability of antioxidants against ABTS radical cation (ABTS^{o+}), a blue chromophore (Liang and Kitts, 2014). Unlike DPPH radicals, which is sensitive towards acidic condition, Trolox equivalent antioxidant capacity assay can be applied to reaction wider range of pH (Ou *et al.*, 2002). Prior to this assay, the ABTS^{o+} is generated from the reaction between ABTS salt and an oxidising agent, potassium persulfate (Shalaby and Shanab, 2013). The decolorization of green colour ABTS indicates the quenching of the radical cations by sample antioxidants (Ilyasov *et al.*, 2020).

3.3.2.3.2 Procedure

The Trolox equivalent antioxidant capacity assay was performed according to Re *et al.* (1999) with minor modifications. The ABTS reagent was prepared from 7 mM ABTS diammonium salt and 140 mM potassium persulfate. The mixture was incubated in the dark at room temperature for 16 hours. The mixture was then diluted with distilled water in a volume ratio of 1:30. The reaction mixture consisted of 1 mg/ml sample and 2.45 mM ABTS reagent. The reaction mixture was incubated at room temperature for 1 minutes. The decrease of absorbance was monitored at 734 nm with a microplate reader. The sample was replaced with distilled water as negative control. Trolox was used as the standard. The ABTS radical scavenging activity of plant extract was expressed as IC₅₀ in mg/ml, which was derived from the ABTS radical scavenging activity (%) calculated as follows:

$$\text{ABTS radical scavenging activity (\%)} = \left[\frac{A_{\text{control}} - A_{\text{sample}}}{A_{\text{control}}} \right] \times 100\%$$

A_{control} and A_{sample} refer to the respective absorbance of the negative control and sample.

3.3.2.4 Lipid peroxidation inhibitory activity

3.3.2.4.1 Principle

The thiobarbituric acid-reactive species assay is commonly used to estimate the capacity of biological sample in inhibiting lipid peroxides (Upadhyay *et al.*, 2014). In this assay, the egg-yolk homogenate serves as the lipid substances from which lipid peroxides are produced (Upadhyay *et al.*, 2014). The ferrous sulphate induces lipid peroxidation in polyunsaturated fatty acids and yields malondialdehyde, which subsequently reacts with thiobarbituric acid to produce a pinkish-red chromogenic product (Upadhyay *et al.*, 2014). The product is then

extracted with n-butanol and the resulting absorbance is measured spectrophotometrically at 532 nm (Upadhyay *et al.*, 2014).

3.3.2.4.2 Procedure

This assay was based on thiobarbituric acid-reactive species assay described by Upadhyay *et al.* (2014) with minor modifications. The reaction mixture consisted of 10 % egg homogenate, 1 mg/ml sample, distilled water and 0.07 M ferrous sulphate. The reaction mixture was incubated for 30 minutes at room temperature. Next, 20 % acetic acid and 0.8 % thiobarbituric acid in 1.1 % sodium dodecyl sulphate and 20 % TCA were added, vortexed, and heated in a boiling water bath for 60 minutes. After cooling, n-butanol was then added and centrifuged at 3000 rpm for 10 minutes. Ascorbic acid was used as the standard. For negative control, sample was replaced with distilled water. The absorbance of the supernatant was measured at 532 nm against n-butanol. The lipid peroxidation inhibitory activity of plant extract was expressed as IC₅₀ in mg/ml, which was derived from the lipid peroxidation inhibitory activity (%) calculated as follows:

$$\text{Lipid peroxidation inhibitory activity (\%)} = \left[\frac{A_{\text{control}} - A_{\text{sample}}}{A_{\text{control}}} \right] \times 100\%$$

A_{control} and A_{sample} refer to the respective absorbance of the negative control and sample.

3.3.2.5 Antioxidant index (AI)

According to Puttaraju *et al.* (2006), the AI was used to categorise the antioxidant potential of biological sample. To determine the AI of each plant extract, the mean of relative percentage values derived from the 4

antioxidant assays; namely the FRAP, DPPH, ABTS and lipid peroxidation inhibitory assays were used to determine the AI. The highest value in each assay was converted to 100 while the remaining lower values were converted based on the numerical scale. Based on the percentage values, the plant extracts were graded into very high (76-100 %), high (51-75 %), moderate (26-50 %) and low (0-25 %) AI fractions.

3.3.3 Anti-inflammatory activities

3.3.3.1 Cyclooxygenase (COX) 1 and 2 inhibitory activities

3.3.3.1.1 Principle

COXs are myeloperoxidases superfamily of fatty-acid oxygenases that catalyses the production of prostaglandins that are involved in the generation of fever and pain during inflammation (Rouzer and Marnett, 2009). COXs are bifunctional as the enzymes exert both the COX and peroxidase effects (Rouzer and Marnett, 2009). COXs oxidise the substrate AA via its tyrosyl radical to synthesise prostaglandin G₂ and the peroxidase reduces prostaglandin G₂ to Prostaglandin H₂ which is the precursor of thromboxane and prostacyclin (Rouzer and Marnett, 2009).

3.3.3.1.2 Procedure

COXs inhibitory assay was performed according to Gacche *et al.* (2011). The assay was used to evaluate the peroxidase activity by measuring the generation of oxidised N, N, N', N'-tetramethyl-p-phenylenediamine (Cayman Chemical, 2020). The reaction mixture consisted of 0.1 M Tris-hydrochloric acid (pH 8.0), sample (0.5 mg/ml), 0.046x diluted hemin and 0.25x diluted enzyme (COX-1 or COX-2). The plate was gently agitated for few seconds and incubated at room

temperature for 5 minutes. The colorimetric substrate solution was then added, followed by 1.1 mM AA. The plate was gently agitated for few seconds and incubated at room temperature for 2 minutes. The absorbance was measured at 590nm against the sample blank with a microplate reader. Distilled water and buffer were used to replace the sample and enzyme for reagent blank and sample blank, respectively. Acetylsalicylic acid was used as the standard. For negative control, sample was replaced with water. The COX inhibitory activity of plant extract was expressed as percentage inhibition (%) calculated as follows:

$$\text{COX inhibitory activity (\%)} = \left[\frac{A_{\text{control}} - A_{\text{sample}}}{A_{\text{control}}} \right] \times 100\%$$

Acontrol and Asample refer to the respective absorbance of the negative control and sample.

3.3.3.2 5-Lipoxygenase (LOX) inhibitory activity

3.3.3.2.1 Principle

Lipoxygenases are a family of enzymes that catalyse the oxidation of polyunsaturated fatty acids which consist of the Z, Z-pentadienyl fragment in their structure (Peters-Golden and Brock, 2003). Lipoxygenases can be classified into LOX, 8-lipoxygenase, 11-lipoxygenase, 12-lipoxygenase and 15-lipoxygenase with their common substrates being the arachidonic acid (AA) and linoleic acid depending on the origin of lipoxygenases (Butovich and Lukyanova, 2008). Linoleic acid is the substrate for the LOX of plant origin, also known as the lipoxidases (Butovich and Lukyanova, 2008). The final product that forms from the oxidation of linoleic acid is known as hydroperoxyoctadecadienoic acid (Butovich and Lukyanova). The LOX inhibitory activity increases with the concentration of the plant extracts (Butovich and Lukyanova). This was

accompanied with corresponding decrease in the production of hydroperoxyoctadecadienoic acid, which will be indicated by the reduced absorbance (Butovich and Lukyanova).

3.3.3.2.2 Procedure

LOX inhibitory assay was based on the method as described by Perera *et al.* (2016) with minor modifications. The reaction mixture consisted of 1 mg/ml sample and 165 U/ml LOX dissolved in 100 mM sodium phosphate buffer (pH 8.0). The reaction mixture was incubated at 37°C in the dark for 10 minutes. Ten millimolar sodium linoleic acid dissolved in Tween® 20 were then added to the reaction mixture. The change in absorbance was monitored every minute for 10 minutes at 290 nm against the sample blank with a microplate reader. The sample and sodium linoleic acid were replaced by distilled water for negative control and sample blank, respectively. Quercetin solution was used as the standard. The LOX inhibitory activity of plant extract was expressed as IC₅₀ in mg/ml, which was derived from the LOX inhibitory activity (%) calculated as follows:

$$\text{LOX inhibitory activity (\%)} = \left[\frac{A_{\text{control}} - A_{\text{sample}}}{A_{\text{control}}} \right] \times 100\%$$

A_{control} and A_{sample} refer to the respective absorbance of the negative control and sample.

3.3.3.3 Xanthine oxidase (XO) inhibitory activity

3.3.3.3.1 Principle

XO is an enzyme that catalyses the hydroxylation of hypoxanthine to xanthine, and subsequently to uric acid (Kostić *et al.*, 2015). XO has

been implicated in the development of metabolic syndrome through its involvement in oxidative stress and inflammation (Feoli *et al.*, 2014). In this assay, the xanthine served as the substrate for XO and the oxidation of xanthine was monitored kinetically at 295 nm (Noro *et al.*, 1983).

3.3.3.3.2 Procedure

XO inhibitory assay was performed according to Quy and Xuan (2019) with slight modifications. The reaction mixture was consisted of 1 mg/ml sample, 100 mM sodium phosphate buffer (pH 7.5) and 1 U/ml XO dissolved in the same buffer. The reaction mixture was incubated at room temperature for 15 minutes, followed by the addition of 8 mM xanthine. The absorbance was monitored kinetically every minute for 30 minutes at 295 nm against the sample blank with a microplate reader. Quercetin served as the standard. For negative control, the sample was replaced with distilled water. For sample blank, the enzyme was replaced with buffer. The XO inhibitory activity of plant extract was expressed as IC₅₀ in mg/ml, which was derived from the XO inhibitory activity (%) calculated as follows:

$$\text{XO inhibitory activity (\%)} = \left[\frac{A_{\text{control}} - A_{\text{sample}}}{A_{\text{control}}} \right] \times 100\%$$

A_{control} and A_{sample} refer to the respective absorbance of the negative control and sample.

3.3.3.4 Hyaluronidase inhibitory activity

3.3.3.4.1 Principle

Hyaluronidases are a family of enzymes involved in the degradation of HA via the hydrolysis of hexosaminidic β-1,4 bond between N-acetylglucosamine and glucuronic acid (Cavallini *et al.*, 2013). HA is one of the essential components in the extracellular matrix that are known to

involve in the attenuation of inflammatory responses (Buhren *et al.*, 2016). HA is also capable of preventing the formation of blood vessels in addition to its ability in immunosuppression (Buhren *et al.*, 2016). The hyaluronidase inhibitory assay is based on the enzymatic cleavage of HA, producing N-acetylglucosamine (Wilkinson *et al.*, 1996). The calcium chloride solution acts as an enzyme stabilising agent (Ma *et al.*, 2006). An intermediary product forms upon heating of N-acetylglucosamine with alkaline tetraborate (Wilkinson *et al.*, 1996). The reaction between the intermediary product and *p*-dimethylaminobenzaldehyde gives rise to the generation of purple coloured product (Wilkinson *et al.*, 1996).

3.3.3.4.2 Procedure

The hyaluronidase inhibitory assay was performed according to Perera *et al.* (2016) with slight modification. The reaction mixture consisted of 1 mg/ml sample and 4200 U/ml hyaluronidase, both dissolved in acetate buffer (100 mM, pH 3.6). The reaction mixture was incubated at 37°C for 20 minutes. Then 12.5 mM calcium chloride was added and the reaction mixture was incubated at 37°C for 10 minutes. After that, 12 mg/ml sodium hyaluronate was added and incubated at 37°C for 40 minutes. This was followed by the addition of 0.9 M sodium hydroxide and 0.2 M disodium tetraborate. After incubating in boiling water bath for 3 minutes, 67 mM *p*-dimethylaminobenzaldehyde was added. The reaction mixture was incubated at 37°C for 10 minutes. Then the absorbance was measured at 585 nm against the sample blank with a microplate reader. Tannic acid served as the standard. For negative control, the sample was replaced with acetate buffer. For sample blank, the enzyme was replaced with buffer. The hyaluronidase inhibitory activity of plant extract was expressed as IC₅₀ in

mg/ml, which was derived from the hyaluronidase inhibitory activity (%) calculated as follows:

$$\text{Hyaluronidase inhibitory activity (\%)} = \left[\frac{A_{\text{control}} - A_{\text{sample}}}{A_{\text{control}}} \right] \times 100\%$$

A_{control} and A_{sample} refer to the respective absorbance of the negative control and sample.

3.3.3.5 Anti-inflammatory index (AII)

The AII was used to categorise the anti-inflammatory potential of biological sample and it was derived from the AI formulated by Puttaraju *et al.* (2016). The mean of relative percentage values of the plant extracts in the 5 anti-inflammatory assays; namely, the COX-1, COX-2, LOX, XO and hyaluronidase inhibitory assays were used to determine the AII. The highest value in each assay was converted to 100 while the remaining lower values were converted based on the numerical scale. Based on the percentage value, the plant extracts were graded into very high (76-100 %), high (51-75 %), moderate (26-50 %) and low (0-25 %) AII fractions.

3.3.4 Anti-glycaemic activities

3.3.4.1 α -glucosidase inhibitory activity

3.3.4.1.1 Principle

α -glucosidase is an enzyme that catalyses the breakdown of carbohydrates such as starch and disaccharides, thereby leading to the elevation of blood glucose level (Telagari *et al.*, 2015). In this assay, α -glucosidase catalyses the hydrolysis of the substrate, 4-nitrophenyl α -D-glucopyranoside and this results in the formation of glucose and the yellow

product *p*-nitrophenol (Sulistiyani *et al.*, 2016). The reaction is terminated by alkaline sodium carbonate solution and the released *p*-nitrophenol (Kazeem *et al.*, 2013).

3.3.4.1.2 Procedure

α -glucosidase inhibitory assay was performed according to Sancheti *et al.* (2011) with slight modifications. The reaction mixture consisted of 0.1 M sodium phosphate buffer (pH 7.0), 1 mg/ml sample and 40 U/ml α -glucosidase solution dissolved in buffer. The reaction mixture was incubated at 37°C for 10 minutes. 4-nitrophenyl α -D-glucopyranoside was added and the reaction was further incubated at 37°C for 30 minutes. Next, 0.2 M sodium carbonate solution was added to the reaction. The absorbance was measured at 410nm against the sample blank. Acarbose served as the standard. For sample blank, the enzyme was replaced with buffer. For negative control, sample was replaced with distilled water. The α -glucosidase inhibitory activity of plant extract was expressed as IC₅₀ in mg/ml, which was derived from the α -glucosidase inhibitory activity (%) calculated as follows:

$$\alpha\text{-glucosidase inhibitory activity (\%)} = \left[\frac{A_{\text{control}} - A_{\text{sample}}}{A_{\text{control}}} \right] \times 100\%$$

A_{control} and A_{sample} refer to the respective absorbance of the negative control and sample.

3.3.4.2 α -amylase inhibitory activity

3.3.4.2.1 Principle

α -amylase is another carbohydrate-metabolising enzyme found in the saliva and pancreatic juice and it is responsible for the initial digestion of complex carbohydrates into oligosaccharides and disaccharides

(Oyedemi *et al.*, 2017). In this assay, potato starch serves as the substrate, which is hydrolysed by α -amylase into maltose, a reducing sugar (Oyedemi *et al.*, 2017). The presence of reducing sugars converts the orange colour of 3,5-dinitrosalicylic acid reagent into brick-red colour (Hsiao *et al.*, 2019).

3.3.4.2.2 Procedure

α -amylase inhibitory assay was performed according to Manaharan *et al.* (2012) with minor modifications. The reaction mixture consisted of sodium phosphate buffer (100 mM, pH 7.0), 1 mg/ml sample and 40 U/ml α -amylase dissolved in phosphate buffer. The reaction mixture was incubated at 37°C for 20 minutes. Next, 1 % potato soluble starch solution was added and incubated at 37°C for 30 minutes. Following this was the addition of working reagent containing 3,5-dinitrosalicylic acid (10 mg/ml), potassium sodium tartrate tetrahydrate (300 mg/ml), sodium hydroxide (0.2 M) and distilled water. The reaction was incubated at 95°C for 10 minutes. The absorbance was measured at 540 nm against the sample blank. Acarbose was used as the standard. For sample blank, the enzyme was replaced with buffer. For negative control, sample was replaced with distilled water. The α -amylase inhibitory activity of plant extract was expressed as IC₅₀ in mg/ml, which was derived from the α -amylase inhibitory activity (%) calculated as follows:

$$\alpha\text{-amylase inhibitory activity (\%)} = \left[\frac{A_{\text{control}} - A_{\text{sample}}}{A_{\text{control}}} \right] \times 100\%$$

A_{control} and A_{sample} refer to the respective absorbance of the negative control and sample.

3.3.5 Anti-glycation activities

3.3.5.1 AGE formation inhibitory activity

AGE formation inhibitory assay was performed according to Hung *et al.* (2017) with slight modifications. The reaction mixture consisted of 10 mg/mL bovine serum albumin in 50 mM sodium phosphate buffer (pH 7.4), 1 M D-glucose and 1 mg/ml sample (10 mg/ml for aqueous fraction dissolved in distilled water,) which was incubated at 80°C for 7 days. The glycated material was then analysed with three assays: AGE fluorescence analysis, Amadori product analysis and dicarbonyl compound analysis. Aminoguanidine was used as standard.

3.3.5.2 Total AGE inhibition

3.3.5.2.1 Principle

The current assay analysis employed the fluorescent properties of AGEs to determine the inhibitory activity of plant extract against fluorescent AGEs (Zhang *et al.*, 2011). The fluorescence is measured at excitation and emission wavelength of 370 nm and 440 nm, respectively (Zhang *et al.*, 2011).

3.3.5.2.2 Procedure

The assay was based on the method described by Zhang *et al.* (2011) with slight modifications. The glycated material incubated with plant extract were mixed with 1 g/ml trichloroacetic acid. The mixture was then centrifuged at 15000 rpm for 4 minutes at 4°C. The supernatant was discarded and the pellet was dissolved in phosphate-buffered saline. The AGE fluorescence intensity (FI) was measured at excitation wavelength of 360 nm and emission wavelength of 450 nm. The total AGE inhibitory

activity of plant extract was expressed as IC₅₀ in mg/ml, which was derived from the AGE formation inhibition (%) calculated as follows:

$$AGE \text{ formation inhibition } \% = \left[1 - \frac{FI \text{ extract}}{FI \text{ blank}} \right] \times 100$$

FI extract and FI blank refer to the respective fluorescence intensity of the sample and negative control.

3.3.5.3 Amadori product inhibition

3.3.5.3.1 Principle

This assay analyses the formation of Amadori products by estimating the ability of the formed Amadori products in reducing the nitroblue tetrazolium chloride (NBT) reagent (Bohlooli *et al.*, 2016). The reduction process generates tetrazinoyl radical NBT[•] (Bohlooli *et al.*, 2016). The radicals are subsequently disproportionated to form purple coloured formazan dye (Bohlooli *et al.*, 2016).

3.3.5.3.2 Procedure

The Amadori product analysis was performed according to Hung *et al.* (2017) with slight modifications. The reaction mixture consisted of glycated material and 0.3 mM NBT reagent in 0.1 M sodium carbonate buffer (pH 10.35). The reaction mixture was incubated at room temperature for 15 minutes. The absorbance was measured at 530 nm against blank. For blank, the NBT reagent was replaced with distilled water. The Amadori product inhibitory activity of plant extract was expressed as percentage inhibition (%) calculated as follows:

$$\text{Amadori products formation inhibition (\%)} = \left[\frac{A_{\text{control}} - A_{\text{sample}}}{A_{\text{control}}} \right] \times 100\%$$

A_{control} and A_{sample} refer to the respective absorbance of the negative control and sample.

3.3.5.4 Dicarbonyl compound inhibition

3.3.5.4.1 Principle

This assay is based on the reaction between the acidic hydrazide group of Girard's reagent T and dicarbonyl compounds (Wheeler, 1968). The reaction forms hydrazone derivatives, which are soluble in water due to the presence of quaternary ammonium cation in the structure of the hydrazone (Mitchel and Birnboim, 1977).

3.3.5.4.2 Procedure

This assay was performed according to Hung *et al.* (2017) with slight modifications. The reaction mixture consisted of glycated material, 0.5 M Girard's reagent T solution and 0.5 M sodium formate (pH 2.9). The reaction mixture was incubated at room temperature for 1 hour and the absorbance was measured at 295 nm against blank. Glyoxal was used as the standard. For blank, the Girard's reagent T solution was replaced with distilled water. The dicarbonyl compounds inhibitory activity of plant extract was expressed as percentage inhibition (%) calculated as follows:

$$\text{Dicarbonyl compounds formation inhibition (\%)} = \left[\frac{A_{\text{control}} - A_{\text{sample}}}{A_{\text{control}}} \right] \times 100\%$$

A_{control} and A_{sample} refer to the respective absorbance of the negative control and sample.

3.3.5.5 Aldose reductase (AR) inhibitory activity

3.3.5.5.1 Principle

AR is the rate-limiting enzyme in polyol pathway and it has been implicated in the formation of AGEs as well as oxidative stress, both of which are risk factors in the development of DR (Tarr *et al.*, 2013). In this assay, the NADPH acts as the cofactor for the AR that catalyses the reduction of the substrate, DL-glyceraldehyde (Del Corso *et al.*, 2000). The corresponding oxidation of NADPH results in yellow decolourization (Del Corso *et al.*, 2000).

3.3.5.5.2 Procedure

AR inhibitory assay was performed according to Manaharan *et al.* (2012) with slight modifications. The reaction mixture consisted of 0.1 M sodium phosphate buffer (pH 6.2), 20 U/ml AR, 3 mM NADPH, 1 mg/ml sample and 5 mM DL-glyceraldehyde. The decrease in absorbance over a period of 10 minutes was measured at 340 nm. Quercetin served as the standard. For negative control, sample was replaced with distilled water. The AR inhibitory activity of plant extract was expressed as IC₅₀ in mg/ml, which was derived from the AR inhibitory activity (%) calculated as follows:

$$\text{AR inhibitory activity (\%)} = \left[\frac{A_{\text{control}} - A_{\text{sample}}}{A_{\text{control}}} \right] \times 100\%$$

A_{control} and A_{sample} refer to the respective absorbance of the negative control and sample.

3.3.5.6 Anti-glycation index (AGI)

The AGI was derived from the AI formulated by Puttaraju *et al.* (2016) and it was used to rank the anti-glycation potential of plant extracts. The mean of relative percentage values of the plant extracts derived from the 4 anti-glycation assays; namely, the aldose reductase inhibitory assay,

total AGE inhibition, Amadori product and dicarbonyl compound analysis were used to determine the AGI. The highest value in each assay was converted to 100 while the remaining lower values were converted based on the numerical scale. Based on the percentage value, the plant extracts were graded into very high (76-100 %), high (51-75 %), moderate (26-50 %) and low (0-25 %) AGI fractions.

3.3.6 Toxicity evaluation

3.3.6.1 Principle

The brine shrimp toxicity assay determines the ability of the biological sample to cause lethality in the brine shrimp, *Artemia salina* within 24 hours (Wu, 2014). The number of surviving nauplii will be counted after 24 hours to determine the toxicity of the sample (Sarah *et al.*, 2017).

3.3.6.2 Procedure

The brine shrimp toxicity assay was performed according to Asaduzzaman *et al.* (2015) with slight modifications. Three grams of brine shrimp eggs was hatched into nauplii with constant oxygen supply and light. After 48 hours, the test sample was mixed with saltwater containing 10 nauplii. Potassium dichromate was used as the standard. For negative control, DMSO was mixed with brine containing 10 nauplii. After 24 hours, the number of survived nauplii was counted. The toxicity of the plant extract was expressed as 50 % lethality concentration (LC₅₀) in mg/ml based on the percentage of mortality for nauplii calculated as follows:

$$Pt \% = \frac{[(Po - Pc)]}{(100 - Pc)} \times 100$$

Po and Pc refers to observed mortality and control mortality, respectively.

3.4 Phase 2: *In vitro* cellular mechanistic study

3.4.1 Preparation of AGE

3.4.1.1 Principle

The formation of AGE is a non-enzymatic reaction between the reducing sugars and proteins (Fournet *et al.*, 2018). AGE can be taken up by the body system either through diet or formed endogenously under normal physiological condition (Nowotny *et al.*, 2018). In DM, the formation of AGE is accelerated due to the spike in blood glucose level (Fournet *et al.*, 2018). However, the process occurs at a slow rate at 37°C (Bhatwadekar and Ghole, 2005). For the rapid synthesis of AGE, the reaction can be experimentally accelerated by increasing the temperature to 50°C (Bhatwadekar and Ghole, 2005).

3.4.1.2 Procedure

The preparation of AGE was performed as described by Sun *et al.* (2017). The bovine serum albumin (1 mM) was incubated with D-glucose (1 M) in 0.01 M PBS at 50°C for 30 days. Then the clear brown AGE solution was dialysed against PBS to remove free unbound glucose. The dialysed AGE solution was lyophilised, resulting in brown powder.

3.4.2 Cell culture and sample treatment

The ARPE-19 were cultured as described by Arumugam *et al.* (2020) with slight modifications. The cells were grown in basal Dulbecco's Modified Eagle's Medium/Nutrient Mixture F12 cell culture medium supplemented with L-glutamine (2.5 mM), fetal bovine serum (10 %), penicillin-

streptomycin (1 %) and glucose (17 mM) in a 5 % CO₂ incubator at 37°C. The cell culture medium was replaced with fresh medium every second day. Upon 70-80 % confluence, the cell culture was passaged by dissociating in 0.05 % trypsin-ethylenediaminetetraacetic acid solution (pH 7.4). Cells at passage 24 to 27 were utilised for experiments. For moderately high glucose induction studies, ARPE-19 were grown for 48 hours in basal medium containing 34 mM glucose. For high glucose induction studies, ARPE-19 were grown for 48 hours in the basal medium containing 68 mM glucose. For normal glucose AGE induction studies, cells were grown in basal media containing AGE (200 µg/ml) for 48 hours. For high glucose AGE induction studies, high glucose basal medium (34 mM or 68 mM glucose) containing AGE (200 µg/ml) were used. For cell treatment, cells were serum-starved in serum-free media for 24 hours to synchronise the cell cycle and reduce the interference from serum proteins in the cell culture medium. Cell treatment with *P. pellucida* crude methanolic extract or ethyl acetate fraction was continued for 48 hours. To prepare the *P. pellucida* crude methanolic extract (0.75 mg/ml, 1.5 mg/ml, 3 mg/ml) or ethyl acetate fraction (1 mg/ml, 2 mg/ml, 4 mg/ml) for cell treatment, 10 mg/ml of stock sample dissolved in 1 % DMSO was injected into the cell culture medium through a 0.22 µm syringe filter. The final concentration of DMSO in the working medium did not exceed 0.5 %.

3.4.3 Plant cytotoxicity evaluation

3.4.3.1 3-[4,5-dimethylthiazol-2-yl]-2,5 diphenyl tetrazolium bromide (MTT) cell viability assay

3.4.3.1.1 Principle

MTT cell viability assay is a direct colorimetric assay used to measure the metabolic activity of cell culture (Ghasemi *et al.*, 2021). The assay is based on the reduction of MTT, a tetrazolium salt by the enzymes reductase and dehydrogenase located in the mitochondria of metabolically active cells (Ghasemi *et al.*, 2021). The reduction results in the formation of purple insoluble formazan crystals which are dissolved in a solubilising reagent such as DMSO and EtoH (Kim *et al.*, 2007). The absorption spectrum of purple solution, which directly corresponds to the intracellular MTT reduction by viable cells is measured at 570 nm (Kim *et al.*, 2007).

3.4.3.1.2 Procedure

The MTT cell viability assay was based on the method described by Arumugam *et al.* (2020) with minor modifications. ARPE-19 cells were seeded in 96-wells plates at a density of 2.5×10^4 cells per well and treated with *P. pellucida* crude methanolic extract and ethyl acetate fraction. After incubation at 37°C for 48 hours in the 5 % CO₂ incubator, cells were treated with 100 µl of MTT (0.5 mg/ml) in serum-free medium for 4 hours. The formazan crystal was solubilised with 100 µl of DMSO. The absorbance was measured at 570 nm. The cell viability (%) and cell death (%), which derived the IC₅₀ in mg/ml was calculated as follows:

$$(i) \text{ Cell viability \%} = \frac{A \text{ treated sample}}{A \text{ untreated control}} \times 100$$

$$(ii) \text{ Cell death \%} = \frac{(A \text{ untreated control} - A \text{ treated sample})}{A \text{ untreated control}} \times 100$$

A treated sample and A untreated control refer to the respective absorbance of the sample and negative control.

3.4.4 Genes expression

This step aimed to investigate the expression of genes involved in pro-inflammatory and anti-inflammatory signalling pathways within ARPE-19, as part of the second objective of the study to elucidate the underlying modulatory mechanism of *P. pellucida*. The genes involved in inflammatory response include the pro-inflammatory markers, IL-8, MCP-1 and RAGE as well as the angiogenic markers, MMP2 and VEGF. The intracellular antioxidant marker, GPx assumes a critical role in the antioxidant defense system to prevent oxidative stress, which directly contributes to inflammation. In addition, the activation of STAT3 could induce the gene expression of SOCS1, which serves as a negative feedback regulator of STAT3 signalling pathway. These genes were regulated by the transcription factors NF- κ B p65, PPAR- γ and STAT3.

3.4.4.1 RNA extraction

3.4.4.1.1 Principle

The guanidinium thiocyanate-phenol-chloroform extraction of RNA is based on the phase separation of intracellular RNA, DNA and organic components such as protein and lipids (Toni *et al.*, 2018). In this method, deactivation of nucleases, denaturation of protein and disruption of cell membranes were achieved with guanidinium thiocyanate-phenol solution (Shen, 2019a). The addition of chloroform, an organic solvent separates the cell lysate into aqueous layer, interphase layer and organic layer containing the RNA, DNA and organic matters, respectively (Shen, 2019a). Isopropanol is used to precipitate the RNA in the aqueous phase prior to the removal of isopropanol with EtOH of lower (Shen, 2019a). After drying, the RNA purity is assessed by measuring the absorption spectrum at

230nm, 260nm and 280nm (Toni *et al.*, 2018). The absorption spectrum of RNA peaks at 230nm whereas organic matters absorb light at the wavelength of 260nm and 280nm (Toni *et al.*, 2018). An optimal absorbance ratios for 260nm/230nm and 260nm/280nm should exceeds 2.0 (Toni *et al.*, 2018). The extracted pure RNA is often subjected to the treatment of deoxyribonuclease to remove genomic DNA that may otherwise present in the sample (Kipp *et al.*, 2013).

3.4.4.1.2 Procedure

RNA extraction was performed with the guanidinium thiocyanate-phenol-chloroform extraction method as described by the manufacturer's instruction for TRIzol reagent. ARPE-19 was grown to 80-90 % confluence on a 100 mm cell culture dish and washed with 1X PBS twice. The cells were lysed with 1 ml of TRIzol reagent and incubated for 5 minutes in a 2 ml eppendorf tube. Then 200 μ l of chloroform was added and mixed well by gently shaking the tube. After 15 minutes of incubation, the tube was centrifuged at 12000 x g for 15 minutes to promote phase separation. The aqueous layer was aliquoted into a new tube before mixing with 500 μ l of isopropanol. After centrifuged at 12000 x g for 10 minutes, the isopropanol was discarded. The RNA pellet was washed with 1 ml of EtOH and centrifuged at 8000 x g for 5 minutes. After discarding the EtOH, the RNA pellet was air-dried and dissolved in 30 μ l of distilled water. The concentration and purity of RNA sample was analysed with a Nano-Drop spectrophotometer based on the absorbance ratio of 260nm/230nm and 260nm/280nm. RNA with 260nm/230nm and 260nm/280nm ratios of 2.0 or higher was subjected to treatment with ribonuclease-free deoxyribonuclease by following the manufacturer's instruction of a

commercial kit. One unit of deoxyribonuclease was added to 2 µg of RNA in a 10 µL reaction consisting of 40 mM Tris-hydrochloric acid, 10 mM magnesium sulphate and 1 mM calcium chloride. The reaction was incubated at 37°C for 30 minutes and it was terminated with the addition of 2 mM ethylene glycol tetraacetic acid. The deoxyribonuclease was then inactivated at 65°C for 10 minutes.

3.4.4.2 Reverse transcription and complementary DNA (cDNA) synthesis

3.4.4.2.1 Principle

In reverse transcription and cDNA synthesis, the RNA molecule is reversibly converted into cDNA (Mo *et al.*, 2012). The transcription of DNA results in the production of RNA molecules, which serve as the carrier for decoding genetic information into proteins (Harries, 2019). In various downstream transcriptomic analyses, the conversion of RNA into cDNA is necessary for the quantitative measurement of genetic copies, such as real-time polymerase chain reaction (qPCR) (Mo *et al.*, 2012). The process is initiated by oligodeoxythymine primer and the addition of nucleotides to RNA molecules, which is facilitated by the enzyme reverse transcriptase (Mo *et al.*, 2012).

3.4.4.2.2 Procedure

The deoxyribonuclease-treated RNA was subjected to reverse transcription and cDNA synthesis following the manufacturer's instruction for the commercial high-capacity cDNA reverse transcription kit. First-strand cDNA was synthesised in a 20 µL reaction consisting of 2 µg of RNA,

50 units of reverse transcriptase, 4 mM deoxynucleotide mix and 1X random primers. The reaction was carried out on a Bio-Rad T-100 thermal cycler (California, USA) with the following conditions: Primer annealing and activation of reverse transcriptase at 25°C for 10 minutes; reverse transcription at 37°C for 120 minutes and termination of reaction at 85°C for 5 minutes.

3.4.4.3 Reverse transcription real-time polymerase chain reaction (RT-qPCR)

3.4.4.3.1 Principle

Polymerase chain reaction (PCR) is a popular molecular biology technique used to determine gene expression (Krohn *et al.*, 2014). However, PCR is generally used for the qualitative detection of target gene expression (Krohn *et al.*, 2014). On the other hand, qPCR is a highly efficient and upgraded PCR method that enables real-time monitoring and quantitative measurement of target gene expression (Mo *et al.*, 2012). The SYBR green based method is one of the two qPCR methods and it is based on the binding of intercalating SYBR green dye to newly synthesised double-stranded DNA in PCR (Mo *et al.*, 2012). Upon binding, the PCR products release fluorescent signal, which is detected by the camera equipped in the real-time thermocycler (Mo *et al.*, 2012). There are two working mechanisms of qPCR, one-step and two-step qPCR (Wacker and Godard, 2005). In the one-step method, gene-specific primers are used in reverse transcription and synthesis of cDNA, which is directly subjected to qPCR (Wacker and Godard, 2005). Thus this method is less time consuming and allows the handling of more samples (Wacker and Godard, 2005). On the other hand, the two-step method has a separate reverse

transcription and qPCR procedures, which provide greater flexibility on the primer of choice. (Wacker and Godard, 2005).

3.4.4.3.2 Procedure

Gene expression was evaluated with a commercial SYBR green qPCR kit according to the manufacturer's instruction. The target genes, NF- κ B p65, PPAR- γ , STAT3, MCP-1, IL-8, GPx, VEGF, MMP2, RAGE and SOCS1 in the reverse transcribed cDNA, were amplified with respective gene-specific forward and reverse primers (Table 3.1). Briefly, each of forward and reverse primers (0.4 μ M) was mixed with 1 μ g of cDNA template in a 20 μ L reaction with 3 mM magnesium chloride. The qPCR reaction was carried out on a Bio-Rad CFX Connect Real-time PCR Detection System (California, USA) with the following conditions: Initial denaturation and polymerase activation at 95°C for 2 minutes; 40 cycles of 3-step cycling reactions, which consist of denaturation at 95°C for 5 seconds, primer annealing at 60°C for 10 seconds and extension at 72°C for 20 seconds. The amplification specificity was verified with melting curve analysis. The quantitative expression of the genes was determined by using $2^{-\Delta\Delta C_t}$ method in which the relative gene expression level was normalised to the housekeeping genes, β -actin and glyceraldehyde-3-phosphate dehydrogenase (GAPDH).

Table 3.2. The forward and reverse primer sequences for the genes of interest.

Gene	Forward primer (5'-3')	Reverse primer (5'-3')
β-actin	AGA GCT ACG AGC TGC CTG AC	AGC ACT GTG TTG GCG TAC AG
GAPDH	CAT GAG AAG TAT GAC AAC AGC C	AGT CCT TCC ACG ATA CCA AAG
NF-κB p65	GCG AAT GGC TCG TCT GTA GT	GTA TCT GTG CTC CTC TCG CC
PPAR-γ	GGA GCC CAA GTT TGA GTT TGC	GAA ATG TTG GCA GTG GCT CAG
STAT3	GGG TGG AGA AGG ACA TCA GCG GTA A	GCCGACAATACTTTCCGAATCC
MCP-1	GAA TCA CCA GCA GCA AGT GT	GAG TGT TCA AGT CTT CGG AGT T
IL-8	TTG GCA GCC TTC CTG ATT TC	TGG TCC ACT CTC AAT CAC TCT CA
GPx	AGT TCG GAC ATC AGG AGA ATG GCA	TCA CCA TTC ACC TCG CAC TTC TCA
VEGF	CCC ACT GAG GAG TCC AAC AT	TTT CTT GCG CTT TCG TTT TT
MMP2	TGC TGG AGA CAA ATT CTG GA	GAT GGC ATT CCA GGC ATC
RAGE	GAT GGA AAC TGA ACA CAG GC	GTT GGA CTT GGT CTC CTT TC
SOCS1	CAC GCA CTT CCG CAC ATT C	CGA AAA AGC AGT TCC GCT GG

3.4.5 Proteins expression

Together with gene expression study, this study was to fulfill the second objective of the study. In addition to the markers involved in gene expression, including NF-κB p65, PPAR-γ, STAT3, IL-8, MCP-1, MMP2, VEGF, RAGE, GPx and SOCS1, the activation of transcription factors were determined by evaluating the protein expression of phosphorylated NF-κB p65 and STAT3. On the other hand, the investigation also considered the phosphorylation of PPAR-γ, which rendered the nuclear receptor in an

inactive form. The current study also monitored the inhibition of RAGE-induced inflammatory response by *P. pellucida* through the protein quantification of sRAGE, an AGE antagonist.

3.4.5.1 Cell lysis

3.4.5.1.1 Principle

The extraction of whole cell lysate is focused on obtaining the total protein content in the cell membrane and protoplasm following the disruption of cell membrane with detergents (Winter and Steen, 2011). Radioimmunoprecipitation assay lysis buffer is the most commonly used reagent for whole cell lysis and solubilization of proteins (Winter and Steen, 2011). It contains a combination of ionic and non-ionic detergents to efficiently disrupt the cell membrane and separate the soluble proteins from insoluble cellular components (Jain *et al.*, 2021). Protease and phosphatase inhibitors are often added into radioimmunoprecipitation assay lysis buffer to prevent the degradation of protein and achieve the highest protein yield (Jain *et al.*, 2021).

3.4.5.1.2 Procedure

The preparation of cell lysate extract was performed according to the method by Winter and Steen (2011) with slight modification. Briefly, the cells were grown to 80-90 % confluence on a 100 mm cell culture dish and washed twice with cold PBS. Then the cells were detached from the cell culture dish with a cell scraper. After centrifuged at 250 x g for 5 minutes at 4°C, the supernatant was discarded and the cell pellet was suspended in 100 µl of ice-cold radioimmunoprecipitation lysis buffer. The suspension

was incubated on ice for 60 minutes followed by centrifuging at 16000 x g for 15 minutes at 4°C. The supernatant, which contains the soluble cell lysate extract was stored at -80°C until experiment.

3.4.5.2 Nuclear and cytoplasmic proteins extraction

3.4.5.2.1 Principle

Similar to cell lysate extraction, the extraction of nuclear and cytoplasmic protein is focused on obtaining the intracellular proteins (Merck, 2023). Rather than extracting a single component, the nuclear and cytoplasmic extraction is a two-step procedure that involves the disruption of cell membrane and nuclear membrane to isolate the localised proteins from the cytoplasmic and nuclear fractions, respectively (Ogawa and Imamoto, 2021).

3.4.5.2.2 Procedure

The extraction of nuclear and cytoplasmic proteins was performed using commercial nuclear protein extraction kit according to the manufacturer's instructions. The cells were washed twice with cold PBS and remove from the cell culture dish with a cell scraper. After centrifuged at 250 x g for 5 minutes at 4°C, the supernatant was discarded and the cell pellet was disrupted with the addition of 250 µl of ice-cold cytoplasmic lysis buffer. The suspension was incubated on ice for 15 minutes followed by centrifuging at 250 x g for 5 minutes at 4°C. The supernatant was discarded and the cell pellet was suspended in 100 µl of ice-cold cytoplasmic lysis buffer. After centrifuged at 8000 x g for 5 minutes at 4°C, the supernatant was transferred to a pre-chilled tube as cytoplasmic lysate

and stored at -80°C until experiment. The insoluble pellet fraction, which contains crude nuclei, was suspended in 100 µl of ice-cold nuclear extraction buffer. The suspension was incubated on ice for 60 minutes and then centrifuged at 16000 x g for 5 minutes at 4°C. The resulting supernatant, which contains the nuclear protein was stored at -80°C until experiment.

3.4.5.3 Cell culture supernatant proteins precipitation

3.4.5.3.1 Principle

Protein precipitation is a common technique used for the extraction of secretory protein from cell culture supernatant (Paré *et al.*, 2016). Among the protein precipitation methods, the trichloroacetic acid-deoxycholate method often resulted in consistently high protein yield recovery from large volume samples (Paré *et al.*, 2016). In this method, sodium deoxycholate serves as an ionic detergent that lyses remnant of cells in the cell culture supernatant by disrupting the hydrophobic interactions within the lipid membrane (Keane *et al.*, 2016). The secretory proteins were then aggregated and precipitated with the use of trichloroacetic acid and acetone (Paré *et al.*, 2016).

3.4.5.3.2 Procedure

The extraction of cell culture supernatant protein was performed based on the protein precipitation method using trichloroacetic acid and sodium deoxycholate as described by Paré *et al.* (2016). Two percent sodium deoxycholate solution was added to 40 ml of cell culture supernatant at a final concentration of 0.02 %. After incubating on ice for

30 minutes, trichloroacetic acid was added into the mixture at a final concentration of 7.5 % and mixed well. The precipitated proteins were centrifuged at 15000 x g for 20 minutes at 4°C after incubating on ice for 60 minutes. The supernatant was then discarded before the protein pellet was washed with 10 ml of ice-cold acetone twice by incubating at -20°C for 5 minutes. Centrifugation at 15000 x g for 5 minutes at 4°C was done in between washes. After the supernatant was discarded during the second wash, the protein pellet was air-dried in the fumehood for 30 minutes before being dissolved in 100 µl of radioimmunoprecipitation buffer. The cell culture supernatant protein was stored at -80°C until experiment.

3.4.5.4 Proteins quantification

3.4.5.4.1 Principle

The bicinchoninic acid (BCA) protein quantification assay is a copper-based colorimetric assay based on the formation of protein-cupric ion complex (Otieno *et al.*, 2016). Under alkaline condition, the cupric ion is reduced to cuprous ion, which reacts to form BCA-cuprous ion complex (Shen, 2019b). The quantity of BCA-cuprous ion complex formed is directly proportional to the quantity of protein (Otieno *et al.*, 2016). A change from green colour to purple colour complex is caused by the chelating action of cuprous ion by two molecules of BCA. The absorbance of purple BCA-cuprous ion complex is measured at 562 nm (Otieno *et al.*, 2016). In comparison to other assays, BCA assay is suitable for quantifying detergent-containing protein samples (Shen, 2019b).

3.4.5.4.2 Procedure

The quantification of protein in whole cell lysate, cell culture supernatant, nuclear and cytoplasmic fractions was performed with the BCA protein quantification assay method as described by the manufacturer's instruction for BCA assay kit (Thermo Fisher Scientific, 2020). Briefly, ten microliter of protein sample was mixed with 200 μ l of BCA working reagent and incubated at 37°C for 30 minutes. For blank, the sample was replaced with distilled water. The absorbance was measured at 562 nm against blank. Bovine serum albumin was served as the standard (0–2000 μ g/mL). The protein concentration was determined from the standard curve.

3.4.5.5 Sodium dodecyl sulfate-polyacrylamide gel electrophoresis (SDS-PAGE)

3.4.5.5.1 Principle

SDS-PAGE is a proteomic technique used to separate proteins on a polyacrylamide gel with electric current (Manns, 2011). The denaturation of proteins with anionic detergent prior to SDS-PAGE imparts net negative charge to the protein samples (Manns, 2011). This enables the negative charged proteins to migrate to the opposite charged electrode as a function of their molecular size (Nowakowski *et al.*, 2014). Smaller protein tends to migrate at a higher rate when compared to its large counterpart on a polyacrylamide gel (Nowakowski *et al.*, 2014). The rate of migration is also affected by the concentration of polyacrylamide which determines the gel pore size (Manns, 2011).

3.4.5.5.2 Procedure

The protein samples (30 µg) were resolved with SDS-PAGE as described by Mazur *et al.* (2023). Briefly, 4X protein loading buffer with 10 % β-mercaptoethanol was diluted four times with thirty micrograms of protein sample. Then the protein sample was heated at 95°C for 5 minutes and centrifuged at 16000 x g for 15 minutes at 4°C. The protein sample was loaded into the wells on the stacking gel (4 %) and resolved on a resolving gel (8-12 %) at 90 V until the front dye almost reaches the end of the gel.

3.4.5.6 Western blot

3.4.5.6.1 Principle

Western blotting is a highly specific proteomic technique that detects target protein from a complex mixture of proteins (Mahmood and Yang, 2012). This technique is commonly used as a continuation of SDS-PAGE to transfer the separated proteins onto a nitrocellulose or polyvinylidene difluoride membrane by means of electric current (Kurien and Scofield, 2015). The target protein on the membrane is then detected and captured with specific antibodies (Mahmood and Yang, 2012). The antibodies may be tagged with fluorescent dye for subsequent visualising step (Kurien and Scofield, 2015). Alternatively, enzyme-conjugated antibodies are utilised with a chromogenic substrate that reacts to produce a luminescent signal (Kurien and Scofield, 2015).

3.4.5.6.2 Procedure

The resolved proteins were proceed for western blotting and antibody probing as described by Sethi *et al.* (2014) with slight

modification. The resolved proteins on the gel was subjected to electro-transfer onto a polyvinylidene difluoride membrane at 350 mA for 60 minutes. After the membrane was blocked with PBS containing 5 % non-fat dry milk and 0.1 % Tween® 20 for 2 hours, it was probed with the protein-specific primary antibodies (Table 3.2) diluted in PBS containing 5 % non-fat dry milk and 0.1 % Tween® 20 overnight at 4°C with gentle agitation. The blot was then washed twice with PBS containing 0.1 % Tween® 20 for 15 minutes and incubated with horseradish peroxidase-conjugated secondary antibody (Antibody titer= 1:10000) in PBS containing 5 % non-fat dry milk and 0.1 % Tween® 20 for 1 hour at room temperature with gentle agitation. After washing, the blot was exposed to chemiluminescent substrate and visualised with the signal accumulation mode on a Bio-Rad ChemiDoc MP imaging system (California, USA). Densitometric analysis of the bands was performed with the ImageJ software (National Institute of Health, Maryland, USA). The relative protein expression level was expressed as fold change relative to the internal control, β -actin.

Table 3.3. The primary antibodies targeting the proteins of interest.

Protein	Antibody titer	Type of samples	Brand of antibody
β -actin	1:10000	Cell lysate extract, cell culture supernatant, nuclear and cytoplasmic fractions.	St John's Laboratory (London, UK)
NF- κ B p65	1:1000	Nuclear and cytoplasmic fractions.	GeneTex (California, USA)
Phosphorylated-NF- κ B p65	1:500	Nuclear and cytoplasmic fractions.	St John's Laboratory (London, UK)
PPAR- γ	1:1000	Nuclear and cytoplasmic fractions.	Thermo Fisher Scientific (Massachusetts, USA)
Phosphorylated-PPAR- γ	1:500	Nuclear and cytoplasmic fractions.	St John's Laboratory (London, UK)
STAT3	1:1000	Nuclear and cytoplasmic fractions.	GeneTex (California, USA)
Phosphorylated-STAT3	1:1000	Nuclear and cytoplasmic fractions.	GeneTex (California, USA)
MCP-1	1:1000	Cell culture supernatant.	St John's Laboratory (London, UK)
IL-8	1:1000	Cell culture supernatant.	GeneTex (California, USA)
GPx	1:1000	Cell lysate extract.	St John's Laboratory (London, UK)
VEGF	1:1000	Cell culture supernatant.	St John's Laboratory

			(London, UK)
MMP2	1:1000	Cell culture supernatant.	St John's Laboratory (London, UK)
RAGE	1:1000	Cell lysate extract.	St John's Laboratory (London, UK)
SOCS1	1:1000	Cell lysate extract.	GeneTex (California, USA)

3.4.5.7 Soluble RAGE (sRAGE) quantification

3.4.5.7.1 Principle

Enzyme-linked immunosorbent assay (ELISA) is a sensitive immunoassay commonly used for the quantification of specific proteins via antibody-antigen interaction (Sakamoto *et al.*, 2018). In this assay, the captured antibody specific to the protein of interest is coated onto the well of microplate (Anagu and Andoh, 2022). The protein of interest should contain more than one antigenic site for antibody binding (Anagu and Andoh, 2022). The first antigenic site of target protein in the complex protein mixture is captured by the coated antibody (Anagu and Andoh, 2022). This is followed by the binding of enzyme-labelled antibody to the second antigenic site (Anagu and Andoh, 2022). Enzyme-substrate reaction follows the addition of chromogenic substrate, which leads to development of colour for colorimetric measurement (Sakamoto *et al.*, 2018).

3.4.5.7.2 Procedure

The quantification of sRAGE secreted by ARPE-19 cells was performed with sandwich ELISA by following the manufacturer's instruction of a commercial kit. The cell culture supernatant (30 µg/100 µL) was incubated with the captured anti-sRAGE primary antibodies located on the 96-wells microplate. After incubating at 37°C for 90 minutes, the content in the wells were discarded and the wells were washed twice with wash buffer by using a squeeze bottle. The microplate was incubated at room temperature for 2 minutes in between washes. Then biotin-labelled antibody solution (100 µL) was added to the well and incubated at 37°C for 60 minutes. After washing the plate for 3 times, horseradish peroxidase-streptavidin conjugate solution (100 µL) was added and incubated at 37°C for 30 minutes. Ninety microliters of 3,3',5,5'-tetramethylbenzidine substrate solution was then added after the wells were washed for 5 times. The microplate was incubated at 37°C for 20 minutes in the dark. The reaction was then terminated by adding 50 µL of 0.2 M sulphuric acid into the wells. The absorbance was measured at 450 nm with a microplate reader against the sample blank. The human sRAGE provided in the kit was served as the standard (0-1000 pg/mL). The total sRAGE (pg/ml) in ARPE-19 was calculated as follows:

$$\text{Total sRAGE (pg/ml)} = \left[\frac{\text{Concentration of standard equivalent}}{\text{Concentration of cell culture supernatant protein}} \right]$$

3.5 Phase 3: Identification of phytochemicals

3.5.1 Purification of phytochemicals

3.5.1.1 Thin-layer chromatography (TLC)

3.5.1.1.1 Principle

TLC is a low cost and rapid chromatographic technique capable of separating a complex mixture of chemical compounds (Santiago and Strobel, 2013). Due to its reproducibility, TLC is commonly used for phytochemical profiling and to determine the purity of isolated compound (Santiago and Strobel, 2013). In TLC, a thin layer of silica gel on the aluminum or glass plate serves as the stationary phase (Gillings, 2021). Through capillary action, the solvent which acts as the mobile phase transports the samples upward through the plate (Gillings, 2021). The compounds are separated based on their affinity towards the stationary and mobile phases (Gillings, 2021).

3.5.1.1.2 Procedure

TLC was performed to determine the phytochemical profile and identify suitable solvent system for the subsequent purification of phytochemicals from *P. pellucida* crude methanolic extract. The aluminium TLC plate serves as the stationary phase while the solvent system chloroform-hexanes (1:1) serves as the mobile phase. A horizontal line was drawn about 5 mm from the bottom of the plate using pencil. A piece of filter paper was used as a wick to saturate the developing chamber with solvent vapours. The solvent was poured into the chamber about 5 mm in depth. The crude methanolic extract was dissolved with chloroform at a concentration of 10 mg/ml and spotted onto the drawn line with a capillary

spotter. The TLC plate was placed at a 30° angle in the chamber with the top facing upwards. It was carefully taken out using forceps once the solvent front had migrated approximately 10 mm from the top of the plate. The TLC plate was left to dry before being visualised under short-wave (254 nm) or medium wave (315 nm) ultraviolet light. Several TLC spots were only visible under the ultraviolet light, hence these spots were circled with pencil. The retention factor (R_f) values were determined by dividing the distance travelled by the spot (mm) with the distance travelled by the solvent (mm). The solvent system that yielded a R_f value of less than 0.25 was selected as the mobile phase.

3.5.1.2 Silica gel column chromatography

3.5.1.2.1 Principle

The working mechanism of silica gel column chromatography is similar to that of TLC but with a higher sample loading capacity (Srivastava *et al.*, 2021). As the name of the technique suggests, column chromatography involves the packing of stationary phase, silica gel in a glass column (Singh *et al.*, 2021). Prior to separation, the sample is adhered onto the stationary phase either as concentrated solution or preadsorbed solid (Poole, 2003). Rather than capillary action, the separation of components is achieved through the gravitational migration of a suitable mobile phase to the lower end of the column (Srivastava *et al.*, 2021). The movement of mobile phase is facilitated by the vacuum generated at the bottom of the column (Poole, 2003). The separation results in the formation of discrete phytochemical bands, which are eluted out from the column with the mobile phase (Srivastava *et al.*, 2021).

3.5.1.2.2 Procedure

Silica gel column chromatography was performed based on the method described by de Moraes and Kato (2021) with slight modifications. One-third of the glass column was packed with dry silica gel and conditioned with chloroform-hexanes (1:1), which served as the mobile phase. Sodium sulphate was then added on top of the silica gel layer as drying agent to remove moisture from the solvent. The silica gel layer was covered with solvent during the whole process to avoid being dried out. The crude methanolic extract (15 g) was dissolved in the mobile phase and introduced on top of the sodium sulphate layer with glass pasteur pipette. After the sample was entirely adsorbed onto the silica gel layer, two-third of the column was refilled with the mobile phase. This step was critical to prevent dilution of the sample. The semi-purified fractions (250 ml each) were collected in rotary flasks by eluting with a gradient of chloroform-hexanes (50:50-100:0), chloroform-methanol (99:1-80:20) and absolute EtOH. Similar semi-purified fractions were pooled based on TLC profiling and concentrated with rotary evaporator.

3.5.1.3 Preparative radial chromatography (PRC)

3.5.1.3.1 Principle

PRC is a efficient chromatographic technique which utilises centrifugal force to separate a complex mixture of phytochemicals present in plant matrix (Agrawal and Desai, 2015). The spinning rotor in the Chromatotron® generates centrifugal force which propels the eluting mobile phase through a layer of sorbent coated on a circular glass (Muhammad *et al.*, 2013). The sorbent such as silica gel with gypsum and alumina acts as a stationary phase (Muhammad *et al.*, 2013). The mixture

of compounds are separated into circular bands as the mobile phase elutes the sample through the stationary phase (Agrawal and Desai, 2015). The factors affecting the separation of mixture with PRC include the rate of rotation, the thickness of silica as well as the polarity and flow rate of mobile phase (Agrawal and Desai, 2015).

3.5.1.3.2 Procedure

The semi-purified fractions were subjected to further purification with PRC using Harrison Research Chromatotron® 7924T (New Jersey, USA) as described by de Moraes and Kato (2021) with slight modifications. The semi-purified fractions were dissolved in chloroform and applied onto silica gel near the center of the rotating rotor. The samples were eluted with mobile phases of different solvent systems such as chloroform-hexanes, diethyl ether-hexanes or dichloromethane-hexanes. The separated bands were visualised under the 254 nm and 315 nm ultraviolet light. Similar fractions were pooled based on TLC profiling.

3.5.2 Characterisation of phytochemicals

3.5.2.1 Nuclear magnetic resonance (NMR) spectroscopy

3.5.2.1.1 Principle

NMR spectroscopy is a non-destructive characterisation technique that applies radio frequency energy to the isotopes of atomic nucleus of hydrogen-1 (^1H) and carbon-13 (^{13}C) to determine the atomic resonance frequency according to its chemical structure (Stark *et al.*, 2016). The application of radio frequency energy to the molecule will change the nuclear spins of ^1H and ^{13}C , thereby creating a magnetic field (Stark *et al.*,

2016). The electrons in an atom either oppose or circulate along the direction of magnetic field, generating an induced magnetic field at the nucleus (Stark *et al.*, 2016). Furthermore, the electron density around the nucleus differs across molecules, which results in varying strength of electron shielding (Louro, 2013). Electron shielding affects the magnetic field experienced by the nucleus and the radio frequency wave required for the nucleus to achieve resonance (Louro, 2013). As a result, different types of phytochemicals display varying degree of chemical shift, which is expressed in parts per million (ppm) (Louro, 2013).

3.5.2.1.2 Procedure

¹H NMR and ¹³C NMR spectroscopy were carried out with the Bruker Ascend 400 MHz NMR spectrometer (Massachusetts, USA). The semi-purified fractions were dissolved in deuterated chloroform (CDCl₃) containing 0.03 % (v/v) tetramethylsilane and silver foil as stabilisers. Tetramethylsilane was also served as the internal standard. The semi-purified fractions (10 mg/ml) were added into either thin walled or heavy walled NMR tube depending on the sample yield. Heavy walled NMR tubes were used for fractions with low sample concentration (<10 mg/ml) to minimise dilution of the sample. The NMR data were processed with the program MestreNova version 14.2.1-27684. The scale was adjusted to the tetramethylsilane signal as 0.00 ppm.

3.5.2.2 Ultraviolet-visible (UV-Vis) spectroscopy

3.5.2.2.1 Principle

The UV-Vis spectroscopy is another characterisation method which is based on the compound absorption of UV-Vis light with the wavelength ranging from 180 to 750 nm (Rakhee *et al.*, 2018). This spectroscopic method takes advantage of the presence of functional groups or chromophores in phytochemicals for identification (Daéid, 2019). The chromophores absorb UV-Vis light of specific wavelength and undergoes excitation from the ground state (Rakhee *et al.*, 2018). The resultant spectrum then aids in the identification of compounds. According to Beer Lambert law, the concentration of sample is directly proportional to the absorption of light by the chromophores at a specific wavelength (Daéid, 2019).

3.5.2.2.2 Procedure

UV-Vis spectroscopy was carried out on a Shimadzu UV-2600 UV-Vis spectrophotometer (Kyoto, Japan). The semi-purified fractions (0.2 mg) were dissolved in 10 ml of absolute EtOH in the volumetric flask. The quartz cuvette was two-third filled with the dissolved sample and inserted into the cuvette holder of the UV-Vis spectrophotometer. The absorbance was measured with a spectral ranged between 200 nm and 700 nm. The absolute EtOH served as the blank. The UV-Vis data was processed with the LabSolutions UV-Vis program version 1.1.

3.5.2.3 Fourier-transform infrared (FTIR) spectroscopy

3.5.2.3.1 Principle

FTIR spectroscopy is a useful spectroscopic technique that utilises electromagnetic wave in the infrared region to detect different functional

groups present in the phytochemicals (Mallakpour *et al.*, 2020). The transparent zinc selenide crystal with high refractive index is used as the infrared sampling optics as it is highly resistant to a diverse range of chemicals (Perkin Elmer, 2014). The atoms in the functional groups undergo excitation to a vibrational state either through stretching and bending upon exposure to the infrared radiation of a specific wavelength (Shojaei *et al.*, 2018). The FTIR spectrum is the result of the intensity and frequency of vibrations among the bonds of atoms which produces the absorption peak (Daéid, 2019).

3.5.2.3.2 Procedure

The FTIR analysis of purified fractions was carried out on a Perkin Elmer Spectrum 400 FTIR spectrometer (Massachusetts, USA). Fifty microliters of sample (10 mg/ml) was dissolved in chloroform and placed on the zinc selenide crystal located in the center of sample platform. After the sample was fully dried, the metal compression bar was lowered to press the sample against the crystal. Then the FTIR spectrum of sample was measured at a range of 450–4000 cm^{-1} . The spectrometer was blanked with an empty platform prior to analysis. The FTIR spectral data was processed and analysed with the Spectrum 10 spectroscopy software version 10.4.3.

3.5.2.4 Liquid chromatography-mass spectrometry (LC-MS)

3.5.2.4.1 Principle

LC-MS is a powerful metabolomic analytical technique used for separation and identification of polar phytochemicals (Mukherjee, 2019).

The coupling of the separation ability of liquid chromatography with the mass analysis capability of electrospray ionization mass spectrometry (ESIMS) makes LC-MS a highly sensitive and selective tool for compound identification (Tilvi *et al.*, 2014). The eluted compounds in chromatographic separation will be ionised by high electrical voltage in the metal capillary (Chappell *et al.*, 2021). The ionised molecules passages through the magnets and are resolved based on their m/z ratio in the mass spectrometer (Chappell *et al.*, 2021). The signals are then detected by the detector, which results in the mass spectrum that displays the m/z of the compound (Chappell *et al.*, 2021).

3.5.2.4.2 Procedure

Mass analysis of the semi-purified compounds and identification of polar compounds were performed on the Agilent Technologies 1290 Infinity LC system (California, USA) equipped with a binary pump. For mass analysis, the LC system was interfaced with the Agilent Technologies 6490 triple quadrupole (QQQ) mass spectrometer with electrospray ion source (California, USA). Full-scan mode with m/z range of 100 to 1000 was performed with a fragmentation voltage and source temperature of 140 V and 300°C, respectively. The sample (20 ppm) was dissolved in methanol and the injection volume was 2 µl. The stationary phase, Agilent ZORBAX Eclipse XDB-C18 HPLC column (2.1 x 100 mm, 1.8 µm) was maintained at 40°C. The mobile phase, acetonitrile-water (6:4) was delivered at a total flow rate of 1.4 ml/min. LC-QQQ-MS post-run analysis was performed with the Agilent MassHunter software version B.07.00.

For the identification of polar compounds in *P. pellucida*, the LC system was interfaced with the Agilent Technologies 6520 Accurate-Mass

quadrupole time-of-flight (QToF) mass spectrometer with dual electrospray ion source (California, USA). Positive and negative ionization were used to acquire the data with m/z range of 100 to 3200. Full-scan mode was performed with a fragmentation voltage and source temperature of 125V and 300°C, respectively. The sample (1000 ppm) was dissolved in EtOH and the injection volume was 2 μ l. The stationary phase, Agilent ZORBAX Eclipse XDB-C18 HPLC column (2.1 x 150 mm, 3.5 μ m) was maintained at 25°C. The mobile phase, 0.1 % formic acid in water (A) and 0.1 % formic acid in acetonitrile (B) was delivered at a total flow rate of 0.5 ml/min and a total time of 30 minutes in the following settings: 0 to 20 minutes, 5 % B; 20 to 30 minutes, linear gradient from 5 % to 100 % B. LC-QToF-MS post-run analysis was performed with the Agilent MassHunter software version B.07.00. The mass spectrum of the compounds was matched against the METLIN metabolomics Database and Library (Metlin_AM_PCDL-N-170502.cdb) for the identification of polar compounds (Sana *et al.*, 2008). Briefly, the compounds that are present in the solvent blank were omitted from sample analysis. The shortlisted compounds meeting the criteria of a database (Db) score or molecular formula generator (MFG) score of 90 % or higher, and falling within the range of -2 to +2 for Diff(Db.ppm) or Diff(MFG.ppm) values were selected.

3.5.2.5 Gas chromatography-mass spectrometry (GC-MS)

3.5.2.5.1 Principle

GC-MS is an efficient metabolomic analytical method employed to detect non-polar volatile compounds (Rockwood *et al.*, 2018). It is based on the specific retention time, elution and mass fragmentation pattern of each individual constituent in a complex mixture of compounds (Mani *et al.*,

2017). GC-MS begins with the separation of gaseous mixture of compounds through the analytical column under high temperature (Rockwood *et al.*, 2018). The individual compounds are fragmented into ions in the MS ionising chamber after eluting from the column (Mani *et al.*, 2017). The fragments with specific mass to charge ratio are then detected by the electron multiplier in the detector (Mani *et al.*, 2017). This produces a mass spectrum that displays the relative abundance of the individual compounds with different mass to charge (m/z) ratio (Rockwood *et al.*, 2018).

3.5.2.5.2 Procedure

The identification of non-polar volatile compounds in *P. pellucida* crude methanolic extract was performed with GC-MS on Shimadzu GCMS-QP2010 Ultra (Kyoto, Japan) equipped with Rtx 5MS silica capillary column (30 m \times 0.25 mm \times 0.25 μ m). One microliter of sample (20 ppm) was dissolved in dichloromethane and injected splitless with the autosampler and subjected to GC-MS analysis under the programmed temperature of 60–250°C with a thermal ramp rate of 3°C per minute. The flow rate of carrier gas helium was 1.6 ml/min with linear velocity of 46 cm/s and 70 eV electron ionization. The temperature of injector, ion source and transfer line was 250°C for the Shimadzu gas chromatograph GC-2010 Plus (Kyoto, Japan). The mass spectrum was recorded at a mass scan range of 30–400 m/z with 70 eV electron ionization. GC-MS real-time and post-run analysis were performed with the Shimadzu GCMSsolution software version 2.6. The compounds were identified by comparison of mass spectrum and RI of known compounds in the National Institute of Standards and Technology library.

3.6 Statistical analysis

All experiments were performed in triplicate and the data was expressed as mean \pm standard deviation. The normality of the data distribution was evaluated prior to the data analysis. Statistical significance of the mean values among the samples was determined by using unpaired T-test and one-way ANOVA with Tukey post test. Pearson's linear correlation test was used to determine the correlation between the biological activities and phytochemicals. Principal component analysis (PCA) was carried out to evaluate the variables that were responsible for the variation in biological activity. P-values of less than 0.05 were considered statistically significant. All data was analysed by using GraphPad Prism® for Windows® version 8.4.3 and XLSTAT 2018 software for Microsoft Excel program (Addinsoft Inc., New York, U.S.).

Chapter IV

Results

4.1 Phase 1: The biological activities and phytochemicals of *P. pellucida*

4.1.1 Plant extraction yield

In this study, the extraction yield of *P. pellucida* crude methanolic extract was determined to be 14.22 % of the coarse plant powder. On the other hand, the extraction yield of plant solvent fractions ranged from 0.99 % to 5.93 % (Table 4.1). The yield of plant fractions decreased in the following order: hexane > aqueous > ethyl acetate > chloroform > n-butanol, which was different from the solvent polarity trend as followed: aqueous > n-butanol > ethyl acetate > chloroform > hexane. The above contrasting findings clearly showed that both non-polar (hexane) and polar (aqueous) fractions gave the highest extraction yield among the solvent fractions derived from *P. pellucida* crude methanolic extract. Nevertheless, low extraction yield was also observed for the non-polar chloroform fraction. Both ethyl acetate and n-butanol fractions of medium polarity also displayed relative low extraction yield when compared to the aqueous and hexane fractions. Interestingly, the extraction yield of ethyl acetate fraction was higher than that of chloroform fraction. The lowest extraction yield was observed in the n-butanol fraction.

4.1.2 Phytochemicals

The TPC of *P. pellucida* crude methanolic extract and solvent fractions ranged from 10.29 mg GAE/g to 24.10 mg GAE/g, in which non-polar chloroform fraction and moderately-polar n-butanol and ethyl acetate

fractions displayed relatively high TPC (Table 4.1). This were preceded by the polar crude methanolic extract and aqueous fraction, respectively. The lowest TPC was found in the non-polar hexane fraction. On the other hand, the TFC of *P. pellucida* fractions spanned from 4.88 mg Qct/g to 25.91 mg Qct/g. The n-butanol fraction showed the highest TFC, followed by the hexane fraction. Both ethyl acetate and aqueous fractions exhibited relative similar TFC. This was followed by the crude methanolic extract, which demonstrated a 15 % lower in TFC than the ethyl acetate and aqueous fractions. Despite the high TPC, the chloroform fraction displayed the lowest TFC. On the contrary, non-polar hexane fraction with low TPC contained significant amount of TFC.

In this study, the tannin content of *P. pellucida* solvent fractions ranged between 0.06 mg TAE/g and 1.04 mg TAE/g while the alkaloid content of *P. pellucida* varied from 3.07 mg BCE/g to 44.27 mg BCE/g. Among the plant solvent fractions, chloroform fraction showed the highest level of tannins (1.04 mg TAE/g) and alkaloids (44.27 mg BCE/g). The tannin content was preceded by the ethyl acetate fraction with 0.40 mg BCE/g. The crude methanolic extract, hexane and n-butanol fractions shared similar tannin content. The lowest tannin content was observed in the aqueous fraction. Except chloroform fraction, a similar alkaloid level was found in the remaining solvent fractions. Furthermore, *P. pellucida* solvent fractions showed a wider range of saponin, from 4.15 mg QSE/g to 249.43 mg QSE/g. The highest saponin content was detected in the moderately polar ethyl acetate fraction, followed by n-butanol (79.65 QSE/g) fraction. Both non-polar hexane and chloroform showed similar level of saponin content (34.01-36.60 mg QSE/g), which was twice the amount observed for crude methanolic extract (19.06 mg QSE/g). The lowest saponin content was shown by the aqueous fraction.

Table 4.1. The extraction yield, total phenolic, flavonoid, tannin, saponin and alkaloid content of *P. pellucida* crude methanolic extract and fractions.

<i>P. pellucida</i> extracts	Extraction yield (%)	TPC (mg GAE/g)	TFC (mg Qct/g)	Tannin content (mg TAE/g)	Saponin content (mg QSE/g)	Alkaloid content (mg BCE/g)
Crude methanolic extract	14.22 ± 3.7 ^a	16.69 ± 0.48 ^a	10.36 ± 0.41 ^a	0.13 ± 0.07 ^a	19.06 ± 5.69 ^a	10.53 ± 1.82 ^a
Hexane fraction	5.93 ± 3.06 ^{b**}	10.29 ± 0.52 ^{b****}	21.39 ± 0.68 ^{b****}	0.21 ± 0.01 ^a	36.60 ± 7.91 ^{b*}	15.41 ± 1.80 ^a
Chloroform fraction	1.08 ± 0.83 ^{c***}	22.04 ± 1.28 ^{c****}	4.88 ± 0.67 ^{c***}	1.04 ± 0.15 ^{b*}	34.01 ± 4.91 ^{b*}	44.27 ± 2.61 ^{b*}
Ethyl acetate fraction	1.65 ± 0.93 ^{c***}	22.25 ± 1.19 ^{c****}	13.77 ± 1.30 ^{d*}	0.40 ± 0.01 ^{c****}	249.43 ± 3.50 ^{c****}	3.07 ± 0.72 ^a
n-Butanol fraction	0.99 ± 0.70 ^{c***}	24.10 ± 0.26 ^{c****}	25.91 ± 1.33 ^{e****}	0.16 ± 0.01 ^a	79.65 ± 1.97 ^{d*}	14.32 ± 3.15 ^a
Aqueous fraction	5.08 ± 2.53 ^{b**}	13.38 ± 0.14 ^{d**}	12.13 ± 1.22 ^{d*}	0.06 ± 0.00 ^{d**}	4.15 ± 0.96 ^{e*}	6.96 ± 2.54 ^a

Note: Values are mean ± standard deviation of three independent determinations. Different superscript letters within the same column indicate significant ($p < 0.05$) differences of means among the fractions. The level of significance is expressed as $p < 0.05$ (*), $p < 0.01$ (**), $p < 0.005$ (***), $p < 0.001$ (****). mg BCE, miligram berberine chloride equivalent; mg GAE, miligram gallic acid equivalent; mg Qct, miligram quercetin equivalent; mg QSE, miligram quillaja saponin equivalent; mg TAE, miligram tannic acid equivalent; TFC, total flavonoid content; TPC, total phenolic content.

4.1.3 Antioxidant activities and indices

The *P. pellucida* crude methanolic extract and five solvent fractions displayed FRAP value ranging from 0.09 mmol Fe²⁺/g to 0.80 mmol Fe²⁺/g (Table 4.2). The ethyl acetate fraction showed the highest FRAP activity among the plant fractions, followed by n-butanol (0.52 mmol Fe²⁺/g) and chloroform (0.47 mmol Fe²⁺/g) fractions. Both crude methanolic extract and hexane fraction displayed similar FRAP value. The aqueous fraction displayed the lowest FRAP activity. The ethyl acetate, n-butanol and chloroform fractions with high TPC showed relatively high FRAP activity.

The IC₅₀ for DPPH and ABTS radicals scavenging activities varied from 0.08 mg/ml to 0.69 mg/ml, and 0.24 mg/ml to 1.16 mg/ml, respectively (Table 4.2). For both DPPH and ABTS radical scavenging, the strongest radical scavenging activity was found in moderately polar ethyl acetate fraction due to the lowest IC₅₀ for DPPH and ABTS scavenging activities. The non-polar hexane fraction displayed the weakest radical scavenging activity. In general, the DPPH radical scavenging activity for all *P. pellucida* solvent fractions were higher than their ABTS radical scavenging activity. However, both DPPH and ABTS radicals scavenging activities of solvent fractions were still weaker when compared to their respective standards ascorbic acid (IC₅₀ = 0.004 mg/ml) and Trolox (IC₅₀ = 0.01 mg/ml). The DPPH radical scavenging activity trends in crude methanolic extract, hexane, chloroform and aqueous fractions were different than their ABTS radical scavenging trend. For instance, the aqueous fraction showed comparable DPPH scavenging activity with crude methanolic extract and chloroform fraction, but lowest ABTS scavenging activity along with hexane fraction.

Table 4.2. The antioxidant activity of *P. pellucida* crude methanolic extract and fractions.

<i>P. pellucida</i> extracts	FRAP (mmol Fe ²⁺ /g)	DPPH radical scavenging activity (IC ₅₀ , mg/ml) ¶	ABTS radical scavenging activity (IC ₅₀ , mg/ml) †	Lipid peroxidation inhibitory activity (IC ₅₀ , mg/ml) ‡
Crude methanol extract	0.19 ± 0.01 ^a	0.21 ± 0.01 ^a	0.54 ± 0.01 ^a	0.022 ± 0.002 ^a
Hexane fraction	0.21 ± 0.01 ^a	0.69 ± 0.06 ^{b****}	1.16 ± 0.02 ^{b****}	0.022 ± 0.003 ^a
Chloroform fraction	0.47 ± 0.03 ^{b****}	0.21 ± 0.02 ^a	0.79 ± 0.01 ^{c****}	0.019 ± 0.001 ^{b*}
Ethyl acetate fraction	0.80 ± 0.02 ^{c****}	0.08 ± 0.00 ^{d****}	0.24 ± 0.00 ^{d****}	0.010 ± 0.00 ^{c****}
n-Butanol fraction	0.52 ± 0.01 ^{d****}	0.14 ± 0.01 ^{c*}	0.29 ± 0.00 ^{e****}	0.030 ± 0.00 ^{d***}
Aqueous fraction	0.09 ± 0.00 ^{e****}	0.28 ± 0.01 ^a	1.19 ± 0.01 ^{b****}	0.021 ± 0.002 ^a

Note: Values are mean ± standard deviation of three independent determinations. Different superscript letters within the same column indicate significant (p<0.05) differences of means among the fractions. The level of significance is expressed as p<0.05 (*), p<0.01 (**), p<0.005 (***), p<0.001 (****). ABTS, 2, 2'-azino-bis (3-ethylbenzothiazoline-6-sulfonate); DPPH, 2, 2-diphenyl-2-picrylhydrazyl; IC₅₀, half-maximal inhibitory concentration; FRAP, ferric-reducing antioxidant power; mmol Fe²⁺, millimole ferrous ions equivalent.

¶ The IC₅₀ for standard ascorbic acid was 0.004 mg/ml. † The IC₅₀ for standard Trolox was 0.010 mg/ml. ‡ The IC₅₀ for standard ascorbic acid was 0.004 mg/ml.

In this study, the ethyl acetate fraction displayed high lipid peroxidation inhibitory activity ($IC_{50} = 0.01$ mg/ml) that was comparable to that of the standard ascorbic acid ($IC_{50} = 0.004$ mg/ml). However, the weakest lipid peroxidation inhibitory activity was found in the other moderately polar n-butanol fraction with the largest IC_{50} value at 0.03 mg/ml. The lipid peroxidation inhibitory activity ($IC_{50} = 0.019$ - 0.022 mg/ml) among the crude methanolic extract, hexane, chloroform and aqueous fractions were not significantly different. Interestingly, moderate lipid peroxidation inhibitory activity was exhibited in the polar and non-polar solvent fractions.

The AI index of *P. pellucida* crude methanolic extract and solvent fractions was determined based on their performance in antioxidant assays, including FRAP, ABTS, DPPH and lipid peroxidation inhibitory assays. Based on the results, the ethyl acetate and n-butanol fractions were ranked as very high and high antioxidant fractions, respectively while the rest of fractions were classified as moderate AI fractions (Table 4.3). Interestingly, none of the extracts were graded as low AI fraction. The ethyl acetate fraction was classified as very high AI fraction due to its highest FRAP, DPPH and ABTS radicals scavenging and lipid peroxidation inhibitory activities among the solvent fractions. For n-butanol fraction, the high AI can be derived from its relatively high FRAP, DPPH and ABTS scavenging activities. The moderate AI observed in the remaining solvent fractions can be derived from their distinctive effects in various antioxidant assays. For instance, both aqueous and hexane fractions exhibited moderate lipid peroxidation inhibitory activity. In addition to that, crude methanolic extract and chloroform fraction demonstrated moderate ABTS scavenging activity and FRAP activity, respectively.

Table 4.3. The antioxidant index of *P. pellucida* crude methanolic extract and fractions.

<i>P. pellucida</i> extracts	FRAP (mmol Fe ²⁺ /g)	DPPH (IC ₅₀ , mg/ml)	ABTS (IC ₅₀ , mg/ml)	Lipid peroxidation (IC ₅₀ , mg/ml)	Relative % FRAP	Relative % DPPH	Relative % ABTS	Relative % Lipid peroxidation inhibition	AI	Category
Ethyl acetate fraction	0.80	0.08	0.24	0.01	100	100	100	100	100	Very high
n-Butanol fraction	0.52	0.14	0.29	0.03	65	57	83	33	60	High
Chloroform fraction	0.47	0.20	0.79	0.02	59	38	30	50	44	Moderate
Crude methanolic extract	0.19	0.21	0.54	0.02	24	38	44	50	39	Moderate
Aqueous fraction	0.09	0.28	1.19	0.02	11	29	20	50	27	Moderate
Hexane fraction	0.21	0.69	1.16	0.02	26	12	21	50	28	Moderate

Note: The plants are graded into very high (76-100 %), high (51-75 %), moderate (26-50 %) and low (0-25 %) antioxidant potentials. The percentage relative value for each sample in each assay is based on the highest value in each assay. ABTS, 2, 2'-azino-bis (3-ethylbenzothiazoline-6-sulfonate; AI, antioxidant index; DPPH, 2, 2-diphenyl-2-picrylhydrazyl; IC₅₀, half-maximal inhibitory concentration; FRAP, ferric-reducing antioxidant power; mmol Fe²⁺, millimole ferrous ions equivalent.

4.1.4 Anti-inflammatory activities and indices

4.1.4.1 COXs inhibitory activity

In this study, the overall COX-1 and COX-2 inhibitory activities of *P. pellucida* fractions ranged from 10.60 % to 82.60 %. The non-polar hexane fraction showed the highest inhibitory activity against COX-1 and COX-2 at 82.6 % and 76.65 %, respectively (Table 4.4). This was preceded by the *P. pellucida* crude methanolic extract with 71.18 % and 72.89 % of inhibition against COX-1 and COX-2, respectively. Interestingly, the chloroform and aqueous fractions exhibited greater COX-1 inhibitory activity compared to the ethyl acetate fraction, while demonstrating lower COX-2 inhibitory activity than the latter. The lowest COX-1 and COX-2 inhibitory activities were observed in n-butanol fraction. Based on the overall trend in COXs inhibitory activity, the majority of the *P. pellucida* solvent fractions expressed higher COX-1 inhibition than COX-2.

4.1.4.2 LOX inhibitory activity

The IC₅₀ for the LOX inhibitory activity of solvent fractions ranged from 0.01 mg/ml to 0.03 mg/ml (Table 4.4). The strongest LOX inhibitory activity was observed in the ethyl acetate, n-butanol and hexane fractions, which equally displayed the lowest IC₅₀ without any significant difference. This was followed by the chloroform fraction with IC₅₀ of 0.02 mg/ml. The crude methanolic extract and aqueous fraction each displayed similar LOX inhibitory activity (IC₅₀ = 0.03 mg/ml). Remarkably, the IC₅₀ of LOX inhibitory activities for ethyl acetate, n-butanol and hexane fractions were comparable to that of the standard quercetin (0.007 mg/ml).

Table 4.4. The anti-inflammatory activity of *P. pellucida* crude methanolic extract and fractions.

<i>P. pellucida</i> extracts	COX-1 inhibition (%) #	COX-2 inhibition (%) #	LOX inhibition (IC ₅₀ , mg/ml) Δ	XO inhibition (IC ₅₀ , mg/ml) Ⓔ	hyaluronidase inhibition (IC ₅₀ , mg/ml) Ω
Crude methanolic extract	71.18 ± 1.25 ^a	72.89 ± 0.23 ^a	0.03 ± 0.01 ^a	0.052 ± 0.01 ^a	0.22 ± 0.01 ^a
Hexane fraction	82.60 ± 4.77 ^{b**}	76.65 ± 2.28 ^a	0.010 ± 0.002 ^{b****}	0.093 ± 0.02 ^a	0.233 ± 0.003 ^a
Chloroform fraction	40.09 ± 0.57 ^{c****}	12.45 ± 0.99 ^{b****}	0.02 ± 0.00 ^{c*}	0.102 ± 0.01 ^a	0.233 ± 0.004 ^a
Ethyl acetate fraction	31.94 ± 3.91 ^{d****}	49.59 ± 2.09 ^{c****}	0.013 ± 0.001 ^{b****}	0.085 ± 0.02 ^a	0.43 ± 0.00 ^{b****}
n-Butanol fraction	19.72 ± 3.12 ^{e****}	10.60 ± 1.37 ^{b****}	0.013 ± 0.002 ^{b****}	0.042 ± 0.01 ^a	0.50 ± 0.02 ^{c****}
Aqueous fraction	38.85 ± 1.39 ^{c****}	21.12 ± 1.37 ^{d****}	0.03 ± 0.00 ^a	0.112 ± 0.03 ^{b*}	0.61 ± 0.03 ^{d****}

Note: Values are mean ± standard deviation of three independent determinations. Different superscript letters within the same column indicate significant (p<0.05) differences of means among the fractions. The level of significance is expressed as p<0.05 (*), p<0.01 (**), p<0.005 (***), p<0.001 (****). COX, cyclooxygenase; IC₅₀, Half-maximal inhibitory concentration; LOX, lipoxygenase; XO, xanthine oxidase.

Δ The IC₅₀ for standard quercetin was 0.007 mg/ml. Ⓔ The IC₅₀ for standard quercetin was 0.001 mg/ml. Ω The IC₅₀ for standard tannic acid was 0.017 mg/ml.

Sample concentration at 0.5 mg/ml.

4.1.4.3 XO inhibitory activity

In this study, ethyl acetate, n-butanol, hexane fractions and crude methanolic extract shared the strongest XO inhibitory activities (Table 4.4) among the plant fractions. This was preceded by the chloroform ($IC_{50} = 0.102$ mg/ml) fraction. Besides, the lowest XO inhibitory activity was detected in the polar aqueous fraction with IC_{50} of 0.112 mg/ml. The overall IC_{50} for XO inhibitory activity of *P. pellucida* extracts was also found to be higher, ranging from 0.052 mg/ml to 0.112 mg/ml, compared to the IC_{50} of standard quercetin at 0.001 mg/ml.

4.1.4.4 Hyaluronidase inhibitory activity

The IC_{50} of hyaluronidase inhibition activity for *P. pellucida* crude methanolic extract and solvent fractions ranged from 0.22 mg/ml to 0.61 mg/ml (Table 4.4). The standard tannic acid displayed significant hyaluronidase inhibitory activity ($IC_{50} = 0.017$ mg/ml). Among the *P. pellucida* fractions, the crude methanolic extract, hexane and chloroform fractions displayed the strongest hyaluronidase inhibitory activity (lowest IC_{50} values). This was followed by the moderately polar ethyl acetate ($IC_{50} = 0.43$ mg/ml) and n-butanol ($IC_{50} = 0.50$ mg/ml) fractions, respectively. The weakest hyaluronidase inhibitory activity was exhibited by the polar aqueous fraction with the highest IC_{50} value. The trend of hyaluronidase inhibitory activity among the solvent fractions indicated that the hyaluronidase inhibitory activity decreased with increasing solvent polarity of the plant fractions.

Based on the AII index, six *P. pellucida* solvent fractions were equally grouped into either very high AII, high AII or moderate AII categories (Table 4.5). Out of the six plant fractions, four were ranked as

high AII category and above while no plant fraction was grouped into low AII category. Both hexane fraction and crude methanolic extract were graded as very high AII fractions due to their relatively high inhibitory activities against COXs and hyaluronidase while hexane fraction also showed strong LOX inhibitory activity. The moderately polar ethyl acetate and n-butanol fractions, which were ranked as high AI fractions were also classified as high AII fractions in the current study.

Table 4.5. The anti-inflammatory index of *P. pellucida* crude methanolic extract and fractions.

<i>P. pellucida</i> extracts	COX-1 inhibition (%)	COX-2 inhibition (%)	LOX inhibition (IC ₅₀ , mg/ml)	XO inhibition (IC ₅₀ , mg/ml)	Hyaluronidase inhibition (IC ₅₀ , mg/ml)	Relative % COX-1 inhibition	Relative % COX-2 inhibition	Relative % LOX inhibition	Relative % XO inhibition	Relative % hyaluronidase inhibition	AII	Category
Hexane fraction	82.60	76.65	0.010	93.72	0.23	100	100	100	45	95	88	very high
Crude methanolic extract	71.18	72.89	0.034	52.18	0.22	86	95	29	81	100	78	very high
Ethyl acetate fraction	31.94	49.59	0.013	85.75	0.43	39	65	77	49	51	56	high
n-Butanol fraction	19.72	10.60	0.013	42.43	0.50	24	14	77	100	44	52	high
Chloroform fraction	40.09	12.45	0.024	102.35	0.23	49	16	41	41	95	48	moderate
Aqueous fraction	38.85	21.12	0.026	112.30	0.61	47	28	38	38	36	37	moderate

Note: The plants are graded into very high (76-100 %), high (51-75 %), moderate (26-50 %) and low (0-25 %) anti-inflammatory potentials. The percentage relative value for each sample in each assay is based on the highest value in each assay. AII, anti-inflammatory index; COX, cyclooxygenase; IC₅₀, half-maximal inhibitory concentration; LOX, lipoxygenase; XO, xanthine oxidase.

4.1.5 Anti-glycaemic activities

4.1.5.1 α -glucosidase and α -amylase inhibitory activities

To date, the α -glucosidase and α -amylase inhibitory activities of *P. pellucida* is yet to be explored. Based on the current result, the IC_{50} for α -glucosidase inhibitory activity of *P. pellucida* crude methanolic extract and plant solvent fractions ranged from 0.07 mg/ml to 1.17 mg/ml (Table 4.6). There was no significant difference between the ethyl acetate and chloroform fractions, which displayed the strongest α -glucosidase inhibitory activity with the lowest IC_{50} relative to that of other solvent fractions. This was followed by the n-butanol fraction and crude methanolic extract. The lowest α -glucosidase inhibitory activity was observed in the non-polar hexane and polar aqueous fractions with the highest IC_{50} . The result showed that moderately polar fractions displayed stronger α -glucosidase inhibitory activity than the polar fractions. With the exception of hexane and aqueous fractions, the *P. pellucida* crude methanolic extract and the remaining solvent fractions also exhibited greater inhibition against α -glucosidase than the anti-diabetic drug acarbose, which served as the standard ($IC_{50} = 0.70$ mg/ml) in this study.

The IC_{50} for the α -amylase inhibitory activity ranged from 0.002 mg/ml to 0.009 mg/ml, in which the ethyl acetate, hexane fractions and crude methanolic extract, displayed relatively strong α -amylase inhibitory activity (Table 4.6). This was followed by n-butanol ($IC_{50} = 0.004$ mg/ml) and chloroform ($IC_{50} = 0.007$ mg/ml) fractions. The weakest α -amylase inhibitory activity was found in the aqueous fraction. The α -amylase inhibitory activity of crude methanolic extract and solvent fractions were generally stronger than the standard acarbose ($IC_{50} = 0.01$ mg/ml). In addition, the solvent fractions of *P. pellucida* exhibited greater inhibition against α -amylase compared to α -glucosidase.

Table 4.6. The anti-glycaemic and anti-glycation activities of *P. pellucida* crude methanolic extract and fractions.

<i>P. pellucida</i> extracts	Anti-glycaemic activity			Anti-glycation activity		
	α -glucosidase inhibition (IC ₅₀ , mg/ml) \ae	α -amylase inhibition (IC ₅₀ , mg/ml) \ae	Aldose reductase inhibition (IC ₅₀ , mg/ml) \ae	AGE inhibition (IC ₅₀ , mg/ml) \ae	Inhibition of dicarbonyl compound formation (%)#	Inhibition of Amadori product formation (%)#
Crude methanolic extract	0.48 \pm 0.02 ^a	0.003 \pm 0.00 ^a	0.12 \pm 0.01 ^a	0.800 \pm 0.02 ^a	9.08 \pm 2.06 ^a	25.27 \pm 1.85 ^a
Hexane fraction	0.92 \pm 0.22 ^{b***}	0.003 \pm 0.01 ^a	0.16 \pm 0.01 ^{b*}	0.801 \pm 0.02 ^a	11.49 \pm 1.14 ^a	30.16 \pm 4.05 ^a
Chloroform fraction	0.13 \pm 0.01 ^{c**}	0.007 \pm 0.01 ^{b****}	0.07 \pm 0.02 ^{c**}	0.793 \pm 0.02 ^a	4.89 \pm 1.03 ^{b*}	27.58 \pm 4.43 ^a
Ethyl acetate fraction	0.07 \pm 0.00 ^{c**}	0.002 \pm 0.00 ^a	0.07 \pm 0.01 ^{c**}	0.05 \pm 0.00 ^{b****}	10.69 \pm 1.06 ^a	31.42 \pm 2.90 ^a
n-Butanol fraction	0.40 \pm 0.02 ^a	0.004 \pm 0.00 ^{c*}	0.08 \pm 0.01 ^{c*}	0.790 \pm 0.00 ^a	7.29 \pm 0.94 ^a	27.05 \pm 3.96 ^a
Aqueous fraction	1.17 \pm 0.05 ^{b****}	0.009 \pm 0.01 ^{d****}	0.02 \pm 0.01 ^{d****}	1.12 \pm 0.02 ^{c****}	7.52 \pm 2.16 ^{ψa}	28.52 \pm 1.80 ^{ψa}

Note: Values are mean \pm standard deviation of three independent determinations. Different superscript letters within the same column indicate significant ($p < 0.05$) differences of means among the fractions. The level of significance is expressed as $p < 0.05$ (*), $p < 0.01$ (**), $p < 0.005$ (***), $p < 0.001$ (****). AGE, advanced glycation end product; IC₅₀, half-maximal inhibitory concentration.

\ae The IC₅₀ for standard acarbose was 0.70 mg/ml. \ae The IC₅₀ for standard acarbose was 0.01 mg/ml. \ae The IC₅₀ for standard quercetin was 0.002 mg/ml. \ae The IC₅₀ for positive control aminoguanidine was 0.36 mg/ml.

Sample concentration at 1 mg/ml. ψ Sample concentration at 10 mg/ml.

4.1.6 Anti-glycation activities and indices

4.1.6.1 AR inhibitory activity

Based on Table 4.7, the polar aqueous fraction of *P. pellucida* with low anti-inflammatory and anti-glycaemic activities displayed the highest AR inhibitory activity (the smallest IC₅₀ at 0.02 mg/ml). This was followed by the ethyl acetate, chloroform and n-butanol plant fractions with similar IC₅₀ values (0.07-0.08 mg/ml) for AR inhibitory activity. The crude methanolic extract preceded with IC₅₀ of 0.12 mg/ml while the hexane fraction exhibited the weakest AR inhibitory potential at IC₅₀ of 0.16 mg/ml. Nevertheless, the overall AR inhibitory potential of standard quercetin (IC₅₀ = 0.002 mg/ml) was much stronger than all plant fractions.

4.1.6.2 Total AGE inhibition analysis

In total AGE inhibition analysis, the moderately polar ethyl acetate fraction of *P. pellucida* showed the strongest fluorescent AGEs inhibition (IC₅₀ = 0.05 mg/ml) (Table 4.7). The total AGE inhibitory activities of crude methanolic extract, hexane, chloroform and n-butanol fractions (IC₅₀ = 0.79-0.80 mg/ml) were not significantly different. In contrary to the AR inhibitory activity, the weakest total AGE inhibitory activity was observed in the aqueous fraction (IC₅₀ = 1.12 mg/ml). Interestingly, the total AGE inhibitory activity of ethyl acetate fraction was even stronger than that of the positive control aminoguanidine (IC₅₀=0.36 mg/ml).

4.1.6.3 Dicarbonyl compound analysis

In this study, the dicarbonyl compound inhibitory activity of *P. pellucida* fractions ranged from 4 % to 12 % at a concentration of 1 mg/ml

for all solvent fractions, except for the aqueous fraction (Table 4.7). Although the aqueous fraction shared similar dicarbonyl compound inhibitory activity with n-butanol and chloroform fractions, ten mg/ml was used for aqueous fraction to obtain a detectable activity. Likewise, the dicarbonyl compound inhibitory activity were similar among the ethyl acetate, hexane fractions and crude methanolic extract, which were considered relatively strong among the six solvent fractions.

4.1.6.4 Amadori product analysis

All six solvent fractions of *P. pellucida* shared similar Amadori products inhibitory activities, ranging from 25 % to 32 % (Table 4.7). Similar to dicarbonyl compound analysis, the inhibitory activity of aqueous fraction against the formation of Amadori products was only detectable at 10 mg/ml. Notably, the overall Amadori product inhibitory activities of all *P. pellucida* crude methanolic extract and solvent fractions were higher than their dicarbonyl compound inhibitory potential. Based on the AGI analysis, the ethyl acetate fraction of *P. pellucida* was the only solvent fraction ranked as very high AGI fraction while the aqueous and hexane fractions were categorised as high AGI fractions (Table 4.8). The other 3 plant solvent fractions were grouped as moderate AGI fractions. Overall, none of the solvent fractions belonged in the low AI, AII and AGI groups. The ethyl acetate fraction was classified as such based on its potent inhibitory activity on the total AGE and Amadori products. Besides, it was shown that the significant aldose reductase and dicarbonyl compound inhibitory activities supported the respective aqueous and hexane fractions as high AGI plant fractions.

Table 4.7. The anti-glycation index of *P. pellucida* crude methanolic extract and fractions.

<i>P. pellucida</i> extracts	Total AGE inhibition (IC ₅₀ , mg/ml)	Amadori product inhibition (%)	Dicarbonyl compound inhibition (%)	Aldose reductase inhibition (IC ₅₀ , mg/ml)	Relative % Total AGE inhibition	Relative % Amadori product inhibition	Relative % Dicarbonyl compound inhibition	Relative % aldose reductase inhibition	AGI	Category
Ethyl acetate fraction	0.05	31.42	10.69	0.07	100	100	93	25	79	very high
Aqueous fraction	1.12	28.52	7.52	0.02	4	91	65	100	65	high
Hexane fraction	0.80	30.15	11.49	0.16	6	96	100	11	53	high
n-Butanol fraction	0.79	27.05	7.29	0.08	6	86	63	23	45	moderate
Crude methanolic extract	0.80	25.27	9.08	0.12	6	80	79	15	45	moderate
Chloroform fraction	0.79	27.58	4.89	0.07	6	88	43	27	41	moderate

Note: The plants are graded into very high (76-100 %), high (51-75 %), moderate (26-50 %) and low (0-25 %) anti-glycation potentials. The percentage relative value for each sample in each assay is based on the highest value in each assay. AGE, advanced glycation end product; AGI, anti-glycation index; IC₅₀, half-maximal inhibitory concentration.

4.1.7 *In vivo* toxicity assay

According to Hamidi *et al.* (2014), the toxicity of solvent fractions towards the brine shrimps can be classified into non-toxic ($LC_{50} > 1$ mg/ml), mildly toxic ($LC_{50} = 0.5 - 1$ mg/ml), moderately toxic ($LC_{50} = 0.1 - 0.5$ mg/ml) or highly toxic ($LC_{50} = 0 - 0.1$ mg/ml) based on the sample concentration that causes death in 50 % of brine shrimp population. The result clearly indicated that the aqueous fraction of *P. pellucida* was non-toxic against brine shrimps with LC_{50} exceeding 1 mg/ml (5.48 ± 0.85 mg/ml) (Table 4.8). The ethyl acetate plant fraction and crude methanolic plant extract were mildly toxic against the brine shrimp nauplii at LC_{50} of 0.55 mg/ml and 0.71 mg/ml, respectively. This was closely followed by the n-butanol ($LC_{50} = 0.40$ mg/ml) and chloroform fractions ($LC_{50} = 0.42$ mg/ml) with moderate toxicity towards brine shrimps. The lowest LC_{50} was observed in the hexane fraction (0.35 ± 0.08 mg/ml), indicating the high toxicity of the non-polar fraction.

In the current study, the positive control, potassium dichromate displayed the highest toxicity with LC_{50} of 0.26 mg/ml, which was only slightly lower than the non-polar hexane fraction (0.35 ± 0.08 mg/ml). Out of the six plant fractions, the polar aqueous fraction of *P. pellucida* was the only non-toxic plant fraction based on the *in vivo* toxicity finding. The crude methanolic extract and ethyl acetate fraction of *P. pellucida* which displayed strong antioxidant, anti-inflammatory, anti-glycaemic and anti-glycation properties were considered mildly toxic.

Table 4.8. The *in vivo* toxicity of *P. pellucida* crude methanolic extract and fractions.

<i>P. pellucida</i> extracts	<i>In vivo</i> toxicity (LC ₅₀ , mg/ml) §
Crude methanolic extract	0.71 ± 0.06 ^a
Hexane fraction	0.35 ± 0.08 ^{b*}
Chloroform fraction	0.42 ± 0.04 ^{b*}
Ethyl acetate fraction	0.55 ± 0.11 ^a
n-Butanol fraction	0.40 ± 0.05 ^{b*}
Aqueous fraction	5.48 ± 0.85 ^{c*}

Note: Values are mean ± standard deviation of three independent determinations. Different superscript letters within the same column indicate significant ($p < 0.05$) differences of means among the fractions. The level of significance is expressed as $p < 0.05$ (*), $p < 0.01$ (**), $p < 0.005$ (***), $p < 0.001$ (****).

§ The IC₅₀ for positive control potassium dichromate was 0.26 mg/ml.

4.1.8 Correlation analysis

Based on correlation analysis (Table 4.9), a significant positive correlation was established between the TPC and FRAP ($r = 0.80$, $p < 0.001$). The significant positive correlation observed between saponin and FRAP ($r = 0.89$, $p < 0.001$) may also strengthen the reducing potential of saponins. Besides, there was a strong inverse correlation ($p < 0.001$) between TPC and the IC_{50} for DPPH ($r = -0.82$) and ABTS ($r = -0.83$) radical scavenging activities, respectively. Similarly, a moderate inverse correlation was also spotted between the saponin and IC_{50} for ABTS radical scavenging activity ($r = -0.68$, $p < 0.005$). Moreover, the significant correlation among the FRAP, DPPH and ABTS radicals scavenging activities indicated that hydrogen atom transfer and SET-based reactions are closely related to one another. In addition, FRAP was negatively correlated with the IC_{50} for lipid peroxidation inhibitory activity of plant extracts ($r = -0.53$, $p < 0.05$). Likewise, the saponin content with strong association with FRAP and ABTS radical scavenging activities, also displayed significant inverse correlation with the IC_{50} of lipid peroxidation inhibition ($r = -0.71$, $p < 0.001$). However, this study has found that TFC was not associated with the antioxidant activities in *P. pellucida* based on the non-significant correlation of TFC with FRAP activity, DPPH and ABTS radicals scavenging activities. In terms of *in vivo* toxicity, there was a mild inverse correlation of the LC_{50} values of *P. pellucida* fractions with TPC ($r = -0.40$, $p < 0.05$) and TFC ($r = -0.18$, $p < 0.05$). Additionally, there was also a moderate negative correlation ($r = -0.52$, $p < 0.05$) between the FRAP values and LC_{50} of *in vivo* toxicity.

Furthermore, correlation studies showed that the inhibition of COX-1 and 2 was not associated with the alkaloids, phenolic compounds and saponins of *P. pellucida*. On the other hand, there was a significant inverse relationship shared between IC_{50} for LOX with TFC ($r = -0.65$, $p < 0.005$)

and saponin ($r = -0.50$, $p < 0.05$) contents (Table 4.9), hinting at the role of flavonoids and saponins on the LOX inhibitory activity of *P. pellucida*. Additionally, a significant positive correlation was found between XO inhibitory activity and ABTS radical scavenging activity ($r = 0.61$, $p < 0.01$). Despite the lack of correlation among the hyaluronidase inhibitory activity, TPC and TFC, the alkaloid content of *P. pellucida* was inversely correlated with the IC_{50} of hyaluronidase inhibitory activity ($r = -0.49$, $p < 0.05$).

Although correlation studies indicated that TFC was not associated with the α -glucosidase inhibitory activity of *P. pellucida* ($r = 0.25$, $p > 0.05$), the IC_{50} of α -glucosidase inhibitory activity was inversely correlated with TPC ($r = -0.82$, $p < 0.001$), tannin ($r = -0.61$, $p < 0.01$) and saponin contents ($r = -0.60$, $p < 0.01$) (Table 4.9). Besides, the α -glucosidase inhibitory activity (IC_{50}) of *P. pellucida* demonstrated significant inverse correlation with the antioxidant parameters such as FRAP, DPPH and ABTS radical scavenging activities. On the contrary, there was a weak inverse correlation of α -amylase inhibitory activity (IC_{50}) with TPC ($r = -0.16$) and TFC ($r = -0.37$). Nevertheless, a moderate inverse correlation was observed between the α -amylase inhibitory activity (IC_{50}) of *P. pellucida* and antioxidant parameters.

This study also revealed that the AR inhibitory activity was positively associated with DPPH radical scavenging activity ($r = 0.63$, $p < 0.005$) but inversely correlated with TPC ($r = -0.32$, $p < 0.05$) (Table 4.9). The total AGE inhibitory activity of *P. pellucida* was significantly associated with the α -glucosidase ($r = 0.70$, $p < 0.05$) and α -amylase ($r = 0.71$, $p < 0.05$) inhibitory activities of *P. pellucida*. Besides, there was a significant inverse association of total AGE inhibition activity with TPC ($r = -0.47$, $p < 0.05$), saponin content ($r = -0.96$, $p < 0.001$) and FRAP ($r = -0.87$, $p < 0.001$). The dicarbonyl compound inhibitory activity of *P. pellucida*

fractions was positively correlated with the IC_{50} of α -amylase ($r = 0.58$, $p < 0.05$), COX-1 ($r = 0.49$, $p < 0.05$) and COX-2 ($r = 0.75$, $p < 0.001$) inhibitory activities. Correlation analysis also showed that TFC was positively correlated with the Amadori product inhibitory activity ($r = 0.41$, $p < 0.05$) and dicarbonyl compound inhibitory activity ($r = 0.18$, $p < 0.05$). Between the dicarbonyl compound and Amadori product inhibitory activities, a moderate positive correlation ($r = 0.55$, $p < 0.05$) was established.

Table 4.9. Linear correlation and regression of biological activities in *P. pellucida*.

Assays	Pearson <i>r</i>	R²	p-value
Phytochemical content versus antioxidant activity			
TPC vs FRAP	0.798	0.637	****
TPC vs DPPH radical scavenging activity	-0.818	0.668	****
TPC vs ABTS radical scavenging activity	-0.832	0.692	****
TFC vs lipid peroxidation inhibitory activity	0.478	0.229	*
Saponin content vs ABTS radical scavenging activity	-0.680	0.460	***
Saponin content vs FRAP	0.889	0.790	****
Saponin content vs lipid peroxidation	-0.711	0.510	****
Phytochemical content versus anti-glycaemic activity			
TPC vs α -glucosidase inhibitory activity	-0.819	0.671	****
Saponin content vs α -glucosidase inhibitory activity	-0.601	0.360	**
Tannin content vs α -glucosidase inhibitory activity	-0.615	0.380	**
Phytochemical content versus anti-inflammatory activity			
TPC vs COX-1 inhibitory activity	-0.764	0.584	****
TPC vs COX-2 inhibitory activity	-0.577	0.334	*
TFC vs LOX inhibitory activity	-0.652	0.426	***
Alkaloid content vs hyaluronidase inhibitory activity	-0.491	0.240	*
Saponin content vs LOX inhibitory activity	-0.497	0.250	*
Phytochemical content versus anti-glycation activity			
TPC vs total AGE inhibition analysis	-0.470	0.221	*
Saponin content vs total AGE inhibition analysis	-0.960	0.920	****

Note: The *r* value denotes the significant Pearson's correlation value of 6 fractions. The level of significance is expressed as $p < 0.05$ (*), $p < 0.01$ (**), $p < 0.005$ (***), $p < 0.001$ (****).

Table 4.9 (continued)

Assays	Pearson <i>r</i>	R²	p-value
Antioxidant activity			
FRAP vs DPPH radical scavenging activity	-0.567	0.322	*
FRAP vs ABTS radical scavenging activity	-0.778	0.605	****
FRAP vs lipid peroxidation inhibitory activity	-0.526	0.276	*
DPPH scavenging activity vs ABTS scavenging activity	0.748	0.559	****
Antioxidant activity versus anti-glycaemic activity			
FRAP vs α -glucosidase inhibitory activity	-0.824	0.679	****
DPPH scavenging activity vs α -glucosidase inhibitory activity	0.637	0.406	***
ABTS scavenging activity vs α -glucosidase inhibitory activity	0.795	0.632	****
ABTS scavenging activity vs α -amylase inhibitory activity	0.621	0.385	**
Antioxidant activity versus anti-inflammatory activity			
FRAP vs COX-1 inhibitory activity	-0.585	0.342	*
DPPH scavenging activity vs COX-1 inhibitory activity	0.770	0.593	****
DPPH scavenging activity vs COX-2 inhibitory activity	0.527	0.278	*
ABTS scavenging activity vs COX-1 inhibitory activity	0.514	0.265	*
ABTS scavenging activity vs XO inhibitory activity	0.609	0.371	**
Antioxidant activity versus anti-glycation activity			
FRAP vs total AGE inhibition analysis	-0.866	0.750	****
DPPH scavenging activity vs aldose reductase inhibitory activity	0.631	0.398	***
ABTS scavenging activity vs total AGE inhibition analysis	0.684	0.468	***
Lipid peroxidation inhibitory activity vs total AGE inhibition analysis	0.755	0.570	****

Note: The *r* value denotes the significant Pearson's correlation value of 6 fractions. The level of significance is expressed as $p < 0.05$ (*), $p < 0.01$ (**), $p < 0.005$ (***), $p < 0.001$ (****).

Table 4.9 (continued)

Assays	Pearson <i>r</i>	R²	p-value
Antioxidant activity versus <i>in vivo</i> toxicity			
FRAP vs <i>in vivo</i> toxicity	-0.525	0.275	*
ABTS scavenging activity vs <i>in vivo</i> toxicity	0.544	0.296	*
Anti-inflammatory activity			
COX-1 inhibitory activity vs COX-2 inhibitory activity	0.852	0.726	****
COX-1 inhibitory activity vs hyaluronidase inhibitory activity	-0.691	0.477	***
COX-2 inhibitory activity vs hyaluronidase inhibitory activity	-0.562	0.316	*
Anti-inflammatory activity versus anti-glycaemic activity			
COX-2 inhibitory activity vs α-amylase inhibitory activity	-0.637	0.406	***
XO inhibitory activity vs α-amylase inhibitory activity	0.554	0.307	*
Anti-inflammatory activity versus anti-glycation activity			
COX-1 inhibitory activity vs aldose reductase inhibitory activity	0.759	0.576	****
COX-1 inhibitory activity vs dicarbonyl compound analysis	0.488	0.238	*
COX-2 inhibitory activity vs aldose reductase inhibitory activity	0.771	0.594	****
COX-2 inhibitory activity vs dicarbonyl compound analysis	0.745	0.555	****
XO inhibitory activity vs Amadori product analysis	0.549	0.302	*
Hyaluronidase inhibitory activity vs aldose reductase inhibitory activity	-0.725	0.525	****
Anti-inflammatory activity versus <i>in vivo</i> toxicity			
XO inhibitory activity vs <i>in vivo</i> toxicity	0.498	0.248	*
Hyaluronidase inhibitory activity vs <i>in vivo</i> toxicity	0.685	0.469	***

Note: The *r* value denotes the significant Pearson's correlation value of 6 fractions. The level of significance is expressed as p<0.05 (*), p<0.005 (***), p<0.001 (****).

Table 4.9 (continued)

Assays	Pearson <i>r</i>	R²	p-value
Anti-glycaemic activity versus anti-glycation activity			
α-glucosidase inhibitory activity vs total AGE inhibition analysis	0.703	0.494	***
α-amylase inhibitory activity vs aldose reductase inhibitory activity	-0.633	0.401	***
α-amylase inhibitory activity vs total AGE inhibition analysis	0.709	0.503	****
α-amylase inhibitory activity vs dicarbonyl compound analysis	-0.575	0.330	*
Anti-glycaemic activity versus <i>in vivo</i> toxicity			
α-glucosidase inhibitory activity vs <i>in vivo</i> toxicity	0.692	0.479	***
α-amylase inhibitory activity vs <i>in vivo</i> toxicity	0.725	0.526	****
Anti-glycation activity			
Aldose reductase inhibitory activity vs dicarbonyl compound analysis	0.595	0.354	**
Dicarbonyl compound analysis vs Amadori product analysis	0.551	0.303	*
Anti-glycation activity versus <i>in vivo</i> toxicity			
Aldose reductase inhibitory activity vs <i>in vivo</i> toxicity	-0.653	0.427	***
Total AGE inhibition analysis vs <i>in vivo</i> toxicity	0.524	0.275	*

Note: The *r* value denotes the significant Pearson's correlation value of 6 fractions. The level of significance is expressed as p<0.05 (*), p<0.01 (**), p<0.005 (***), p<0.001 (****).

4.1.9 Principal component analysis (PCA)

Based on the PCA biplot (Figure 4.1), the highest variation was observed among the components in F1 and F2, which collectively accounted for 63.02 % of the total variance. On the horizontal axis of biplot, the F1 components showed 33.22 % of activity variation among the *P. pellucida* fractions. The variation was also characterised by a distinct separation of aqueous and hexane fractions from chloroform, ethyl acetate and n-butanol fractions. Interestingly, both aqueous and hexane fractions were solvent fractions with higher extraction yield when compared to the chloroform, ethyl acetate and n-butanol fractions. This may indicate that the biological activity variation was due in part to the plant extraction yield. On the contrary, the F2 component (vertical axis) has accounted for the 29.81 % of variation in biological activity, which was partly achieved through the positioning of non-polar hexane fraction away from the polar aqueous fraction and semi-polar solvent fractions. Furthermore, a noticeable separation of biological activity variables can be observed in all four quadrants of the PCA biplot. The solvent fractions that exhibited parallel vector direction with the biological activity variables in every region of the biplot was an indication of association to one another. In the lower left quadrant of biplot, FRAP was placed together with ethyl acetate and n-butanol fractions. The same plant fractions also displayed high FRAP values (Table 4.2). Hexane plant fraction was associated with high COX inhibitory activities (Table 4.5) and thus it was placed together with the COX-1 and COX-2 variables in the biplot. In addition, the aqueous fraction was the only non-toxic solvent fraction towards the brine shrimps (Table 4.9). Due to the high LC_{50} , the aqueous fraction was grouped with the *in vivo* toxicity variable in the lower right quadrant of the biplot.

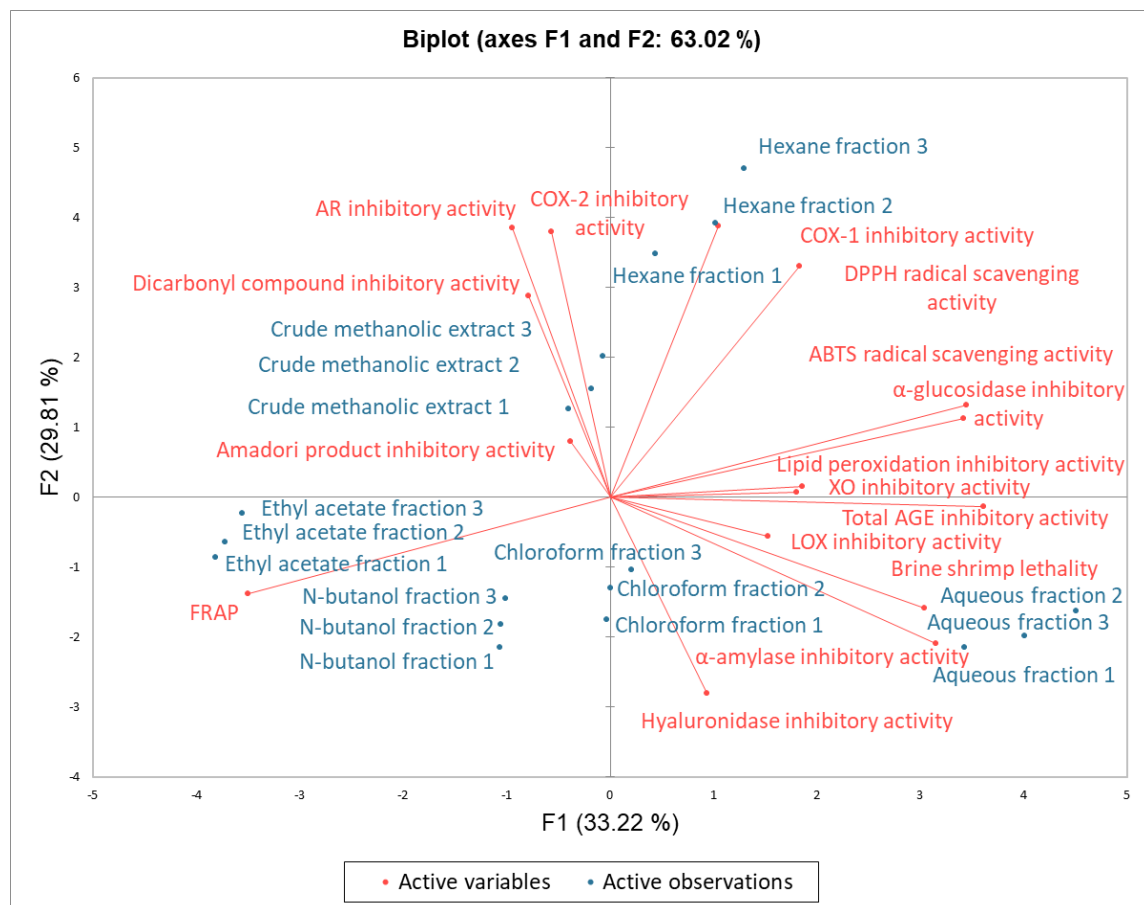


Figure 4.1. The PCA biplot of biological activities in *P. pellucida* crude methanolic extract and solvent fractions. ABTS, 2, 2'-azino-bis (3-ethylbenzothiazoline-6-sulfonic acid); AGE, advanced glycation end product; AR, aldose reductase; COX-1, cyclooxygenase 1; COX-2, cyclooxygenase 2; DPPH, 2,2-diphenyl-1-picrylhydrazyl; FRAP, ferric-reducing antioxidant power; LOX, 5-lipoxygenase; XO, xanthine oxidase.

4.2 Phase 2: *In vitro* cellular study

In this study, the modulatory effect of ethyl acetate fraction and crude methanolic extract on the gene and protein expression of angiogenic, antioxidant and pro-inflammatory markers implicated in NF- κ B, PPAR- γ and STAT3 signalling pathways were investigated with an *in vitro* ARPE-19 cellular model subjected to high glucose and AGE-induced stress. In addition, MTT cell viability assay was also carried out to evaluate the ARPE-19 cytotoxicity of *P. pellucida* crude methanolic extract and ethyl acetate fraction under high glucose and glycativ stresses.

4.2.1 Plant cytotoxicity in ARPE-19

4.2.1.1 Normal glucose condition

In order to evaluate the cytotoxicity of *P. pellucida* crude methanolic extract and ethyl acetate fraction towards ARPE-19, the cells were subjected to treatment with the plant extracts (0.1-10 mg/ml). The morphology of ARPE-19 treated with different concentration of crude methanolic extract and ethyl acetate fraction was also monitored to evaluate the impact of sample concentration on cell structure and appearance (Figure 4.2). Following the plant extracts treatment, ARPE-19 in the negative control (Figure 4.2A) and 0.5 % DMSO vehicle control (Figure 4.2B) retained its cobblestone morphology. Although the IC₅₀ of crude methanolic extract and ethyl acetate fraction for ARPE-19 cytotoxicity was determined to be respective 8.70 mg/ml and 7.34 mg/ml (Figure 4.3), the cells treated with 4 mg/ml and 5 mg/ml onwards of the respective crude methanolic extract (Figure 4.2C) and ethyl acetate fraction (Figure 4.2D) appeared shrivel. The ARPE-19 has also completely lost its characteristic cobblestone morphology and apical-basal polarity.

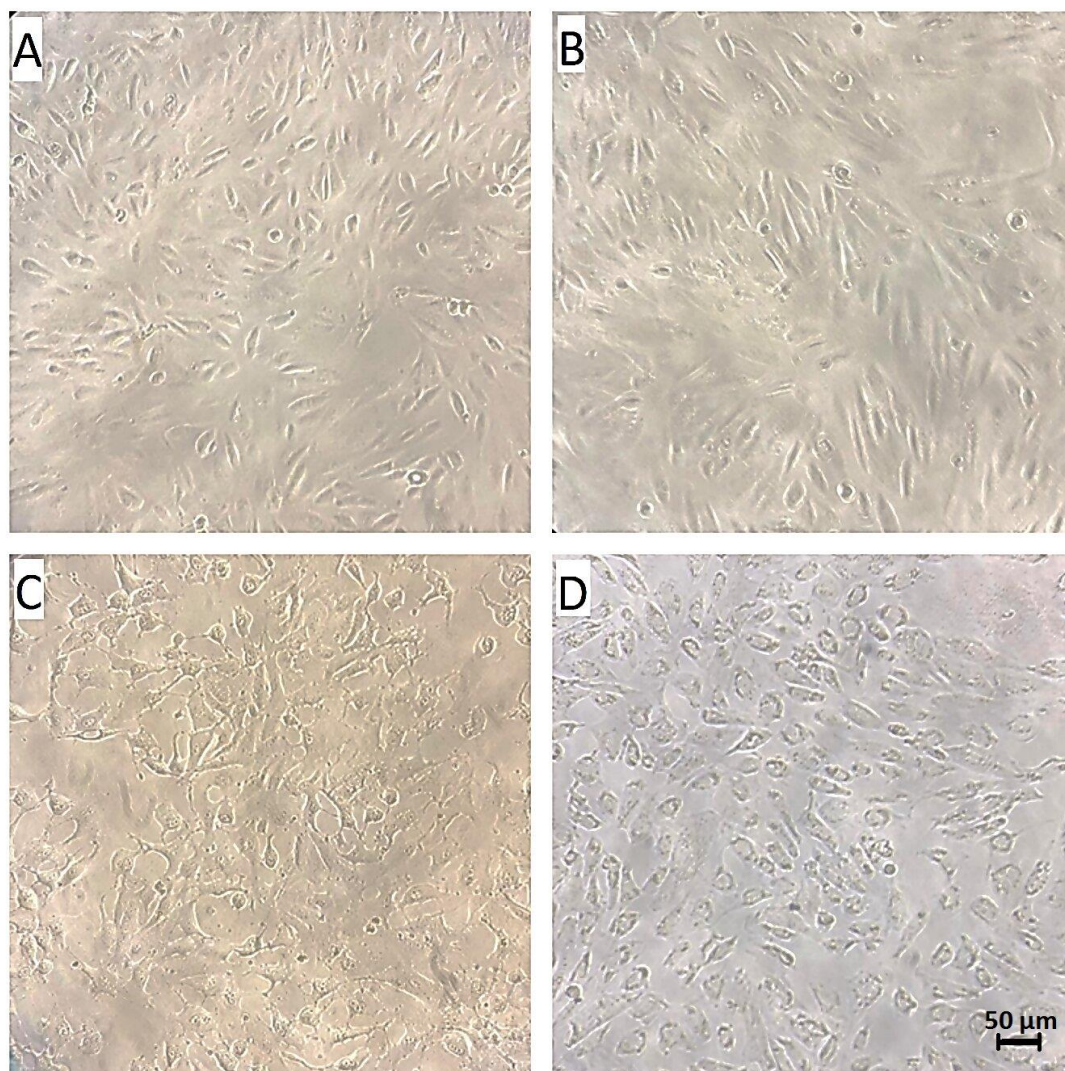


Figure 4.2. The morphology of ARPE-19. (A) negative control group. (B) 0.5 % DMSO vehicle control group. (C) crude methanolic extract (4 mg/ml onwards). (D) ethyl acetate fraction (5 mg/ml onwards).

Based on the result (Figure 4.3), the ARPE-19 cell viability has reduced by 13 % in the 0.5 % DMSO vehicle control when compared to the normal glucose control. The viability of ARPE in the plant treatment group (3 mg/ml for crude methanolic extract and 4 mg/ml for ethyl acetate fraction) was not significantly different from those of 0.5 % DMSO vehicle control group. At 4 mg/ml, the crude methanolic extract led to lower ARPE-19 cell viability (77.86 %) when compared to the ethyl acetate fraction (86.66 %). Besides, the ARPE-19 cell viability decreased gradually from 4 mg/ml (crude methanolic extract) and 5 mg/ml (ethyl acetate fraction) onwards. The ARPE-19 cell viability was leveled at a treatment concentration of 6 mg/ml for both plant extracts. From 7 mg/ml onwards, the ethyl acetate fraction resulted in the greater cell death among the ARPE-19 population with a 8.58 % lower in ARPE-19 cell viability compared to the crude methanolic extract. The disparity in ARPE-19 cell viability between treatment with crude methanolic extract and ethyl acetate fraction continued to escalate from 7 mg/ml to 10 mg/ml. At the highest plant sample concentration (10 mg/ml), the ARPE-19 cell viability upon treatment with crude methanolic extract and ethyl acetate fraction was 23.02 % and 2.15 %, respectively. Based on the above findings, it was determined that ARPE-19 could tolerate up to 3 mg/ml and 4 mg/ml of crude methanolic extract and ethyl acetate fraction, respectively.

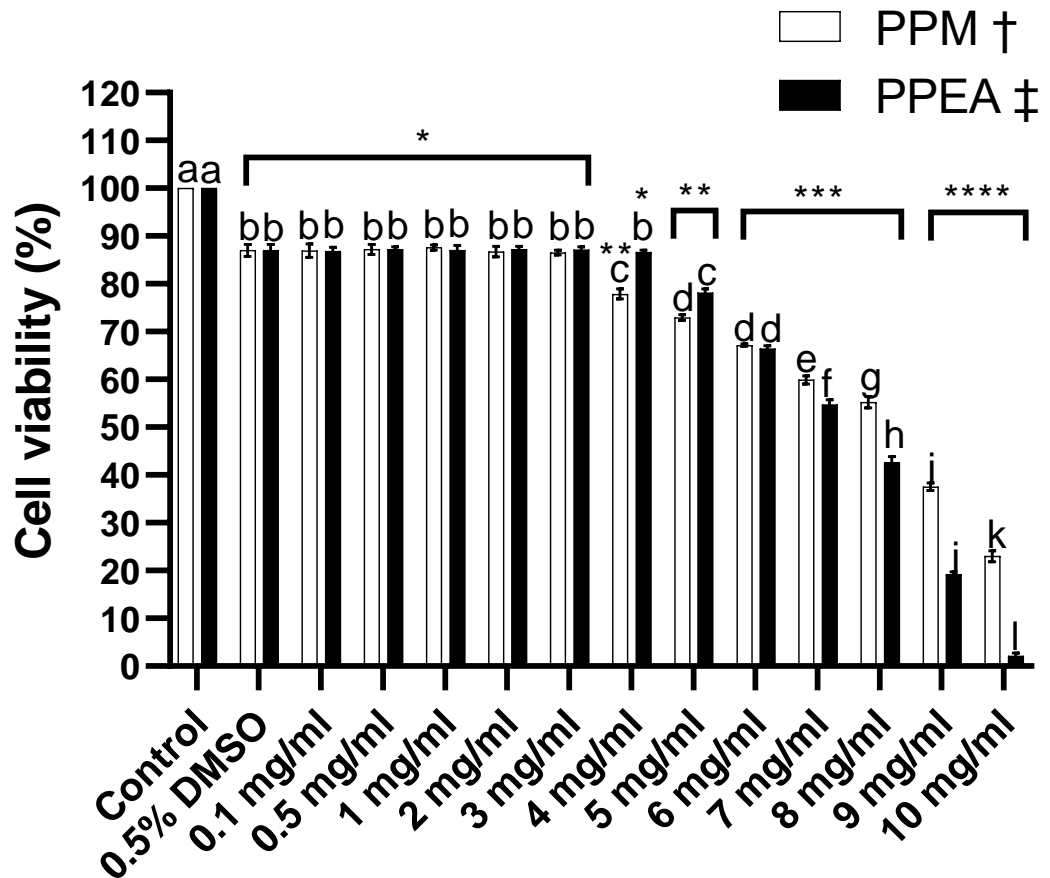


Figure 4.3. The cell viability (%) of ARPE-19 treated with *P. pellucida* crude methanolic extract and ethyl acetate fraction under normal glucose condition after 24 hours. Control refers to untreated cells cultured in basal medium. The 0.5 % DMSO vehicle control refers to untreated cells cultured in medium supplemented with 0.5 % DMSO. Data were expressed as mean \pm standard deviation of four independent determinations. Different alphabetical letters indicated significant ($p < 0.05$) means difference among the plant treatment groups. The level of significance is expressed as $p < 0.05$ (*), $p < 0.01$ (**), $p < 0.005$ (***), $p < 0.001$ (****). † The IC_{50} for ARPE-19 cytotoxicity was 8.70 mg/ml. ‡ The IC_{50} for ARPE-19 cytotoxicity was 7.34 mg/ml. DMSO, dimethyl sulfoxide; PPEA, *P. pellucida* ethyl acetate fraction; PPM, *P. pellucida* crude methanolic extract.

4.2.1.2 Hyperglycaemic stress

In this study, the effect of *P. pellucida* crude methanolic extract and ethyl acetate fraction on ARPE-19 cell viability under high glucose and AGE-treated conditions was investigated. Since the maximum tolerable concentrations of *P. pellucida* crude methanolic extract and ethyl acetate fraction towards ARPE-19 have been determined as 3 mg/ml and 4 mg/ml respectively, the cells were subjected to an individual three-point concentration treatment of crude methanolic extract (0.75 mg/ml, 1.5 mg/ml, 3 mg/ml) and ethyl acetate fraction (1 mg/ml, 2 mg/ml, 4 mg/ml) via the two-fold serial dilution method.

Under high glucose condition (34 mM, 68 mM) (Figure 4.4), the ARPE-19 cell viability has been reduced by 10 % when compared to the normal glucose control (17 mM). The ARPE-19 cell viability in 0.5 % DMSO vehicle control groups were also found to be lower than the respective untreated normal glucose and high glucose groups (17 mM, 34 mM, 68 mM). It can be observed that the ARPE-19 cell viability under normal glucose condition was higher in the 48-hour treatment groups of crude methanolic extract (1.5 mg/ml onwards) and ethyl acetate fraction (2 mg/ml onwards) than those in the 24-hour treatment groups. The same cell viability trend was observed for ARPE-19 treated with crude methanolic extract and ethyl acetate fraction under 34 mM and 68 mM glucose conditions.

Treatment with the *P. pellucida* extracts for 48 hours also showed prominent concentration-dependent increment in the ARPE-19 cell viability under normal glucose and high glucose conditions. Under both normal glucose (17 mM) and moderately high glucose (34 mM) conditions, the crude methanolic extract (1.5 mg/ml onwards) and ethyl acetate fraction

(4 mg/ml) restored the ARPE-19 cell viability back to the normal glucose control level. The crude methanolic extract treated ARPE-19 group also displayed higher cell viability and greater cytoprotective effect than ethyl acetate fraction under the same conditions. The crude methanolic extract has maintained the ARPE-19 cell viability in normal glucose condition (17 mM) at a starting concentration of 1.5 mg/ml onwards. Even at low plant sample concentration of 0.75 mg/ml, the ARPE-19 treated with crude methanolic extract could sustain its cell viability against the impact of moderately high glucose (34 mM). When compared to the crude methanolic extract, a higher concentration of ethyl acetate fraction (4 mg/ml) was required to produce similar cytoprotective effect in ARPE-19. Despite an increase in ARPE-19 cell viability after 24 hours treatment of crude methanolic extract, the ethyl acetate fraction (starting from 2 mg/ml) induced a further 12 % increase in ARPE-19 cell viability under high glucose (68 mM) conditions after 48 hours of treatment.

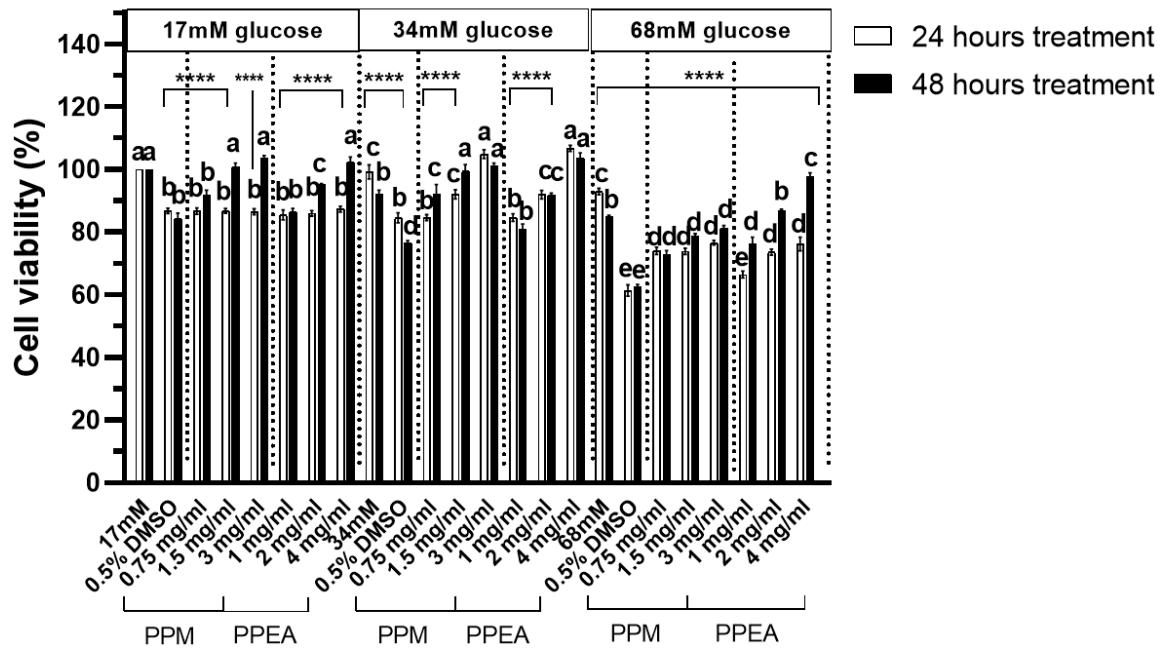


Figure 4.4. The cell viability (%) of ARPE-19 treated with *P. pellucida* crude methanolic extract and ethyl acetate fraction under normal glucose (17 mM) and the high glucose (34 mM, 68 mM) conditions. Control refers to untreated cells cultured in basal medium. The 0.5 % DMSO vehicle control refers to untreated cells cultured in medium supplemented with 0.5 % DMSO. Data are expressed as mean \pm standard deviation of four independent determinations. Different alphabetical letters indicate significant ($p < 0.05$) differences of means among the treatment groups. The level of significance is expressed as $p < 0.05$ (*), $p < 0.01$ (**), $p < 0.005$ (***), $p < 0.001$ (****). DMSO, dimethyl sulfoxide; PPEA, *P. pellucida* ethyl acetate fraction; PPM, *P. pellucida* crude methanolic extract.

4.2.1.3 AGE-induced stress

In the current study, the ARPE-19 cell viability was significantly reduced by AGE when compared to the normal glucose control (Figure 4.5). The AGE-treated ARPE-19 cell viability was further reduced by 15 % under the high glucose (34 mM, 68 mM) conditions. The ARPE-19 cell viability in 0.5 % DMSO vehicle group under normal glucose and high glucose (34 mM, 68 mM) AGE-treated conditions were lower than their respective untreated control groups. It was worth noting that the ARPE-19 cell viability under all AGE-treated conditions increased with the duration of plant treatment. Treatment of crude methanolic extract and ethyl acetate fraction displayed concentration-dependent restoration of ARPE-19 cell viability in the normal glucose and high glucose (34 mM) AGE-treated condition. Similar to the moderately high glucose (34 mM) group, the sample concentration required by crude methanolic extract (1.5 mg/ml) to restore the ARPE-19 cell viability back to the level of normal glucose control was lower than ethyl acetate fraction (4 mg/ml) under normal glucose AGE-treated condition. The ARPE-19 cell viability was further increased by 10 % with 3 mg/ml of crude methanolic extract.

Although 48 hours treatment of either crude methanolic extract or ethyl acetate fraction managed to raise the ARPE-19 cell viability under the high glucose (34 mM, 68 mM) AGE-treated condition, it failed to reach the level of normal glucose control group. Nevertheless, the crude methanolic extract and ethyl acetate fraction showed similar cytoprotective effect on ARPE-19 across all plant concentrations treatments under high glucose AGE-treated (68 mM) condition. Since 48-hour treatment of crude methanolic extract (0.75 mg/ml, 1.5 mg/ml, 3 mg/ml) and ethyl acetate fraction (1 mg/ml, 2 mg/ml, 4 mg/ml) increased the ARPE-19 cell viability under the high glucose AGE-treated conditions, the similar plant

concentration series of treatment and duration were applied in subsequent experiments to investigate the regulatory role of *P. pellucida* extracts on the gene and protein expression of angiogenic, antioxidant, anti-inflammatory and pro-inflammatory markers in high glucose and AGE-stimulated ARPE-19.

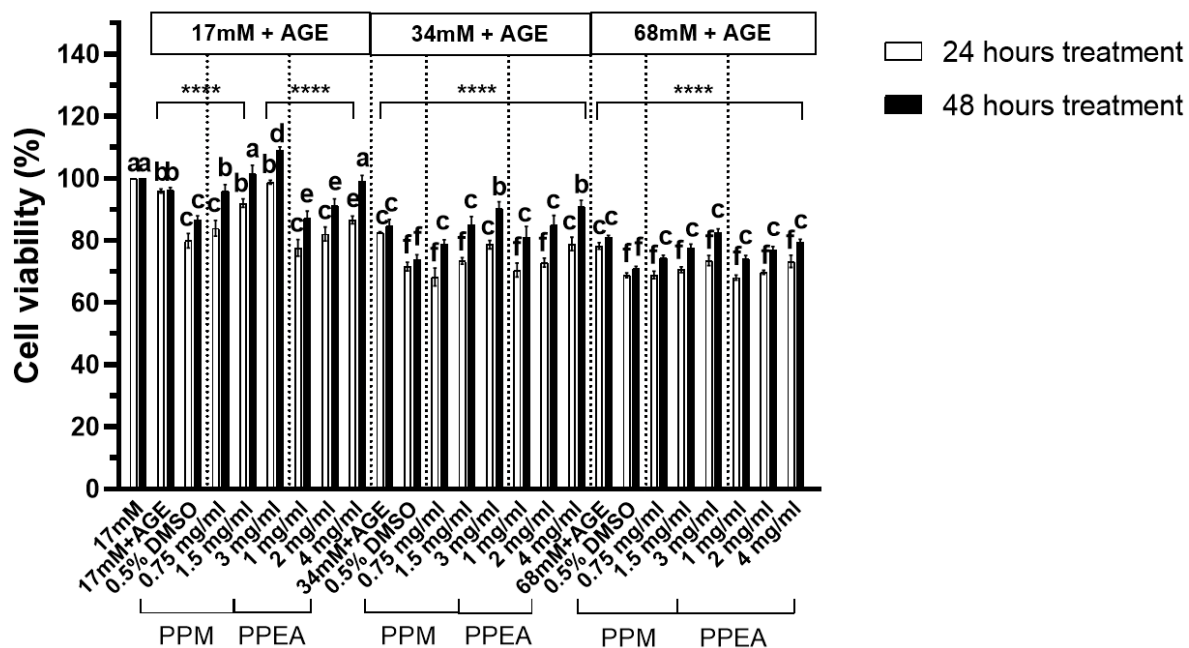


Figure 4.5. The cell viability (%) of ARPE-19 treated with *P. pellucida* crude methanolic extract and ethyl acetate fraction under normal glucose (17 mM), high glucose (34 mM, 68 mM) and AGE-treated conditions. Control refers to untreated cells cultured in basal medium. The 0.5 % DMSO vehicle control refers to untreated cells cultured in medium supplemented with 0.5 % DMSO. Data are expressed as mean \pm standard deviation of four independent determinations. Different alphabetical letters indicate significant ($p < 0.05$) differences of means among the treatment groups. The level of significance is expressed as $p < 0.05$ (*), $p < 0.01$ (**), $p < 0.005$ (***), $p < 0.001$ (****). AGE, advanced glycation end product; DMSO, dimethyl sulfoxide; PPEA, *P. pellucida* ethyl acetate fraction; PPM, *P. pellucida* crude methanolic extract.

4.2.2 Gene and protein expression

4.2.2.1 NF- κ B p65

In this study, the relative fold change of NF- κ B p65 gene expression in ARPE-19 varies from 7.86 to 14.22 folds under the high glucose (34 mM, 68 mM) and AGE-treated (17 mM, 34 mM, 68 mM) conditions when compared to the normal glucose (17 mM) control (Figure 4.6). This increased trend was also observed in the NF- κ B p65 (1.50-1.67 folds) and phosphorylated NF- κ B p65 proteins expression (1.40-1.91 folds) (Figure 4.7-4.8). The relative gene and protein expression of NF- κ B p65 were most pronounced in both the high glucose (68 mM) and its corresponding AGE-treated group, in comparison to the normal glucose control. Similarly, the highest protein expression level of phosphorylated NF- κ B p65 was detected in both conditions. Furthermore, AGE alone has also resulted in 1.5 fold increase in the protein levels of both NF- κ B p65 and phosphorylated NF- κ B p65 in relative to normal glucose control. Nevertheless, the combination of AGE and high glucose did not further escalate the gene and protein expression of NF- κ B p65 and phosphorylated NF- κ B p65.

P. pellucida extracts treatment did not alter the gene and protein expression of NF- κ B p65 and phosphorylated NF- κ B p65 in the normal glucose condition, when compared to the untreated control. In both the moderately high glucose (34 mM) group and its AGE-treated counterpart, treatment of ARPE-19 with crude methanolic extract and ethyl acetate fraction down-regulated the NF- κ B p65 gene and protein (including phosphorylated NF- κ B p65) expression in a concentration-dependent manner. Despite that, crude methanolic extract, at the highest concentration (3 mg/ml) suppressed the gene expression of NF- κ B p65 in all glucose conditions while ethyl acetate fraction could only exert the same effect under the high glucose (34 mM, 68 mM) stimulation. In terms of protein expression, treatment with increasing concentration of *P. pellucida* extracts reduced the level of protein NF- κ B p65 and phosphorylated NF- κ B p65 expression.

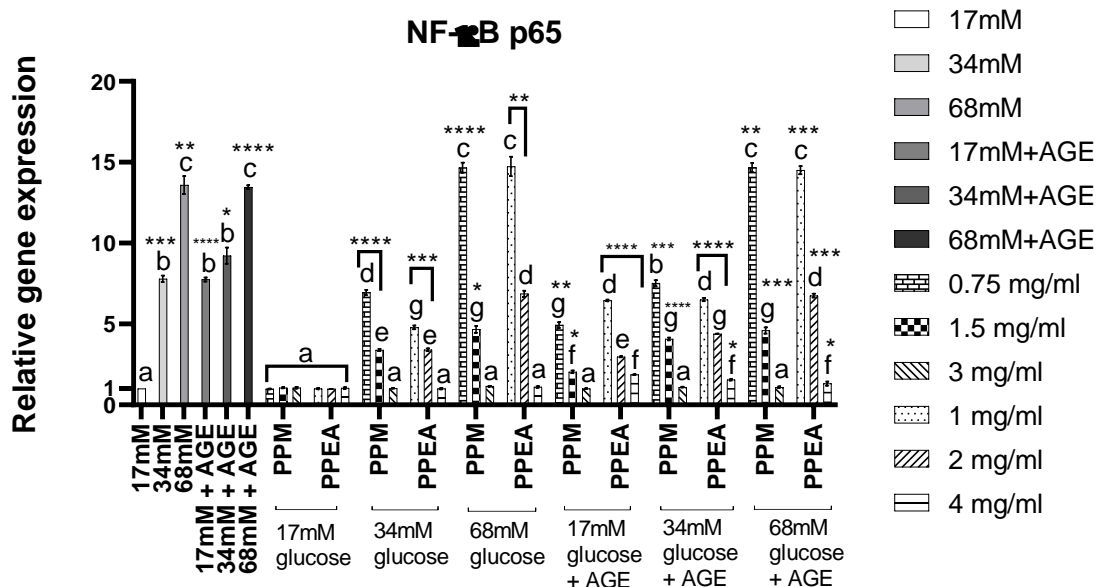


Figure 4.6. The relative gene expression of NF-κB p65 in ARPE-19 treated with *P. pellucida* crude methanolic extract and ethyl acetate fraction under normal glucose (17 mM), high glucose (34 mM, 68 mM) and AGE-treated conditions. Control refers to untreated cells cultured in basal medium. Data are expressed as mean ± standard deviation of three independent determinations. Different alphabetical letters indicate significant ($p < 0.05$) differences of means among the treatment groups. The level of significance is expressed as $p < 0.05$ (*), $p < 0.01$ (**), $p < 0.005$ (***), $p < 0.001$ (****). AGE, advanced glycation end product; PPEA, *P. pellucida* ethyl acetate; PPM, *P. pellucida* crude methanolic extract; NF-κB, nuclear factor kappa B.

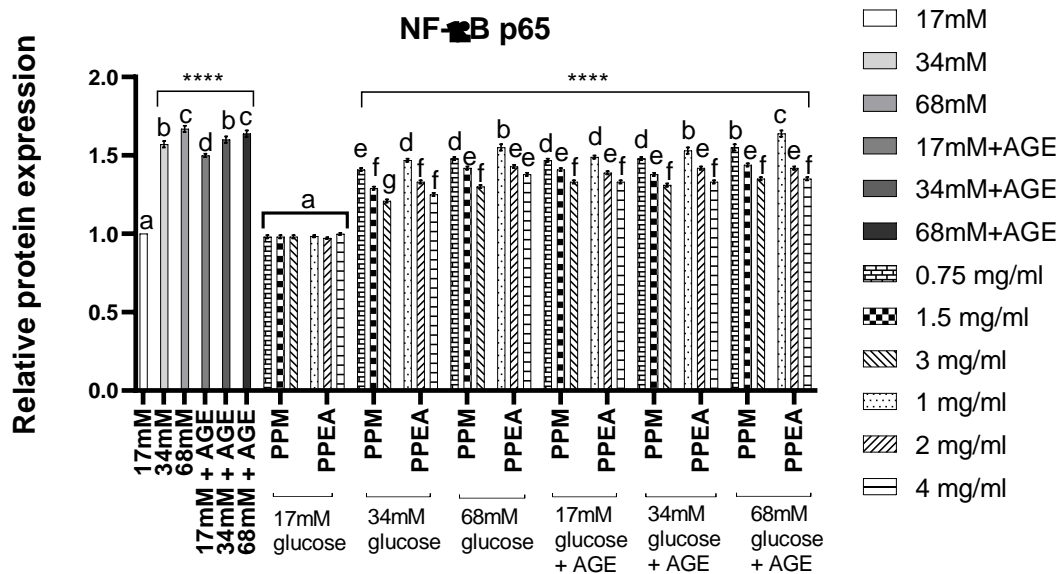


Figure 4.7. The relative protein expression of NF-κB p65 in ARPE-19 treated with *P. pellucida* crude methanolic extract and ethyl acetate fraction under normal glucose (17 mM), high glucose (34 mM, 68 mM) and AGE-treated conditions. Control refers to untreated cells cultured in basal medium. Data are expressed as mean ± standard deviation of three independent determinations. Different alphabetical letters indicate significant ($p < 0.05$) differences of means among the treatment groups. The level of significance is expressed as $p < 0.05$ (*), $p < 0.01$ (**), $p < 0.005$ (***), $p < 0.001$ (****). AGE, advanced glycation end product; PPEA, *P. pellucida* ethyl acetate; PPM, *P. pellucida* crude methanolic extract; NF-κB, nuclear factor kappa B.

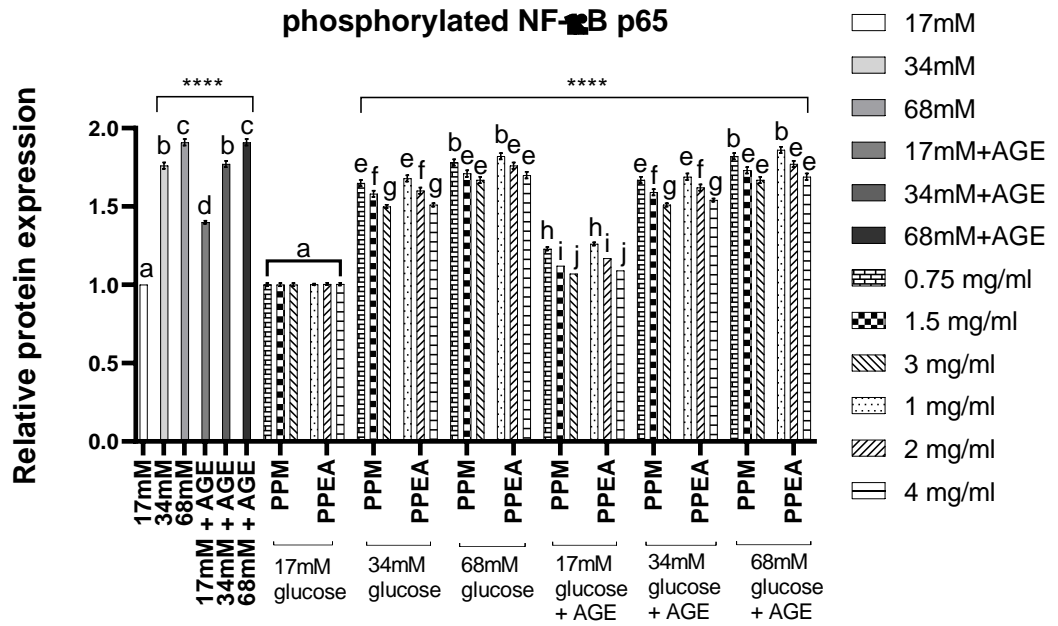


Figure 4.8. The relative protein expression of phosphorylated NF-κB p65 in ARPE-19 treated with *P. pellucida* crude methanolic extract and ethyl acetate fraction under normal glucose (17 mM), high glucose (34 mM, 68 mM) and AGE-treated conditions. Control refers to untreated cells cultured in basal medium. Data are expressed as mean ± standard deviation of three independent determinations. Different alphabetical letters indicate significant ($p < 0.05$) differences of means among the treatment groups. The level of significance is expressed as $p < 0.05$ (*), $p < 0.01$ (**), $p < 0.005$ (***), $p < 0.001$ (****). AGE, advanced glycation end product; PPEA, *P. pellucida* ethyl acetate; PPM, *P. pellucida* crude methanolic extract; NF-κB, nuclear factor kappa B.

4.2.2.2 STAT3

In the current study, the gene expression of STAT3 was found to be increased under the high glucose (34 mM, 68 mM) and their corresponding AGE-treated groups (Figure 4.9). Similar to NF- κ B p65, STAT3 gene expression showed the largest fold change at 8.58 folds under both high glucose (68 mM) and its AGE-treated counterpart, as compared to the normal glucose control. However, the expression of STAT3 proteins remained constant across all experimental groups (Table 4.10, Appendix B1a). The phosphorylated STAT3 protein expression was up-regulated under all high glucose and AGE-treated conditions, ranging from 1.30 to 1.81 folds (Appendix B1b). The highest phosphorylated STAT3 protein expression was achieved in ARPE-19 incubated under high glucose (68 mM) and all AGE-treated conditions.

The STAT3 gene and phosphorylated STAT3 protein levels in the normal glucose control remained unchanged with the increased concentration of *P. pellucida* crude methanolic extract and ethyl acetate fraction. Under both high glucose (68 mM) and its corresponding AGE-treated condition, treatment of *P. pellucida* (1.5 mg/ml crude methanolic extract onwards and 2 mg/ml ethyl acetate fraction onwards) showed concentration-dependent reduction in STAT3 gene and phosphorylated STAT3 protein expression of ARPE-19. Although the lowest concentration of crude methanolic extract and ethyl acetate fraction was inadequate to prevent the activation of STAT3 in high glucose (68 mM) and AGE-treated (17 mM, 34 mM, 68 mM) environments, it was noteworthy to highlight that the crude methanolic extract (3 mg/ml) and ethyl acetate fraction (4 mg/ml) suppressed the phosphorylated STAT3 proteins under the high glucose (34 mM, 68 mM) conditions. The crude methanolic extract (3 mg/ml) also inhibited the phosphorylation of STAT3 under the AGE-treated (17 mM, 34 mM) environment.

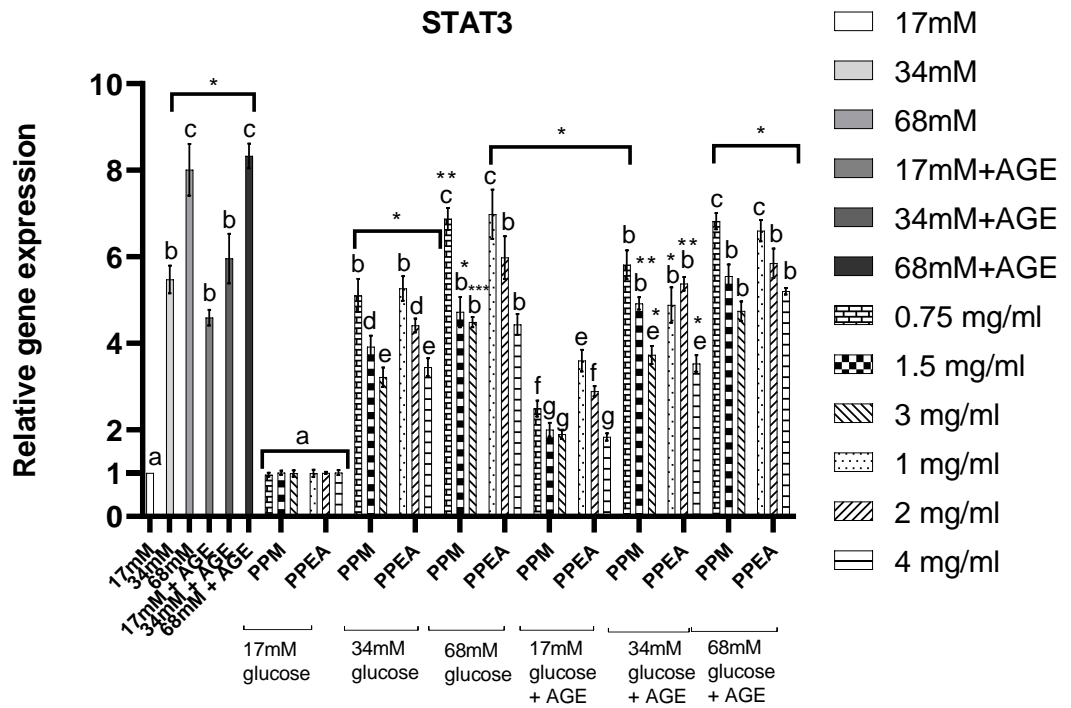


Figure 4.9. The relative gene expression of STAT3 in ARPE-19 treated with *P. pellucida* crude methanolic extract and ethyl acetate fraction under normal glucose (17 mM), high glucose (34 mM, 68 mM) and AGE-treated conditions. Control refers to untreated cells cultured in basal medium. Data are expressed as mean \pm standard deviation of three independent determinations. Different alphabetical letters indicate significant ($p < 0.05$) differences of means among the treatment groups. The level of significance is expressed as $p < 0.05$ (*), $p < 0.01$ (**), $p < 0.005$ (***)). AGE, advanced glycation end product; PPEA, *P. pellucida* ethyl acetate; PPM, *P. pellucida* crude methanolic extract; STAT3, signal transducer and activator of transcription 3.

Table 4.10. The relative protein expression of STAT3 and phosphorylated STAT3 in ARPE-19 treated with *P. pellucida* crude methanolic extract and ethyl acetate fraction under normal glucose (17 mM), high glucose (34 mM, 68 mM) and AGE-treated conditions.

Group		Relative expression (fold change)			
		STAT3 protein		Phosphorylated-STAT3 protein	
	17mM (control)	1.000 ±	0.000	1.000 ±	0.000
	0.75 mg/ml	0.995 ±	0.004	1.302 ±	0.009
PPM	1.5 mg/ml	0.993 ±	0.000	1.003 ±	0.003
	3 mg/ml	0.991 ±	0.009	1.008 ±	0.003
	1 mg/ml	0.991 ±	0.013	1.006 ±	0.003
PPEA	2 mg/ml	0.996 ±	0.004	1.005 ±	0.003
	4 mg/ml	1.009 ±	0.002	1.009 ±	0.003
	34mM	1.001 ±	0.001	0.998 ±	0.003**
	0.75 mg/ml	0.990 ±	0.011	1.176 ±	0.005
PPM	1.5 mg/ml	1.000 ±	0.000	1.050 ±	0.002**
	3 mg/ml	1.005 ±	0.005	0.996 ±	0.000**
	1 mg/ml	1.000 ±	0.006	1.199 ±	0.006
PPEA	2 mg/ml	0.996 ±	0.009	1.086 ±	0.003**
	4 mg/ml	0.997 ±	0.003	1.006 ±	0.003*
	68mM	0.985 ±	0.018	1.759 ±	0.022**
	0.75 mg/ml	0.996 ±	0.002	1.794 ±	0.023**
PPM	1.5 mg/ml	0.996 ±	0.005	1.697 ±	0.020**
	3 mg/ml	1.006 ±	0.003	1.499 ±	0.014
	1 mg/ml	0.992 ±	0.021	1.016 ±	0.003**
PPEA	2 mg/ml	0.998 ±	0.005	1.705 ±	0.020**
	4 mg/ml	0.998 ±	0.003	1.448 ±	0.013
	17mM + AGE	0.992 ±	0.005	1.059 ±	0.002**
	0.75 mg/ml	1.012 ±	0.012	1.728 ±	0.021**
PPM	1.5 mg/ml	1.022 ±	0.005	1.537 ±	0.016**
	3 mg/ml	1.004 ±	0.004	1.057 ±	0.002
	1 mg/ml	0.997 ±	0.007	1.742 ±	0.021**
PPEA	2 mg/ml	0.996 ±	0.003	1.497 ±	0.014**
	4 mg/ml	1.001 ±	0.009	1.274 ±	0.004***
	34mM + AGE	0.993 ±	0.005	1.792 ±	0.023**
	0.75 mg/ml	1.025 ±	0.002	1.814 ±	0.023**
PPM	1.5 mg/ml	1.018 ±	0.004	1.765 ±	0.022**
	3 mg/ml	1.007 ±	0.009	1.562 ±	0.016
	1 mg/ml	0.986 ±	0.001	1.096 ±	0.001**
PPEA	2 mg/ml	1.002 ±	0.010	1.777 ±	0.022**
	4 mg/ml	1.017 ±	0.005	1.548 ±	0.016***
	68mM + AGE	0.992 ±	0.001	1.286 ±	0.005**
	0.75 mg/ml	1.014 ±	0.003	1.786 ±	0.023**
PPM	1.5 mg/ml	1.010 ±	0.001	1.608 ±	0.018**
	3 mg/ml	1.002 ±	0.009	1.175 ±	0.005**
	1 mg/ml	0.997 ±	0.013	1.806 ±	0.023**
PPEA	2 mg/ml	0.995 ±	0.007	1.658 ±	0.019**
	4 mg/ml	1.013 ±	0.009	1.317 ±	0.009**

The level of significance is expressed as p<0.05 (*), p<0.01 (**), p<0.005

(***). AGE, advanced glycation end product; PPEA, *P. pellucida* ethyl acetate;

PPM, *P. pellucida* crude methanolic extract; STAT3, signal transducer and

activator of transcription 3.

4.2.2.3 PPAR- γ

In the current study, the gene expression of PPAR- γ , varies from 0.17 to 0.53 fold across all high glucose and AGE-treated conditions, in relative to that of normal glucose control (Table 4.11, Appendix B1c). When stimulated by AGE, the gene expression of PPAR- γ was further reduced with increased glucose concentration. On the contrary, the protein expression of PPAR- γ was up-regulated under high glucose (34 mM, 68 mM) conditions, with and without AGE (Appendix B1d). The PPAR- γ protein expression showed down-regulation (0.73 fold) under normal glucose AGE-treated condition whereas phosphorylated PPAR- γ proteins were increased (≥ 1.68 folds) in the high glucose and AGE-treated groups (Table 4.11, Appendix B1e).

Under normal glucose (17 mM) and moderately high glucose (34 mM) conditions, the expression of PPAR- γ gene increased with the treatment concentration of *P. pellucida* extracts. Interestingly, treatment of crude methanolic extract with concentration of 1.5 mg/ml onwards was able to maintain the PPAR- γ gene expression level of ARPE-19 under high glucose condition within the range of normal glucose control. The ethyl acetate fraction was able to emulate the same effect at 4 mg/ml plant concentration. Besides, the PPAR- γ gene expression in normal glucose ARPE-19 was higher than that of normal glucose control when treated with either 1.5 mg/ml crude methanolic extract or 4 mg/ml ethyl acetate fraction. In the high glucose (68 mM) and all AGE-treated conditions, *P. pellucida* extracts treatment did not yield noticeable effect on the expression of PPAR- γ gene compared to the respective untreated control groups.

Table 4.11. The relative gene and protein expression of PPAR- γ in ARPE-19 treated with *P. pellucida* crude methanolic extract and ethyl acetate fraction under normal glucose (17 mM), high glucose (34 mM, 68 mM) and AGE-treated conditions.

Group	Relative expression (fold change)		
	PPAR- γ gene	PPAR- γ protein	Phosphorylated-PPAR- γ protein
17mM (control)	1.000 \pm 0.000	1.000 \pm 0.000	1.000 \pm 0.000
PPM	0.75 mg/ml	0.519 \pm 0.015	2.381 \pm 0.095
	1.5 mg/ml	1.022 \pm 0.010*	0.987 \pm 0.018
	3 mg/ml	1.231 \pm 0.029*	0.990 \pm 0.019
PPEA	1 mg/ml	1.281 \pm 0.055	0.992 \pm 0.019
	2 mg/ml	0.987 \pm 0.018	0.991 \pm 0.019
	4 mg/ml	1.055 \pm 0.027*	0.991 \pm 0.019
34mM	1.204 \pm 0.041***	1.107 \pm 0.027****	0.988 \pm 0.018****
PPM	0.75 mg/ml	0.698 \pm 0.008**	2.643 \pm 0.043****
	1.5 mg/ml	0.807 \pm 0.018	2.518 \pm 0.040****
	3 mg/ml	0.944 \pm 0.016	2.399 \pm 0.037****
PPEA	1 mg/ml	0.566 \pm 0.010****	2.658 \pm 0.044****
	2 mg/ml	0.650 \pm 0.019*	2.540 \pm 0.040****
	4 mg/ml	0.811 \pm 0.031	2.461 \pm 0.038****
68mM	0.406 \pm 0.013****	2.731 \pm 0.046****	2.737 \pm 0.115****
PPM	0.75 mg/ml	0.489 \pm 0.014****	0.727 \pm 0.036****
	1.5 mg/ml	0.476 \pm 0.003****	2.685 \pm 0.044****
	3 mg/ml	0.434 \pm 0.011****	2.569 \pm 0.041****
PPEA	1 mg/ml	0.481 \pm 0.002****	2.428 \pm 0.037****
	2 mg/ml	0.422 \pm 0.007****	2.697 \pm 0.045****
	4 mg/ml	0.429 \pm 0.017****	2.584 \pm 0.042****
17mM + AGE	0.417 \pm 0.009****	2.445 \pm 0.038**	1.608 \pm 0.051****
PPM	0.75 mg/ml	0.572 \pm 0.017****	0.777 \pm 0.034*
	1.5 mg/ml	0.504 \pm 0.025****	0.808 \pm 0.034*
	3 mg/ml	0.539 \pm 0.009****	0.910 \pm 0.031
PPEA	1 mg/ml	0.532 \pm 0.009****	0.743 \pm 0.035*
	2 mg/ml	0.518 \pm 0.010****	0.790 \pm 0.034*
	4 mg/ml	0.497 \pm 0.001****	0.899 \pm 0.031
34mM + AGE	0.266 \pm 0.013****	2.570 \pm 0.041****	2.536 \pm 0.104****
PPM	0.75 mg/ml	0.172 \pm 0.003****	2.652 \pm 0.043****
	1.5 mg/ml	0.303 \pm 0.004****	2.513 \pm 0.040****
	3 mg/ml	0.305 \pm 0.009****	2.398 \pm 0.037****
PPEA	1 mg/ml	0.253 \pm 0.004****	2.176 \pm 0.031****
	2 mg/ml	0.277 \pm 0.009****	2.557 \pm 0.041****
	4 mg/ml	0.315 \pm 0.004****	2.441 \pm 0.038****
68mM + AGE	0.242 \pm 0.010****	2.216 \pm 0.032****	1.659 \pm 0.054****
PPM	0.75 mg/ml	0.210 \pm 0.004****	2.614 \pm 0.042****
	1.5 mg/ml	0.210 \pm 0.003****	2.430 \pm 0.037****
	3 mg/ml	0.177 \pm 0.006****	2.310 \pm 0.034****
PPEA	1 mg/ml	0.206 \pm 0.004****	2.641 \pm 0.043****
	2 mg/ml	0.209 \pm 0.003****	2.468 \pm 0.038****
	4 mg/ml	0.213 \pm 0.009****	2.365 \pm 0.036****

The level of significance is expressed as $p < 0.05$ (*), $p < 0.01$ (**), $p < 0.005$ (***), $p < 0.001$ (****). AGE, advanced glycation end product; PPAR- γ , peroxisome proliferator-activated receptor; PPEA, *P. pellucida* ethyl acetate; PPM, *P. pellucida* crude methanolic extract

For protein expression study, the *P. pellucida* crude methanolic extract (3 mg/ml) and ethyl acetate fraction (4 mg/ml) managed to restore the PPAR- γ protein expression of AGE-treated ARPE-19 back to the normal glucose level. However, the plant extracts demonstrated negligible impact on the protein expression of PPAR- γ in ARPE-19 treated with up to 1.5 mg/ml and 2 mg/ml of the respective crude methanolic extract and ethyl acetate fraction across all high glucose and AGE-treated conditions. *P. pellucida* extracts treatment did not cause PPAR- γ phosphorylation in ARPE-19 as reflected by the similar protein level of phosphorylated PPAR- γ in the control group and plant treatment groups under normal glucose condition. Under all high glucose and AGE-treated conditions, the crude methanolic plant extract and ethyl acetate plant fraction down-regulated the expression of phosphorylated PPAR- γ protein in a concentration-dependent trend. Although *P. pellucida* crude methanolic extract (0.75 mg/ml) and ethyl acetate fraction (1 mg/ml) could not prevent the phosphorylation of PPAR- γ in ARPE-19, the expression of phosphorylated PPAR- γ proteins in the normal glucose AGE-treated APRE-19 was suppressed with 3 mg/ml and 4 mg/ml of crude methanolic extract and ethyl acetate fraction, respectively.

4.2.2.4 IL-8

In the current study, the gene and protein expression of pro-inflammatory cytokine IL-8 was up-regulated in the high glucose (34 mM, 68 mM) and AGE-treated ARPE-19 (Table 4.12, Appendix B2a and B3a). The highest increment of 5.50 folds for IL-8 gene expression was observed in the high glucose (68 mM) AGE-treated APPE-19 when compared to the normal glucose control. A significant increase in IL-8 protein can also be observed in the high glucose (68 mM) and AGE-treated (17 mM, 34 mM,

68 mM) conditions. When compared to moderately high glucose (34 mM) condition, there was an increase in both IL-8 gene and protein expression in the normal glucose AGE-treated condition, with differences of 43 % and 27 %, respectively.

In general, treatment of *P. pellucida* extracts on ARPE-19 led to a concentration-dependent down-regulation of IL-8. Interestingly, the gene and protein expression levels of IL-8 in the plant-treated normal glucose ARPE-19 reduced by ≥ 13 % when compared to the normal glucose control. In addition, both crude methanolic extract (1.5 mg/ml) and ethyl acetate fraction (2 mg/ml) suppressed the gene and protein expression of IL-8 in normal glucose AGE-treated condition. Although the *P. pellucida* crude methanolic extract (0.75 mg/ml) and ethyl acetate fraction (1 mg/ml) did not affect the IL-8 gene expression under high glucose (68 mM) AGE-treated condition, the protein level of IL-8 was reduced with the treatment of similar concentration of crude methanolic extract and ethyl acetate fraction.

Table 4.12. The relative gene and protein expression of IL-8 and MCP-1 in ARPE-19 treated with *P. pellucida* crude methanolic extract and ethyl acetate fraction under normal glucose (17 mM), high glucose (34 mM, 68 mM) and AGE-treated conditions.

Group		Relative expression (fold change)							
		IL-8 gene		IL-8 protein		MCP-1 gene		MCP-1 protein	
17mM (control)		1.000 ± 0.000		1.000 ± 0.000		1.000 ± 0.000		1.000 ± 0.000	
PPM	0.75 mg/ml	2.148 ± 0.046*		1.575 ± 0.021*		6.652 ± 0.213		2.491 ± 0.034	
	1.5 mg/ml	0.783 ± 0.024*		0.894 ± 0.004*		0.975 ± 0.020		0.962 ± 0.001	
	3 mg/ml	0.765 ± 0.020*		0.880 ± 0.004*		1.088 ± 0.024		0.980 ± 0.001	
PPEA	1 mg/ml	0.753 ± 0.035		0.864 ± 0.005*		1.042 ± 0.049		0.994 ± 0.001	
	2 mg/ml	0.975 ± 0.031*		0.874 ± 0.005*		1.017 ± 0.029		0.994 ± 0.001	
	4 mg/ml	0.796 ± 0.027*		0.839 ± 0.006*		0.994 ± 0.004		0.962 ± 0.001	
34mM		0.852 ± 0.021**		0.832 ± 0.006*		1.134 ± 0.017**		0.957 ± 0.001****	
PPM	0.75 mg/ml	1.950 ± 0.023****		1.321 ± 0.012*		7.301 ± 0.047****		1.729 ± 0.016****	
	1.5 mg/ml	1.365 ± 0.025*		1.229 ± 0.009*		5.128 ± 0.111****		1.356 ± 0.008****	
	3 mg/ml	1.192 ± 0.040		1.148 ± 0.006*		4.495 ± 0.183*		1.182 ± 0.005****	
PPEA	1 mg/ml	1.951 ± 0.047*		1.352 ± 0.013*		6.877 ± 0.109****		1.899 ± 0.021****	
	2 mg/ml	1.557 ± 0.013****		1.284 ± 0.011*		6.166 ± 0.226**		1.540 ± 0.012****	
	4 mg/ml	1.192 ± 0.042		1.175 ± 0.007*		5.044 ± 0.080****		1.397 ± 0.009****	
68mM		4.291 ± 0.032****		2.260 ± 0.047*		11.35 ± 0.642*		3.077 ± 0.044****	
PPM	0.75 mg/ml	3.778 ± 0.162**		2.174 ± 0.043*		5.804 ± 0.189****		2.045 ± 0.024****	
	1.5 mg/ml	3.605 ± 0.108*		1.709 ± 0.026*		11.71 ± 0.307***		2.370 ± 0.031****	
	3 mg/ml	2.396 ± 0.095****		1.395 ± 0.015*		8.750 ± 0.259****		1.797 ± 0.018****	
PPEA	1 mg/ml	2.243 ± 0.008*		1.176 ± 0.007*		8.342 ± 0.150****		1.461 ± 0.010****	
	2 mg/ml	3.552 ± 0.126**		1.768 ± 0.028*		10.98 ± 0.288**		2.451 ± 0.031****	
	4 mg/ml	3.100 ± 0.066****		1.470 ± 0.017*		9.839 ± 0.309**		2.113 ± 0.024****	
17mM + AGE		2.318 ± 0.034*		1.262 ± 0.010*		8.118 ± 0.251**		1.972 ± 0.022****	
PPM	0.75 mg/ml	0.867 ± 0.030		1.634 ± 0.023*		1.524 ± 0.068*		1.481 ± 0.011****	
	1.5 mg/ml	0.744 ± 0.020*		1.019 ± 0.001		1.341 ± 0.038*		1.089 ± 0.002	
	3 mg/ml	0.697 ± 0.015*		0.921 ± 0.003**		1.080 ± 0.046		1.004 ± 0.001	
PPEA	1 mg/ml	2.779 ± 0.062**		1.647 ± 0.024*		1.585 ± 0.023**		1.574 ± 0.013****	
	2 mg/ml	0.781 ± 0.009**		1.045 ± 0.002		1.092 ± 0.012*		1.287 ± 0.007****	
	4 mg/ml	0.653 ± 0.010**		0.939 ± 0.002**		1.003 ± 0.037		0.971 ± 0.001	
34mM + AGE		4.810 ± 0.143**		2.160 ± 0.090*		14.87 ± 1.192*		2.626 ± 0.037****	
PPM	0.75 mg/ml	5.509 ± 0.125*		2.334 ± 0.049*		31.30 ± 1.152**		3.623 ± 0.058****	
	1.5 mg/ml	2.400 ± 0.091*		1.477 ± 0.018*		17.47 ± 0.565**		1.888 ± 0.020****	
	3 mg/ml	1.888 ± 0.106*		1.270 ± 0.010*		16.44 ± 0.535****		1.492 ± 0.011****	
PPEA	1 mg/ml	1.222 ± 0.015**		1.122 ± 0.005*		11.82 ± 0.200****		1.304 ± 0.007****	
	2 mg/ml	2.858 ± 0.069*		1.445 ± 0.016*		15.47 ± 0.065**		2.003 ± 0.022****	
	4 mg/ml	2.150 ± 0.072*		1.302 ± 0.011*		17.42 ± 0.696****		1.737 ± 0.017****	
68mM + AGE		1.347 ± 0.031****		1.149 ± 0.006*		12.19 ± 0.168**		1.505 ± 0.012****	
PPM	0.75 mg/ml	5.839 ± 0.175**		1.869 ± 0.032*		33.72 ± 1.592*		2.481 ± 0.033****	
	1.5 mg/ml	4.800 ± 0.049****		1.463 ± 0.017*		32.87 ± 1.178**		1.905 ± 0.020****	
	3 mg/ml	3.320 ± 0.021****		1.193 ± 0.007*		27.76 ± 1.523*		1.624 ± 0.014****	
PPEA	1 mg/ml	6.026 ± 0.102****		1.857 ± 0.031*		32.20 ± 0.872****		2.733 ± 0.037****	
	2 mg/ml	4.779 ± 0.137**		1.484 ± 0.018*		30.27 ± 1.553*		2.550 ± 0.035****	
	4 mg/ml	3.759 ± 0.125**		1.231 ± 0.009*		29.55 ± 1.848*		2.098 ± 0.025****	

The level of significance is expressed as p<0.05 (*), p<0.01 (**), p<0.005 (***), p<0.001 (****). AGE, advanced glycation end product; IL-8, interleukin 8; MCP-1, monocyte chemoattract protein; PPEA, *P. pellucida* ethyl acetate; PPM, *P. pellucida* crude methanolic extract

4.2.2.5 MCP-1

When compared to the normal glucose control, the relative fold change of MCP-1 gene and protein expression across the high glucose (34 mM, 68 mM) and AGE-treated groups ranged from 2.04 to 32.22 folds (Table 4.12, Appendix B2b and B3b). Similar to IL-8, the highest increment for the gene expression of MCP-1 was observed in the high glucose (68 mM) AGE-treated ARPE-19. This was followed by the high glucose (68 mM) and moderately high glucose (34 mM) AGE-treated ARPE-19. The modest increase in MCP-1 gene expression was observed in the moderately high glucose (34 mM) and normal glucose AGE-treated conditions. On the contrary, the smallest increase in MCP-1 protein expression was observed in the normal glucose AGE-treated ARPE-19, followed by both the moderately high glucose (34 mM) and its corresponding AGE-treated condition.

Unlike IL-8, *P. pellucida* extracts treatment did not significantly affect the gene and protein expression of MCP-1 in ARPE-19 under normal glucose condition. It was worth noting that the crude methanolic extract and ethyl acetate fraction decreased the gene expression of MCP-1 by at least 23 % in moderately high glucose (34 mM) stimulated ARPE-19. The maximum inhibition of MCP-1 protein expression was also observed in ARPE-19 treated with 1.5 mg/ml of crude methanolic extract and 2 mg/ml of ethyl acetate fraction under the same condition. On the other hand, a decrease in MCP-1 gene expression of ARPE-19 was attained after treating with 1.5 mg/ml of crude methanolic extract and 4 mg/ml ethyl acetate fraction for *P. pellucida*. Besides, the crude methanolic extract (3 mg/ml) and ethyl acetate fraction (4 mg/ml) suppressed the transcription of MCP-1 under normal glucose AGE-treated condition, in which the gene and protein expression of MCP-1 were similar to the normal glucose control. Similar to

the scenario observed with IL-8, while the expression of MCP-1 protein was reduced by *P. pellucida* extracts treatment in high glucose (68 mM) and AGE-treated (34 mM, 68 mM) conditions, the gene expression remained consistent across varying treatment concentration of crude methanolic extract and ethyl acetate fraction.

4.2.2.6 MMP2

Across the high glucose (34 mM, 68 mM) and AGE-treated conditions, increased gene and protein expression of MMP2 compared to the normal glucose control was observed (Table 4.13, Appendix B2c and 3c). The relative fold change of MMP2 gene expression in the high glucose (68 mM) and AGE-treated (34 mM, 68 mM) ARPE-19 was the highest (4.27-7.79 folds). This was followed by the moderately high glucose (34 mM) and normal glucose AGE-treated ARPE-19 with similar gene expression of MMP2. In terms of protein expression, a significant increase can be observed in the high glucose (34 mM, 68 mM) and their AGE-treated counterparts. The smallest increase in MMP2 protein expression was observed in the normal glucose AGE-treated condition.

The gene and protein expression of MMP2 remain unchanged in ARPE-19 after treating with *P. pellucida* crude methanolic extract and ethyl acetate fraction. Except for the high glucose AGE-treated (68 mM) condition, *P. pellucida* extracts have reduced the gene expression of MMP2 by $\geq 14\%$ in the remaining high glucose and AGE-treated conditions. The most significant decrease in MMP2 gene expression occurred in the normal glucose AGE-treated condition (74%). On the other hand, the crude methanolic extract (0.75 mg/ml) and ethyl acetate fraction (1 mg/ml) decreased the production of MMP2 protein by 8% in the high glucose AGE-treated (68 mM) condition. Furthermore, the crude methanolic extract and

ethyl acetate fraction also suppressed the gene expression of MMP2 in normal glucose AGE-treated condition from as low as 1.5 mg/ml and 2 mg/ml, respectively. In addition to reducing the gene expression of MMP2 in moderately high glucose AGE-treated (34 mM) condition, the highest concentration of crude methanolic extract and ethyl acetate fraction suppressed the protein expression of MMP2.

Table 4.13. The relative gene and protein expression of MMP2 and VEGF in ARPE-19 treated with *P. pellucida* crude methanolic extract and ethyl acetate fraction under normal glucose (17 mM), high glucose (34 mM, 68 mM) and AGE-treated conditions.

Group	Relative expression (fold change)							
	MMP2 gene		MMP2 protein		VEGF gene		VEGF protein	
17mM (control)								
		1.000 ± 0.000		1.000 ± 0.000		1.000 ± 0.000		1.000 ± 0.000
PPM	0.75 mg/ml	5.181 ± 0.151		2.626 ± 0.029		2.976 ± 0.024		1.486 ± 0.014
	1.5 mg/ml	1.050 ± 0.007		0.997 ± 0.001		0.973 ± 0.020		0.984 ± 0.006
	3 mg/ml	1.040 ± 0.043		0.989 ± 0.001		1.047 ± 0.025		0.986 ± 0.019
PPEA	1 mg/ml	1.042 ± 0.035		1.000 ± 0.001		0.958 ± 0.005		0.995 ± 0.023
	2 mg/ml	1.026 ± 0.025		0.990 ± 0.001		0.998 ± 0.029		0.918 ± 0.017
	4 mg/ml	1.006 ± 0.007		0.981 ± 0.001		0.970 ± 0.018		0.924 ± 0.017
34mM								
		1.008 ± 0.004*		1.007 ± 0.001****		1.048 ± 0.057****		0.966 ± 0.018***
PPM	0.75 mg/ml	4.947 ± 0.127***		2.106 ± 0.020****		2.872 ± 0.043****		1.260 ± 0.008**
	1.5 mg/ml	3.613 ± 0.060****		1.767 ± 0.014****		2.153 ± 0.060*		1.130 ± 0.025
	3 mg/ml	3.344 ± 0.115*		1.325 ± 0.006****		1.986 ± 0.050*		1.020 ± 0.023
PPEA	1 mg/ml	4.941 ± 0.166**		2.225 ± 0.022****		2.854 ± 0.033****		1.379 ± 0.038*
	2 mg/ml	4.061 ± 0.091***		1.804 ± 0.015****		2.507 ± 0.111*		1.218 ± 0.030
	4 mg/ml	3.250 ± 0.172*		1.440 ± 0.008****		2.043 ± 0.054*		1.121 ± 0.025
68mM								
		7.256 ± 0.427*		2.747 ± 0.031****		3.710 ± 0.137*		1.731 ± 0.023***
PPM	0.75 mg/ml	4.270 ± 0.168*		2.272 ± 0.023****		2.416 ± 0.047****		1.390 ± 0.012*
	1.5 mg/ml	4.399 ± 0.172*		2.305 ± 0.023****		3.811 ± 0.044**		1.466 ± 0.028
	3 mg/ml	3.184 ± 0.131*		1.820 ± 0.015****		2.888 ± 0.074**		1.242 ± 0.031
PPEA	1 mg/ml	2.837 ± 0.146****		1.410 ± 0.008****		2.717 ± 0.064*		1.063 ± 0.023*
	2 mg/ml	4.608 ± 0.025*		2.377 ± 0.024****		3.513 ± 0.167****		1.573 ± 0.047***
	4 mg/ml	3.824 ± 0.134**		1.866 ± 0.016****		3.523 ± 0.067*		1.314 ± 0.010
17mM + AGE								
		3.037 ± 0.078*		1.565 ± 0.010****		3.003 ± 0.099***		1.125 ± 0.006***
PPM	0.75 mg/ml	1.333 ± 0.030*		1.457 ± 0.009****		1.273 ± 0.065		1.237 ± 0.006****
	1.5 mg/ml	1.036 ± 0.062		1.247 ± 0.005****		1.077 ± 0.035		1.153 ± 0.028
	3 mg/ml	0.946 ± 0.036		1.029 ± 0.001		0.987 ± 0.020		1.027 ± 0.005
PPEA	1 mg/ml	1.292 ± 0.033*		1.529 ± 0.010****		1.500 ± 0.025*		1.314 ± 0.025*
	2 mg/ml	1.026 ± 0.024		1.323 ± 0.007****		1.291 ± 0.019*		1.219 ± 0.023*
	4 mg/ml	0.964 ± 0.018		1.050 ± 0.002		1.058 ± 0.063		1.050 ± 0.022
34mM + AGE								
		7.445 ± 0.197**		2.667 ± 0.030****		4.066 ± 0.202*		1.573 ± 0.016****
PPM	0.75 mg/ml	7.894 ± 0.105****		2.748 ± 0.031****		5.102 ± 0.185****		1.790 ± 0.059****
	1.5 mg/ml	7.325 ± 0.093****		2.247 ± 0.022****		4.593 ± 0.055*		1.515 ± 0.013*
	3 mg/ml	6.842 ± 0.064****		1.836 ± 0.015****		4.541 ± 0.157**		1.245 ± 0.024
PPEA	1 mg/ml	5.042 ± 0.088****		1.390 ± 0.008****		3.796 ± 0.088**		1.100 ± 0.022*
	2 mg/ml	6.549 ± 0.089****		2.201 ± 0.022****		4.134 ± 0.044****		1.546 ± 0.028****
	4 mg/ml	7.315 ± 0.128**		1.792 ± 0.015****		4.714 ± 0.106***		1.302 ± 0.007
68mM + AGE								
		5.533 ± 0.203****		1.437 ± 0.009****		3.639 ± 0.126**		1.119 ± 0.027*
PPM	0.75 mg/ml	7.705 ± 0.211***		2.527 ± 0.027****		5.044 ± 0.060*		1.649 ± 0.017****
	1.5 mg/ml	7.775 ± 0.038****		2.097 ± 0.020****		5.117 ± 0.154**		1.340 ± 0.026*
	3 mg/ml	6.966 ± 0.113****		1.654 ± 0.012****		5.118 ± 0.144**		1.138 ± 0.022
PPEA	1 mg/ml	7.853 ± 0.063****		2.368 ± 0.025****		5.156 ± 0.087****		1.701 ± 0.031**
	2 mg/ml	7.624 ± 0.229**		2.140 ± 0.021****		4.930 ± 0.068****		1.425 ± 0.011****
	4 mg/ml	7.201 ± 0.225**		1.726 ± 0.013****		5.027 ± 0.079*		1.221 ± 0.031

The level of significance is expressed as p<0.05 (*), p<0.01 (**), p<0.005 (***), p<0.001 (****). AGE, advanced glycation end product; MMP2, matric metalloproteinase 2; PPEA, *P. pellucida* ethyl acetate; PPM, *P. pellucida* crude methanolic extract ; VEGF, vascular endothelial growth factor

4.2.2.7 VEGF

In this study, higher expression of VEGF gene and protein (Table 4.13, Appendix B2d and B3d) was observed across all high glucose (34 mM, 68 mM) and AGE-treated groups, as compared to the normal glucose control. The relative fold change of VEGF gene expression among the high glucose and AGE-treated ARPE-19 groups varies from 2.37 to 4.96 folds, in relative to that of normal glucose control. On the other hand, the relative fold change of VEGF protein expression ranged between 1.39 and 1.79 folds. The highest VEGF gene expression can be observed in the high glucose (68 mM) AGE-treated ARPE-19. This was followed by high glucose (68 mM) group, moderately high glucose (34 mM) and its AGE-treated counterpart. For both VEGF gene and protein expression, the smallest increment was observed in the normal glucose AGE-treated ARPE-19. Besides, the overall increased of MMP2 gene and protein expression were about 44 % higher than those of VEGF.

Similar to MMP2, the administration of *P. pellucida* crude methanolic extract or ethyl acetate fraction did not significantly affect the gene and protein expression of VEGF in normal glucose ARPE-19. Under moderately high glucose (34 mM) condition, the gene expression of VEGF decreased by 28 % and 16 % folds with the treatment of 1.5 mg/ml and 2 mg/ml, respectively, of the crude methanolic extract and ethyl acetate fraction. Intriguingly, the *P. pellucida* extracts suppressed the gene expression of VEGF, which was up-regulated in the normal glucose AGE-treated ARPE-19. Furthermore, *P. pellucida* crude methanolic extract (3 mg/ml) and ethyl acetate fraction (4 mg/ml), succeeded in reducing the protein expression of VEGF across the high glucose and AGE-treated conditions to a level similar to normal glucose control.

4.2.2.8 GPx

Among the different ARPE-19 groups, their relative fold change of GPx gene expression ranged from 0.12 to 1.00 fold and decreased in the following order: normal glucose control > moderately high glucose (34 mM) > AGE-treated (17 mM) > high glucose (68 mM) > moderately high glucose AGE-treated (34 mM) > high glucose AGE-treated (68 mM) (Table 4.14, Appendix B2e). The expression of GPx proteins showed similar trend among the normal glucose (17 mM) AGE-treated and moderately high glucose (34 mM) groups, as well as in the moderately high glucose (34 mM) AGE-treated and high glucose (68 mM) AGE-treated group (Appendix B3e). The GPx proteins were significantly reduced by $\geq 56\%$ when compared to the normal glucose control.

In general, the gene expression of GPx in ARPE-19 was lower in the presence of AGE compared to the untreated high glucose counterpart without AGE. However, the protein expression of GPx was similar between the AGE-treated (17 mM, 34 mM) ARPE-19. Further reduction in GPx protein expression was observed in high glucose (68 mM) ARPE-19. The lowest protein expression of GPx can be observed in the high glucose (34 mM, 68 mM) AGE-treated groups. *P. pellucida* extracts treatment collectively increased the gene and protein expression of GPx under the high glucose (34 mM, 68 mM) groups and AGE-treated counterparts. Nevertheless, these were unaffected in the normal glucose condition. It was noteworthy to highlight that treatment with ethyl acetate plant fraction from 2 mg/ml onwards increased the gene and protein expression of GPx in high glucose (34 mM, 68 mM) ARPE-19. The crude methanolic extract (3 mg/ml) and ethyl acetate fraction (4 mg/ml) also maintained the GPx gene expression under high glucose (34 mM) condition at a similar level as normal glucose control. However, the same concentration of *P. pellucida* extracts was insufficient to restore the protein level of GPx under the high glucose (34 mM, 68 mM) and AGE-treated conditions.

Table 4.14. The relative gene and protein expression of GPx and SOCS1 in ARPE-19 treated with *P. pellucida* crude methanolic extract and ethyl acetate fraction under normal glucose (17 mM), high glucose (34 mM, 68 mM) and AGE-treated conditions.

Group	Relative expression (fold change)							
	GPx gene		GPx protein		SOCS1 gene		SOCS1 protein	
17mM								
(control)								
		1.000 ± 0.000		1.000 ± 0.000		1.000 ± 0.000		1.000 ± 0.000
PPM	0.75 mg/ml	0.557 ± 0.007		0.400 ± 0.017		1.479 ± 0.012		3.877 ± 0.096
	1.5 mg/ml	0.951 ± 0.011		1.000 ± 0.000		0.966 ± 0.028		0.994 ± 0.001
	3 mg/ml	1.107 ± 0.028		1.006 ± 0.000		1.082 ± 0.039		1.003 ± 0.001
PPEA	1 mg/ml	1.090 ± 0.036		1.005 ± 0.000		1.064 ± 0.045		0.984 ± 0.001
	2 mg/ml	0.967 ± 0.027		1.003 ± 0.000		1.002 ± 0.020		0.987 ± 0.001
	4 mg/ml	1.058 ± 0.030		1.001 ± 0.000		1.006 ± 0.048		0.993 ± 0.001
34mM								
		1.064 ± 0.033****		1.009 ± 0.000****		1.075 ± 0.041****		0.999 ± 0.001**
PPM	0.75 mg/ml	0.641 ± 0.003****		0.400 ± 0.017****		1.558 ± 0.029*		3.021 ± 0.068**
	1.5 mg/ml	0.687 ± 0.004****		0.523 ± 0.013***		1.156 ± 0.014		1.780 ± 0.027**
	3 mg/ml	0.877 ± 0.005		0.628 ± 0.010****		1.121 ± 0.049		1.039 ± 0.002
PPEA	1 mg/ml	0.716 ± 0.008****		0.389 ± 0.017****		1.530 ± 0.037*		3.155 ± 0.073**
	2 mg/ml	0.859 ± 0.029		0.517 ± 0.014****		1.323 ± 0.037*		1.776 ± 0.026***
	4 mg/ml	0.901 ± 0.027		0.601 ± 0.011****		1.048 ± 0.043		1.090 ± 0.003
68mM								
		0.328 ± 0.010****		0.246 ± 0.021****		2.486 ± 0.096*		4.441 ± 0.115**
PPM	0.75 mg/ml	0.419 ± 0.016****		0.441 ± 0.016****		1.222 ± 0.036****		4.810 ± 0.126**
	1.5 mg/ml	0.393 ± 0.001****		0.258 ± 0.021***		2.230 ± 0.010*		4.032 ± 0.101**
	3 mg/ml	0.372 ± 0.003****		0.373 ± 0.018****		1.472 ± 0.038		3.324 ± 0.078**
PPEA	1 mg/ml	0.405 ± 0.005****		0.510 ± 0.014****		1.169 ± 0.018*		1.980 ± 0.033***
	2 mg/ml	0.395 ± 0.011****		0.256 ± 0.021****		2.304 ± 0.080***		4.120 ± 0.103**
	4 mg/ml	0.418 ± 0.011****		0.397 ± 0.017****		1.870 ± 0.025		3.452 ± 0.082**
17mM + AGE								
		0.439 ± 0.007**		0.436 ± 0.016****		1.269 ± 0.033*		2.483 ± 0.050**
PPM	0.75 mg/ml	0.495 ± 0.012***		0.520 ± 0.013****		1.288 ± 0.029*		4.409 ± 0.114**
	1.5 mg/ml	0.473 ± 0.008****		0.589 ± 0.012****		0.938 ± 0.019		3.698 ± 0.093**
	3 mg/ml	0.527 ± 0.013***		0.679 ± 0.009****		1.009 ± 0.031		2.305 ± 0.043**
PPEA	1 mg/ml	0.470 ± 0.005****		0.493 ± 0.014****		1.264 ± 0.022*		4.744 ± 0.126**
	2 mg/ml	0.527 ± 0.006****		0.555 ± 0.013****		0.985 ± 0.009		3.606 ± 0.085***
	4 mg/ml	0.571 ± 0.009****		0.613 ± 0.011****		0.924 ± 0.035		2.509 ± 0.050**
34mM + AGE								
		0.203 ± 0.009****		0.176 ± 0.023****		1.800 ± 0.071*		5.276 ± 0.143**
PPM	0.75 mg/ml	0.119 ± 0.003****		0.116 ± 0.025****		2.219 ± 0.077*		5.415 ± 0.146**
	1.5 mg/ml	0.268 ± 0.002****		0.176 ± 0.023****		1.652 ± 0.050		4.910 ± 0.130**
	3 mg/ml	0.304 ± 0.004****		0.244 ± 0.021****		1.323 ± 0.060		4.420 ± 0.115***
PPEA	1 mg/ml	0.285 ± 0.009****		0.457 ± 0.015****		0.914 ± 0.030*		3.019 ± 0.067***
	2 mg/ml	0.237 ± 0.004****		0.181 ± 0.023****		1.683 ± 0.078		5.022 ± 0.133***
	4 mg/ml	0.316 ± 0.010****		0.217 ± 0.022****		1.547 ± 0.073		4.489 ± 0.116**
68mM + AGE								
		0.278 ± 0.009****		0.401 ± 0.017****		0.987 ± 0.035*		3.203 ± 0.074***
PPM	0.75 mg/ml	0.154 ± 0.003****		0.120 ± 0.024****		1.993 ± 0.085*		5.142 ± 0.139**
	1.5 mg/ml	0.168 ± 0.001****		0.171 ± 0.023****		1.669 ± 0.011****		4.791 ± 0.130**
	3 mg/ml	0.320 ± 0.006****		0.211 ± 0.022****		1.123 ± 0.054		3.358 ± 0.078***
PPEA	1 mg/ml	0.157 ± 0.004****		0.120 ± 0.024****		2.109 ± 0.059*		5.285 ± 0.144**
	2 mg/ml	0.161 ± 0.001****		0.160 ± 0.023****		1.626 ± 0.026*		4.692 ± 0.121***
	4 mg/ml	0.166 ± 0.003****		0.255 ± 0.021****		1.161 ± 0.028		3.732 ± 0.091**

The level of significance is expressed as p<0.05 (*), p<0.01 (**), p<0.005 (***), p<0.001 (****).

AGE, advanced glycation end product; GPx, glutathione peroxidase; PPEA, *P. pellucida* ethyl acetate;

PPM, *P. pellucida* crude methanolic extract; SOCS1, suppressor of cytokine signalling 1

4.2.2.9 SOCS1

In this study, the gene and protein expression of SOCS1 were up-regulated across the high glucose (34 mM, 68 mM) and AGE-treated conditions (Table 4.14, Appendix B4a and B4b). Among the untreated groups, the high glucose (68 mM) and AGE-treated conditions caused the highest expression of SOCS1 gene (2.35 folds higher than the normal glucose condition). On the other hand, the protein expression of SOCS1 was elevated in the high glucose conditions of 34 mM (3.88 folds) and 68 mM (4.44 folds). Stimulation by AGE further increased the level of SOCS1 protein (4.81 folds) in ARPE-19. Relatively high protein expression of SOCS1 was observed in the high glucose AGE-treated conditions (34 mM, 68 mM), which was 5.35 folds higher than the normal glucose control. However, the gene expression of SOCS1 among the high glucose (34 mM, 68 mM) and corresponding AGE-treated groups were similar.

The gene and protein expression of SOCS1 were unaffected by *P. pellucida* crude methanolic extract and ethyl acetate fraction as they were comparable to the normal glucose control. The increased gene and protein expression of SOCS1 in the high glucose and AGE-treated ARPE-19 were reversed with the treatment of *P. pellucida* extracts in a concentration-dependent manner. In the high glucose (68 mM) group and its corresponding AGE-treated condition, the gene expression of SOCS1 remained unchanged when treated with *P. pellucida* crude methanolic extract (0.75 mg/ml) and ethyl acetate fraction (1 mg/ml). Despite that, it was interesting to point out that the gene and protein expression of SOCS1 in moderately high glucose (34 mM) condition were maintained at the similar level as that in normal glucose control when treated with the highest concentration of crude methanolic extract (3 mg/ml) and ethyl acetate fraction (4 mg/ml).

4.2.2.10 RAGE

Based on the findings of this study, the gene and protein expression of RAGE was up-regulated across all the high glucose and AGE-treated conditions. There were no significant difference observed in the gene expression of RAGE among the high glucose ARPE-19 (34 mM, 68 mM), both of which were 6.50 folds higher than the normal glucose condition (Table 4.15, Appendix B4c). On the contrary, the relative protein expression of RAGE (Table 4.15, Appendix B4d) was higher in the high glucose (68 mM) ARPE-19 (7.07 folds), as compared to the moderately high glucose (34 mM) condition (4.97 folds). The gene and protein expressions of RAGE were further elevated under the high glucose (34 mM, 68 mM) AGE-treated conditions. Conversely, the protein level of sRAGE decreased in all high glucose and AGE-treated ARPE-19, compared to the normal glucose condition (Table 4.15, Appendix B4e). The protein level of sRAGE was suppressed in the high glucose (68 mM) and high glucose AGE-treated (68 mM) conditions. Nevertheless, a higher level of sRAGE was observed in moderately high glucose (34 mM) and AGE-treated (17 mM, 34 mM) conditions, which was 30 % lower than the level observed in the normal glucose control.

The gene and protein expression of RAGE in the *P. pellucida*-treated normal glucose ARPE-19 were comparable to the normal glucose control. Besides, a reduction in gene and protein expression for RAGE was observed with increased concentration of *P. pellucida* extracts under high glucose and AGE-treated conditions. Although the lowest concentration of crude methanolic extract (0.75 mg/ml) and ethyl acetate fraction (1 mg/ml) did not alter the RAGE gene expression in high glucose (68 mM) AGE-treated condition, the crude methanolic extract (3 mg/ml) and ethyl acetate fraction (4 mg/ml) suppressed the gene expression of RAGE under high glucose (34 mM, 68 mM) and normal glucose AGE-treated conditions.

Table 4.15. The relative gene and protein expression of RAGE and sRAGE in ARPE-19 treated with *P. pellucida* crude methanolic extract and ethyl acetate fraction under normal glucose (17 mM), high glucose (34 mM, 68 mM) and AGE-treated conditions.

Group	Relative expression (fold change)		
	RAGE gene	RAGE protein	sRAGE protein
17mM (control)	1.000 ± 0.000	1.000 ± 0.000	1.000 ± 0.000
PPM	0.75 mg/ml	6.264 ± 0.080	4.968 ± 0.193
	1.5 mg/ml	0.944 ± 0.030	1.044 ± 0.002
	3 mg/ml	1.053 ± 0.036	0.996 ± 0.000
PPEA	1 mg/ml	1.047 ± 0.028	0.995 ± 0.000
	2 mg/ml	0.983 ± 0.028	0.991 ± 0.000
	4 mg/ml	0.985 ± 0.041	1.050 ± 0.002
34mM	1.050 ± 0.033****	1.020 ± 0.001*	1.124 ± 0.009*
PPM	0.75 mg/ml	3.013 ± 0.048****	4.943 ± 0.193*
	1.5 mg/ml	1.484 ± 0.029*	3.953 ± 0.145*
	3 mg/ml	1.049 ± 0.045	2.661 ± 0.081*
PPEA	1 mg/ml	3.745 ± 0.028****	4.706 ± 0.181*
	2 mg/ml	1.359 ± 0.046*	4.245 ± 0.161*
	4 mg/ml	0.965 ± 0.010	2.799 ± 0.087*
68mM	6.738 ± 0.325*	7.065 ± 0.293*	0.491 ± 0.001*
PPM	0.75 mg/ml	13.50 ± 0.418****	5.630 ± 0.226*
	1.5 mg/ml	4.281 ± 0.086*	6.337 ± 0.265*
	3 mg/ml	2.004 ± 0.051	4.979 ± 0.192*
PPEA	1 mg/ml	1.227 ± 0.012****	3.813 ± 0.135*
	2 mg/ml	3.495 ± 0.059*	6.219 ± 0.250*
	4 mg/ml	1.865 ± 0.082	5.821 ± 0.241*
17mM + AGE	1.116 ± 0.026**	4.165 ± 0.154*	0.712 ± 0.009*
PPM	0.75 mg/ml	8.249 ± 0.298**	4.863 ± 0.189*
	1.5 mg/ml	3.404 ± 0.055****	4.036 ± 0.149*
	3 mg/ml	1.446 ± 0.052	3.251 ± 0.110*
PPEA	1 mg/ml	8.621 ± 0.139****	5.433 ± 0.217*
	2 mg/ml	2.929 ± 0.059***	4.403 ± 0.169*
	4 mg/ml	1.254 ± 0.047	3.457 ± 0.118*
34mM + AGE	20.08 ± 0.712**	6.075 ± 0.245*	0.637 ± 0.022*
PPM	0.75 mg/ml	26.23 ± 0.255***	7.787 ± 0.331*
	1.5 mg/ml	13.90 ± 0.394*	5.641 ± 0.231*
	3 mg/ml	7.677 ± 0.356**	4.512 ± 0.170*
PPEA	1 mg/ml	3.537 ± 0.090****	3.846 ± 0.137*
	2 mg/ml	11.48 ± 0.073*	5.702 ± 0.226*
	4 mg/ml	7.085 ± 0.289****	5.027 ± 0.201*
68mM + AGE	2.971 ± 0.045****	4.200 ± 0.156*	0.774 ± 0.051*
PPM	0.75 mg/ml	25.66 ± 1.029**	6.915 ± 0.289*
	1.5 mg/ml	14.01 ± 0.179****	6.030 ± 0.247*
	3 mg/ml	6.185 ± 0.115****	4.842 ± 0.187*
PPEA	1 mg/ml	26.27 ± 0.777***	7.053 ± 0.296*
	2 mg/ml	12.91 ± 0.048****	6.541 ± 0.276*
	4 mg/ml	5.381 ± 0.567*	5.023 ± 0.194*

The level of significance is expressed as p<0.05 (*), p<0.01 (**), p<0.005 (***), p<0.001 (****). AGE, advanced glycation end product; PPEA, *P. pellucida* ethyl acetate; PPM, *P. pellucida* crude methanolic extract; RAGE, receptor for advanced glycation end product; sRAGE, soluble receptor for advanced glycation end product

On the other hand, the protein level of sRAGE was escalated when treated with the highest possible concentration of crude methanolic extract (3 mg/ml) and ethyl acetate fraction (4 mg/ml). Interestingly, the level of sRAGE in the *P. pellucida* extracts-treated normal glucose groups was even higher than that of normal glucose control. Similar to RAGE, the crude methanolic extract (0.75 mg/ml) and ethyl acetate fraction (1 mg/ml) failed to raise the sRAGE proteins in the high glucose (34 mM, 68 mM) ARPE-19 and their AGE-treated counterparts. Despite that, treatment with ethyl acetate fraction (4 mg/ml) restored the protein level of sRAGE in normal glucose AGE-treated condition to the level of normal glucose control. Under high glucose (68 mM) and its corresponding AGE-treated conditions, sRAGE proteins increased with the treatment of crude methanolic extract at a starting treatment concentration of 1.5 mg/ml onwards, which was lower than the ethyl acetate fraction (4 mg/ml). Appendix B5-7 depicts the western blot bands of the biomarkers in ARPE-19, under normal glucose, high glucose and AGE-treated conditions.

4.3 Phase 3: Phytochemicals identification

The phytochemical profile of *P. pellucida* was evaluated with TLC to optimise the purification process and subsequent identification of phytochemicals from the plant. The findings from TLC in the optimization step indicated that all plant solvent fractions of *P. pellucida* demonstrated similar phytochemical profiles as that of crude methanolic extract (Appendix C1). Based on TLC, a higher concentration of phytochemical content was expected in crude methanolic extract as the plant fractions were derived from the crude extract. Hence, the crude methanolic extract of *P. pellucida* was chosen for further purification and identification of phytochemicals.

In order to characterise the complex mixture of phytochemicals from *P. pellucida*, the phytochemicals present in the crude methanolic extract of the plant were initially purified with silica gel column chromatography to yield semi-purified fractions of increasing polarity. This allowed for the separation of different compounds based on their affinity to the stationary phase. Subsequently, the semi-purified fractions were further purified using PRC, a process that enables finer separation and purification of phytochemicals. The purified fractions were subjected to subsequent chemical characterisation with ^1H NMR, ^{13}C NMR, FTIR, UV-Vis and ESIMS analyses.

4.3.1 Purification and identification of fraction 1

P. pellucida crude methanolic extract was subjected to silica gel column chromatography purification and yielded a total of thirty-five semi-purified fractions. Fractions with similar TLC profile were pooled together. The semi-purified fractions, PPM/A and PPM/B were proceeded to

phytochemical characterisation with ^1H NMR analysis. Based on the results (Appendix C2-3), the ^1H NMR chemical shifts of PPM/A and PPM/B were comparable to literature values for a mixture of non-polar phenylpropanoids such as dillapiole and 2,4,5-trimethoxystyrene and fatty acids (de Moraes and Kato, 2021). To confirm the identity of the compounds, PPM/A and PPM/B were selected for purification with PRC on silica gel by eluting with 100 % hexane and chloroform-hexanes (1:5), respectively. The resulting fractions, PPM/A/5-7 and PPM/B/2-4 were further purified with PRC, eluted with diethyl ether-hexanes (1:50) to yield the respective fractions, PPM/A/5-7/2-3 and PPM/B/2-4/7. The fractions each displayed a TLC spot of similar R_f value (Figure 4.10). The fractions were then characterised with ^1H NMR, which suggested comparable spectral value to dillapiole (Appendix C4-5) (de Moraes and Kato, 2021). On the other hand, the TLC profile of fraction PPM/B/5-6 (Figure 4.11) revealed two TLC spots. The first spot was identified as fraction 1 by eluting with diethyl ether-hexanes (1:15). Fraction 1 was characterised with ^1H NMR, ^{13}C NMR, FTIR, UV-Vis and ESIMS analysis by comparing the spectral values with previous reports for dillapiole.

4.3.1.1 Fraction 1

$\text{C}_{12}\text{H}_{14}\text{O}_4$ (150 mg), Pale yellow oil. UV λ_{max} (EtOH) nm: 222, 286. FTIR ν_{max} cm^{-1} : 2933.94, 1626.68, 1462.26, 1047.86, 914.16. ^1H NMR (400 MHz, CDCl_3): δ_{H} 6.35 (1H, s, H-6), 5.95 (1H, m, H-8), 5.88 (2H, s, O-CH₂-O), 5.05 (1H, d, $J=6.6$, H-9), 5.03 (1H, s, H-9), 4.01 (3H, s, 3-OCH₃), 3.75 (3H, s, 2-OCH₃), 3.31 (2H, d, $J=6.5$, H-7). ^{13}C NMR (100 MHz, CDCl_3): δ_{C} 144.60 (C-4), 144.31 (C-3), 137.39 (C-2), 135.94 (C-5), 126.05 (C-1), 115.54 (C-9), 102.76 (C-6), 101.10 (O-CH₂-O), 61.28 (2-OCH₃), 59.96 (3-OCH₃), 33.91 (C-7). ESIMS m/z : 223 $[\text{M}+\text{H}]^+$ ($\text{C}_{12}\text{H}_{14}\text{O}_4$).

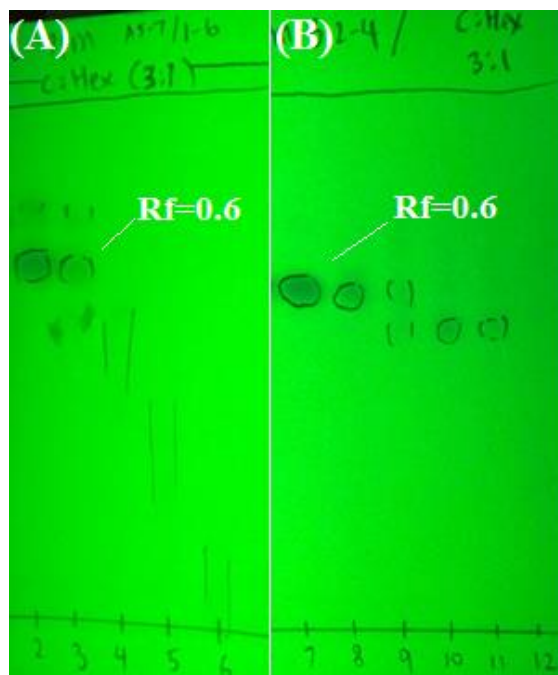


Figure 4.10. The TLC profiles of PPM/A/5-7 (A) and PPM/B/2-4 (B). Rf: retention factor.

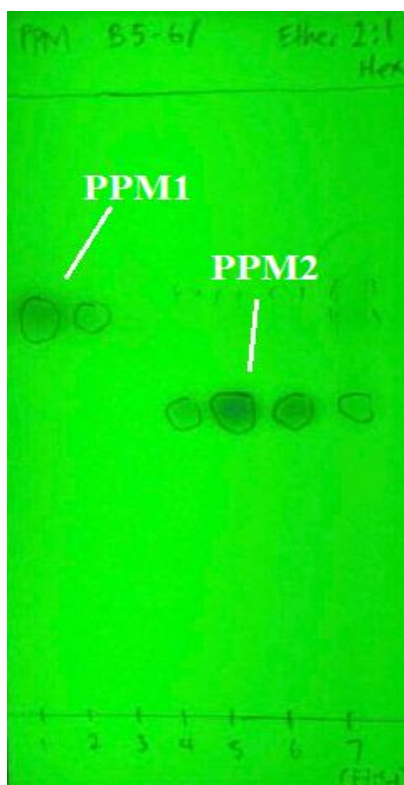


Figure 4.11. The TLC profile of PPM/B/5-6.

4.3.1.2 Chemical characterisation of fraction 1

The ^1H NMR, ^{13}C NMR (de Moraes and Kato, 2021), UV-Vis and FTIR (Fatope *et al.*, 2006; Iqbal *et al.*, 2020) spectral data of fraction 1 (Appendix D1-4) were compared with previous studies. The spectra data collectively suggested fraction 1 was mainly consisted of phenylpropanoid. The ^1H NMR chemical shifts at δ_{H} 5.95 ppm, 5.05 ppm, 5.03 ppm and 3.31 ppm were attributed to the presence of allyl groups in the chemical structure (Appendix D1) (Vučković *et al.*, 2021). The presence of methylenedioxy group was indicated by the singlet at δ_{H} 5.88 ppm while the methoxy groups resulted in the signals at δ_{H} 4.01 ppm and 3.75 ppm (Vučković *et al.*, 2021). The chemical compound in fraction 1 shared some structural similarities with dillapiole and apiole (Alam *et al.*, 2013). According to Alam *et al.* (2013), the major structural difference between dillapiole and apiole lies in the chemical shift of quaternary carbon and C-6. The chemical shift of quaternary carbons in dillapiole was in the range of δ_{C} 126 to 144 ppm (Appendix D2) whereas the quaternary carbons of apiole should remain below δ_{C} 140 ppm (Alam *et al.*, 2013). Besides, the chemical shift for C-6 (δ_{C} 108.5 ppm) in apiole should be located downfield when compared to that (δ_{C} 102.75 ppm) in dillapiole (Alam *et al.*, 2013). Hence, the findings suggested that fraction 1 was majorly composed of dillapiole rather than apiole.

The UV-Vis spectrum of fraction 1 showed two absorption bands at 222 nm and 286 nm, in which the highest absorbance was observed at 222 nm (Appendix D3). This observation was comparable to previous report for dillapiole (Alam *et al.*, 2013; Fatope *et al.*, 2006). The maximum peak at 222 nm was indicative of the presence of methoxy group on the structure of dillapiole (Kitanovski *et al.*, 2014) while the absorption band at the region near 280 nm was attributed to the presence of fatty acids (Saito *et*

al., 2023). FTIR analysis of fraction 1 (Appendix D4) demonstrated that the absorption band at 2933 cm^{-1} was due to the C–H stretching of methyl and methylene groups in the structure of dillapiole (Iqbal *et al.*, 2020). The absorption at 1627 cm^{-1} may suggest the presence of C=C stretching for the aromatic ring on dillapiole (Iqbal *et al.*, 2020). When coupled with the absorption band at 1462 cm^{-1} , this could indicate that the compound adopted a benzodioxole ring system (Iqbal *et al.*, 2020). The presence of methoxy groups in dillapiole was illustrated by the absorption bands of C–H bending and C–O stretching, which ranged from 1462 cm^{-1} to 1048 cm^{-1} (Iqbal *et al.*, 2020; Merck, 2022). Furthermore, the co-occurrence of C=C bending at 914 cm^{-1} and methylene group may suggest the presence of an allyl functional group (Merck, 2022). The FTIR spectral data of fraction 1 conformed with a previous study for dillapiole (Iqbal *et al.*, 2020). In addition, the molecular ion (MH^+) of fraction 1 displayed m/z value of 223 (Appendix D5), which was comparable to the molecular formula, $\text{C}_{12}\text{H}_{14}\text{O}_4$ for dillapiole (Vučković *et al.*, 2021). The chemical structure of dillapiole was shown in Figure 4.12.

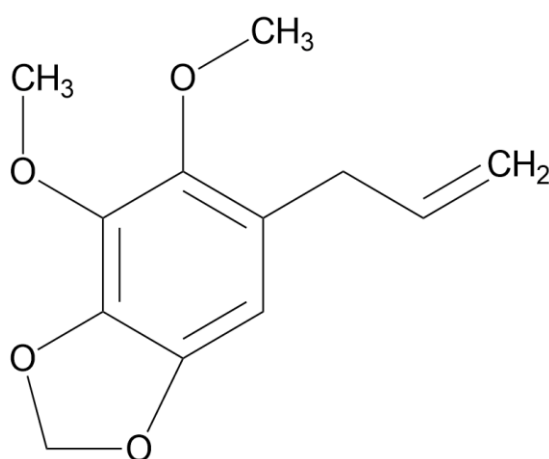


Figure 4.12. The chemical structure of dillapiole.

4.3.2 Purification and identification of fraction 2

Through ^1H NMR analysis, the chemical shifts of dillapiole and 2,4,5-trimethoxystyrene were detected together in fraction PPM/B (Appendix C3). Thus, the fraction PPM/B was subjected to purification with PRC. Purification of PPM/B resulted in two major TLC spots. The second TLC spot from PPM/B/5-6 was eluted as fraction 2 (Figure 4.31) with diethyl ether-hexanes (1:15) using PRC. Fraction 2 was characterised with ^1H NMR, ^{13}C NMR, FTIR, UV-Vis and ESIMS analysis and by comparison with previous literature values.

4.3.2.1 Fraction 2

$\text{C}_{11}\text{H}_{14}\text{O}_3$ (75 mg), Yellow solid; UV λ_{max} (EtOH) nm: 222, 258, 314. FTIR ν_{max} cm^{-1} : 2924.19, 1607.59, 1508.40, 1034.65, 993.03. ^1H NMR (400 MHz, CDCl_3): δ_{H} 7.03 (1H, dd, $J=9.8$, H-7), 7.02 (1H, s, H-6), 6.51 (1H, s, H-3), 5.62 (1H, dd, $J=1.9$, H-8 $_{\text{T}}$), 5.18 (1H, dd, $J=1.9$, H-8 $_{\text{C}}$), 3.90 (3H, s, 2-OCH $_3$), 3.87 (3H, s, 4-OCH $_3$), 3.83 (3H, s, 5-OCH $_3$). ^{13}C NMR (100 MHz, CDCl_3): δ_{C} 151.42 (C-2), 149.67 (C-4), 143.37 (C-5), 130.97 (C-1), 118.62 (C-6), 112.08 (C-3), 109.57 (C-7), 97.79 (C-8), 56.74 (2-OCH $_3$), 56.52 (4-OCH $_3$), 56.09 (5-OCH $_3$). ESIMS m/z : 195 $[\text{M}+\text{H}]^+$ ($\text{C}_{11}\text{H}_{14}\text{O}_3$).

4.3.2.2 Chemical characterisation of fraction 2

Fraction 2 was characterised with ^1H , ^{13}C NMR, FTIR, UV-Vis, MS (Appendix E1-5) and by comparison with previous reported data. The ^1H NMR and ^{13}C NMR data of fraction 2 were consistent with de Moraes and Kato (2021) for 2,4,5-trimethoxystyrene. The MH^+ of fraction 2 exhibited m/z value of 195 in ESIMS (Appendix E5), which was compatible with the molecular formula, $\text{C}_{11}\text{H}_{14}\text{O}_3$ for 2,4,5-trimethoxystyrene (National Center

for Biotechnology Information, 2022a). Analysis of ^1H NMR data (Appendix E1) revealed that the doublet of doublets at δ_{H} 7.02-7.03 ppm and singlet at δ_{H} 6.51 ppm were the signals for the resonating protons on 1,2,4,5-tetrasubstituted aromatic ring of 2,4,5-trimethoxystyrene (Bayma *et al.*, 2000). Besides, the signals at δ_{H} 3.90 ppm, 3.87 ppm and 3.83 ppm were attributed to the three methoxy groups on the aromatic ring, whereby a superimposed multiplet at δ_{H} 3.90 ppm represented the methine proton on the vinyl group (Bayma *et al.*, 2000). A total of seven chemical shifts may reflect the carbon structure (Appendix E2) on the aromatic ring of 2,4,5-trimethoxystyrene (Bayma *et al.*, 2000). Among the signals are δ_{C} 112.08 and 97.79 ppm which represented the two methines; δ_{C} 151.42 ppm, 149.67 ppm and 143.37 ppm for the three carbonyl groups; δ_{C} 118.62 ppm for the quaternary carbon; and δ_{C} 130.97 ppm for the C-1 bonded to a vinyl group (Bayma *et al.*, 2000). Furthermore, three methoxy groups on the aromatic ring were indicated by the chemical shifts at δ_{C} 56.74 ppm, 56.52 ppm and 56.09 ppm (Bayma *et al.*, 2000).

The high intensity of absorbance was observed at 222 nm and 258 nm in the UV-Vis spectrum of fraction 2 (Appendix E3). The absorbance of lower intensity was observed at 314 nm. Similar to dillapiole, the presence of three methoxy groups in 2,4,5-trimethoxystyrene can be indicated by the absorption band at 222 nm (Kitanovski *et al.*, 2014). At 0.3 mg, fraction 2 displayed higher intensity of absorbance at 222 nm when compared to the fraction 1. This could be due to the higher number of methoxy groups on 2,4,5-trimethoxystyrene when compared to dillapiole. Moreover, the UV-Vis spectrum of fraction 2 was comparable to pellucidin A (Quiroz *et al.*, 2020). However, the presence of a styrene structure in 2,4,5-trimethoxystyrene may give rise to the absorbance at 258 nm (National Institute of Standards and Technology, 2022; Rodebush and

Feldman, 1946). This may have explained the absence of absorption band at 258 nm for pellucidin A due to the substituted vinyl group (Queiroz *et al.*, 2020). The FTIR analysis also suggested that the major compound in fraction 2 adopted a phenylpropanoid structure (Appendix E4). The C-H stretching in the methyl and methylene groups of 2,4,5-trimethoxystyrene was indicated by the absorption at 2924 cm^{-1} (Iqbal *et al.*, 2020). The presence of aromatic ring on 2,4,5-trimethoxystyrene can be highlighted by the absorption band at 1608 cm^{-1} (Iqbal *et al.*, 2020). The trimethoxy groups in 2,4,5-trimethoxystyrene was indicated by the C-H bending and C-O stretching, which spanned an absorption range between 1508 cm^{-1} and 1034 cm^{-1} (Iqbal *et al.*, 2020; Merck, 2022). In addition, the absorption at 993 cm^{-1} may indicate the C=C bending for vinyl group in the styrene structure of 2,4,5-trimethoxystyrene (Merck, 2022). The NMR, UV-Vis and FTIR spectral data collectively suggested that fraction 2 was largely comprised of 2,4,5-trimethoxystyrene. The chemical structure of 2,4,5-trimethoxystyrene was shown in Figure 4.13.

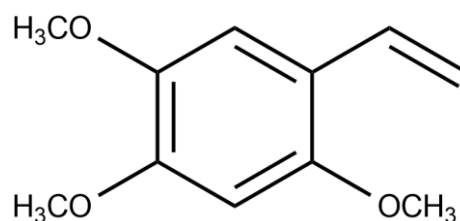


Figure 4.13. The chemical structure of 2,4,5-trimethoxystyrene.

4.3.3 Purification and identification of fraction 3

Purification of PPM/B/7-9 (107.5 mg) with PRC was performed by eluting with diethyl ether-hexanes (1:15), which resulted in 12 fractions. Among the fractions, PPM/B/7-9/1 and PPM/B/7-9/4-5 displayed R_f values

similar to that of dillapiole and 2,4,5-trimethoxystyrene, respectively. In between the fractions, the PPM/B/7-9/2-3 contained an isolated bright blue spot when visualized under 315 nm UV light. It was then separated and eluted as fraction 3, following fraction 1 (dillapiole) but preceding fraction 2 (2,4,5-trimethoxystyrene) using PRC (Figure 4.14). Fraction 3 was characterised by comparing the ^1H NMR, ^{13}C NMR, FTIR, UV-Vis and ESIMS data with previous reports.

4.3.3.1 Fraction 3

$\text{C}_{19}\text{H}_{36}\text{O}_2$ (3.5 mg), Pale yellow oil; UV λ_{max} (EtOH) nm: 225. FTIR ν_{max} cm^{-1} : 2924.34, 1745.08, 1166.61, 772. ^1H -NMR (400 MHz, CDCl_3): δ_{H} 5.34 (1H, s, CH=CH), 5.27 (1H, s, CHO), 4.29 (2H, d, CH_2O), 4.14 (2H, d, CH_2O), 2.77 (2H, s, C=C- CH_2 C=C), 2.32 (2H, s, CH_2 -COO), 2.06 (2H, s, CH_2 -CH=CH), 1.60 (2H, s, CH_2 - CH_2 -COO), 1.25 (2H, s, CH_2), 0.88 (3H, s, CH_3). ^{13}C NMR (100 MHz, CDCl_3): δ_{C} 173.46 (C-1), 130.13 (C-10), 129.83 (C-9), 128.23 (C-13), 128.03 (C-12), 69.03 (β - CH_2O), 62.25 (α - CH_2O), 31.68 (C-16), 25.78 (C-11), 25.02 (C-3), 22.85 (β - CH_3), 14.27 (α - CH_3). ESIMS m/z : 297 $[\text{M}+\text{H}]^+$ ($\text{C}_{19}\text{H}_{36}\text{O}_2$).

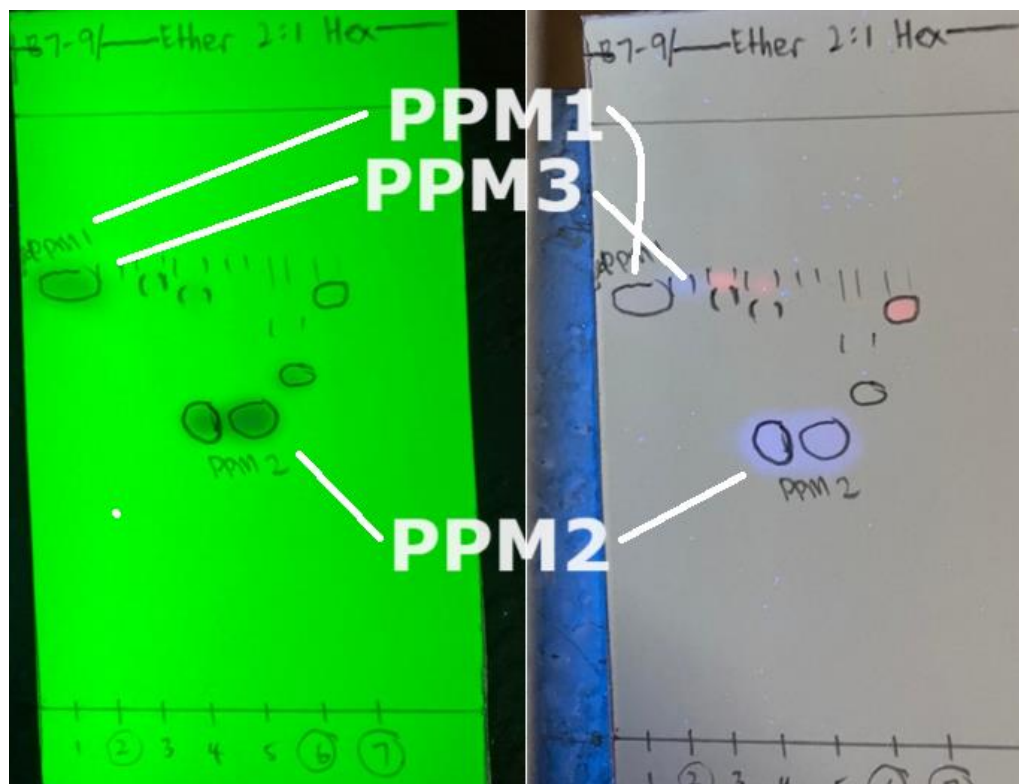


Figure 4.14. The TLC profile of PPM/B/7-9.

4.3.3.2 Chemical characterisation of fraction 3

The ^1H NMR and ^{13}C NMR spectral data of fraction 3 (Appendix F1-2) were in accordance to previous studies for methyl 9-octadecenoic acid (Santos *et al.*, 2018; Thoss *et al.*, 2012). The signals at δ_{H} 0.88 ppm and 1.25 ppm represented the protons that resonate in the respective terminal methyl and methylene groups of methyl 9-octadecenoic acid (Thoss *et al.*, 2012). The rich presence of terminal methyl group also indicated that fraction 3 was majorly composed of fatty acid (Thoss *et al.*, 2012). The signals for protons attached to acyl chains (δ_{H} 1.60 ppm) were also present in all types of fatty acids (Santos *et al.*, 2018). Nevertheless, the protons on allyl group (δ_{H} 2.06 and 2.77 ppm) suggested that fraction 3 was largely comprised of unsaturated fatty acid (Thoss *et al.*, 2012). This was further confirmed by the signal at δ_{H} 5.27, which was attributed to the

presence of olefinic protons linked by a double bond (Santos *et al.*, 2018). The C-1 on fatty acid chain was indicated by the signal at δ_c 173.46 (Thoss *et al.*, 2012). Besides, the chemical shifts ranging from δ_c 14.27 to 31.68 ppm represented the carbons on acyl group (Thoss *et al.*, 2012). From δ_c 128 to 130 ppm, the alkene carbons could be used to determine the position of the double bond present on unsaturated fatty acids (Thoss *et al.*, 2012). In this study, the signal difference between C-9 (δ_c 129.83 ppm) and C-10 (δ_c 130.13 ppm) was 0.3 ppm. For unsaturated fatty acid such as 9-octadecenoic acid, in which the position of double bond was at C-9, the signal difference between C-9 and C-10 is 0.32 ppm (Thoss *et al.*, 2012). Hence, the finding suggested that fraction 3 was majorly composed of methyl 9-octadecenoic acid.

The UV-Vis spectrum of fraction 3 (Appendix F3) displayed one major peak at 225 nm, which may indicate the abundance of methyl or methylene groups in the fraction (Antosiewicz and Shugar, 2016). The faint absorption peak around the region of 280 nm may also suggest the presence of fatty acids (Saito *et al.*, 2023). These findings strongly suggested that fraction 3 was a fraction rich in fatty acid methyl ester since the plant was subjected to extraction with methanol (Kandasamy *et al.*, 2020). The high intensity of absorption bands can be observed in the infrared spectrum of fraction 3 (Appendix F4) at 2924 cm^{-1} that corresponded to the C-H stretching of long chain fatty acids and methyl ester (Merck, 2022). This was followed by the presence of C-O and C=O stretching as indicated by the respective absorptions at 1167 cm^{-1} and 1745 cm^{-1} (Merck, 2022). The two functional groups collectively made up the carboxyl groups of fatty acids. Furthermore, the alkene carbons that imparted the unsaturation to fatty acids were indicated by C=C bending at the absorption band of 772 cm^{-1} (Merck, 2022). ESIMS analysis (Appendix

F5) has demonstrated that fraction 3 displayed MH^+ at m/z of 297, which matched the chemical formula, $C_{19}H_{36}O_2$ for methyl 9-octadecenoic acid (National Center for Biotechnology Information, 2022b). The spectral data collectively confirmed that the fraction 3 was largely comprised of methyl 9-octadecenoic acid. The compound is also known as omega-9 monounsaturated fatty acid. The chemical structure of methyl 9-octadecenoic acid was shown in Figure 4.15.

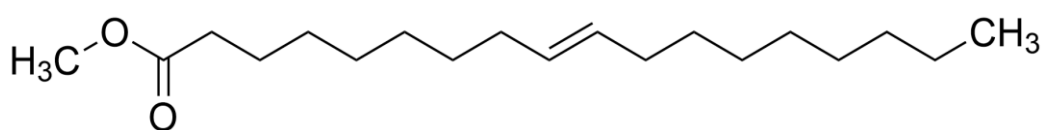


Figure 4.15. The chemical structure of methyl 9-octadecenoic acid.

4.3.4 Purification and identification of fraction 4

The purification of PPM/B/13-15 has resulted in 14 fractions. Among the fractions eluted with chloroform-hexanes (1:1) using PRC, PPM/B/13-15/8 displayed a major reddish broad spot, which was likely a chlorophyll pigment along with stretch of TLC bands that present in the subsequent fractions (Figure 4.16). Further purification of the fraction with dichloromethane-hexanes (9:1) yielded fraction 4 (4.4 mg). Fraction 4 was characterised with 1H NMR, ^{13}C NMR, FTIR, UV-Vis and ESIMS analysis and by comparing with previous spectral data.

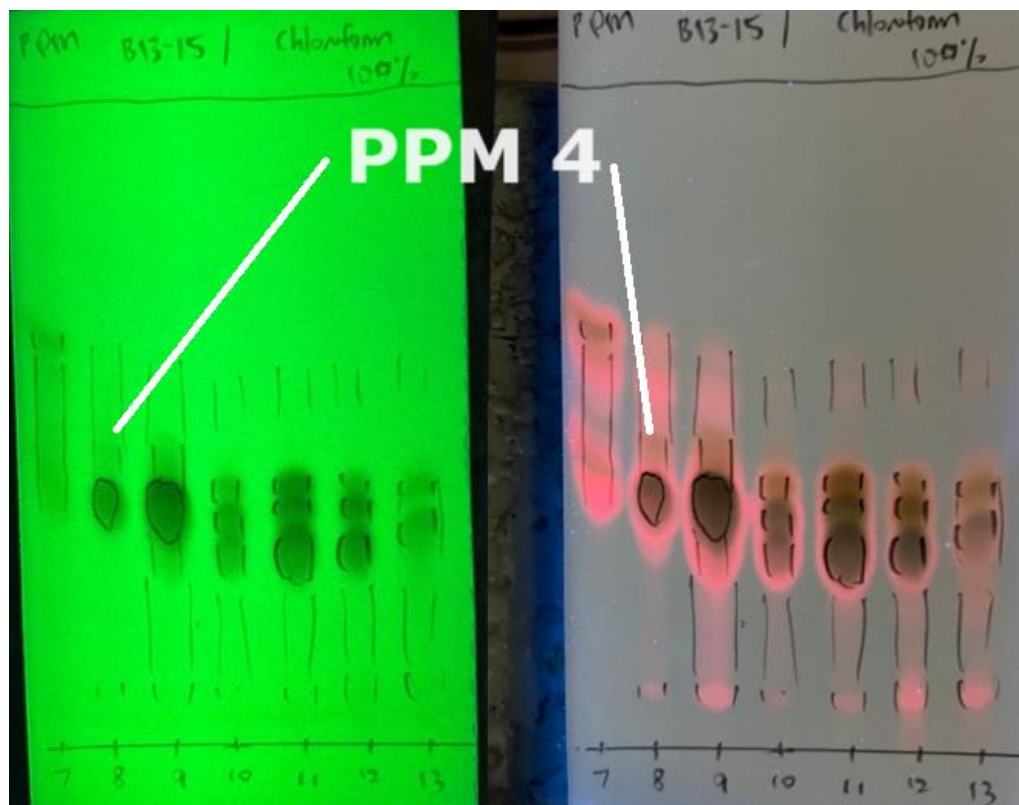


Figure 4.16. The TLC profile of PPM/B/13-15.

4.3.4.1 Fraction 4

$C_{36}H_{38}N_4O_5$ (80 mg), black amorphous solid; UV λ_{max} (EtOH) nm: 401, 500, 530, 612, 669. FTIR ν_{max} cm^{-1} : 2924.77, 1731.21, 1603.82, 1455.52, 1165, 985.55. 1H NMR (400 MHz, $CDCl_3$): δ_H 9.74 (1H, s, H-10), 9.52 (1H, s, H-5), 8.70 (1H, s, H-20), 8.01 (1H, dd, H-3_a), 6.34 (1H, s, H-13_b), 4.44 (1H, q, H-18), 3.89 (3H, s, 13_b-CO₂-CH₃), 3.74 (2H, q, 8-CH₂), 3.43 (3H, s, 2-CH₃), 3.26 (3H, s, 7-CH₃), 1.71 (3H, d, 18_a-CH₃), 1.63 (1H, s, NH). ^{13}C NMR (100 MHz, $CDCl_3$): δ_C 173.21 (C-19), 170.91 (C-13_b-CO₂), 161.07 (C-16), 155.74 (C-6), 149.93 (C-9), 145.55 (C-8), 142.84 (C-1), 138.68 (C-11), 136.48 (C-4), 136.04 (C-3), 131.49 (C-2), 128.98 (C-3_a), 122.70 (C-3_b), 104.13 (C β), 100.51 (C γ), 99.63 (C α), 93.88 (C δ), 61.45 (C-13_b), 54.14 (C-13_b-CO₂-CH₃), 50.31 (C-18), 31.00 (C-17_a), 29.71 (C-17_b), 19.64

(C-8a), 17.57 (C-8b), 12.44 (C-2a), 11.28 (C-7a). ESIMS m/z : 607 $[M+H]^+$ ($C_{36}H_{38}N_4O_5$).

4.3.4.2 Chemical characterisation of fraction 4

The 1H NMR, ^{13}C NMR, UV-Vis, FTIR and MS data of fraction 4 (Appendix G1-5) were consistent with previous literature values for methyl pheophorbide-a (Figure 4.17), a chlorophyll derivative. The upfield signal (δ_H 1.71 ppm) and downfield signals (δ_H 9.74, 9.52 and 8.70 ppm) for the protons (Appendix G1) collectively suggested that the compound contained a pyrrole ring (Ina *et al.*, 2007; Miranda *et al.*, 2017). The presence of vinyl group was indicated by the chemical shift at δ_H 6.34 ppm (Ina *et al.*, 2007). Furthermore, the 1H NMR spectral range of any chlorophyll pigment and its derivatives may vary due to the aromatic ring current effect and different compound concentration used for analysis (Abraham and Rowan, 1981). The aromatic ring current effect was caused by the large conjugated pi system of methyl pheophorbide-a, which gave rise to the shielding of protons located in the center while exposing the peripheral protons (Abraham and Rowan, 1981). However, the central amine will be deshielded, which resulted in the upfield shift at δ_H 1.63 ppm in this study (Chee *et al.*, 2005). Besides, non-covalent bonding may occur among aromatic rings in a phenomenon known as pi-pi stacking (Abraham and Rowan, 1981). This phenomenon may be attributed to the increased concentration of chlorophyll derivative which eventually magnifying the resonances (Abraham and Rowan, 1981). In addition, the lack of phytol in the structure of methyl pheophorbide-a could also lead to a downfield shift when compared to other chlorophyll pigments. The ^{13}C spectral data for fraction 4 was comparable to a previous study (Chee *et al.*, 2005). The

assignment of ^{13}C NMR chemical shift for chlorophyll and derivatives was relative straightforward (Appendix G2). The upfield shift in ^{13}C NMR spectrum was mainly attributed to the peripheral carbons on the pyrrole ring whereas the inner carbon resonates at a higher frequency and shifted downfield (Chee *et al.*, 2005). For instance, the four central carbon atoms of tetrapyrrole structure resonate in the range of δ_{C} 93 to 104 ppm (Chee *et al.*, 2005).

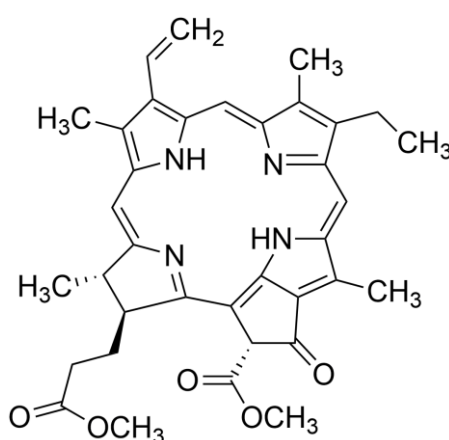


Figure 4.17. The chemical structure of methyl pheophorbide-a.

A total of six absorption bands were observed at 401 nm, 500 nm, 530 nm, 612 nm and 669 nm in the UV-Vis spectrum of fraction 4 (Appendix G3). The UV-Vis data was comparable to previous values (Kuznetsov *et al.*, 2014). Among the absorption bands, the highest absorbance was measured at 401 nm, also known as the Soret band (Tahoun *et al.*, 2021). The Soret band was caused by the delocalised electrons in porphyrins, which have undergone pi-pi transitions (Tahoun *et al.*, 2021). Porphyrin is a natural-occurring pigment that has a characteristic tetrapyrrole ring (Tahoun *et al.*, 2021). The subsequent absorbance at 500 nm, 530 nm, 612 nm and 669 nm were known as the

Q-bands as a result of the conjugation between unsaturated carbons and pyrrole nitrogens in pi-pi transitions (Tahoun *et al.*, 2021). The presence of unsaturated carbons also suggested that fraction 4 was majorly composed of methyl ester of the chlorophyll derivative. In FTIR analysis (Appendix G4), the abundance of C=O and C-H bond stretching was indicated by the high intensity of absorption bands at 1731 cm^{-1} and 2924 cm^{-1} , respectively (Merck, 2022). The central amine of pyrrole ring was evidenced by the N-H bending at 1604 cm^{-1} (Merck, 2022). The absorption at 985 cm^{-1} and 1456 cm^{-1} was a result of the distribution of C=C stretching and C-H bending throughout the tetrapyrrole structure of methyl pheophorbide-a (Merck, 2022). The C-O stretching (1165 cm^{-1}) and C-H bending (1456 cm^{-1}) may hint at the methyl ester structure of the compound. The MH^+ of fraction 4 ($m/z=607$) was compatible with the chemical formula, $\text{C}_{36}\text{H}_{38}\text{N}_4\text{O}_5$ for methyl pheophorbide-a (Appendix G5) (National Center for Biotechnology Information, 2022c). The spectral data collectively suggested that fraction 4 was largely comprised of methyl pheophorbide-a, a derivative of chlorophyll. The overall purification and identification of the major compounds from fraction 1, fraction 2, fraction 3 and fraction 4 from *P. pellucida* crude methanolic extract was summarised in Figure 4.18.

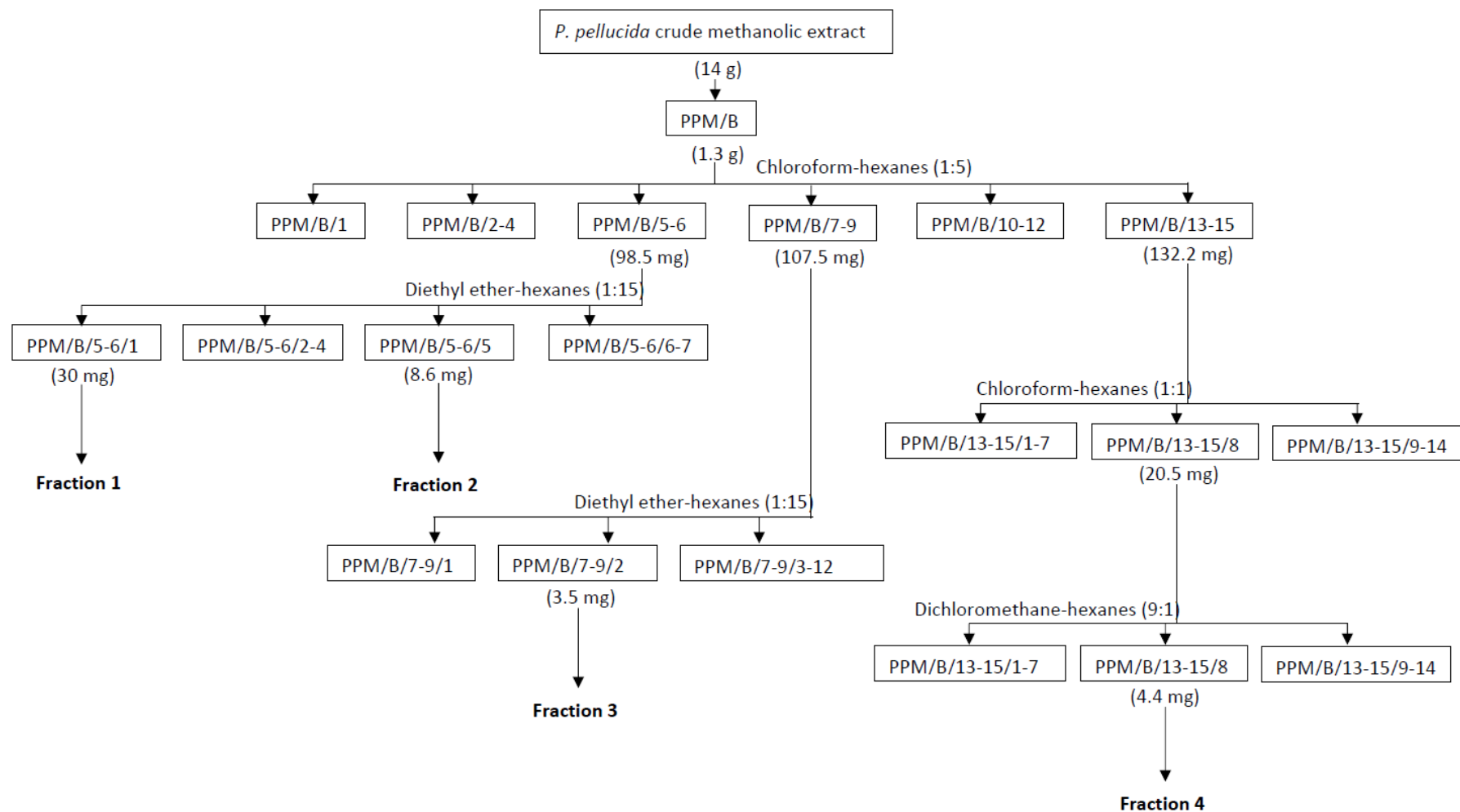


Figure 4.18. The schematic diagram of the purification and isolation of fraction 1, fraction 2, fraction 3 and fraction 4 from *P. pellucida* crude methanolic extract.

4.3.5 Identification of polar compounds with LC-QToF-MS

The presence of polar compounds in *P. pellucida* was detected and characterised with LC-QToF-MS and METLIN database. A total of six classes of minor phytochemicals were detected together with majority of fatty acids-derived alkyl hydrocarbons in the polar subfractions of *P. pellucida*, PPM/B/16-18/2, PPM/E/8 and PPM/E/11. Among the phytochemicals, the minor compounds included the alkaloids, ketones, naphthalenes, phenolic compounds and terpenes. The chlorophyll derivative, methyl pheophorbide-a (13.30 %), which was purified and identified in B13-15/8, was also detected in PPM/E/11 by using LC-QToF-MS analysis. Methyl pheophorbide-a was considered a major polar compound for *P. pellucida*. In PPM/B/16-18/2 and PPM/E/11, the ketone, n-cyclohexanecarbonylpentadecylamine (2.85 %-8.14 %) can be found together with the alkaloids, chlorophyll derivatives, naphthalenes, phenolic compounds and terpenoids. Besides, a minority of naphthalenes, (1R, 2S)-naphthalene 1, 2-oxide (0.27 %) were also detected in PPM/B/16-18/2. In addition, there was a minor portion of phenolic compounds detected in the semi-purified fractions, such as luteolin 5,3'-dimethyl ether (4.07 %), longistylin C (2.38 %), dihydroeuparin (1.95 %), carpelastofuran (0.20 %) and clusin (0.16 %). Further analysis revealed that PPM/E/11 contained higher amount of phenolic compounds compared to PPM/E/8. On the other hand, three distinct varieties of phenolic compounds can be detected in PPM/E/8. LC-QToF-MS analysis also revealed the presence of sesquiterpene, ishwarol (1.30 %) as well as alkaloids such as dictyoquinazol C (6.41 %), homaline (0.78 %), uplandicine (0.34 %) and 5-methoxycanthin-6-one (0.22 %). Interestingly, alkaloids and phenolic compounds were exclusively detected in the semi-purified fractions (PPM/E/8 and PPM/E/11). Likewise, naphthalene can only be identified in PPM/B/16-18/2. Furthermore,

PPM/E/8 and PPM/E/11 can be distinguished by the presence of specific types of alkaloids and phenolic compounds in each fraction. Table 4.16 has summarised the polar compounds detected in PPM/B/16-18/2, PPM/E/8 and PPM/E/11 with LC-QToF-MS.

Table 4.16. The polar compounds detected in PPM/B/16-18/2, PPM/E/8 and PPM/E/11 with liquid chromatography-mass spectrometry quadrupole time-of-flight.

Fraction	Polar compounds	Chemical composition (%)	Phytochemical class	Reported biological effects	References
PPM/B/16-18/2	N-cyclohexanecarbonylpentadecylamine	8.14	Ketone	Anti-inflammatory, analgesic	Tsuboi <i>et al.</i> (2004)
	(1R,2S)-Naphthalene 1,2-oxide	0.27	Naphthalenes	No reported effect	-
PPM/E/8	Dihydroeuparin	1.95	Phenolic compounds	Hypotensive	Ortega <i>et al.</i> (2020)
	Homaline	0.78	Alkaloids	Anti-microbial	Kanhar and Sahoo (2021)
	Uplandicine	0.34			Angelini <i>et al.</i> (2019)
	Carpelastofuran	0.20	Phenolic compounds	Anti-cancer	Cidade <i>et al.</i> (2021)
	Clusin	0.16		No reported effect	-
PPM/E/11	Luteolin 5,3'-dimethyl ether	4.07		Anti-inflammatory	Jegal <i>et al.</i> (2021)

Table 4.16. (continued)

Fraction	Polar compounds	Chemical composition (%)	Phytochemical class	Reported biological effects	References
PPM/E/1 1	N-cyclohexanecarbonylpentadecylamine	2.85	Ketone	Anti-inflammatory, analgesic	Tsuboi <i>et al.</i> (2004)
	Longistylin C	2.38	Phenolic compounds	Anti-cancer, anti-microbial, hypocholesterolemic	Pal <i>et al.</i> (2011)
	Ishwarol	1.30	Terpenes	Anti-microbial	Lago <i>et al.</i> (2007)
	Methylpheophorbide-a	13.30	Chlorophyll derivatives	Anti-cancer, anti-inflammatory	Saide <i>et al.</i> (2020)
	Dictyoquinazol C	6.41	Alkaloids	Neuroprotective	Lee <i>et al.</i> (2002)
	5-Methoxycanthin-6-one	0.22		Anti-microbial	Farouil <i>et al.</i> (2022)

4.3.6 GC-MS analysis of non-polar volatile compounds

4.3.6.1 PPM/A

A total of twenty-seven volatile compounds were detected in the non-polar fraction, PPM/A with GC-MS analysis. The mass spectrum and RI of the identified compounds were compared with the known compounds in NIST library. The identified compounds mainly belonged to the four major classes of phytochemicals such as alkyl hydrocarbons, naphthalenes, phenylpropenes and terpenes. Volatile compounds which occupy more than 5 % are classified as major compounds (Fan *et al.*, 2018). In this study, the predominant phytochemicals identified in PPM/A were the sesquiterpenes, which is a subclass of terpenes. The sesquiterpenes occupied about two-third of the total amount of volatile compounds in PPM/A. This was preceded by the phenylpropanoid compounds, dillapiole and apiole which accounted for 15.46 % of the total volatile compounds. The alkyl hydrocarbons (11.84 %) were lower than the phenylpropenes. In addition, five naphthalene-based sesquiterpenes were identified in PPM/A, namely the α -amorphene, α -selinene, β -selinene, δ -cadinene and γ -cadinene.

This study has demonstrated that the major sesquiterpenes in the crude methanolic extract of *P. pellucida* was β -santalene, which recorded a marked 25.62 % of the total composition. As the dominant sesquiterpene, β -santalene occupied 35.24 % of the total sesquiterpenoid constituents. The elemene-based sesquiterpenes, (-)- β -elemene (4.52 %), (-)-cis- β -elemene (4.63 %), δ -elemene (4.25 %) and γ -elemene (3.96 %) have collectively recorded 23.86 % of the sesquiterpenes. Furthermore, the isocaryophyllene (5.18 %) and β -caryophyllene (5.59 %) occupied 15 % of the total sesquiterpenoid constituents. The minor sesquiterpenes, α -

chamigrene, germacrenes and α -cubebene have accounted for respective 3.78 %, 3.12 % and 2.11 % of the total constituents.

On the other hand, two minor sesquiterpenes, β -copaene (1.72 %) and γ -muurolene (1.89 %) were identified from PPM/A in this study. It was noteworthy to highlight that carotol (1.68 %) has amounted to just 2.32 % of the total sesquiterpenes. The remaining minor sesquiterpenes each constituted lesser than 1 % of the total chemical composition were α -amorphene (0.49 %), α -guaiene (0.33 %), α -selinene (0.37 %), aromadendrene (0.74 %), β -selinene (0.43 %), δ -cadinene (0.16 %) and ledene (0.05 %).

The naphthalene-based sesquiterpenes, α -amorphene, α -selinene, β -selinene, δ -cadinene and γ -cadinene have accounted for 5 % of the sesquiterpenes in *P. pellucida*. The concentration of γ -cadinene was the highest among the naphthalenes. The remaining naphthalenes composed lesser than 1 % of the total chemical composition in the plant. In this study, dillapiole (15.30 %) was the major phenylpropene present in the crude methanolic extract of *P. pellucida*. Dillapiole was also purified from fraction 1 with silica gel column chromatography and PRC through this study. Another phenylpropene, apiole (0.16 %) was detected as a minor compound in this study. In addition, long chain alkyl hydrocarbons that derived from free fatty acids were detected by GC-MS. These were composed of the hexadecane, eicosane, and 8-heptadecene, which accounted for respective 7.1 %, 3.41 % and 1.32 % of the total chemical composition, respectively. Table 4.17 has summarised the non-polar volatile compounds detected in PPM/A with GC-MS.

Table 4.17. The non-polar volatile compounds detected in PPM/A with gas chromatography-mass spectrometry.

Phytochemical class	Volatile compounds	m/z	Chemical composition (%)	Reported biological effects	References
Terpenes	β -santalene	94.10	25.62	Anti-cancer, anti-inflammatory,	El Hachlafi <i>et al.</i> (2024)
	β -caryophyllene	41.00	5.59	anti-microbial	Fidyf <i>et al.</i> (2016)
	Isocaryophyllene	41.00	5.18		Di Sotto <i>et al.</i> (2020)
	(-)-cis- β -elemene	81.10	4.63	Anti-cancer, anti-inflammatory	Chen <i>et al.</i> (2021)
	(-)- β -elemene	81.10	4.52		
	δ -elemene	121.10	4.25		
	γ -elemene	121.15	3.96		
	α -chamigrene	121.10	3.78	Anti-cancer, anti-microbial	White <i>et al.</i> (2010)
	α -cubebene	105.05	2.11	Anti-cancer	Gong <i>et al.</i> (2022)
	Germacrene D	161.15	1.98	Anti-microbial	Pérez Zamora <i>et al.</i> (2018)

Table 4.17 (continued)

Phytochemical class	Volatile compounds	m/z	Chemical composition (%)	Reported biological effects	References
Terpenes	γ -muurolene	161.15	1.89	Anti-microbial	Zuccolotto <i>et al.</i> (2019)
	β -copaene	105.05	1.72	Antioxidant	Roman <i>et al.</i> (2023)
	Carotol	161.15	1.68	Anti-microbial	Sharma <i>et al.</i> (2019)
	Germacrene B	121.10	1.14		Pérez Zamora <i>et al.</i> (2018)
	Aromandendrene	41.00	0.74		Mulyaningsih <i>et al.</i> (2011)
	α -guaiene	105.05	0.33		Anggraeni <i>et al.</i> (2020)
	Ledene	105.05	0.05		Riyadi <i>et al.</i> (2023)
Naphthalenes	γ -cadinene	161.15	2.13		Aghajani <i>et al.</i> (2009)
	α -amorphene	161.15	0.49		Morocho <i>et al.</i> (2023)

Table 4.17 (continued)

Phytochemical class	Volatile compounds	m/z	Chemical composition (%)	Reported biological effects	References
Naphthalenes	β -selinene	79.05	0.43	Anti-inflammatory, analgesic	Chandra <i>et al.</i> (2017)
	α -selinene	79.10	0.37	Anti-cancer, anti-microbial	Keawsaard <i>et al.</i> (2012)
	δ -cadinene	105.10	0.16	Anti-microbial	Kačániová <i>et al.</i> (2022)
Phenylpropanoids	Dillapiole	222.10	15.30	Anti-inflammatory	Rojas-Martínez <i>et al.</i> (2013)
	Apiole	222.15	0.16		Kartika <i>et al.</i> (2020)
Alkyl hydrocarbons	Hexadecane	57.05	7.10	Anti-cancer, anti-microbial	Wei <i>et al.</i> (2011)
	Eicosane	57.05	3.41	Anti-microbial	Bhat <i>et al.</i> (2024)
	8-heptadecene	55.05	1.32	Anti-cancer, anti-microbial	Rahayu <i>et al.</i> (2022)

4.3.6.2 PPM/A/1 and PPM/A/2

The first two eluted sub-fractions of PPM/A in PRC, PPM/A/1 and PPM/A/2 both shared a similar isolated spot in TLC analysis (Figure 4.19). GC-MS analysis has detected a total 13 compounds in PPM/A/1 whereas 14 compounds were spotted in PPM/A/2 (Table 4.18). These compounds belonged to the phytochemical class of alkyl hydrocarbons, aromatic heterocyclics, esters, phenylpropanoids and terpenes. With the exception of an additional compound (nonenyl acetate ester) detected in PPM/A/2, 13 other compounds were shared between the two sub-fractions. The major non-polar compounds that predominated PPM/A/1 and PPM/A/2 belonged to the class of terpenes and phenylpropanoids, similar to PPM/A. Apiole (15.40 %-15.81 %) was the sole phenylpropanoid that can be detected in PPM/A/1 and PPM/A/2. The sesquiterpenes accounted for more than 60 % of the total composition of PPM/A/1 and PPM/A/2. Interestingly, carotol predominates the detectable sesquiterpenes in the sub-fractions with a range of 31.90 % to 35.08 %. This was followed by the other major sesquiterpenes, (-)- β -elemene (14.59 %-14.95 %) and β -caryophyllene (12.29 %-13.92 %). The subfractions also contained a minor sesquiterpene (<5 %), which was α -caryophyllene (3.55 %-3.04 %). Similar to PPM/A, several long chain alkyl, aromatic hydrocarbons and esters that derived from free saturated and unsaturated fatty acids can also be found in the sub-fractions as minor components in GC-MS. Among them, 1,3,6-heptatriene topped the list with 5.08 % and 4.46 % in PPM/A/1 and PPM/A/2, respectively. This was followed by chlorooctadecane (3.98-4.74 %), propanoic acid ester (2.31-3.43 %), 1,4-methanocyclooctapyridazine (2.16-2.87 %), oxalic acid ester (1.61-1.95 %), heptadecane (1.60-1.74 %), 3-octadecene (0.61-1.40 %) and 1,3,6-octatriene (0.66-0.70 %). In addition, an overall higher concentration of each phytochemical was observed in the PPM/A/1 compared to PPM/A/2. Table 4.18 has summarised the non-polar volatile compounds detected in PPM/A/1 and PPM/A/2 with GC-MS.



Figure 4.19. The TLC profile of PPM/A/1 and PPM/A/2.

Table 4.18. The non-polar volatile compounds detected in PPM/A/1 and PPM/A/2 with gas chromatography-mass spectrometry.

Phytochemical class	Volatile compounds	m/z	Chemical composition (%) in PPM/A/1	Chemical composition (%) in PPM/A/2	Reported biological effects	References
Alkyl hydrocarbons	1,3,6-heptatriene	93.00	5.08	4.46	Insecticidal	Mahi <i>et al.</i> (2023)
	Chlorooctadecane	57.00	4.74	3.98	Insecticidal	Hussain and AlJabr (2020)
	Heptadecane	69.00	1.74	1.60	Anti-inflammatory	Kim <i>et al.</i> (2013)
	3-octadecene	57.00	1.40	0.61	Analgesic	Altameme <i>et al.</i> (2015)
	1,3,6-octatriene	93.10	0.70	0.66	Anti-cancer, anti-microbial	Amirzadeh <i>et al.</i> (2022)
Aromatic heterocyclics	1,4-methanocyclo-octapyridazine	107.00	2.87	2.16	Anti-microbial	El-Shamy <i>et al.</i> (2023)

Table 4.18. (continued)

Phytochemical class	Volatile compounds	m/z	Chemical composition (%) in PPM/A/1	Chemical composition (%) in PPM/A/2	Reported biological effects	References
Esters	Propanoic acid ester	47.00	3.43	2.31	Anti-microbial	Goldberg and Rokem (2009)
	Oxalic acid ester	57.00	1.95	1.61	Anti-microbial, anti-cancer	Wiraswati <i>et al.</i> (2023)
	Nonenyl acetate	43.00	-	0.16	No reported effect	-
Phenylpropa-noids	Apiole	222.15	15.40	15.81	Anti-inflammatory	Kartika <i>et al.</i> (2020)
Terpenes	Carotol	161.15	31.90	35.08	Anti-microbial	Sharma <i>et al.</i> (2019)
	(-)- β -elemene	81.10	14.95	14.59	Anti-cancer, anti-inflammatory	Chen <i>et al.</i> (2021)
	β -caryophyllene	41.00	12.29	13.92		Fidy <i>et al.</i> (2016)
	α -caryophyllene	93.00	3.55	3.04		

Chapter V

Discussion

5.1 Biological activities and phytochemicals in *P. pellucida*

5.1.1 The influence of extraction parameters on the yield of *P. pellucida*

Based on the extraction yield of *P. pellucida* (Table 4.1), the yield of crude methanolic extract (14.22 %) obtained in this study was higher than those (10.28 %) reported by Phongtongpasuk and Poadang (2014), who macerated the plant samples in a solid-solvent ratio of 1:20 for 24 hours at room temperature. While the previous study employed a lower solid-solvent ratio, the duration of maceration was shorter compared to the 72-hour period utilised in this study. This finding indicated that the extraction yield of *P. pellucida* was dependent on the duration of maceration. According to Hamdan *et al.* (2008), the solid-solvent ratio may cause an exponential increase in the extraction yield when arrived at the solute-solvent equilibrium constant. Hence, the lower solid-solvent ratio used in the previous study did not further increase the extraction yield of *P. pellucida*. In addition, the extraction yield of crude methanolic extract was higher than that of Ng *et al.* (2020) (8.78 %), where maceration was carried out at 1:12 solid-solvent ratio for 7 days. This study also suggested that a 3-day maceration was sufficient to yield the maximum extraction from *P. pellucida* at a solid-solvent ratio of 1:10.

Among the plant solvent fractions, the higher extraction yield observed in the polar (aqueous) and non-polar (hexane) fractions could be attributed to the abundance of polar and non-polar materials in *P. pellucida* (Widyawati *et al.*, 2014). Besides, the particle size of plant powder may also affect the extraction yield (Rezazi *et al.*, 2017). In the current study,

coarse plant powder was selected in the extraction process as there was no significant difference in extraction yield between the use of coarse and fine plant powders (Zhang *et al.*, 2016b). However, the use of fine plant powders may hinder the interaction of phytochemicals with extraction solvent due to the increased tendency to clump (Vuong *et al.*, 2011). More importantly, the slimy texture of fine plant powder could pose difficulty in filtration upon contacting the solvents (Makanjuola, 2017). This study also found that the ethyl acetate fraction displayed higher extraction yield than the chloroform fraction. This observation was comparable to Nakamura *et al.* (2017), who reported similar findings while the non-polar hexane and polar aqueous fractions produced the highest plant extraction yield. According to Nakamura *et al.* (2017), solvents of high polarity may lead to high extraction yield. The aqueous fraction showed the highest plant yield possibly due to the abundance of water soluble and polar substances in the plant (Abu *et al.*, 2017). The high extraction yield of the non-polar hexane fraction may be attributed to the solvent fractionation process utilised in this study for extraction (Nakamura *et al.*, 2007).

In step-wise solvent fractionation, hexane was the first extraction solvent being used due to its non-polar nature (Nawaz *et al.*, 2020). This was followed by chloroform, ethyl acetate and n-butanol with increased polarities. Hence, all of the non-polar materials that are present in *P. pellucida* crude methanolic extract, such as fatty acids esters would have been extracted into the hexane fraction (Maimulyanti and Prihadi, 2016). Besides, hexane is often used for defatting purpose to extract hydrophobic substances during the plant extraction process (Laroche *et al.*, 2019). As most of the fatty materials have been extracted into the hexane layer, this may result in a lower extraction yield of subsequent non-polar organic layer (chloroform). In addition to the extraction method, the plant

extraction yield can also be influenced by the use of fertilizers such as chicken manure and hydroponic fertilizers (Roshidi *et al.* 2020). Based on Stalikas (2007), there are other factors that could affect the extraction yield of a plant. Factors such as duration of storage, temperature and plant anatomical parts may play significant roles in affecting the overall plant extraction yield. In conjunction with PCA analysis (Figure 4.1), this study confirmed that the extraction yield of *P. pellucida* could be influenced by parameters such as the duration of extraction, solid-solvent ratio and solvent polarity.

5.1.2 Phytochemicals

The extraction yield did not reflect the TPC and TFC of *P. pellucida* fractions (Table 4.1). For instance, ethyl acetate, n-butanol and chloroform fractions with low extraction yields showed relatively high TPC (Table 4.1), which concurred with a previous study (Moshawih *et al.*, 2017). The solvent polarity has been reported to influence the extractability of compounds (Ng *et al.*, 2020). Since phenolic compounds present in plants are of differing polarities, the amount of phenolic compounds in each solvent fraction also varied (Do *et al.*, 2014). Moshawih *et al.* (2017) suggested that the presence of phenolic compounds in solvent fractions were influenced by the solvent polarity. Therefore, the polarity of most phenolic compounds presented in *P. pellucida* were compatible to that of ethyl acetate, n-butanol and chloroform, leading to high TPC in these fractions. However, the complex mixture of phytochemicals in the crude methanolic extract could also shield specific class of phytochemicals such as phenolic compounds, saponins and alkaloids in the extract from being detected by *in vitro* colorimetric assays (Weng *et al.*, 2015). Hence, this

shielding effect could be overcome by the subsequent solvent fractionation process (Ismail and Chua, 2021).

The TPC and TFC trend findings also suggested that the solvents with moderate polarities were effective in the extraction of phenolic and flavonoid compounds from *P. pellucida*. Chloroform plant fraction with high TPC but low TFC may imply that the solvent was suitable for the extraction of non-flavonoid phenolic compounds. As TFC in *P. pellucida* fractions did not correlate with the antioxidant parameters (FRAP, DPPH and ABTS radicals scavenging activities), this may suggest that the amount of phytochemical content did not necessarily reflect the overall antioxidant activity of the plant (Supriatno and Lelifajri, 2018). The structural role of flavonoids such as the degree of polymerization and chemical interaction could influence the antioxidant activity of the plant (Supriatno and Lelifajri, 2018). Although flavonoids are part of the polyphenols, there are other classes of phenolic compounds such as phenolic acids and tannins (King and Young, 1999). The release of flavonoids from the plant is also influenced by temperature, whereby a proportional relationship exists between them (Peleg *et al.*, 1991). It is possible that some flavonoids are either concealed in the cellular components of the plant or bound to non-polar substances that are extracted in the non-polar hexane fraction (Supriatno and Lelifajri, 2018). Besides, hydrophobic phenolic compounds can be extracted using hexane (Akomeng and Adusei, 2021). Hence, high TFC can be observed in the hexane fraction in this study (Table 4.1). Based on the phase 3 study findings, dihydroeuparin, carpelastofuran, clusin, luteolin and longistylin were some of the phenolic compounds and flavonoids identified in the crude methanolic extract of *P. pellucida*.

Tannins are high molecular weight polyphenols that are responsible for the astringency and bitterness of plant-based foods (Soares *et al.*,

2020). On the contrary, alkaloid is considered one of the largest phytochemical group in medicinal plants (Ferreira, 2022). Due to the structural complexity, alkaloids possess a diverse range of therapeutic properties (Ferreira, 2022). Alves *et al.* (2019) previously reported the presence of alkaloid and tannin in *P. pellucida*. This study found high level of alkaloid and tannin in the chloroform fraction. On the other hand, saponins are glycosides that derived from either triterpenoids or steroids, which include both the glycone and aglycone moieties (Xi *et al.*, 2008). The significant saponin content in the moderately polar ethyl acetate and n-butanol fractions (Table 4.1) indicated that the majority of saponins present in *P. pellucida* tend to solubilise in solvents of moderate polarities, which also reflected the polarity of these compounds (Do *et al.*, 2014). Likewise, the low tannin and saponin contents in the aqueous fraction may suggest the lack of polar tannins and saponins in *P. pellucida*, and this may explain the absence of tannins and saponins detected in LC-QToF-MS analysis. Several alkaloids were found in *P. pellucida* such as dictyoquinazol, homaline, 5-methoxycanthin-6-one and uplandicine (Table 4.12). The overall high levels of alkaloid, flavonoids, phenolic compounds, saponin and tannin in the moderately-polar fractions (Table 4.1) of *P. pellucida* crude methanolic extract signified the abundance of similar moderately polar compounds in *P. pellucida*.

In phase 3 investigation, the similar phytochemical profiles observed among the *P. pellucida* crude methanolic extract and its solvent fractions during the optimization step using TLC can be attributed to the fact that the plant fractions were derived from the crude extract (Appendix C1). The higher concentration of phytochemicals observed in the crude methanolic extract compared to the solvent plant fractions may indicate that the extraction of phytochemicals from *P. pellucida* with diverse polarity

and functional activities, as displayed in phases 1 and 2 studies, can be achieved effectively using methanol. Likewise, the varying biological activities that can be observed in the *P. pellucida* crude methanolic extract and solvent fractions could be ascribed to the various chemico-biological interactions among the phytochemicals (Rasoanaivo *et al.*, 2011). These interactions can exist as additive, antagonistic and synergistic interactions, contributing to the overall observed biological effects in this study (Rasoanaivo *et al.*, 2011).

In GC-MS analysis, the four detected major classes of compounds including alkyl hydrocarbons, naphthalenes, phenylpropenes and terpenes were in accordance with Alves *et al.* (2019). Besides, the predominance of sesquiterpenes and phenylpropenes in *P. pellucida* agreed with the previous study (Alves *et al.*, 2019). The major sesquiterpenes detected in PPM/A/1 and PPM/A/2 were also comparable to Verma *et al.* (2014). In this study, β -santalene was identified as a major sesquiterpene in *P. pellucida*. The compound was previously identified as a minor phytoconstituent in the essential oil derived from the root of *P. pellucida* (Usman and Ismaeel, 2020). Hence, this finding suggested that β -santalene can be found abundantly in the aerial part of the plant. The composition percentage of (-)- β -elemene was comparable to previous studies (Alves *et al.*, 2022; Verma *et al.*, 2014). However, the amount of δ -elemene was higher than those reported in previous finding (Verma *et al.*, 2014). The different climates and geographical regions in which the plant was grown could be the reason behind this discrepancy. The biosynthesis of secondary metabolites such as terpenes could be affected by temperature, sun exposure and precipitation frequency (Romero *et al.*, 2021). For instance, the biosynthesis of pellucidin A from 2,4,5-trimethoxystyrene could be promoted by ultraviolet light (de Moraes and Kato, 2021). In addition, the

extraction method and soil composition of the plant could cause the variation of chemical composition in *P. pellucida* (Verma *et al.*, 2014).

According to Alves *et al.* (2019), caryophyllene-based sesquiterpenes is another major sesquiterpenes that can be found in the essential oil of *P. pellucida*. In this study, the amount of β -caryophyllene was also comparable to a previous report (Alves *et al.*, 2019). The concentration of β -caryophyllene is usually higher than (-)- β -elemene and this agreed with previous reports (Alves *et al.*, 2022; Verma *et al.*, 2014). Additionally, α -caryophyllene, also known as humulene, is an isomer of β -caryophyllene. These compounds are commonly found together as a mixture and have been previously demonstrated to possess anti-inflammatory properties (Hartsel *et al.*, 2016). On the other hand, the presence of minor sesquiterpenes, including α -chamigrene, germacrene and γ -cadinene in the *Piper* genus of plants has also been previously documented (Oliveira *et al.*, 2013; Silva *et al.*, 2017). Besides, germacrene was commonly detected in the leaf essential oil of *P. pellucida* (Alves *et al.*, 2019). Based on Usman and Ismaeel (2020), α -cubebene had recorded 1.2 % of the chemical composition in the root of *P. pellucida*. Since this study has identified α -cubebene (2.11 %) in PPM/A, it was indicated that the aerial part displayed double the amount of α -cubebene in the root of the plant (Usman and Ismaeel, 2020).

Furthermore, the minor sesquiterpenes, β -copaene and γ -muurolene were commonly identified along with β -caryophyllene, β -elemene and germacrene in *Peperomia* species (Mesquita *et al.*, 2021). The concentration of γ -muurolene in this study was also slightly higher than previously reported (Mesquita *et al.*, 2021). The reduction of γ -muurolene could be due to the removal of fruiting spikes in the previous study (Mesquita *et al.*, 2021). Additionally, this study has also detected carotol as

a minor compound in *P. pellucida*. The presence of carotol may differentiate *P. pellucida* from other *Peperomia* species (de Lira *et al.*, 2009). According to Alves *et al.* (2019), carotol also constituted 32.1 % of the total chemical composition in the essential oil of *P. pellucida*. This observation has deduced that hydrodistillation was the ideal extraction method to recover carotol from the plant.

The remaining sesquiterpenes, such as α -amorphene, α -guaiene, α -selinene, aromadendrene, β -selinene, δ -cadinene and ledene, which constituted less than 1 % of the total chemical composition of *P. pellucida* were minor compounds that can be commonly found in plants of genus *Piper* (Nayaka *et al.*, 2021; Oliveira *et al.*, 2017). Besides, the concentration of γ -cadinene was the highest among the naphthalene-based sesquiterpenes and this agreed with previous reports (Oliveira *et al.*, 2017; Usman and Ismaeel, 2020). It was suggested that higher concentration of γ -cadinene was present in the stem compared to the root of *P. pellucida* (Oliveira *et al.*, 2017; Usman and Ismaeel, 2020).

Dillapiole is a major compound present in the whole plant of *P. pellucida*, including the leaves, roots and stems (Alves *et al.*, 2019). Previous studies have demonstrated the anti-inflammatory, anti-osteoporotic and gastro-protective activities of dillapiole isolated from the plant (Parise-Filho *et al.*, 2011; Rojas-Martínez *et al.*, 2013). The current study has characterised the compound with GC-MS and spectroscopic methods. The presence of dillapiole may highlight the therapeutic significance of *P. pellucida* against DR. Apiole is commonly identified along with dillapiole from *P. pellucida* (Alves *et al.*, 2019; Kartika *et al.*, 2020). Although both compounds share some structural similarities, the marked anti-inflammatory activity of dillapiole could be attributed to the steric and electronic effects that resulted from the covalent bonds in the compound

(Pineda *et al.*, 2018). In this study, apiole was detected in PPM/A/1 and PPM/A/2. It can be indicated that apiole is less polar than its phenylpropanoids counterpart, due to it being eluted earlier in the first two sub-fractions during PRC. On the other hand, this study has also identified another phenylpropanoid, 2,4,5-trimethoxystyrene from *P. pellucida*. Interestingly, this compound serves as a precursor to pellucidin A, with its formation being facilitated by exposure to UV light (de Moraes and Kato, 2021). Besides, the absence of naphthalenes in PPM/A/1 and PPM/A/2 also indicated that naphthalenes found in PPM/A were more polar comparatively. Hence, they were eluted later and not detected in both fractions.

This study also revealed the presence of a mixture of alkyl hydrocarbons alongside other classes of phytochemicals. According to Wei *et al.* (2011), alkyl hydrocarbons that derived from the saturated and unsaturated fatty acids are among the major compounds that can be detected in the crude methanolic extract of *P. pellucida*. Hexadecane (16 carbons) and 8-heptadecene (17 carbons) were previously identified as the two main components present in the essential oil of *Piper longum* from the *Piperaceae* family (Dash *et al.*, 2022). Hexadecane was derived from the saturated fatty acid, hexadecanoic acid (Wei *et al.*, 2011). The identification of hexadecanoic acid from the crude methanolic extract of *P. pellucida* agreed with the previous study (Wei *et al.*, 2011). Furthermore, the current study also characterised 9-octadecenoic acid methyl ester as a major compound, which was in accordance to Okoh *et al.* (2017) and Teoh *et al.* (2021). The 20 carbons alkyl hydrocarbons, eicosane detected in this study as a minor constituent, can be also found in other plants belonging to the *Piperaceae* family (Asadi, 2022).

In addition, several polar compounds such as ketones, naphthalenes, phenolic compounds, alkaloids and terpenes were detected in *P. pellucida*

using LC-QToF-MS. Ketones are naturally occurring substances that are commonly found in natural products including plants (Farmer and Reusch, 2023). Similar to esters, the presence of ketones may impart characteristic scent to the plants (Farmer and Reusch, 2023; Silva *et al.*, 2018). On the contrary, naphthalenes were known to display anti-inflammatory and antioxidant activities due to the presence of stable benzene rings (Luo *et al.*, 2021). Besides, the presence of phenolic compounds, such as luteolin 5,3'-dimethyl ether, longistylin C, dihydroeuparin, carpelastofuran and clusin in PPM/E/8 and PPM/E/11 may reflect the TPC and TFC quantified from *P. pellucida*. The presence of these compounds could potentially contribute to the observed biological activities in phase 1 study. Furthermore, alkaloids and terpenes are important secondary metabolites in plants, which display a broad spectrum of biological activities, such as anti-glycaemic and anti-inflammatory activities (Adamski *et al.*, 2020; Lv *et al.*, 2022). Additionally, the presence of alkaloids and phenolic compounds was observed in the semi-purified fractions (PPM/E), which was eluted later during silica gel column chromatography. This may indicate the high polarity of the majority of alkaloids and phenolic compounds present in *P. pellucida*. The same theory can be applied to the presence of naphthalenes in the PPM/B/16-18/2.

5.1.3 Antioxidant effect

The presence of high amount of phenolic compounds could explain why certain fraction possessed higher FRAP activity than the other plant fractions (Abu *et al.*, 2017). The significant positive correlation observed between TPC and FRAP (Table 4.9) could be explained by the metal-reducing power of phenolic compounds that are present in *P. pellucida*

fractions. In other words, this can be ascribed to the redox properties of phenolic compounds (Nagarajan *et al.*, 2017). Besides, it was also suggested that the metal ion reducing capability of plant extract was due to the presence of phenolic compounds (Nagarajan *et al.*, 2017). The donation of hydrogen atom by phenolic compounds to ferric complex reflects the metal chelating action of phenolic compounds, which is based on the SET mechanism (Nagarajan *et al.*, 2017). Furthermore, the modest positive correlation observed between saponin and FRAP confirmed the ferric-reducing properties of saponins (Table 4.9), which was in agreement with a previous study (Chen *et al.*, 2014). As the FRAP activity is also inversely correlated with the IC₅₀ for DPPH and ABTS radicals scavenging activities of *P. pellucida*, this may suggested that the antioxidants present in the plant may possess ferric-reducing properties in addition to its free radicals scavenging ability. The above finding also indicated the ability of antioxidants of *P. pellucida* in utilising hydrogen atom transfer and SET-based reactions simultaneously to neutralise the harmful effect of free radicals (Liang and Kitts, 2014).

The low DPPH radical scavenging activity of hexane fraction agreed with a study conducted by Shoeb (2019), which also showed that the non-polar fraction displayed the lowest DPPH radical scavenging activity. This study also demonstrated an overall higher DPPH radical scavenging activity of *P. pellucida* fractions compared to ABTS radical scavenging activity. This was observed as a lower IC₅₀ of plant solvent fractions was required to inhibit the DPPH radicals compared to ABTS radicals. This could be attributed to the different affinity of bioactive compounds in the plant towards the DPPH or ABTS radicals (Liang and Kitts, 2014). According to Lee *et al.* (2015b), the high ABTS radical scavenging activity was associated with the presence of phenolic compounds and flavonoids. This

could explained the high ABTS radical scavenging activity in the ethyl acetate and n-butanol fractions with high TPC and TFC. Besides, the abundance of hydrophobic compounds in *P. pellucida*, such as terpenes, phenylpropanoids, and fatty acids, may account for the higher DPPH radical scavenging activity compared to ABTS radical scavenging activity (Lee *et al.*, 2015b). The high DPPH radical scavenging activity also suggested that the majority antioxidants in *P. pellucida* acted through the SET mechanism (Liang and Kitts, 2014). In addition, the IC₅₀ of the standards ascorbic acid and Trolox for DPPH and ABTS radicals scavenging activities, were comparable to those reported in previous studies (Noreen *et al.*, 2017; Shoeb, 2019).

The different trends of DPPH and ABTS radicals scavenging activities in different plant solvent fractions could be due to the varying reactivities of bioactive compounds towards the two types of radicals. (Okoh *et al.*, 2017). Based on the correlation study (Table 4.4), the TPC was closely associated with DPPH and ABTS radicals scavenging activities in *P. pellucida*. This may suggest that the phenolic compounds identified in this study were partly responsible for the radicals scavenging activities (Anggraini *et al.*, 2019; Cao *et al.*, 2018). According to Liang and Kitts (2014), the radical scavenging activity of phenolic compounds could be ascribed to its ability to donate hydrogen atom to free radicals, thus sequestering its harmful effects. Likewise, the correlation established between saponin and ABTS radical scavenging activity may also implied that the antioxidant activity of *P. pellucida* was partially attributed to the presence of saponins (Chen *et al.*, 2014).

The overall high FRAP, DPPH and ABTS radicals scavenging activities also qualified the moderately polar ethyl acetate and n-butanol fraction as very high AI fraction and 'high' AI fraction, respectively. This

finding concurred with a previous report on their significant antioxidant activities due to the rich phytochemical content (Zhang *et al.*, 2015b). Although polar solvent displayed high extraction yield, it was the solvent of moderate polarity that favoured the extraction of phytochemicals that contribute to the high antioxidant activity in *P. pellucida* (Jing *et al.*, 2015).

On the other hand, the supplementation of *P. pellucida* leaves has previously been shown to inhibit lipid peroxidation in a rat model using thiobarbituric acid-reactive species method (Hamzah *et al.*, 2012). In this study, the lipid peroxidation inhibitory activity of *P. pellucida* solvent fractions was determined. The strong lipid peroxidation inhibitory activity in *P. pellucida* ethyl acetate fraction was in accordance to Oloyede *et al.* (2011). However, this study contradicted the previous finding, as it revealed that the n-butanol and aqueous fractions exhibited the highest lipid peroxidation inhibitory activity. This was likely due to the omission of chloroform in the previous study, leading to the extraction of compounds with high lipid peroxidation inhibitory activity in the moderate-polar and polar fractions. The IC₅₀ of ascorbic acid for inhibiting the hydroxyl radicals was also comparable to a previous study (Nehete *et al.*, 2010). The significant inverse correlation between the FRAP and lipid peroxidation inhibitory activities of the plant was mostly likely due to the induction of lipid peroxidation by iron, which is also the target metal of chelation in FRAP assay (Khan *et al.*, 2014). The weak correlation between TPC and lipid peroxidation inhibitory activity in *P. pellucida* suggested that phenolic compounds were less likely to inhibit lipid peroxidation. The significant correlation observed between saponin and lipid peroxidation inhibitory activity of *P. pellucida* further strengthened the antioxidant role of saponins in *P. pellucida* by combating oxidative stress. Moreover, the aerial part of *P. pellucida* has been previously associated with strong lipid peroxy radical

scavenging effect (Okoh *et al.*, 2017). Hence, this study suggested that the lipid peroxidation inhibitory activity was partly derived from the saponins detected in the aerial part of *P. pellucida*. Dillapiole, the phytochemical previously isolated from the aerial part of *P. pellucida* by Rojas-Martínez *et al.* (2013), has been demonstrated to inhibit lipid peroxidation (Rojas-Martínez *et al.*, 2013). In the current study, the presence of the major compound dillapiole may have explained the high lipid peroxidation inhibitory activity of *P. pellucida*.

5.1.4 Anti-inflammatory effect

The COXs and LOX are the two main families of enzymes that could initiate the AA pathway through the generation of pro-inflammatory mediators (Perera *et al.*, 2016). Thus the inhibition of COXs and LOX could lead to suppression of inflammation. The overall higher inhibitory activity on COX-1 compared to COX-2 among the *P. pellucida* fractions, contradicted with the trend observed in the study conducted by Gacche *et al.* (2011). The previous study showed better COX-2 inhibition among the different medicinal plants (Gacche *et al.*, 2011). This study found that *P. pellucida* could be a potential COX-1 antagonist. As COX-1 and COX-2 inhibitory activities were not associated with the phytochemical content of the solvent fractions, this finding suggested that the high COX-1 and COX-2 inhibitory activities displayed by non-polar hexane fraction could be due to the presence of non-polar unsaturated fatty acid such as 9-octadecenoic acid. This was indicated by a previous study, which reported COX inhibitory activity of 9-octadecenoic acid (Xie *et al.*, 2022). In the current study, the identification of such non-polar fatty acids in *P. pellucida* could support its COX-1 and COX-2 inhibitory properties.

It was noteworthy to highlight that the LOX inhibitory activities of ethyl acetate, n-butanol and hexane fractions of *P. pellucida* were comparable to the standard quercetin. Although the IC₅₀ of quercetin in another study was much lower at 0.0002 mg/ml (Kwon *et al.*, 2011), the method employed was based on the formation of final product cysteinyl leukotrienes, rather than the intermediary product hydroperoxyoctadecadienoic acid as described in this study. The formation of hydroperoxyoctadecadienoic acid is an elementary reaction (Miyata *et al.*, 2020). Conversely, the formation of cysteinyl leukotrienes involves a multi-step reaction aided by the presence of glutathione (Miyata *et al.*, 2020). Hence, this phenomenon may have led to the lower IC₅₀ observed for inhibiting the formation of the final product in the previous study.

The significant correlation among TFC, saponin content and LOX inhibitory activity of *P. pellucida* also indicated flavonoids and saponins as strong inhibitors of LOX. This study has indicated the crucial role of flavonoids and saponins on the LOX inhibitory activity of *P. pellucida*. It was also previously reported that both flavonoids and saponins displayed LOX inhibitory activity (Bildziukevich *et al.*, 2023; Ibrahim *et al.*, 2018). Ibrahim *et al.* (2018) has reported that flavonoids were major contributors to LOX inhibition. The LOX inhibitory activity of flavonoids was best explained by its planar structure whereby the hydroxyl groups played a huge role in anti-inflammatory action (Alaba and Chichioco-Hernandez, 2014; Ibrahim *et al.*, 2018). Likewise, the presence of hydroxyl groups in triterpenoid saponins was likely to be responsible for the anti-inflammatory action of *P. pellucida*, as the plant is rich in terpenoids (Bildziukevich *et al.*, 2023).

Besides, the COXs and LOX inhibitory activities could also be attributed to the presence of non-polar compounds such as dillapiole and

2,4,5-trimethoxystyrene (Saldanha *et al.*, 2020) identified from *P. pellucida* in this study. Dillapiole is a major compound found in the plant's aerial part (Alves *et al.*, 2019). The therapeutic significance of dillapiole lies with the presence of specific functional groups on the phenylpropanoid structure. Previous study has suggested that the anti-inflammatory activity of dillapiole was attributed to the presence of its allyl side chain, benzodioxole ring and methoxy groups on the structure of the compound (Parise-Filho *et al.*, 2011).

Along with dillapiole, 2,4,5-trimethoxystyrene is a major compound of *P. pellucida* and a precursor of pellucidin A (Bayma *et al.*, 2000; de Moraes and Kato, 2021). The anti-inflammatory action of 2,4,5-trimethoxystyrene was often related to the inhibition of pro-inflammatory mediators, including COXs and LOX (Saldanha *et al.*, 2020). This may have attributed to the presence of three methoxy groups in the structure of the compound (Parise-Filho *et al.*, 2011). According to Xie *et al.* (2022), 9-octadecenoic acid has been previously shown to exhibit anti-inflammatory effect by inhibiting the production of COX-2. The presence of fatty acid methyl ester is a product from the transesterification of methanol with the acyl groups that are present in fats and oils (Kandasamy *et al.*, 2020). This phenomenon could have arose from the utilization of methanol as the extraction solvent (Kandasamy *et al.*, 2020). Hence, the COXs and LOX inhibitory activities displayed by *P. pellucida* may be attributed to the presence of phytochemicals like 2,4,5-trimethoxystyrene, 9-octadecenoic acid and dillapiole that specifically targeted the AA pathway.

On the other hand, the traditional usage of *P. pellucida* as an anti-gout agent has been previously documented (Abu Bakar *et al.*, 2018) due to its ability to suppress inflammation by inhibiting the enzyme XO (Fachriyah *et al.*, 2018). The trend of XO inhibitory activity for *P. pellucida*

showed that solvent fractions of moderate polarity displayed stronger XO inhibitory activity than the polar and non-polar fractions, suggesting that phytochemicals of equivalent polarities may play a significant role in XO inhibition (Sakti *et al.*, 2020). The IC₅₀ of standard quercetin for XO inhibitory activity was in accordance to a previous report (Zhang *et al.*, 2018). The low IC₅₀ value also suggested that the standard displayed significantly greater XO inhibitory activity compared to the *P. pellucida* fractions. The significant correlation established between XO inhibitory activity and ABTS radical scavenging activity may suggest that the bioactive compounds present in *P. pellucida* were both effective radicals and XO inhibitors in preventing inflammation. According to Feoli *et al.* (2014), XO is responsible for oxidative stress and the subsequent occurrence of inflammation. This study showed that the bioactive compounds present in *P. pellucida* could be effective in preventing oxidative stress and inflammation by inhibiting XO.

Methanol has been used as the preferred solvent for extracting bioactive compounds with excellent hyaluronidase inhibitory activity (Ao *et al.*, 2010). Hence, the highest hyaluronidase inhibitory activity can be observed in the *P. pellucida* crude methanolic extract in this study. Among the plant solvent fractions, non-polar hexane and chloroform fractions displayed higher hyaluronidase inhibitory activity than the other plant fractions in this study. According to Addotey *et al.* (2018), the presence of phenolic compounds, including flavonoids contributed to hyaluronidase inhibition. However, this study did not observe any correlation among TPC, TFC and hyaluronidase inhibitory activity. Furthermore, the IC₅₀ of hyaluronidase inhibitory activity for the standard tannic acid was comparable to previous study (Tokeshi *et al.*, 2007).

Based on the correlation study, there was a significant negative correlation between alkaloid and hyaluronidase inhibitory activity. Hence, the strong hyaluronidase inhibitory activity of crude methanolic extract could also be ascribed to the presence of alkaloids. Nevertheless, the hyaluronidase inhibitory activity of *P. pellucida* might also be due to the presence of other phytochemicals, such as β -caryophyllene, β -elemene and dillapiole, which were identified from the crude methanolic extract in phase 3 study. These compounds were previously associated with high hyaluronidase inhibitory activity (Hou *et al.*, 2022). According to Ling *et al.* (2003), the hyaluronidase inhibitory activity is related to the presence of terpenes. The enzyme inhibitory action of this phytochemical class depends on either the presence of nitrogenous compounds such as proteins through a cross-linking mechanism or the action of its intermediate products (Ling *et al.*, 2003). Several major terpenes identified from this study include the β -caryophyllene, β -elemene and β -santalene. Besides, the synthesis of substrate for hyaluronidase, HA occurs at the apical surface of RPE (Senanayake *et al.*, 2000) and HA could suppress the production of angiogenic and inflammatory cytokines (He *et al.*, 2017; Takahashi and Tanihara, 2012). Therefore, this study further proposed that the inhibition of hyaluronidase by *P. pellucida* could attenuate neovascularization, a common occurrence in the development of DR.

For AII, the ethyl acetate and hexane fractions as well as crude methanolic extract were classified as excellent AII fractions, partly due to their high COXs and LOX inhibitory activities. This result also indicated the potential anti-inflammatory role of *P. pellucida* in targeting the AA pathway, in which the enzyme COX and LOX are the main players contributing to the inflammatory outcomes (Hanna and Hafez, 2018). The relatively high hyaluronidase inhibition activity in crude methanolic extract and hexane

fraction may suggest that *P. pellucida* could modulate the regulation of neovascularisation and inflammatory events in PDR through the modulation of HA (Wolk *et al.*, 2020, He *et al.*, 2017). As *P. pellucida* displayed significant inhibitory activity against COXs, LOX and hyaluronidase, it may harbour phytochemicals such as dillapiole, 9-octadecenoic acid and terpenoids that exhibit anti-inflammatory properties.

5.1.5 Anti-glycaemic effect

The higher α -glucosidase inhibitory activity of most *P. pellucida* solvent fractions compared to the standard drug acarbose, implied that the herbal plant is a good anti-glycaemic source. The overall IC₅₀ for α -glucosidase inhibition of the plant solvent fractions, ranging from 0.07 mg/ml to 1.17 mg/ml, was also lower than that of the anti-diabetic medicinal plant *Orthosiphon stamineus* ethanolic extract (4.63 mg/ml) in a previous study (Mohamed *et al.*, 2012), suggesting the comparatively stronger α -glucosidase inhibitory activity of *P. pellucida*. However, the lack of association between TFC and IC₅₀ for α -glucosidase inhibitory activity agreed with Wibisono *et al.* (2019), which suggested that flavonoids were unlikely α -glucosidase inhibitors. On the other hand, the significant inverse correlation established between TPC and IC₅₀ for α -glucosidase inhibitory activity confirmed that non-flavonoid phenolic compounds may have contributed to the α -glucosidase inhibitory activity of *P. pellucida* (Table 4.9). Besides, the IC₅₀ for α -glucosidase inhibitory activity was inversely correlated with the tannin and saponin content of *P. pellucida*. The α -glucosidase inhibitory activities of phenolic compounds, tannins and saponins have been previously documented (Telagari and Hullatti, 2015).

Interestingly, the IC₅₀ for α-amylase inhibitory activity of *P. pellucida* crude methanolic extract and solvent fractions were also much lower than that of acarbose, reflecting the high anti-glycaemic potential of *P. pellucida*. When compared to *O. stamineus* ethanolic extract, the α-amylase inhibitory activity of *P. pellucida* extracts was stronger due to the lower IC₅₀ values in this study. The lack of correlation of α-amylase inhibitory activity with either TPC or TFC implied that both phenolic compounds and flavonoids were less effective in α-amylase inhibition. The phytochemicals detected in phase 3 study such as the sesquiterpenes β-caryophyllene, β-elemene and β-santalene could be responsible for the inhibition of α-amylase (Kidane *et al.*, 2018).

The overall higher α-amylase inhibitory activity than the α-glucosidase inhibitory activity in *P. pellucida* fractions could be partly due to the presence of varying types and amount of bioactive compounds that specifically targeting the α-amylase (Telagari and Hullatti, 2015). In human saliva, α-amylase is the carbohydrate metabolising enzyme that breakdown polysaccharides into oligosaccharides (Telagari and Hullatti, 2015). The stronger inhibitory action against α-amylase than α-glucosidase may suggest the potential application of *P. pellucida* as anti-glycaemic agent by reducing the bioavailability of oligosaccharides in human gut (Telagari and Hullatti, 2015). The correlation of α-glucosidase and α-amylase inhibitory activities with the antioxidant activities was similar to that reported by Hamzah *et al.* (2012). This may indicate the presence of bioactive compounds in *P. pellucida* with both antioxidant and anti-glycaemic activities (Hamzah *et al.*, 2012). Furthermore, this study has identified methyl pheophorbide-a from *P. pellucida* for the first time. The compound has been demonstrated to reduce the risk of developing DM due to its

inhibitory action against carbohydrate-digesting enzymes, α -amylase and α -glucosidase (Kim *et al.*, 2019).

5.1.6 Anti-glycation effect

In DM, the excessive activation of polyol pathway promotes the conversion of glucose into sorbitol (Fournet *et al.*, 2018). With the enzyme AR being the catalyst of the reaction, the formation of sorbitol could contribute to the formation of AGE (Fournet *et al.*, 2018). In this study, the AR inhibitory activity of standard quercetin was comparable to previous studies although different sources of AR were being used (Hwang *et al.*, 2019; Patel *et al.*, 2012b). The finding of AR inhibitory activity trend in this study showed that *P. pellucida* solvent fractions of moderate to high polarities exhibited stronger AR inhibition than non-polar plant fractions. Since the AR inhibitory activity was correlated with DPPH radical scavenging activity of *P. pellucida* fractions, this study deduced that the antioxidants in moderately polar and polar fractions of *P. pellucida* were also effective AR inhibitors. The correlation observed between TPC and AR inhibitory activity provides additional evidence suggesting that the presence of phenolic compounds, which associate with DPPH scavenging activity, may contribute to the AR inhibitory effect of *P. pellucida*. A docking study by Akhila *et al.* (2012) reported that the *P. pellucida* extract displayed high binding energy towards AR. This may be attributed to the presence of phenolic compounds such as dihydroeuparin, longistylin and luteolin detected in *P. pellucida*.

Under DM condition, the accumulation of blood glucose promotes the glycation process, which results in the formation of AGEs, including fluorescent AGEs (Guerin-Dubourg *et al.*, 2017). Among the *P. pellucida*

solvent fractions, the IC₅₀ of AGE inhibition for ethyl acetate fraction was 0.05 mg/ml, whereas the medicinal plant *F. deltoidei* with anti-glycation potential, was reported in a previous study to exhibit a comparatively higher IC₅₀ at 0.125 mg/ml (Dom *et al.*, 2020). In this study, a significant positive correlation between the total AGE inhibition and anti-glycaemic activity of *P. pellucida* was observed. This finding further supported the relationship between glycaemic control and inhibition of AGEs formation (Rhee and Kim, 2018). Furthermore, the correlation of total AGE inhibition analysis with TPC, saponin and FRAP activity agreed with Starowicz *et al.* (2019), which suggested that the anti-glycation activity could be attributed to the antioxidant activity, phenolic and saponin content in medicinal plants (Valdivieso-Ugarte *et al.*, 2019). The metal chelating properties of saponin and phenolic compounds could have an impact on the synthesis of AGE (Hung *et al.*, 2017; Yeh *et al.*, 2017).

The formation of AGE intermediaries, Amadori product and dicarbonyl compounds is crucial for the synthesis of AGE (Fournet *et al.*, 2018) while most of the total AGE is composed of dicarbonyl compounds (Hung *et al.*, 2017). The interaction of AGE and its ligand subsequently leads to pro-inflammatory responses that contribute to the pathological development of DR (Chuah *et al.*, 2013). As the formation of AGE is a major risk factor for DR, the inhibition of Amadori products and dicarbonyl compound formation is valuable for the prevention of DR (Ng *et al.*, 2013). In this study, the Amadori product and dicarbonyl compound inhibitory activities were only detectable in 10 mg/ml of *P. pellucida* aqueous fraction when compared to the other solvent fractions (1 mg/ml). This finding showed that the aqueous plant fraction displayed weak inhibitory activity against the formation of Amadori products and dicarbonyl compound. Nevertheless, the dicarbonyl compound inhibitory activity was positively

correlated with COX-1 and COX-2 inhibitory activities and inversely correlated with α -amylase inhibitory activity. These findings collectively indicated that the bioactive compounds in *P. pellucida* possessed anti-glycation, anti-glycaemic and anti-inflammatory effects. Likewise, the positive correlation of TFC with Amadori product and dicarbonyl compound inhibitory activities concurred with Hung *et al.* (2017), who reported that flavonoid with antioxidant activity may partly contribute to the anti-glycation activity in *P. pellucida*.

The strong Amadori product and dicarbonyl compound inhibitory activities of ethyl acetate and hexane fractions for *P. pellucida* suggested the presence of moderately-polar and non-polar bioactive compounds that could interfere with the formation of AGE (Fournet *et al.*, 2018). In general, *P. pellucida* solvent fractions displayed stronger Amadori product inhibitory activity than their dicarbonyl compound inhibitory activity. This may indicate that *P. pellucida* exerts its inhibitory effect at the initial phase of AGEs formation, during which the Amadori product was formed (Fournet *et al.*, 2018). As dicarbonyl compounds are mainly derived from Amadori product during the AGE synthesis, the inhibition of Amadori production formation by *P. pellucida* could also interfere the formation of the dicarbonyl compounds (Fournet *et al.*, 2018). This could have explained the modest positive correlation found between the Amadori product and dicarbonyl compound inhibitory activities in the plants. In addition, the marked inhibition against the total AGEs and Amadori products qualified ethyl acetate plant fraction as a worthy anti-glycation source. Based on the correlation study (Table 4.9), the high saponin, TPC and antioxidant activity displayed by ethyl acetate fraction may also contribute to its high AGI. On the other hand, the high anti-glycation potential displayed by the

aqueous and hexane fractions was partly attributed to the significant inhibition on AR activity and dicarbonyl compounds.

5.2 The anti-retinopathy mechanisms of *P. pellucida* in ARPE-19

5.2.1 Regulation on the transcription factors implicated in inflammation and angiogenesis

Based on the phase 1 investigation on *in vitro* biological activity of *P. pellucida*, it can be deduced that the ethyl acetate fraction of the plant exhibited high antioxidant, anti-inflammatory, and anti-glycation activities in addition to its relatively high phytochemical content. The same fraction also displayed higher α -amylase and α -glucosidase inhibitory activities than the standard anti-diabetic drug, acarbose. In terms of the biological activity indices, the ethyl acetate fraction was identified as a plant fraction with very high AI and high AII. Furthermore, AGI also ranked the ethyl acetate fraction as an excellent anti-glycation fraction. The ethyl acetate fraction was classified as mildly toxic together with crude methanolic extract based on the *in vivo* toxicity assay. Although the aqueous fraction was non-toxic against brine shrimps, the biological activities shown by the fraction were insufficient to justify its potential as an anti-retinopathy agent. In addition, the chloroform, hexane and n-butanol fractions were considered moderately to highly toxic. From the above findings, it is pertinent to suggest that the ethyl acetate fraction derived from crude methanolic extract may harbour potential anti-retinopathy effect. This has prompted further investigation to study the modulatory role of ethyl acetate fraction and crude methanolic extract on the gene and protein expression of angiogenesis, antioxidant and inflammatory mediators implicated in high glucose and glycation induced stress. For this reason, an ARPE-19 cellular model was utilised to evaluate the anti-retinopathy potential of ethyl acetate fraction and crude methanolic extract against high glucose and AGE induced oxidative-glycative stress related to DR.

The major risk factors that contribute to the development of DR include the manifestation of pathological processes in the retina such as angiogenesis, inflammation and oxidative stress (Safi *et al.*, 2014). These risk factors are controlled by transcription factors in the cells that act as the master switch for gene and protein expression of angiogenic, pro-inflammatory and antioxidant biomarkers (Al-Kharashi, 2018). In the present study, the negative impact of high glucose and AGE towards the gene and protein expression of transcription factors, NF- κ B p65, STAT3 and PPAR- γ in ARPE-19 was investigated. While not all mRNA transcripts are translated into proteins, analysing the gene and protein expression provides insights into the transcriptional regulation of specific genes and proteins (Alberts *et al.*, 2022). The impact of *P. pellucida* crude methanolic extract and ethyl acetate fraction on the behavior of transcription factors in ARPE-19 subjected to high glucose and AGE induced stress was discussed in this section.

5.2.1.1 Effect of AGE and high glucose-induced oxidative stress on NF- κ B p65 and STAT3 in ARPE-19

The NF- κ B p65 transcription factor regulates a variety of genes that control the innate and adaptive immune functions (Liu *et al.*, 2017). According to Suryavanshi and Kulkarni (2017), the gene and protein expression of NF- κ B p65 can be induced under prolonged high glucose environment through oxidative stress and the formation of AGE, which collectively lead to the development of macrovascular and microvascular complications. This is accomplished through the activation of toll-like receptor-induced myeloid differentiation primary response 88 pathway, which in turn stimulates the enzyme IKK to degrade the protein I κ B that is

sequestering the action of NF- κ B p65 (Liu *et al.*, 2017). Alternatively, the *de novo* synthesis of diacylglycerol in high glucose condition could stimulate PKC-induced ROS formation, leading to the activation of IKK and release of NF- κ B p65 (Mittal *et al.*, 2014; Tarr *et al.*, 2013). Subsequently, this led to the activation of NF- κ B p65 as indicated by the increased protein level of phosphorylated NF- κ B p65 (Figure 4.8). Hence, this mechanism may explain how the exposure of ARPE-19 to increased concentration of glucose could up-regulate the gene expression of NF- κ B p65 through the induction of oxidative stress in this study (Figure 4.6). Besides, the binding of AGE to RAGE is known to trigger the NF- κ B p65 signalling pathway through PKC-mediated ROS formation, resulting in the activation of IKK and liberation of NF- κ B p65. This cascade results in the generation of downstream inflammatory responses (Vanhooren *et al.*, 2015). Although AGE did increase the gene expression of NF- κ B p65 under normal glucose condition in this study, there was no further escalation in the gene and protein expression of NF- κ B p65 and phosphorylated-NF- κ B p65 in the high glucose AGE-treated conditions. This finding suggested that both high glucose and AGE may share a similar mechanism for the activation of NF- κ B p65, likely through the stimulation of IKK. Figure 5.1 illustrates the comprehensive molecular mechanism, which involves the NF- κ B p65 and STAT3 signal transduction pathways.

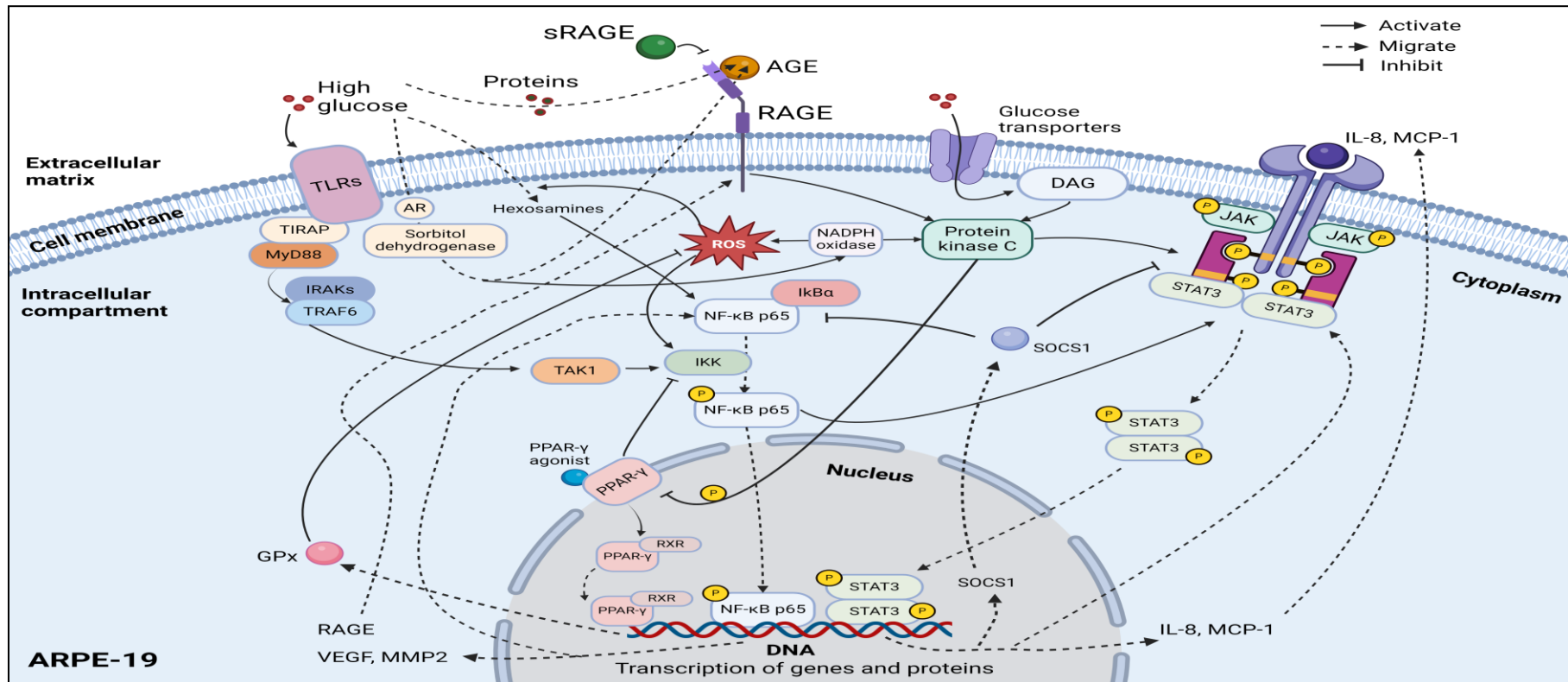


Figure 5.1. The overall molecular mechanism of signal transduction pathways implicated in the gene and protein expression of antioxidant, angiogenic and inflammatory markers. AGE, advanced glycation end product; AR, aldose reductase; DAG, diacylglycerol; DNA, deoxyribonucleic acid; GPx, glutathione peroxidase; IκBα, inhibitor of nuclear factor kappa B alpha; IKK, inhibitor of nuclear factor-kappa B kinase; IL-8, interleukin 8; IRAK, interleukin receptor-associated kinase; JAK, Janus kinase; MCP-1, monocyte chemoattractant protein 1; MMP2, matrix metalloproteinase 2; MyD88, Myeloid differentiation primary response protein 88; NF-κB p65, nuclear factor kappa B p65; NADPH, nicotinamide adenine dinucleotide phosphate; P, phosphate; PPAR-γ, peroxisome proliferator activated-receptor gamma; RAGE, receptor for advanced glycation end product; ROS, reactive oxygen species; RXR, retinoid X receptor; SOCS1, suppressor of cytokine signalling 1; STAT3, signal transducer and activator of transcription 3; TAK1, transforming growth factor-β-activated kinase 1; TIRAP, toll-interleukin receptor domain-containing adaptor protein; TLR, toll-like receptor; TRAF6, Tumor necrosis factor receptor-associated factor 6; VEGF, vascular endothelial growth factor.

Under normal physiological condition, the activation of STAT3 is negligible (Rébé *et al.*, 2013). In previous reports, ARPE-19 grown in high glucose condition has been associated with apoptosis and inflammation through the activation of STAT3 signalling pathway (Liang *et al.*, 2022; Wang *et al.*, 2021a). As the activation of STAT3 is insignificant under normal condition (Rébé *et al.*, 2013), this may cause an unaltered STAT3 band signal across the experimental groups (Table 4.10). The reason was that the C-terminal region (702-716 amino acids) of STAT3 protein was the target site of anti-STAT3 antibody, which was also the same region for the dimerization of phosphorylated STAT3 during activation (Sethi *et al.*, 2014). Therefore, any activation of STAT3 would result in negligible changes in the observable STAT3 signal, which was derived from both the STAT3 and undimerised phosphorylated STAT3 proteins (Figure 5.1). This phenomenon was in accordance with previous reports, which showed that the band signal of STAT3 was unaltered under normal glucose, high glucose and AGE-treated groups (Johnston *et al.*, 2013; Yang *et al.*, 2019).

The current study reported that high glucose (68 mM) significantly stimulated STAT3 activation in ARPE-19 (Table 4.10). The high gene expression and activation of STAT3 under high glucose (>60 mM) condition was in agreement with a previous report (Yang *et al.*, 2021). As STAT3 forms an important element in the JAK-STAT3 signalling pathway, the up-regulation of STAT3 in ARPE-19 under normal glucose AGE-treated condition could be related to the activation of JAK-STAT3 via AGE-RAGE interaction (Sun *et al.*, 2017). In contrast to NF- κ B, this study observed significant activation of STAT3 in response to the combination of high glucose and AGE, particularly when comparing moderate high glucose (34 mM) with its AGE-treated counterpart. This could be attributed to the combination of factors induced by high glucose and AGE, such as NF- κ B

p65 signalling, cytokine receptor signalling and PKC-mediated oxidative stress (Figure 5.1) (Prakash *et al.*, 2008). Under normal physiological condition, JAK-STAT3 is implicated in the regulation of the cellular functions such as cell growth, cell differentiation and immune response (Bharadwaj *et al.*, 2020). However, the activation of JAK-STAT3 under pathologic conditions could result in increased gene expression and subsequent phosphorylation of STAT3, leading to inflammatory response and apoptosis (Bharadwaj *et al.*, 2020). The inflammatory response was further amplified due to the transcription of inflammatory cytokines such as IL-8 and MCP-1, which activate JAK by binding to the respective cytokine receptors (Figure 5.1) (Fan *et al.*, 2013). Besides, previous studies have reported the transactivation of both NF- κ B p65 and JAK-STAT3 (Fan *et al.*, 2013; McFarland *et al.*, 2013). It was plausible that the activation of NF- κ B p65 and JAK-STAT3 took place concurrently under high glucose and AGE-treated conditions in this study, which leads to inflammation and subsequent ARPE-19 cell injury.

5.2.1.2 Effect of AGE and high glucose on PPAR- γ

In contrary to NF- κ B p65 and STAT3, the PPAR- γ pathway is involved in the regulation of insulin sensitivity and glucose homeostasis in most cell types, including the RPE (Zhang *et al.*, 2015a). Interestingly, PPAR- γ also acts as an immunomodulator by counteracting the production of pro-inflammatory mediators (Hernandez-Quiles *et al.*, 2021). In other words, NF- κ B p65 and STAT3 promote inflammation in the retina whereas PPAR- γ elicits anti-inflammatory response (Tarr *et al.*, 2013; Zhang *et al.*, 2015a). As PPAR- γ was involved in the stimulation of insulin-mediated glucose uptake (Hernandez-Quiles *et al.*, 2021), the increased PPAR- γ

protein expression in ARPE-19 in the current study was a response to high glucose in an attempt to stimulate glucose uptake in ARPE-19 (Jiang *et al.*, 2018; Panchapakesan *et al.*, 2004). However, the up-regulation of PPAR- γ under hyperglycaemic condition has been linked to reduced cell viability (Panchapakesan *et al.* 2004). As a result, the increased protein expression of PPAR- γ (Figure 4.13) could have involved in the decreased ARPE-19 cell viability under high glucose conditions. This study found that increased phosphorylated PPAR- γ protein expression under high glucose conditions (Table 4.11) led to a downregulation of PPAR- γ gene expression. This downregulation occurred due to alterations in transcriptional activity caused by the phosphorylation of PPAR- γ . (Frkic *et al.*, 2021).

On the other hand, AGE-induced stress was accompanied by decreased expressions of PPAR- γ gene and protein in normal glucose ARPE-19 (Table 4.11). The anti-inflammatory action of PPAR- γ lies in its ability to suppress the enzyme IKK, which activates NF- κ B p65 (Ju *et al.*, 2020). With the gene and protein expression of PPAR- γ reduced under normal glucose AGE-treated condition, this could justify the up-regulation of NF- κ B p65 in ARPE-19 (Figure 5.1). The antagonistic relationship between the gene expression of NF- κ B p65 and PPAR- γ has been previously reported (Wang *et al.*, 2021b). Likewise, the down-regulation of PPAR- γ protein expression under normal glucose AGE-treated condition could be a result of NF- κ B p65 activation, which repressed the action of PPAR- γ (Chen *et al.*, 2013, Wang *et al.*, 2009). Besides, reduced level of PPAR- γ protein was linked to increased pro-inflammatory response (Sobolev *et al.*, 2020). This was in accordance to a previous study, which suggested that reduced PPAR- γ expression was related to high incidence of oxidative stress event while PPAR- γ level could be a predictor of diabetic progression (Ekun *et al.*, 2021). In this study, the level of phosphorylated PPAR- γ protein was

increased in the high glucose (34 mM, 68 mM) and AGE-treated groups (Table 4.11). The phosphorylation of PPAR- γ protein may occur as a result of high glucose and AGE-induced PKC activation (Figure 5.1) (Burns and Heuvel, 2007). The phosphorylation of PPAR- γ has been shown to modify the transcriptional activity of PPAR- γ , thereby leading to subsequent down-regulation of important anti-inflammatory markers (Burns and Heuvel, 2007; Dias *et al.*, 2020). The altered behaviour of PPAR- γ as a result of phosphorylation may indicate that the transcriptional activity of NF- κ B p65 could no longer be suppressed, which caused a continuous generation of pro-inflammatory response in ARPE-19 under the influence of high glucose and AGE (Chen *et al.*, 2013).

5.2.1.3 Effect of *P. pellucida* on NF- κ B p65, STAT3 and PPAR- γ transcription factors

The unaltered gene and protein expression of NF- κ B p65 (Figure 4.6-4.8), STAT3 (Figure 4.9, Table 4.10) and PPAR- γ (Table 4.11), including their phosphorylated counterparts in plant-treated normal glucose ARPE-19 may indicate that the crude methanolic extract and ethyl acetate fraction did not affect the expression or activation of these transcriptional proteins. Several studies have previously reported that treatment with natural product extracts was unlikely to result in the activation of transcription factors and nuclear receptors (Kim *et al.*, 2020; Koraneeyakijkulchai *et al.*, 2023). In the current study, it was suggested that the administration of *P. pellucida* will not trigger the NF- κ B p65, JAK-STAT3 and PPAR- γ signalling pathways in the retina of normoglycaemic individuals.

Interestingly, *P. pellucida* extracts treatment was shown to prevent the activation of NF- κ B p65 and STAT3 by reducing the expression of their phosphorylated counterparts under high glucose and AGE-treated conditions (Figure 4.8, Table 4.10). This finding indicated a decreased downstream pro-inflammatory response, which is controlled by the NF- κ B p65 and STAT3 signalling pathways (Liu *et al.*, 2017; Zegeye *et al.*, 2018). As the up-regulation of PPAR- γ was linked to reduced cell viability (Panchapakesan *et al.* 2004), the restoration of PPAR- γ back to normal control level by crude methanolic extract and ethyl acetate fraction under normal glucose AGE-treated condition could have explained the ARPE-19 cytoprotective effect of *P. pellucida*. Besides, the ability of *P. pellucida* extracts in suppressing the phosphorylation of PPAR- γ proteins was crucial to confirm its anti-inflammatory mechanism in preventing cell death of ARPE-19 (Frkic *et al.*, 2021). Furthermore, a lower sample concentration of *P. pellucida* crude methanolic extract was required when compared to the ethyl acetate fraction to suppress the phosphorylation of NF- κ B p65, STAT3, and PPAR- γ under high glucose and glycated conditions. This may be due to the higher phytochemical concentration in the crude extract from which the ethyl acetate fraction was derived. This observation also applies to the downstream inhibition of pro-inflammatory and angiogenic mediators.

The impact of *P. pellucida* on the transcription factors could be ascribed to the presence of phytochemicals with functional properties. In phase 3 investigation, the purification and characterisation of phytochemicals have resulted in the identification of 4 major phytochemicals, namely the dillapiole, 2,4,5-trimethoxystyrene, methyl 9-octadecenoic acid and methyl pheophorbide-a from *P. pellucida* crude methanolic extract. In GC-MS analysis, the detected non-polar volatile compounds belonged to four phytochemical classes, such as alkyl

hydrocarbons, naphthalenes, phenylpropanoids and terpenes. On the other hand, six classes of polar compounds including alkaloids, chlorophyll derivatives, ketones, naphthalenes, phenolic compounds and terpenes were detected with LC-QToF-MS analysis. The majority of the compounds detected in *P. pellucida* were composed of functional groups such as allyl, benzodioxole, methoxy and quinazoline units, which could be associated with the functional activities of *P. pellucida* (Parise-Filho *et al.*, 2011).

Dillapiole, a major phenylpropanoid compound was known to suppress the production of pro-inflammatory cytokines by targeting the NF- κ B p65 signalling pathway (Li *et al.*, 2021; Rojas-Martínez *et al.*, 2013). Dillapiole was previously shown to exhibit gastroprotective activity against EtOH-induced gastric lesion that raised the NF- κ B p65 activity (Li *et al.*, 2021; Rojas-Martínez *et al.*, 2013). The long chain unsaturated fatty acid detected in *P. pellucida* called 9-octadecenoic acid, was able to inhibit NF- κ B p65 signalling pathway by increasing the NF- κ B sequestering activity of I κ B (Kang *et al.*, 2018). An *in-silico* docking study has suggested that 9-octadecenoic acid may inhibit STAT3 due to its high binding affinity to the protein (Anjum *et al.*, 2023). In addition, it was previously reported that 9-octadecenoic acid was a potential ligand and agonist for PPAR- γ (Ikeguchi *et al.*, 2018). Hence, the activation of PPAR- γ may subsequently lead to the suppression of pro-inflammatory response.

The abundance of sesquiterpenes in *P. pellucida* also plays a crucial role in the inhibition of NF- κ B p65 and JAK-STAT3 signalling pathways. Several major sesquiterpenes have been found in *P. pellucida*, including the β -caryophyllene, β -elemene, β -santalene and carotol (Table 4.18). Among the sesquiterpenes, β -caryophyllene and β -elemene could reduce gene and protein expression of NF- κ B p65 (Ahmad *et al.*, 2020). The sesquiterpenes also interrupted the production of pro-inflammatory

cytokines by targeting the NF- κ B p65 signalling pathway (Liu *et al.*, 2021). According to Ahmad *et al.* (2020), β -elemene inhibited the action of NF- κ B p65. The anti-NF- κ B p65 activity of β -caryophyllene lies with its inhibitory action against IKK, which is responsible for the degradation of I κ B and activation of NF- κ B p65 (Gui *et al.*, 2013).

According to Youssef *et al.* (2019), the agonist of type 2 cannabinoid receptor, β -caryophyllene could intercept the NF- κ B p65 signalling through the activation of PPAR- γ . The activation of PPAR- γ by the sesquiterpene was accompanied by diminished inflammation and oxidative stress (Youssef *et al.*, 2019). Additionally, β -caryophyllene was associated with the inhibition of hexosamine and ROS formation (Hashiesh *et al.*, 2020). The suppression of hexosamine pathway eventually results in the inhibition of NF- κ B p65 (Figure 5.1) (Hashiesh *et al.*, 2020; Li *et al.*, 2017). Thus, *P. pellucida* could hinder the pro-inflammatory signalling pathway through the inhibitory action of sesquiterpenes on NF- κ B p65.

Besides, β -caryophyllene (Gui *et al.*, 2013; Zhang *et al.*, 2022a) have been demonstrated to ameliorate inflammation by inhibiting the activation of STAT3. The molecular mechanism behind the anti-inflammatory activity of β -caryophyllene was through the inhibition of JAK, which may regulate the downstream activation of STAT3 (Kim *et al.*, 2014; Sun *et al.*, 2022). According to Sim *et al.* (2019), NF- κ B p65 may enhance the interaction of STAT3 via p300 proteins, which subsequently activate specific response element in the gene promoter region for the transcription of pro-inflammatory and angiogenic mediators (Sim *et al.*, 2019). Hence, it was likely that the sesquiterpenes could also prevent NF- κ B mediated STAT3 signalling pathway.

Furthermore, the presence of chlorophyll derivative pheophorbide-a methyl ester, which was reported for the first time for *P. pellucida* in this study, could potentially suppress NF- κ B p65 by preventing the phosphorylation of its protein counterpart (Lee *et al.*, 2021). It was previously suggested that flavonoids could inhibit the activation of NF- κ B p65 (Gao *et al.*, 2023). A previous study has demonstrated that the flavonoid luteolin attenuated inflammation by targeting the gene and protein expression of NF- κ B p65 (Gao *et al.*, 2023). According to Kim and Jobin (2005), this was accomplished with the same action as sesquiterpenes, through the suppression of the enzyme IKK.

Additionally, luteolin could also mitigate inflammation by activating PPAR- γ (Li *et al.*, 2022a), leading to the inhibition of NF- κ B p65 signalling pathway and diminished production of pro-inflammatory cytokines (Gao *et al.*, 2023; Li *et al.*, 2022a). Luteolin is has been demonstrated to suppress STAT3 activation (Li *et al.*, 2022b). This study has suggested that *P. pellucida* could prevent the activation of STAT3 by selectively targeting AGE. This can be associated with the findings in phase 1 study, in which *P. pellucida* was found to display strong anti-glycation activity. Hence, this study suggested that *P. pellucida* extracts could intercept AGE-RAGE interaction that is widely implicated in the PKC-mediated downstream activation of STAT3.

The presence of major bioactive compounds identified in this study, such as 9-octadecenoic acid, β -caryophyllene, β -elemene, dillapiole, luteolin and pheophorbide-a methyl ester may support *P. pellucida* as a potential NF- κ B p65 and STAT3 antagonists that regulate inflammatory response in ARPE-19. The suppression of NF- κ B p65 and STAT3 signalling pathways by *P. pellucida* is crucial to intervene the downstream pro-inflammatory and angiogenic responses. Interestingly, the presence of

PPAR- γ agonist in *P. pellucida* such as 9-octadecenoic acid, β -caryophyllene and luteolin may also contribute to promoting the anti-inflammatory response in high glucose and AGE-treated ARPE-19. Therefore, the presence of these bioactive compounds may potentiate *P. pellucida* as a therapeutic remedy for reducing inflammation in DR.

5.2.2 Regulation on pro-inflammatory markers

This section aimed to discuss the effect of high glucose and AGE on the gene and protein expression of pro-inflammatory cytokines: IL-8 and MCP1 in ARPE-19. In eukaryotes, the expression of the pro-inflammatory cytokines are regulated by NF- κ B p65 transcription factor (Liu *et al.*, 2017). In recent studies, it was found that the activation of JAK-STAT3 is also associated with the expression of IL-8 (Hsu *et al.*, 2021) and MCP-1 (Basu *et al.*, 2020). As the activation of NF- κ B p65 and STAT3 are involved in the modulation of transcription for IL-8 and MCP-1, the regulatory mechanism of *P. pellucida* crude methanolic extract and ethyl acetate fraction on the gene and protein expression of pro-inflammatory cytokines in ARPE-19 from high glucose and AGE-treated conditions was elaborated in this section.

5.2.2.1 Effect of AGE and high glucose-induced oxidative stress on pro-inflammatory markers in STAT3 and NF- κ B p65 signalling pathway

The up-regulation of IL-8 and MCP-1 under high glucose and AGE-treated conditions has highlighted that gene and protein expression of the inflammatory markers can be induced in ARPE-19 through NF- κ B p65 and

JAK-STAT3 signalling pathways under the stimulation of high glucose and AGE. This finding agreed with previous studies, which reported increased IL-8 gene and protein expression in normal human cell lines subjected to high glucose and AGE stimulation (Lan *et al.*, 2013; Rasheed *et al.*, 2011). The significant increment of IL-8 gene and protein expression in the normal glucose AGE-treated condition compared to the moderately elevated glucose (34 mM) condition suggests that the influence of AGE on the up-regulation of IL-8 in ARPE-19 was more pronounced than that of the high glucose environment. Among the different ARPE-19 conditions being studied, IL-8 showed the highest increment under high glucose AGE-treated conditions. Chiu *et al.* (2016) reported a synergistic increased of IL-8 gene and protein expression in an environment of high glucose and AGE. Similarly, the MCP-1 expression is regulated by NF- κ B p65 and STAT3 signalling pathways that respond to the AGE and high glucose (Liu *et al.*, 2017; Zegeye *et al.*, 2018). Together with the earlier findings, it can be deduced that high glucose and AGE stimulated the gene and protein expression of pro-inflammatory cytokines: IL-8 and MCP-1 in ARPE-19 via the activation of NF- κ B p65 and STAT3. Additionally, the combination of high glucose and AGE could have resulted in the synergistic activation of NF- κ B p65 and STAT3 signalling pathways, which eventually boosted the expression of IL-8 and MCP-1 under high glucose AGE-treated conditions. IL-8 and MCP-1 are chemotactic cytokines involved in the generation of inflammatory response in DR (Hernández *et al.*, 2005; Taghavi *et al.*, 2019). Both IL-8 and MCP-1 are responsible for chemotaxis, which can be described as the activation and recruitment of leukocytes to the site of inflammation (Deshmane *et al.*, 2009; Silva, 2010). In DR, the migration and subsequent extravasation of leukocytes during inflammation could ultimately lead to the breakdown of BRB, which is the hallmark

manifestation of DME (Wang and Lo, 2018). Hence, the overexpression of IL-8 and MCP-1 could have a negative impact on the severity of DR.

5.2.2.2 Effect at early phase of inflammation

This study has indicated that *P. pellucida* could suppress the gene and protein expression of transcription factors NF- κ B p65 and STAT3 in ARPE-19 subjected to high glucose-induced oxidative glycation stress. The lower expression of IL-8 gene and protein in plant-treated ARPE-19 when compared to the untreated control under normal glucose condition, also suggested that *P. pellucida* could suppress the gene and protein expression of pro-inflammatory cytokines in healthy individuals. Unlike IL-8, the gene and protein expression of MCP-1 under normal glucose ARPE-19 remain unchanged after *P. pellucida* treatment. This finding showed that the application of *P. pellucida* may not affect the MCP-1 expression in the retina of healthy individual. Under high glucose (68 mM) AGE-treated condition, the expression of IL-8 protein was suppressed by crude methanolic extract (≥ 0.75 mg/ml) and ethyl acetate fraction (≥ 1 mg/ml). Besides, *P. pellucida* extracts also suppressed the gene and protein expression of MCP-1 and IL-8, especially in the normal glucose AGE-treated condition. The suppression of IL-8 and MCP-1 gene and protein expression has indicated that the *P. pellucida* extracts, is capable of targeting the early phases of inflammation, especially through AGE inhibition. On the other hand, this study also observed a stronger inhibition on the MCP-1 protein expression in ARPE-19 by crude methanolic extract when compared to the ethyl acetate fraction (Table 4.12). As IL-8 is involved specifically in the early phase of inflammation whereas MCP-1 is implicated in both the early and late phase of inflammation (Silva, 2010; Deshmane *et al.*, 2009), the

down-regulation of gene and protein expression for IL-8 and MCP-1 implied that *P. pellucida* could target the early phase of inflammatory response.

Several bioactive compounds that specifically targeted IL-8 and MCP-1 have been detected in *P. pellucida* (Table 4.17-4.18). Dillapiole, the major phenylpropanoid in *Peperomia* species has been previously demonstrated to reverse carrageenan-induced rat paw edema and writhing (de Cássia *et al.*, 2014; Pinheiro *et al.*, 2011). The stimulation of paw edema by carrageenan was associated with an increase of IL-8 and MCP-1 expression via NF- κ B p65 signalling (de Cássia *et al.*, 2014; Zhang *et al.*, 2022b). Likewise, the gene and protein expression of IL-8, MCP-1 and NF- κ B p65 in rat model of EtOH-induced gastric lesion was also reduced by dillapiole treatment (Li *et al.*, 2021; Rojas-Martínez *et al.*, 2013). Therefore, the regulation of *P. pellucida* on IL-8 and MCP-1 expression in ARPE-19 were most likely attributed to the presence of phenylpropanoid such as dillapiole.

All pheophorbide derivatives, including pheophorbide-a methyl ester have been previously reportedly to inhibit NF- κ B p65 activation and subsequently the down-regulation of IL-8 (Lee *et al.*, 2021). Pheophorbide-a methyl ester has been demonstrated to reduce the gene and protein expression of MCP-1 in AGE-treated NF- κ B p65 signalling pathway (Nam *et al.*, 2013). In addition, previous study has demonstrated that the administration of luteolin, a flavonoid, to ARPE-19 effectively inhibited IL-8 and MCP-1 expression via the NF- κ B p65 signalling pathway (Huang *et al.*, 2020). According to Liu *et al.* (2021), β -caryophyllene, a cannabinoid receptor agonist, inhibited the gene and protein expression of IL-8 by selectively preventing the activation of NF- κ B p65. Both IL-8 and NF- κ B p65 expression in osteosarcoma model were also suppressed in the presence of β -elemene (Fang *et al.*, 2018). Both β -caryophyllene and β -

elemene treatments down-regulated MCP-1 and subsequently macrophage accumulation (Gullì *et al.*, 2022; Yu *et al.*, 2019). Furthermore, PPAR- γ agonists like 9-octadecenoic acid, β -caryophyllene and luteolin could indirectly reduce the expression of IL-8 and MCP-1 by inhibiting NF- κ B p65 (Ikeguchi *et al.*, 2018; Youssef *et al.*, 2019). Since β -caryophyllene and β -elemene reportedly inhibited STAT3 activation by intercepting the NF- κ B p65 signalling pathway, the present study suggested that the presence of β -caryophyllene, β -elemene, dillapiole, luteolin and pheophorbide-a methyl ester in *P. pellucida* were responsible in suppressing the gene and protein expression of IL-8 and MCP-1 by targeting the NF- κ B p65, PPAR- γ , STAT3 signalling pathways.

5.2.3 Regulation on the angiogenic markers

In DR, the MMP2 and VEGF are two important angiogenic factors that contribute equally to neovascularisation (Kowluru *et al.*, 2012). MMP2 is involved in the breakdown of vascular matrix for subsequent vascular development, which is signalled by VEGF (Hazzaa *et al.*, 2020; Quintero-Fabián *et al.*, 2019). In this section, the impact of high glucose and AGE on the gene and protein expression of MMP2 and VEGF in ARPE-19 was discussed. This section also aimed to elaborate the regulatory effect of *P. pellucida* crude methanolic extract and ethyl acetate fraction towards the expression of MMP2 and VEGF in ARPE-19 subjected to high glucose and glycation stress.

5.2.3.1 Effect of AGE and high glucose on STAT3 and NF- κ B p65 implicated in angiogenesis

The activation of STAT3 could directly regulate the transcription of MMP2 (Xie *et al.*, 2004) through the IL-8-STAT3 signalling axis (Quintero-Fabián *et al.*, 2019). The up-regulation of MMP2 via the NF-κB p65 signalling pathway in the presence of high glucose and AGE has been demonstrated previously (Li *et al.*, 2016; Mohammad and Kowluru, 2010). In this study, the gene and protein expression of MMP2 may have increased due to the high glucose and AGE-induced activation of STAT3 and NF-κB p65 signalling pathway (Figure 5.1). This may also reflect the tendency of high glucose and AGE in promoting the degradation of matrix proteins for vascular development in the retina (Nikolov and Popovski, 2021). Although there was a comparatively lower gene and protein expression of VEGF observed in the normal glucose AGE-treated ARPE-19 compared to those in the high glucose (34 mM, 68 mM) conditions, the significant elevated gene and protein expression of VEGF in the high glucose (68 mM) AGE-treated ARPE-19 could be attributed to the combined effect of high glucose and AGE. (Chiu *et al.*, 2016). According to Bandyopadhyay and Rohrer (2012), the up-regulation of VEGF was associated with the expression of MMP2. Furthermore, the gene and protein expression of MMP2 and VEGF was regulated by the NF-κB p65 and STAT3 signalling pathways (Apte *et al.*, 2019; Safi *et al.*, 2014). Hence, this study suggested that the gene and protein expression of MMP2 and VEGF were up-regulated via the activation of NF-κB p65 and STAT3 in ARPE-19 under the stimulation of high glucose and AGE.

5.2.3.2 Effect of *P. pellucida* on angiogenic response in ARPE-19

This study showed that the application of *P. pellucida* did not induce an angiogenic response in healthy retina. This was evidenced by the

unchanged gene and protein expression of MMP2 and VEGF following the administration of crude methanolic extract and ethyl acetate fraction in normal glucose ARPE-19 (Table 4.13). In addition, the ability of *P. pellucida* extracts in suppressing the gene and protein expression of MMP2 and VEGF under the stimulation of AGE showed that the plant could inhibit AGE-induced angiogenic response in ARPE-19. Interestingly, a stronger down-regulation of MMP2 (33 %) than VEGF (16 %) might indicate that *P. pellucida* extracts specifically targeted the degradation of vascular matrix. Regardless, the overall ability of *P. pellucida* in regulating the expression of MMP2 and VEGF could reflect its potential in mitigating retinal neovascularisation and prevent the abnormal development of new blood vessels, especially in PDR (Bandyopadhyay and Rohrer, 2012).

The presence of selected bioactive compounds may be responsible for the anti-angiogenic potential of *P. pellucida* (Ho *et al.*, 2022b). Previous study has reported a reduction of blood vessel formation in an *ex vivo* chorioallantoic membrane model after the administration of *P. pellucida* crude methanolic extract (Camposano *et al.*, 2016). They suggested that the anti-angiogenic effect of *P. pellucida* was linked to the presence of phenolic compounds and alkaloids (Camposano *et al.*, 2016). In this study, the anti-angiogenic potential of *P. pellucida* was likely to be ascribed to the high TPC discovered from crude methanolic extract and ethyl acetate fraction in phase 1 study (Table 4.1). Bioactive compounds such as the carpelastofuran, clusin, dihydroeuparin, longistylin C and luteolin were the phenolic compounds identified in phase 3 study (Table 4.16). Besides, several alkaloids identified with LC-QToF-MS analysis may also contribute to the anti-angiogenic potential of *P. pellucida*, including 5-methoxycanthin-6-one, dictyoquinazol, homaline and uplandicine (Table 4.16). Among the characterised phenolic compounds and alkaloids, luteolin

and dictyoquinazol have been shown to suppress the gene and protein expression of MMP2 in previous studies (Nazir *et al.*, 2021; Pandurangan *et al.*, 2014). The anti-angiogenic activity of luteolin have been described in a previous study (Ambasta *et al.*, 2015). It was found that luteolin was effective in inhibiting the gene and protein expression of VEGF (Ambasta *et al.*, 2015). Hence, it was apparent that the significant down-regulation of VEGF was partly due to the presence of luteolin.

A previous study has demonstrated that β -caryophyllene inhibited the gene and protein expression of MMP2 by targeting the STAT3 signalling pathway (Di Sotto *et al.*, 2022). β -caryophyllene also displayed anti-angiogenic potential by decreasing the gene and protein expression of VEGF (Dahham *et al.*, 2021). According to Zhang *et al.* (2021), β -elemene treatment was accompanied by down-regulated MMP2, which was associated with the inhibition of focal adhesion kinase-Src dependent STAT3 activation. In addition, Zhou *et al.* (2020b) also highlighted the inhibitory effect of β -elemene on the gene and protein expression of VEGF.

Pheophorbide-a methyl ester, a recently discovered chlorophyll derivative in *P. pellucida* in this study, has reduced MMP2 expression through its selective inhibitory activity against NF- κ B p65 (Lee *et al.*, 2021). This study has highlighted the potential of *P. pellucida* crude methanolic extract and ethyl acetate fraction in mitigating the degradation of vascular matrix protein and subsequent vascular development caused by high glucose and AGE in ARPE-19 through NF- κ B p65 and STAT3 mediated expression of MMP2 and VEGF.

5.2.4 Regulation on the antioxidant defense and cytokine signalling

In retina, ROS contributes significantly to inflammation and subsequent pathogenesis of DR (Li *et al.*, 2017). The antioxidant enzyme, GPx plays a crucial role in mitigating oxidative stress by sequestering ROS, thereby safeguarding the retina from oxidative stress (Birben *et al.*, 2012). On the other hand, SOCS1 operates within the mechanism of negative feedback loop to limit the production of pro-inflammatory cytokines from NF- κ B and STAT3 signalling (Liau *et al.*, 2018). This section aimed to discuss about the effect of high glucose and AGE on the gene and protein expression of GPx and SOCS1 in ARPE-19. The regulatory action of *P. pellucida* crude methanolic extract and ethyl acetate fraction towards the expression of GPx and SOCS1 was also described in this section.

5.2.4.1 Effect of AGE and high glucose on antioxidant enzyme GPx

In the current study, the low gene and protein expression of GPx may reflect the presence of oxidative stress in the AGE-treated ARPE-19. This was in agreement with prior report, which suggested that AGE could decrease the production of antioxidant enzymes through the RAGE-NF- κ B p65 signalling axis (Nowotny *et al.*, 2015). In addition, the stimulation of ARPE-19 with AGE and increased concentration of glucose was associated with reduced gene expression and protein level of GPx (Table 4.14). This indicated that the accumulation of glucose further deteriorated the antioxidant status in ARPE-19 due to the accelerated formation of AGE (Nowotny *et al.*, 2015). Furthermore, the PPAR- γ pathway was implicated in the activation of antioxidant defense system (Mannan *et al.*, 2021). Hence, a decreased expression of PPAR- γ in ARPE-19 under AGE-induced stress could have caused the down-regulation of GPx. Besides, the decreased gene and protein expression of GPx were associated with high

glucose-induced NF- κ B p65 activation, which regulates inflammation and apoptosis (Lubos *et al.*, 2011). Therefore, the up-regulated NF- κ B p65 under high glucose and AGE-induced oxidative stress could be related to the reduced GPx level in ARPE-19.

5.2.4.2 The negative feedback response towards STAT3 activation

The up-regulation of SOCS1 under high glucose condition (Figure 4.25-4.26) concurred with a previous report (Chen *et al.*, 2016), indicating the expression of SOCS1 as a result of STAT3 activation. Furthermore, this study also showed that AGE could trigger the gene and protein expression of SOCS1 in ARPE-19 (Table 4.14). According to Sun *et al.* (2017), AGE stimulation induced the expression of SOCS1 via STAT3 activation. In response to AGE, it was plausible that SOCS1 was expressed as a negative feedback regulator of JAK-STAT3 signalling pathway in ARPE-19. Besides, the observed increased SOCS1 protein level, alongside the stagnant gene expression of SOCS1 among the high glucose (34 mM, 68 mM) and AGE-treated (34 mM, 68 mM) conditions (Table 4.14), indicated that SOCS1 protein expression was significantly affected by high glucose condition, while AGE did not further escalate the gene expression of SOCS1. On the contrary, the protein expression of SOCS1 was accelerated by high glucose and AGE in ARPE-19 (Table 4.14). The up-regulation of SOCS1 may correlate with the decreased ARPE-19 cell viability under high glucose and AGE-treated conditions. This was supported by a previous study demonstrating an up-regulated SOCS1 expression due to JAK-STAT3 activation may reflect mitochondrial impairment and subsequent cell death (Chen *et al.*, 2016).

5.2.4.3 Effect of *P. pellucida* on antioxidant status and cytokine signalling

The observed restoration of GPx gene and protein expression by *P. pellucida* could be attributed to the antioxidant activity of the plant. In addition to the metal-reducing and radicals scavenging properties displayed by *P. pellucida* in phase 1 study, the current study showed that the plant could potentially shield ARPE-19 from high-glucose-induced oxidative stress through the up-regulation of GPx. On the other hand, the treatment of *P. pellucida* extracts did not affect the gene and protein expression of SOCS1 in normal glucose ARPE-19 (Table 4.14), which may be translated to the effect of *P. pellucida* on SOCS1 in healthy retina. Furthermore, the down-regulation of SOCS1 under pathologic conditions following plant sample treatment may suggest that the *P. pellucida* extracts suppressed STAT3 signalling pathway, which was regulated by SOCS1 as part of a negative feedback response (Liau *et al.*, 2018). This study also showed that *P. pellucida* could suppress the gene expression of SOCS1 in ARPE-19 when the crude methanolic extract (3 mg/ml) and ethyl acetate fraction (4 mg/ml) was administered. As SOCS1 expression was linked to reduced ARPE-19 cell viability (Chen *et al.*, 2016), the ARPE-19 cytoprotective activity of crude methanolic extract and ethyl acetate fraction could be partly related to the down-regulation of SOCS1 upon *P. pellucida* extracts treatment.

The restoration of GPx gene and protein expression by *P. pellucida* extracts could be related to the presence of bioactive compounds regulating the antioxidant defense system in ARPE-19. In phase 1 study, the TPC was associated with the antioxidant activity of *P. pellucida* fractions (Table 4.9). The antioxidant activity of phenolic compounds are often related to their ability in scavenging harmful free radicals (Anggraini

et al., 2019; Cao *et al.*, 2018). Apart from their antioxidant nature, it was found that some flavonoids provide cells with antioxidant support by increasing the intracellular gene and protein expression of GPx. For instance, the flavonoid identified from *P. pellucida* in phase 3 study (Table 4.16), luteolin could up-regulate the expression of GPx to combat oxidative stress (Albarakati *et al.*, 2020). It was also suggested that treatment with luteolin alone significantly increased the activity of GPx, which is probably a direct result of PPAR- γ activation (Li *et al.*, 2022a; Owumi *et al.*, 2020). In this study, the TFC was significantly correlated with lipid peroxidation inhibitory activity of *P. pellucida*. The restoration of GPx levels by *P. pellucida* extracts further validated the plant's antioxidant role in suppressing lipid peroxidation, given the pivotal role of GPx in inhibiting this process (Ighodaro and Akinloye, 2018).

However, there are several phytochemicals that could indirectly down-regulate SOCS1 by targeting the STAT3 signalling pathway. For instance, the major sesquiterpenes like β -caryophyllene, β -elemene as well as flavonoid luteolin have been shown to inhibit STAT3 activation in previous studies (Bose *et al.*, 2020; Sun *et al.*, 2022; Wang *et al.*, 2020). Hence, this study has demonstrated that the presence of sesquiterpenes and flavonoids in *P. pellucida* down-regulated SOCS1 through STAT3 inhibition. According to Gushiken *et al.* (2022), β -caryophyllene increased the expression and activity of GPx in rat model. It was plausible that β -caryophyllene up-regulates GPx through the activation of PPAR- γ signalling pathway (Youssef *et al.*, 2019). β -elemene was also found to improve the cellular antioxidant status by enhancing the expression of GPx (Nuutinen, 2018).

The major fatty acids 9-octadecenoic acid in *P. pellucida* has been previously described to restore the expression of GPx, possibly through

PPAR- γ activation (Hosseinipour *et al.*, 2022). The unsaturated fatty acid could also inhibit STAT3 activation and decreased the negative feedback response of SOCS1 (Anjum *et al.*, 2023). This could be arised from the high binding affinity of 9-octadecenoic acid towards STAT3 protein (Anjum *et al.*, 2023). This study indicated that the presence of phytochemicals in *P. pellucida* such as luteolin, β -caryophyllene, β -elemene and 9-octadecenoic acid may improve the antioxidant parameters and cytokine signalling in ARPE-19 against high glucose and AGE-induced oxidative stress by targeting the NF- κ B p65, STAT3 and PPAR- γ signalling pathways.

5.2.5 Regulation on the expression of RAGE and sRAGE

The binding AGE to RAGE has been previously shown to trigger inflammation through the activation of NF- κ B p65 and STAT3 signalling pathways (Huang *et al.*, 2001; Safi *et al.*, 2014). On the other hand, sRAGE is the modified form of RAGE that is secreted as a competitive inhibitor to prevent the binding of ligands to RAGE due to its high affinity towards the receptor (Juraneck *et al.*, 2016). This section aimed to discuss the impact of high glucose and AGE stimulation on the gene and protein expression of RAGE and sRAGE in ARPE-19. The regulatory effect of *P. pellucida* crude methanolic extract and ethyl acetate fraction on the gene and protein expression of RAGE and sRAGE in ARPE-19 subjected to high glucose and AGE stress was also elaborated in this section.

5.2.5.1 Effect of high glucose and AGE-induced oxidative stress on RAGE and sRAGE level

Glycation is a process that can be accelerated in the presence of high glucose (Fournet *et al.*, 2018). In previous studies, high glucose is

also known to stimulate the expression of RAGE, which may trigger a cascade of reactions that cause inflammation and oxidative stress (Hu *et al.*, 2021; Yao *et al.*, 2010). According to Zong *et al.* (2010), the gene expression of RAGE reached its peak after 48 hours of exposure to high glucose stimulation. Hence, these could explain the similar gene expression of RAGE in ARPE-19 under both high glucose (34 mM, 68 mM) conditions. Conversely, the elevated RAGE protein level in the high glucose (68 mM) condition may reflect the increased production of RAGE protein through high glucose-induced post-translational modification (Khalid *et al.*, 2022). Besides, the gene and protein expression of RAGE in ARPE-19 was further increased when AGE was introduced alongside an elevated glucose concentrations. This was in accordance with a previous study, which demonstrated that the combination of AGE and high glucose could amplify the up-regulation of RAGE (Ogawa *et al.*, 2007). Previous study has suggested that the expression of RAGE depended on the activation of NF- κ B p65 (Figure 5.1), which was induced by the activation of RAGE through a signal transduction cycle (Tóbon-Velasco *et al.*, 2014). The current study suggested that the combination of AGE and high glucose could synergistically promote the increased expression of RAGE in ARPE-19 via NF- κ B p65 activation.

On the other hand, reduced sRAGE expression in high glucose and AGE-treated ARPE-19 was in accordance with a previous plan that demonstrated low circulating sRAGE in hyperglycaemic patients (Nadali *et al.*, 2021; Wang *et al.*, 2018). Besides, reduced level of sRAGE in ARPE-19 under normal glucose AGE-treated condition could be related to the AGE-induced inflammatory response (Nadali *et al.*, 2021; Zhang *et al.*, 2016c). This study suggested that the sRAGE expression was lowered in ARPE-19 stimulated by high glucose and AGE.

5.2.5.2 Effect of *P. pellucida* on RAGE and sRAGE expression in ARPE-19

The current study has found that the *P. pellucida* crude methanolic extract and ethyl acetate fraction did not alter the gene and protein expression of RAGE in ARPE-19 under normal glucose condition (Table 4.15). Interestingly, sRAGE expression increased in the normal glucose control when ARPE-19 was treated with the highest concentration of *P. pellucida* extracts. This may suggest the ability of *P. pellucida* to promote sRAGE secretion in the retina of healthy individuals. Apart from the excellent anti-glycation effect of *P. pellucida* extracts discovered in phase 1 study (Table 4.7), this finding also showed that *P. pellucida* treatment could restore the concentration of sRAGE in high glucose and AGE stimulated ARPE-19. Furthermore, as *P. pellucida* extracts treatment decreased the activation of NF- κ B p65 and STAT3, this may have led to the subsequent down-regulation of RAGE in the pathologic conditions (Tóbon-Velasco *et al.*, 2014). This study clearly showed that the crude methanolic extract and ethyl acetate fraction could disrupt the NF- κ B p65 and STAT3 signalling processes, which regulate the expression of pro-inflammatory mediators, including RAGE.

This study showed that several bioactive compounds that have been documented to inhibit RAGE expression have been identified in *P. pellucida*. These compounds could be further classified into sesquiterpenes and chlorophyll derivatives. Among the sesquiterpenes, the administration of β -caryophyllene was accompanied with reduced NF- κ B p65 dependent expression of RAGE in previous reports (Hashiesh *et al.*, 2023; Youssef *et al.*, 2019). Besides, it was also likely that the inhibition of IKK by β -

caryophyllene prevented the activation of I κ B-bound NF- κ B p65 (Gui *et al.*, 2013). As a result, this may have prevented the transcription of gene that encodes for RAGE. Interestingly, a chlorophyll derivative, pheophorbide-a methyl ester was reportedly a RAGE antagonist that inhibit the interaction between AGE and RAGE (Matsumoto *et al.*, 2021). The inhibition of RAGE could disrupt the NF- κ B p65 signalling pathway and led to decreased expression of pro-inflammatory mediators (Tóbon-Velasco *et al.*, 2014). In addition, it was previously demonstrated that the presence of unsaturated fatty acids were positively correlated with sRAGE (Deo *et al.*, 2023). As the major unsaturated fatty acid, 9-octadecenoic acid was characterised from *P. pellucida* in phase 2. Hence, it can be deduced that the presence of the fatty acid may assume a crucial role in restoring the protein concentration of sRAGE in high glucose and AGE-treated ARPE-19.

5.3 *In vitro* and *in vivo* toxicity of *P. pellucida*

5.3.1 *In vitro* cytotoxicity

Under normal physiological condition, the ARPE-19 forms a single layer of epithelium with its characteristic cobblestone morphology (Hellinen *et al.*, 2019). The MTT cell viability assay from this study showed that treatment of ARPE-19 with 4 mg/ml of crude methanolic extract and 5 mg/ml of ethyl acetate fraction led to the loss of typical cell morphology despite their high IC₅₀ values. This was largely due to the hypertonicity generated from the increased concentration of plant extracts, thereby leading to the loss of cytoplasmic matrix through osmotic movement (Argyropoulos *et al.*, 2016). Furthermore, the loss of morphology caused by the administration of crude methanolic extract (3 mg/ml) and ethyl acetate fraction (4 mg/ml) corresponded to the gradual decrease in ARPE-

19 cell viability at respective concentrations. These findings have collectively indicated that the maximum concentrations of crude methanolic extract and ethyl acetate fraction that could be sustained by ARPE-19 were limited to respective 3 mg/ml and 4 mg/ml. Hence, the dose response effect of crude methanolic extract (0.75, 1.5, 3 mg/ml) and ethyl acetate fraction (1, 2, 4 mg/ml) on high glucose and AGE-induced stress in ARPE-19 were evaluated via a two-fold serial dilution approach. This was to determine whether the ARPE-19 cell viability would display concentration-dependent response towards the serially diluted crude methanolic extract and ethyl acetate fraction under high glucose and AGE-treated conditions.

When compared to ethyl acetate plant fraction at 4 mg/ml, crude methanolic extract caused a greater reduction in ARPE-19 cell viability (Figure 4.3). On the other hand, ethyl acetate plant fraction was cytotoxic towards ARPE-19 from 7 mg/ml onwards. This could be ascribed to the higher concentration of phytochemicals present in the crude methanolic extract of *P. pellucida*, which derived the ethyl acetate fraction. According to Pappachen (2013), plant extract is considered cytotoxic at an IC_{50} of less than 100 $\mu\text{g/ml}$ *in vitro*. However, the IC_{50} threshold established by the American National Cancer Institute for any given plant extract to be considered cytotoxic was even lower at 30 $\mu\text{g/ml}$ (Canga *et al.* 2022). In this study, both crude methanolic extract and ethyl acetate fraction clearly have exceeded the IC_{50} thresholds required to be considered cytotoxic against ARPE-19. Therefore, this study suggested that *P. pellucida* crude methanolic extract and ethyl acetate fraction were non-cytotoxic towards ARPE-19.

5.3.2 *In vivo* toxicity

Based on the LC₅₀ of *in vivo* toxicity trend across the six *P. pellucida* solvent fractions, the polar aqueous fraction was found to be the only non-toxic fraction with a LC₅₀ of 5.48 ± 0.85 mg/ml (Table 4.9) against the brine shrimps. The LC₅₀ value of *P. pellucida* aqueous fraction has exceeded the minimal value of 1 mg/ml to be defined as toxic (Hamidi *et al.*, 2014). Despite that, the biological activity of aqueous fraction was less ideal and this was insufficient to justify its anti-retinopathy potential. On the other hand, the LC₅₀ value of hexane fraction was comparable to that of the positive control, potassium dichromate (0.26 mg/ml) (Table 4.8), implying the high toxic profile of the non-polar fraction. For n-butanol and chloroform fractions, they were ranked as moderately toxic fraction although they displayed high TPC (Table 4.1). Interestingly, the ethyl acetate fraction with promising functional activities and phytochemical content was considered mildly toxic together with the crude methanolic extract (Table 4.8).

The overall trend of toxicity finding for *P. pellucida* concurred with another study by Oloyede *et al.* (2011), who suggested that the hexane fraction was toxic. However, the study also indicated that the ethyl acetate fraction was toxic (Oloyede *et al.*, 2011). The discrepancy was largely due to the extraction process, from which the chloroform was omitted in the previous study (Oloyede *et al.*, 2011). This may have resulted in the extraction of toxic components into the ethyl acetate fraction. In addition, the LC₅₀ for potassium dichromate was comparable to that reported by Sahgal *et al.* (2010). The toxicity of the solvent fractions could be attributed to the presence of selected phytochemical compounds (Oloyede *et al.*, 2011). According to Asaduzzaman *et al.* (2015), the presence of alkaloids may corroborate to the toxicity of the solvent fractions. Furthermore, phenolic compounds and flavonoids were found to be mildly

toxic due to their tendency to inhibit cellular DNA (Asaduzzaman *et al.*, 2015). The mild toxicity of phenolic compounds and flavonoids could have explained the moderate inverse correlation of TPC and TFC with the LC₅₀ of plant fractions. Due to the metal chelating properties of phenolic compounds, this may lead to a modest correlation between the FRAP and LC₅₀ of plant toxicity (Table 4.9).

5.3.3 Cytoprotective effect of *P. pellucida*

Oxidative stress occurs when the production of free radicals exceed the antioxidant capacity of the cell, which leads to cell damage and apoptosis (Yamagishi *et al.*, 2012). ARPE-19 were previously reported to undergo oxidative stress when subjected to high glucose environment (Arumugam *et al.*, 2020). Subsequently, this could lead to reduced cell viability in ARPE-19 (Liang *et al.*, 2022; Wang *et al.*, 2021a). In this high glucose-stimulation study, a decrease in ARPE-19 cell viability indicated the impact of high glucose-induced stress on ARPE-19. This was in agreement with a previous study, which suggested the occurrence of hyperglycaemic-induced oxidative stress in ARPE-19 that leads to the reduction of cell viability (Arumugam *et al.*, 2020). In addition, this study also discovered a decrease in ARPE-19 cell viability under normal glucose AGE-treated condition. The decreased survival in ARPE-19 population was due to the pro-inflammatory effect of AGE that induced cellular damage in ARPE-19 (Safi *et al.*, 2014). The formation of AGE contributes to the development of oxidative stress in DR via intracellular signalling pathways (Nowotny *et al.*, 2015). The binding of AGE to its receptor, RAGE have also been demonstrated to activate STAT3, which increased intracellular ROS formation through the enzyme NADPH oxidase and lead to decreased cell

viability (Nowotny *et al.*, 2015). Besides, AGE-RAGE interaction could also activate NF- κ B p65 through ROS formation, placing the cells under oxidative stress and inflammatory states and lowering cell viability (Nowotny *et al.*, 2015). This study also showed that a combined effect of both high glucose and AGE imparted a significant decrease in ARPE-19 cell viability when compared to the stimulation of either high glucose or AGE alone. Besides, the slight reduction of ARPE-19 cell viability in 0.5 % DMSO vehicle control may be explained by the mild toxic effect of 0.5 % DMSO (Costa *et al.*, 2017).

The restoration of ARPE-19 cell viability by crude methanolic extract (1.5 mg/ml onwards) and ethyl acetate fraction (4 mg/ml) suggested that both samples displayed cytoprotective effect towards ARPE-19 under high glucose and AGE-induced stress (Figure 4.4-4.5). The cytoprotective effect of natural products on ARPE-19 against the high glucose-induced stress have been reported in previous studies (Arumugam *et al.*, 2020). This study has provided strong evidences to support the cytoprotective effect of *P. pellucida* on ARPE-19 against the high glucose and AGE-induced stress. Besides, the crude methanolic extract displayed higher ARPE-19 cytoprotective effect, when compared to the ethyl acetate fraction. This was evidenced by the use of lower concentration of crude methanolic extract to maintain the ARPE-19 cell viability, compared to the ethyl acetate fraction. Since the ethyl acetate plant fraction was derived from the crude methanolic extract of *P. pellucida*, the stronger restoration of ARPE-19 cell viability under high glucose (34 mM) and AGE-treated (17 mM) condition by crude methanolic extract treatment (Figure 4.4) could be attributed, in part, to the higher concentration of phytochemicals possessing anti-inflammatory and cytoprotective effects (Rojas-Martínez *et*

al., 2013) towards ARPE-19, such as 9-octadecenoic acid, β -caryophyllene, dillapiole, luteolin and methyl-pheophorbide a.

On the other hand, the cytoprotective effect of *P. pellucida* ethyl acetate fraction on ARPE-19 against high glucose (68 mM) and AGE induced stress was likely due to the significant antioxidant activities observed in phase 1 study (Table 4.2). For instance, the formation of lipid peroxy radicals is a major factor for the development oxidative stress (Nam, 2011). As demonstrated in phase 1 study, the antioxidant action of ethyl acetate fraction in suppressing lipid peroxidation may partly explain the ARPE-19 cytoprotective effect of the plant against the high glucose induced oxidative stress (Nam, 2011). Besides, the total AGE inhibitory activity of *P. pellucida* may have neutralised the harmful effect of AGE towards ARPE-19, thereby hindering the production of ROS (Nowotny *et al.*, 2015). The inhibition of AR by *P. pellucida* (Table 4.7) could also prevent the depletion of NADPH and subsequent oxidative stress by intercepting the polyol pathway (Yan, 2018). When coupled with the functional activities discovered in phase 1 study, the anti-glycaemic properties of *P. pellucida* further supported the cryoprotective action of crude methanolic extract and ethyl acetate fraction against high glucose induced stress in ARPE-19.

Although the ethyl acetate plant fraction and crude methanolic plant extract of *P. pellucida* were mildly toxic against the *in vivo* brine shrimp nauplii, *in vitro* cell viability assay suggested that the plant extracts were non-cytotoxic towards ARPE-19. Furthermore, *P. pellucida* crude methanolic extract displayed strong ARPE-19 cytoprotective effect under normal glucose, high glucose (34 mM) and normal glucose AGE-treated conditions within the tolerable plant extract concentration. The same applied to the ethyl acetate plant fraction under high glucose (68 mM) condition. Hence, this study implied that the crude methanolic extract and

ethyl acetate fraction of *P. pellucida* displayed cytoprotective effect on ARPE-19 against the high glucose and AGE-induced cellular damage due to oxidative stress and inflammation.

5.4 Future study

It is important to note that the interpretation of experimental result should be taken into account the limitation associated with the application of ARPE-19 cell line, which might not completely reflect the complexity and heterogeneity of primary human retinal epithelium (Oliveira *et al.*, 2021). The reliance on a cell line could potentially overlook elements and responses that are present in the primary human retinal epithelium. Future research should consider the use of primary human retinal epithelial cells to better represent the complex genotype and phenotype of the human retina. Besides, GPx is a crucial component of antioxidant defense system, particularly in neutralising hydrogen peroxides and lipid peroxides (Ighodaro and Akinloye, 2017). However, the exclusion of other antioxidant markers could result in an incomplete understanding of antioxidant response. Hence, the inclusion of other antioxidant markers could result in a more comprehensive understanding of antioxidant response in future studies. Furthermore, despite the *P. pellucida* extracts possess a distinctive chemical profile with therapeutic significance, by investigating isolated pure compounds from *P. pellucida* extracts in the future will provide insights into their individual contributions to therapeutic efficacy, thereby enhancing our understanding of their potential as therapeutic agents (Rasoanaivo *et al.*, 2011). The decision not to utilise a positive control, such as a RAGE inhibitor, in this study was due to the unclear mode of action associated with its use (Sourris *et al.*, 2021). However, its omission may have

hindered the direct comparison between the expected and observed effects in the AGE-treated ARPE-19 groups (Singh and Agrawal, 2022). Additionally, the lack of animal studies in this research has limited the interpretation of findings to *in vitro* contexts (Ho *et al.*, 2022b). Hence, future research should incorporate animal models and positive control with well-defined mechanism of action to provide a more comprehensive understanding of the observed phenomenon by validating the relevance of findings through *in vivo* investigation.

Chapter VI

Conclusion

Based on the findings of biological activities in phase 1 study, it can be concluded that the ethyl acetate plant fraction derived from the crude methanolic extract of *P. pellucida* exhibited strong antioxidant, anti-inflammatory and anti-glycation activities that were associated with its high phytochemical content. The same plant fraction also displayed stronger inhibitory activity against the glycaemic enzymes, α -amylase and α -glucosidase than the standard anti-diabetic drug, acarbose. AGI analysis also ranked ethyl acetate plant fraction as a very high anti-glycation source, which is crucial to prevent the development of DR. Despite being non-toxic, the aqueous fraction demonstrated relatively low functional activities for the management of DR. The toxic characteristics of chloroform, hexane and n-butanol plant fractions were deemed unsuitable to be applied in the DR management. Both the ethyl acetate plant fraction and crude methanolic extract of *P. pellucida* were non-cytotoxic towards ARPE-19 despite being mildly toxic against brine shrimps. Both the plant samples also displayed ARPE-19 cytoprotective effect against inflammatory stress induced by the presence of high glucose and AGE, which could be attributed to the antioxidant properties of *P. pellucida*. *In vitro* cellular mechanistic study has demonstrated the potential of crude methanolic plant extract and ethyl acetate fraction in restoring the level of intracellular antioxidant enzyme GPx and modulating the pro-inflammatory (IL-8, MCP-1, RAGE) and angiogenic (MMP2, VEGF) responses in ARPE-19 via the NF- κ B p65, STAT3 and PPAR- γ signalling pathways. The administration of *P. pellucida* extracts suppressed SOCS1 expression in ARPE-19, which acted as a negative feedback in response to STAT3 signalling. With the exception of IL-8, the exposure of ARPE-19 to ethyl acetate plant fraction and crude methanolic

extract did not influence the selected biomarkers' expression under normal glucose condition. Interestingly, the production of IL-8 in ARPE-19 was reduced by the treatment of plant extracts even under normal glucose condition, suggesting the significant role of *P. pellucida* at the early phase of inflammation. The functional activities demonstrated by *P. pellucida* extracts was mainly attributed to the presence of bioactive compounds, which regulated the biochemical elements along the three signalling pathways. The current study has identified and characterised several major bioactive compounds from *P. pellucida*, including the dillapiole, 2,4,5-trimethoxystyrene, methyl 9-octadecenoic acid and methyl pheophorbide-a. Notably, the methyl pheophorbide-a was reported in *P. pellucida* for the first time. *P. pellucida* also contained non-polar volatile compounds, such as apiole, β -caryophyllene, β -elemene, β -santalene and carotol, along with other polar compounds under the phytochemical categories of alkaloids, chlorophyll derivatives, ketones, naphthalenes, phenolic compounds and terpenes. Among these phytochemicals, β -caryophyllene primarily targeted the NF- κ B p65 and STAT3 signalling pathways by inhibiting Janus kinase, I κ B kinase, and the hexosamine pathway. Alongside 9-octadecenoic acid and luteolin, it served as a PPAR- γ agonist to mitigate the effects of NF- κ B p65. Both 9-octadecenoic acid and luteolin were recognised for their role as STAT3 antagonists while methyl pheophorbide-a is a known RAGE antagonist. Dillapiole and β -elemene have been previously described as inhibitors of NF- κ B p65. All findings generated from this study, which encompassed the toxicity assessments, significant functional activities and the modulation of plant phytochemicals on pro-inflammatory and anti-inflammatory signalling pathways in ARPE-19, could valorise *P. pellucida* as an alternative promising therapeutic source for DR.

References

- Abcouwer, S.F. and Gardner, T.W., 2014. Diabetic retinopathy: loss of neuroretinal adaptation to the diabetic metabolic environment. *Annals of the New York Academy of Sciences*, 1311(1), 174-190. <https://doi.org/10.1111/nyas.12412>.
- Abdullah, F.I., Chua, L.S., Bohari, S.P. and Sari, R., 2020. Rationale of *Orthosiphon aristatus* for healing diabetic foot ulcer. *Natural Product Communications*. 15(9). <https://doi.org/10.1177/1934578X20953308>.
- Abu, F., Taib, C.N.M.T., Moklas, M.A.M. and Akhir, S.M., 2017. Antioxidant Properties of Crude Extract, Partition Extract, and Fermented Medium of *Dendrobium sabin* Flower. *Evidence-based Complementary and Alternative Medicine*, 2017, 2907219. <https://doi.org/10.1155/2017/2907219>.
- Abu Bakar, F.I., Abu Bakar, M.F., Rahmat, A., Abdullah, N., Sabran, S.F. and Endrini, S., 2018. Anti-gout potential of Malaysian medicinal plants. *Frontiers in Pharmacology*, 9, 261. <https://doi.org/10.3389/fphar.2018.00261>.
- Adamis, A.P. and Berman, A.J., 2008. Immunological mechanisms in the pathogenesis of diabetic retinopathy. *Seminars in Immunopathology*, 30(2), 65-84. <https://doi.org/10.1007/s00281-008-0111-x>.
- Adamski, Z., Blythe, L.L., Milella, L. and Bufo, S.A., 2020. Biological activities of alkaloids: From toxicology to pharmacology. *Toxins*, 12(4),

210. [https://doi.org/ 10.3390/toxins12040210](https://doi.org/10.3390/toxins12040210).

Addotey, J.N., Lengers, I., Jose, J., Gampe, N., Beni, S., Petereit, F. and Hensel, A., 2018. Isoflavonoids with inhibiting effects on human hyaluronidase-1 and norneolignan clitorienolactone B from *Ononis spinosa* L. root extract. *Fitoterapia*, 130, 169-174. <https://doi.org/10.1016/j.fitote.2018.08.013>.

Aghajani, Z., Kazemi, M., Dakhili, M. and Rustaiyan, A., 2009. Composition and antimicrobial activity of the essential oil of *Artemisia kulbadica* from Iran. *Natural Product Communications*, 4(9), 1261-1266.

Ahmad, B., Su, P., Shah, S.R.H., Khan, S.Z., Husain, B., Wahid, F., Ullah, H., Uddin, S., Ahmad, M., Begum, N. and Khan J., 2020. Targeting cancer through NF-kb pathway with selected natural products (β -elemene, puerarin and gypenosides). *American Journal of Biomedical Science & Research*, 10(1), AJBSR.MS.ID.001472. <https://doi.org/10.34297/AJBSR.2020.10.001472>

Ahmad, I., Azminah, M.K., Yanuar, A. and Mun'im, A., 2019. Angiotensin-converting enzyme inhibitory activity of polyphenolic compounds from *Peperomia pellucida* (L.) Kunth: An *in silico* molecular docking study. *Journal of Applied Pharmaceutical Sciences*, 9(8), 25-31. <https://doi.org/10.7324/JAPS.2019.90804>.

Akhila, S., Aleykutty, N.A. and Manju P., 2012. Docking studies on *Peperomia pellucida* as antidiabetic drug. *International Journal of Pharmacy and Pharmaceutical Sciences*, 4(4), 76-77.

- Akhtar, S., Nasir, J.A., Ali, A., Asghar, M., Majeed, R. and Sarwar, A., 2022. Prevalence of type-2 diabetes and prediabetes in Malaysia: A systematic review and meta-analysis. *PLoS One*. 17(1), e0263139. <https://doi.org/10.1371/journal.pone.0263139>.
- Akomeng, N. and Adusei, S., 2021. Organic solvent extraction and spectrophotometric quantification of total phenolic content of soil. *Heliyon*, 7(11), e08388. <https://doi.org/10.1016/j.heliyon.2021.e08388>
- Alaba, C.S.M. and Chichioco-Hernandez, C.L., 2014. 15-Lipoxygenase inhibition of *Commelina benghalensis*, *Tradescantia fluminensis*, *Tradescantia zebrina*. *Asian Pacific Journal of Tropical Biomedicine*, 4(3), 184-188. [https://doi.org/10.1016/S2221-1691\(14\)60229-X](https://doi.org/10.1016/S2221-1691(14)60229-X).
- Albarakati, A.J.A., Baty, R.S., Aljouidi, A.M., Habotta, O.A., Elmahallawy, E.K., Kassab, R.B. and Abdel Moneim, A.E., 2020. Luteolin protects against lead acetate-induced nephrotoxicity through antioxidant, anti-inflammatory, anti-apoptotic, and Nrf2/HO-1 signalling pathways. *Molecular Biology Reports*, 47(4), 2591-2603. <https://doi.org/10.1007/s11033-020-05346-1>.
- Alberts, B., Johnson, A., Lewis, J., Raff, M., Roberts, K. and Walter, P., 2014. *Molecular Biology of the Cell*. 4th edition, New York: Garland Science.
- Ali, M.H.M., Draman, N., Mohamed, W.M.I.W., Yaakub, A. and Embong, Z., 2016. Predictors of proliferative diabetic retinopathy among patients with type 2 diabetes mellitus in Malaysia as detected by fundus

photography. *Journal of Taibah University Medical Sciences*, 11(4), 353-358. <https://doi.org/10.1016/j.jtumed.2016.03.002>

Al-Kharashi, A.S., 2018. Role of oxidative stress, inflammation, hypoxia and angiogenesis in the development of diabetic retinopathy. *Saudi Journal of Ophthalmology*, 32(4), 318-323. <https://doi.org/10.1016/j.sjopt.2018.05.002>.

Altameme, H., Hussein, A., Hameed, I. and Kareem, M., 2015. Determination of alkaloid compounds of *Ricinus communis* by using gas chromatography- mass spectroscopy (GC-MS). *Journal of medicinal plant research*. 9, 349-359. <https://doi.org/10.5897/JMPR2015.5750>

Alves, N.S.F., Inoue, S.G.K., Carneiro, A.R., Albino, U.B., Setzer, W.N., Maia, J.G., Andrade, E.H. and da Silva, J.K.R., 2022. Variation in *Peperomia pellucida* growth and secondary metabolism after rhizobacteria inoculation. *PLoS One*, 17(1), e0262794. <https://doi.org/10.1371/journal.pone.0262794>.

Alves, N.S.F., Setzer, W.N. and Silva, J.K.R.D., 2019. The chemistry and biological activities of *Peperomia pellucida* (Piperaceae): A critical review. *Journal of Ethnopharmacology*, 232, 90-102. <https://doi.org/10.1016/j.jep.2018.12.021>.

Amarathunga, A. A. M. D. D. N. and Kankanamge, S. U., 2017. A Review on Pharmacognostic, Phytochemical and Ethnopharmacological Findings of *Peperomia pellucida* (L.) Kunth: Pepper Elder. *International Research Journal of Pharmacy*, 8(11), 16-23. <https://doi.org/10.7897/2230->

8407.0811211.

Ambasta, R.K., Jha, S.K., Kumar, D., Sharma, R., Jha, N.K. and Kumar, P., 2015. Comparative study of anti-angiogenic activities of luteolin, lectin and lupeol biomolecules. *Journal of Translational Medicine*, 13, 307. <https://doi.org/10.1186/s12967-015-0665-z>.

American Diabetes Association 2022. Classification and diagnosis of diabetes: Standards of medical care in diabetes—2022. *Diabetes Care*, 45(1), 17-38.

Amirzadeh, M., Soltanian, S. and Mohamadi, N., 2022. Chemical composition, anticancer and antibacterial activity of *Nepeta mahanensis* essential oil. *BMC complementary medicine and therapies*, 22(1), 173. <https://doi.org/10.1186/s12906-022-03642-w>

Anagu, L.O. and Andoh, N.E., 2022. Chapter 4 - Vaccine development: From the laboratory to the field. In Ashfield,R., Oli, A.N., Esimone, C. and Anagu, L. (eds.) *Developments in Immunology*, 95-131. Academic Press. <https://doi.org/10.1016/B978-0-323-91146-7.00011-1>.

Angelini, P., Girometta, C., Tirillini, B., Moretti, S., Covino, S., Cipriani, M., D'Ellena, E., Angeles, G., Federici, E., Savino, E., Cruciani, G. and Venanzoni, R., 2019. A comparative study of the antimicrobial and antioxidant activities of *Inonotus hispidus* fruit and their mycelia extracts. *International Journal of Food Properties*, 22(1), 768–783. <https://doi.org/10.1080/10942912.2019.1609497>

- Anggraeni, N.D., Nurjanah, S. and Lembong, E., 2020. Antibacterial activity of α -guaiene Patchouli oil on *Staphylococcus aureus* and *Staphylococcus epidermidis*. *Gontor Agrotech Science Journal*, 6(3), 413–423. <https://doi.org/10.21111/agrotech.v6i3.4964>
- Anggraini, T., Wilma, S., Syukri, D. and Azima, F., 2019. Total phenolic, anthocyanin, catechins, DPPH radical scavenging activity, and toxicity of *Lepisanthes alata* (Blume) leenh. *International Journal of Food Science*, 2019, 9703176. <https://doi.org/10.1155/2019/9703176>.
- Anjum, S.M., Kumar, K.S., Umamaheswari, A., Lakhanpal, D., Swargam, S., Riazunnisa, K. and Chandrasekhar, T., 2023. Identification of a natural antagonist for signal transducer and activator of transcription 3 (STAT3) by computational approach. *Results in Chemistry*, 5, 100970. <https://doi.org/10.1016/j.rechem.2023.100970>
- Antônio M.A. and Souza Brito A.R., 1998. Oral anti-inflammatory and anti-ulcerogenic activities of a hydroalcoholic extract and partitioned fractions of *Turnera ulmifolia* (Turneraceae). *Journal of Ethnopharmacology*, 61, 215-228. [https://doi.org/10.1016/s0378-8741\(98\)00049-x](https://doi.org/10.1016/s0378-8741(98)00049-x)
- Ao, C., Higa, T., Ming, H., Ding, Y. and Tawata, S., 2010. Isolation and identification of antioxidant and hyaluronidase inhibitory compounds from *Ficus microcarpa* L. fil. bark. *Journal of Enzyme Inhibition and Medicinal Chemistry*, 25(3), 406-413. <https://doi.org/10.3109/14756360903213473>

- Apte, R.S., Chen, D.S. and Ferrara, N., 2019. VEGF in signaling and disease: Beyond discovery and development. *Cell*, 176(6), 1248-1264. <https://doi.org/10.1016/j.cell.2019.01.021>.
- Argyropoulos, C., Rondon-Berrios, H., Raj, D.S., Malhotra, D., Agaba, E.I., Rohrscheib, M., Khitan, Z., Murata, G.H., Shapiro, J.I. and Tzamaloukas, A.H., 2016. Hypertonicity: Pathophysiologic concept and experimental studies. *Cureus*. 8(5), e596. <https://doi.org/10.7759/cureus.596>
- Arrigoni-Blank, M.F., Dmitrieva, E.G., Franzotti, E.M., Antonioli, A.R., Andrade, M.R. and Marchioro, M., 2004. Anti-inflammatory and analgesic activity of *Peperomia pellucida* (L.) HBK (Piperaceae). *Journal of Ethnopharmacology*, 91(2-3), 215-218. <https://doi.org/10.1016/j.jep.2003.12.030>.
- Asadi, M., 2022. Chemical constituents of the essential oil isolated from seed of black pepper, *Piper nigrum* L., (Piperaceae). *International Journal of Plant Based Pharmaceuticals*, 2(1), 25-29.
- Asaduzzaman, M., Rana, S., Hasan, S.M.R., Hossain, M. and Das, N., 2015. Cytotoxic (brine shrimp lethality bioassay) and antioxidant investigation of *Barringtonia acutangula* (L.). *International Journal of Pharmacological Sciences and Research*, 6(8), 1179-1185.
- Baek, S.M., Yu, S.Y., Son, Y. and Hong, H.S., 2016. Substance P promotes the recovery of oxidative stress-damaged retinal pigmented epithelial cells by modulating Akt/GSK-3B signaling. *Molecular Vision*, 22(1), 1015-1023.

- Bag, G.C., Grihanjali Devi, P. and Bhaigyaba, T., 2015. Assessment of total flavonoid content and antioxidant activity of methanolic rhizome extract of three Hedychium species of Manipur valley. *International Journal of Pharmaceutical Sciences Review and Research*, 30(1), 154-159.
- Bandyopadhyay, M. and Rohrer, B., 2012. Matrix metalloproteinase activity creates pro-angiogenic environment in primary human retinal pigment epithelial cells exposed to complement. *Investigative Ophthalmology and Visual Science*, 53(4), 1953-1961. <https://doi.org/10.1167/iops.11-8638>.
- Basu, A., Das, A.S., Borah, P.K., Duary, R.K. and Mukhopadhyay, R., 2020. Biochanin A impedes STAT3 activation by upregulating p38 δ MAPK phosphorylation in IL-6-stimulated macrophages. *Inflammation Research*, 69, 1143–1156. <https://doi.org/10.1007/s00011-020-01387-1>.
- Bayma, D.C., Arruda, M.S.P., Müller, A.H., Arruda, A.C. and Canto, W.C., 2000. A dimeric ArC2 compound from *Peperomia pellucida*. *Phytochemistry*, 55(7), 779-782. [https://doi.org/10.1016/S0031-9422\(00\)00224-7](https://doi.org/10.1016/S0031-9422(00)00224-7).
- Beisswenger, P.J., Howell, S.K., Smith, K. and Szwegold, B. S., 2003. Glyceraldehyde-3-phosphate dehydrogenase activity as an independent modifier of methylglyoxal levels in diabetes. *Biochimica et Biophysica Acta - Molecular Basis of Disease*, 1637(1), 98-106. [https://doi.org/10.1016/s09254439\(02\)00219-3](https://doi.org/10.1016/s09254439(02)00219-3).
- Beltran-Benjamin, K.S., Co, E.L., Gaspi, S.A.D., Matibag, S.L.R. and Su, G.L.S., 2013. Enzyme activity and histopathology of rat liver treated with crude methanolic extract of *Peperomia pellucida* (L.) HBK. *Journal*

of *Biological Sciences*, 13, 183-195. <https://doi.org/10.3923/jbs.2013.183.195>.

Bharadwaj, U., Kasembeli, M.M., Robinson, P. and Tweardy, D.J., 2020. Targeting Janus kinases and signal transducer and activator of transcription 3 to treat inflammation, fibrosis, and cancer: Rationale, progress, and caution. *Pharmacological Reviews*, 72, 496-526. <https://doi.org/10.1124/pr.119.018440>.

Bharali, P., Sharma, C.L., Singh, B. and Sharma, M., 2017. Ethnobotanical studies of spice and condiment plants used by some communities of Assam. *International Journal of Advances in Scientific Research*, 3(1), 1. <https://doi.org/10.7439/ijasr.v3i1.3843>.

Bhat, M.P., Kumar, R.S., Chakraborty, B., Nagaraja, S.K., Gireesh Babu, K. and Nayaka, S., 2024. Eicosane: An antifungal compound derived from *Streptomyces* sp. KF15 exhibits inhibitory potential against major phytopathogenic fungi of crops. *Environmental Research*, 251(1), 118666. <https://doi.org/10.1016/j.envres.2024.118666>

Bhatwadekar, A.D. and Ghole, V.S., 2005. Rapid method for the preparation of an AGE-BSA standard calibrator using thermal glycation. *Journal of Clinical Laboratory Analysis*, 19(1), 11-15. <https://doi.org/10.1002/jcla.20048>.

Bibanco, F.M.A., Talaba, A.R.R. and Palacio, M.M.D., 2016. Brine shrimp lethality of 'Sinaw-sinaw' *Peperomia pellucida* (Linn.) extracts. *Journal of Multidisciplinary Studies*, 5(2), 127-140.

<https://doi.org/10.7828/jmnds.v5i2.1051>.

Bildziukevich, U., Wimmerová, M. and Wimmer, Z., 2023. Saponins of selected triterpenoids as potential therapeutic agents: A review. *Pharmaceuticals (Basel)*, 16(3), 386. <https://doi.org/10.3390/ph16030386>.

Birben, E., Sahiner, U.M., Sackesen, C., Erzurum, S. and Kalayci, O., 2012. Oxidative stress and antioxidant defense. *World Allergy Organization Journal*, 5(1), 9-19. <https://doi.org/10.1097/WOX.0b013e3182439613>.

Bohlooli, M., Ghaffari-Moghaddam, M., Khajeh, M., Shahraki-Fallah, G., Haghighi-Kekhaiye, B. and Sheibani, N., 2016. The role of acetoacetate in Amadori product formation of human serum albumin. *Journal of Photochemistry and Photobiology B: Biology*, 163, 345-351. <https://doi.org/10.1016/j.jphotobiol.2016.09.004>.

Bordoloi, R., Kashyap, K. and Das, A., 2017. Ethno-medicinal study on the traditional herbal knowledge of the Tiwa tribe of Morigaon district of Assam, India. *Asian Journal of Science and Technology*, 8, 5484-5489.

Bork, P.M., Schmitz, M.L., Kuhnt, M., Escher, C. and Heinrich, M., 1997. Sesquiterpene lactone containing Mexican Indian medicinal plants and pure sesquiterpene lactones as potent inhibitors of transcription factor NF- κ B. *FEBS Letters*, 402(1), 85-90. [https://doi.org/10.1016/S0014-5793\(96\)01502-5](https://doi.org/10.1016/S0014-5793(96)01502-5).

Bose, D., 2011. An ethno-medicobotanical investigation among Rava tribe of Jalpaiguri district. *NBU Journal of Plant Sciences*, 5, 61-65.

- Bose, S., Banerjee, S., Chakraborty, U., Pumarol, J., Croley, C.R. and Bishayee, A., 2020. Targeting the JAK/STAT signaling pathway using phytocompounds for cancer prevention and therapy. *Cells*, 9(6), 1451. <https://doi.org/10.3390/cells9061451>.
- Boyd, S.R., Advani, A., Altomare, F. and Stockl, F., 2013. Retinopathy. *Canadian Journal of Diabetes*, 37(1), 131-147.
- Briones, A., 2019. Evaluation of anti-angiogenic activity and teratogenicity of *Peperomia pellucida* ethanolic extracts using duck-chorioallantoic membrane assay. *International Conference on Science and Technology*.
- Brunmeir, R. and Xu, F., 2018. Functional Regulation of PPARs through Post-Translational Modifications. *International Journal of Molecular Sciences*. 19(6), 1738. <https://doi.org/10.3390/ijms19061738>.
- Buhren, B.A., Schruppf, H., Hoff, N.P., Bölke, E., Hilton, S. and Gerber, P.A., 2016. Hyaluronidase: From clinical applications to molecular and cellular mechanisms. *European Journal of Medical Research*, 21, 5. <https://doi.org/10.1186/s40001-016-0201-5>.
- Buragohain, J., 2011. Ethnomedicinal Plants Used by the ethnic Communities of Tinsukia district of Assam, India. *Recent Research in Science and Technology*, 3(9), 31-42.
- Burns, K.A. and Heuvel, J.P.V., 2007. Modulation of PPAR activity via phosphorylation. *Biochimica et Biophysica Acta*. 1771(8), 952-60. <https://doi.org/10.1016/j.bbali.2007.04.018>.

- Buse, M.G., 2006. Hexosamines, insulin resistance, and the complications of diabetes: Current status. *American Journal of Physiology - Endocrinology and Metabolism*, 290(1), e1-8.
- Butovich, I.A. and Lukyanova, S.M., 2008. Inhibition of lipoxygenases and cyclooxygenases by linoleyl hydroxamic acid: Comparative *in vitro* studies. *Journal of Lipid Research*, 49(6), 1284–1294.
- Calderon, G.D., Juarez, O.H., Hernandez, G.E., Punzo, S.M. and De la Cruz, Z.D., 2017. Oxidative stress and diabetic retinopathy: Development and treatment. *Eye*, 31(8), 1122-1130.
- Camposano J.E., Dela Torre G.L.T., Laxamana J.G. and Larcia II, L.L.H., 2016. Screening for the anti-angiogenic activity of selected Philippine medicinal plants using chorioallantoic membrane assay. *Mahidol University Journal of Pharmaceutical Sciences*, 43, 173-182.
- Canadian Diabetes Association, 2018. Etiologic Classification of Diabetes Mellitus. *Canadian Journal of Diabetes*, 42(1), 308.
- Canga, I., Vita, P., Oliveira, A.I., Castro, M.Á. and Pinho, C., 2022. *In Vitro* Cytotoxic Activity of African Plants: A Review. *Molecules*, 27(15), 4989. <https://doi.org/10.3390/molecules27154989>
- Cao, J., Chen L., Li, M., Cao, F., Zhao, L. and Su, E., 2018. Efficient extraction of proanthocyanidin from *Ginkgo biloba* leaves employing rationally designed deep eutectic solvent-water mixture and evaluation of the antioxidant activity. *Journal of Pharmaceutical and Biomedical*

Analysis, 158, 317-326.

Cavallini, M., Gazzola, R., Metalla, M. and Vaienti, L., 2013. The role of hyaluronidase in the treatment of complications from hyaluronic acid dermal fillers. *Aesthetic Surgery Journal*, 33(8), 1167-1174.

Cecilia, O.M., Alberto, C.J., Jose, N., German, C.E., Karen, L.A., Miguel, R.L., Raul, R.R. and Daniel, R.A., 2019. Oxidative Stress as the Main Target in Diabetic Retinopathy Pathophysiology. *Journal of Diabetes Research*, 2019, e1-21.

Cepas, V., Collino, M., Mayo, J.C. and Sainz, R.M., 2020. Redox signaling and advanced glycation endproducts (AGEs) in diet-related diseases. *Antioxidants (Basel)*. 9(2), 142. <https://doi.org/10.3390/antiox9020142>.

Cerretani, L. and Bendini, A., 2010. Rapid Assays to Evaluate the Antioxidant Capacity of Phenols in Virgin Olive Oil. *Olives and Olive Oil in Health and Disease Prevention*, 625-635.

Chandra, M., Prakash, O., Kumar, R., Bachheti, R.K., Bhushan, B., Kumar, M. and Pant, A.K., 2017. β -selinene-rich essential oils from the parts of *Callicarpa macrophylla* and their antioxidant and pharmacological activities. *Medicines (Basel, Switzerland)*, 4(3), 52. <https://doi.org/10.3390/medicines4030052>

Chappell, D.L., White, M. C. and Damania, B., 2021. Proteomic approaches to investigate gammaherpesvirus biology and associated tumorigenesis. *Advances in Virus Research*, 109, 201-254.

- Chaves, J.O., de Souza, M.C., da Silva, L.C., Lachos-Perez, D., Torres-Mayanga, P.C., Machado, A.P.F., Gonzalez-de-Peredo, A.V., Barbero, G.F. and Rostagno, M.A., 2020. Extraction of flavonoids from natural sources using modern techniques. *Frontiers in Chemistry*, 8, 1-25.
- Chee, C.F., Lee, H.B., Ong, H.C. and Ho, A.S.H., 2005. Photoxytotoxic pheophorbide-related compounds from *Aglaonema simplex*. *Chemistry and Biodiversity*, 2, 1648-1655.
- Chen, M., Wang, W., Ma, J., Ye, P. and Wang, K., 2016. High glucose induces mitochondrial dysfunction and apoptosis in human retinal pigment epithelium cells via promoting SOCS1 and Fas/FasL signaling. *Cytokine*, 79, 94-102. <https://doi.org/10.1016/j.cyto.2015.09.014>
- Chen, Y., Miao, Y., Huang, L., Li, J., Sun, H., Zhao, Y., Yang, J. and Zhou, W., 2014. Antioxidant activities of saponins extracted from *Radix Trichosanthis*: an *in vivo* and *in vitro* evaluation. *BMC Complementary Medicines and Therapies*, 14,86. <https://doi.org/10.1186/1472-6882-14-86>.
- Chen, Y., Zhu, Z., Chen, J., Zheng, Y., Limsila, B., Lu, M., Gao, T., Yang, Q., Fu, C. and Liao, W., 2021. Terpenoids from *Curcumae Rhizoma*: Their anticancer effects and clinical uses on combination and versus drug therapies. *Biomedicine & Pharmacotherapy*, 138,111350. <https://doi.org/10.1016/j.biopha.2021.111350>.
- Chen, Y.J., Sheu, M.L., Tsai, K.S., Yang, R.S. and Liu, S.H., 2013. Advanced glycation end products induce peroxisome proliferator-

activated receptor γ down-regulation-related inflammatory signals in human chondrocytes via toll-like receptor-4 and receptor for advanced glycation end products. *PLoS ONE*, 8(6), e66611. <https://doi.org/10.1371/journal.pone.0066611>

Chithra, M. and Geetha, S., 2016. Plant based remedies for the treatment of rheumatism among six tribal communities in Malappuram district, Kerala. *International Journal of Botanical Studies*, 1, 47-54.

Chiu, H.C., Fu, M.M., Yang, T.S., Fu, E., Chiang, C.Y., Tu, H.P., Chin, Y.T., Lin, F.G. and Shih, K.C., 2016. Effect of high glucose, *Porphyromonas gingivalis* lipopolysaccharide and advanced glycation end-products on production of interleukin-8/-8 by gingival fibroblasts. *Journal of Periodontal Research*, 52(2), 268-276. <https://doi.org/10.1111/jre.12391>

Chuah, Y.K., Basir, R., Talib, H., Tie, T.H. and Nordin, N., 2013. Receptor for advanced glycation end products and its involvement in inflammatory diseases. *International Journal of Inflammation*, 2013, e1-15.

Cidade, H.M., Nascimento, M.S., Pinto, M.M., Kijjoa, A., Silva, A.M. and Herz, W., 2001. Artelastocarpin and carpelastofuran, two new flavones, and cytotoxicities of prenyl flavonoids from *Artocarpus elasticus* against three cancer cell lines. *Planta Medica*, 67(9), 867-70. <https://doi.org/10.1055/s-2001-18845>.

Clement, Y.N., Baksh-Comeau, Y.S. and Seaforth, C.E., 2015. An

ethnobotanical survey of medicinal plants in Trinidad. *Journal of Ethnobiology and Ethnomedicine*, 11(67), e1-28.

Coney, J.M., 2019. Addressing Unmet Needs in Diabetic Retinopathy. *The American Journal of Managed Care*, 25(16), 311-316.

Cosentino-Gomes, D., Rocco-Machado, N. and Meyer-Fernandes, J.R., 2012. Cell signaling through protein kinase C oxidation and activation. *International Journal of Molecular Sciences*, 13(9), 10697-10721.

Costa, L.A., Ottoni, M.H.F., dos Santos, M.G., Meireles, A.B., de Almeida, V.G., Pereira, W.F., de Avelar-Freitas, B.A. and Brito-Melo, G.E.A., 2017. Dimethyl sulfoxide (DMSO) decreases cell proliferation and TNF- α , IFN- γ , and IL-2 Cytokines Production in Cultures of Peripheral Blood Lymphocytes. *Molecules*, 22(11), 1789.
<https://doi.org/10.3390/molecules22111789>

Coucha, M., Elshaer, S.L., Eldahshan, W.S., Mysona, B.A. and El-Remessy, A.B., 2015. Molecular mechanisms of diabetic retinopathy: Potential therapeutic targets. *Middle East African Journal of Ophthalmology*, 22(2), 165-144.

Cunningham, M.A., Edelman, J.L. and Kaushal, S., 2008. Intravitreal steroids for macular edema: the past, the present, and the future. *Survey of Ophthalmology*, 53(2), 139-49.
<https://doi.org/10.1016/j.survophthal.2007.12.005>

Curtis, T.M., Hamilton, R., Yong, P.H., McVicar, C.M., Berner, A., Pringle, R., Uchida, K., Nagai, R., Brockbank, S. and Stitt, A.W., 2011. Müller glial

dysfunction during diabetic retinopathy in rats is linked to accumulation of advanced glycation end-products and advanced lipoxidation end-products. *Diabetologia*, 54(3), 690-698.

Cutler, R.G., 2005. Oxidative stress profiling: Part I. Its potential importance in the optimization of human health. *Annals of the New York Academy of Sciences*. 1055, 93-135.

Daíd, N.N., 2019. Forensic sciences: Systematic drug identification. *Encyclopedia of Analytical Science*, 75-80.

Dahham, S.S., Tabana, Y., Asif, M., Ahmed, M., Babu, D., Hassan, L.E., Ahamed, M.B.K., Sandai, D., Barakat, K., Siraki, A. and Majid A.M.S.A., 2021. β -Caryophyllene induces apoptosis and inhibits angiogenesis in colorectal cancer models. *International Journal of Molecular Sciences*, 22(19), 10550. <https://doi.org/10.3390/ijms221910550>.

Das, P.R., Islam, M.T., Jahan, R. and Rahmatullah, M., 2013. Ethnomedicinal plants used by the Nag clan of the Rai Ghatual tribe of Moulvibazar district, Bangladesh. *Ancient Science of Life*, 32(4), 217-221.

Dash, M., Singh, S., Sahoo, B.C., Sahoo, S., Sahoo, R.K., Nayak, S. and Kar, B., 2021. Potential role of Indian long pepper (*Piper longum* L.) volatiles against free radicals and multidrug resistant isolates, *Natural Product Research*. 20, 1-5.

de Cássia, S.E.S.R., Andrade, L.N., Dos, R.B.O.R. and de Sousa, D.P., 2014.

A review on anti-inflammatory activity of phenylpropanoids found in essential oils. *Molecules*, 19(2), 1459-1480. <https://doi/10.3390/molecules19021459>

de la Monte, S.M. and Wands, J.R., 2008. Alzheimer's disease is type 3 diabetes-evidence reviewed. *Journal of Diabetes Science and Technology*, 2(6), 1101-13. <https://doi.org/10.1177/193229680800200619>

Del Corso, A., Costantino, L., Rastelli, G., Buono, F. and Mura, U., 2000. Aldose reductase does catalyse the reduction of glyceraldehyde through a stoichiometric oxidation of NADPH. *Experimental Eye Research*, 71(5), 515-521.

de Lira, P.N.B., Silva, J.K.R., Andrade, E.H.A., Sousa, P.J., Silva, N.N.S. and Maia, J.G.S., 2009. Essential oil composition of three *Peperomia* species from the Amazon, Brazil. *Natural Product Communications*, 4, 427-430.

Deliyanti, D., Suphapimol, V. and Wilkinson-Berka, J.L., 2022. Neutrophils as regulators of retinal inflammation in ocular neovascular disease. *Investigative Ophthalmology & Visual Science*, 63(7), 947 – A0416.

De Moraes, M.M., Kato, M.J., 2021. Biosynthesis of pellucidin A in *Peperomia pellucida* (L.) HBK. *Frontiers in Plant Science*, 12, 641717. <https://doi.org/10.3389/fpls.2021.641717>.

Deo, P., Dhillon, V.S., Thomas, P. and Fenech, M., 2023. Oleic acid status positively correlates with the soluble receptor for advanced glycation end-products (sRAGE) in healthy adults who are homozygous for G allele

of RAGE G82S polymorphism. *Cells*. 12(12), 1662.
<https://doi.org/10.3390/cells12121662>

Deshmane, S.L., Kremlev, S., Amini, S. and Sawaya, B.R., 2009. Monocyte chemoattractant protein-1 (MCP-1): An overview. *Journal of Interferon & Cytokine Research*, 29(6), 313-326.
<https://doi.org/10.1089/jir.2008.0027>

Di Sotto, A., Gullì, M., Minacori, M., Mancinelli, R., Garzoli, S., Percaccio, E., Incocciati, A., Romaniello, D., Mazzanti, G., Eufemi, M. and Di Giacomo, S., 2022. β -caryophyllene counteracts chemoresistance induced by cigarette smoke in triple-negative breast cancer MDA-MB-468 cells. *Biomedicines*, 10(9), 2257.
<https://doi.org/10.3390/biomedicines10092257>

Dias, M.M.G., Batista, F.A.H., Tittanegro, T.H., de Oliveira, A.G., Le Maire, A., Torres, F.R., Filho, H.V.R., Silveira, L.R. and Figueira, A.C.M., 2020. PPAR γ S273 phosphorylation modifies the dynamics of coregulator proteins recruitment. *Frontiers in Endocrinology*. 11:561256. doi: 10.3389/fendo.2020.561256

Di Sotto, A., Mancinelli, R., Gullì, M., Eufemi, M., Mammola, C.L., Mazzanti, G. and Di Giacomo, S., 2020. Chemopreventive potential of caryophyllane sesquiterpenes: An overview of preliminary evidence. *Cancers (Basel)*, 12(10), 3034.
<https://doi.org/10.3390/cancers12103034>.

Do, Q. D., Angkawijaya, A. R., Tran-Nguyen, P. L., Huynh, L. H.,

Soetaredjo, F. E., Ismadji, S. and Ju, Y.J., 2014. Effect of extraction solvent on total phenol content, total flavonoid content, and antioxidant activity of *Limnophila aromatica*. *Journal of Food and Drug Analysis*, 22(3), 296-302.

Dom, N.S., Yahaya, N., Adam, Z., Nik Abdul Rahman, N.M.A. and Hamid, M., 2020. Antiglycation and antioxidant properties of *Ficus deltoidea* varieties. *Evidence-Based Complementary and Alternative Medicine*. 2020, 6374632. <https://doi.org/10.1155/2020/6374632>.

Dračínský, M., 2017. Chapter 1 - The chemical bond: The perspective of NMR spectroscopy. In *Annual Reports on NMR Spectroscopy*, 1-40. Academic Press. <https://doi.org/10.1016/bs.arnmr.2016.07.001>.

Duh, E.J., Sun, J.K. and Stitt, A.W., 2017. Diabetic retinopathy: current understanding, mechanisms, and treatment strategies. *JCI insight*. 2(14), e1-13.

Dunn, K.C., Aotaki-Keen, A.E., Putkey, F.R. and Hjelmeland, L.M., 1996. ARPE-19, a human retinal pigment epithelial cell line with differentiated properties. *Experimental Eye Research*, 62(2), 155-169. <https://doi.org/10.1006/exer.1996.0020>

Ebay, 2024. [idHerb] Powder suruhan *Peperomia pellucida* natural herbal organic fresh. Available at: <https://www.ebay.com/itm/387023799994> (Accessed: 10 September 2024).

Eddouks, M., Chattopadhyay, D., Feo, V.D. and Cho, W.C.S., 2014. Medicinal Plants in the Prevention and Treatment of Chronic Diseases. 2013 *Evidence Based Complement Alternative Medicine*, 2014: 180981.

<https://doi.org/10.1155/2014/180981>

Egwuche, R.U., Odetola, A.A. and Erukainure, O.L., 2011. Preliminary investigation into the chemical properties of *Peperomia pellucida* L. *Research Journal of Phytochemistry*, 5, 48-53.

Ekun, O.A., Oyekunle, A.O. and Igbadumhe, C.O., 2021. Evaluation of peroxisome proliferator-activated receptor-gamma (Ppar- γ) and metabolic dysfunction among hypertensive nigerians. *Endocrine and Metabolic Science*, 5(1), 100108. <https://doi.org/10.1016/j.endmts.2021.100108>

El Hachlafi, N., Benkhaira, N., Mssillou, I., Touhtouh, J., Tarik, A., Chamkhi, I., El Omari, N., Khalid, A., Abdalla, A., Aboulagras, S., Kadri, K., Abdallah, A., Lee, L., Bakrim, S. and Bouyahya, A., 2024. Natural sources and pharmacological properties of santalenes and santalols. *Industrial Crops and Products*. 214. 118567. <https://doi.org/10.1016/j.indcrop.2024.118567>.

El-Shamy, I.E., Hleli, E., El-Hashash, M.A., Kelnar, I. and Abdel-Mohsen, A.M., 2023. 2-Methyl-6-(4-aminophenyl)-4,5-dihydro-3(2H)-pyridazinone synthon for some new annelated 1,2,3-selena/thiadiazoles and 2H-diazaphospholes with anticipated biological activity and quantum chemical calculations. *Molecules*, 28(3), 1280. <https://doi.org/10.3390/molecules28031280>

Fachriyah, E., Ghifari, M.A. and Anam, K., 2018. Isolation, identification, and xanthine oxidase inhibition activity of alkaloid compound from *Peperomia pellucida*. *IOP Conference Series: Materials Science and*

Engineering, 349, e1-7.

Fang, M., Mei, X., Yao, H., Zhang, T., Lu, N., Liu, Y., Xu, W. and Wan, C., 2018. β -elemene enhances anticancer and anti-metastatic effects of osteosarcoma of ligustrazine *in vitro* and *in vivo*. *Oncology Letters*, 15(3), 3957-3964. <https://doi.org/10.3892/ol.2018.7788>

Fan, S., Chang, J., Zong, Y., Hu, G. and Jia, J., 2018. GC-MS analysis of the composition of the essential oil from *Dendranthema indicum* Var. *Aromaticum* using three extraction methods and two columns. *Molecules*, 23(3), 576.

Fan, W., 2017. Epidemiology in diabetes mellitus and cardiovascular disease. *Cardiovascular Endocrinology and Metabolism*, 6(1), 8-16.

Fan, Y., Mao, R. and Yang, J., 2013. NF- κ B and STAT3 signaling pathways collaboratively link inflammation to cancer. *Protein & Cell*, 4(3), 176-185. <https://doi.org/10.1007/s13238-013-2084-3>

Farmer, S. and Reusch, W., 2023. Natural occurrence of aldehydes and ketones. Available at: [https://chem.libretexts.org/Bookshelves/Organic_Chemistry/Supplemental_Modules_\(Organic_Chemistry\)/Aldehydes_and_Ketones/Properties_of_Aldehydes_and_Ketones/Natural_Occurrence_of_Aldehydes_and_Ketones](https://chem.libretexts.org/Bookshelves/Organic_Chemistry/Supplemental_Modules_(Organic_Chemistry)/Aldehydes_and_Ketones/Properties_of_Aldehydes_and_Ketones/Natural_Occurrence_of_Aldehydes_and_Ketones) (Accessed: 10 April 2023).

Farouil, L., Sylvestre, M., Fournet, A. and Cebrian-Torrejon, G., 2022. Review on canthin-6-one alkaloids: Distribution, chemical aspects and biological activities. *European Journal of Medicinal Chemistry Reports*,

100049. <https://doi.org/10.1016/j.ejmcr.2022.100049>

Fasola, T.R. and Adeboye JO., 2015. Anti-hypertensive potentials of *Peperomia pellucida* (L.) HBK in anaesthetized normotensive rats. *Advances in Life Science and Technology*, 29(2015), 1-4.

Fatope, M.O., Marwah, R.G., Onifade, A.K., Ochei, J.E. and Al Mahroqi, Y.K.S., 2006. ¹³C NMR analysis and antifungal and insecticidal activities of Oman dill herb oil. *Pharmaceutical Biology*, 44(1), 44-49.

Felix-Silva, J., Silva-Junior, A.A., Zucolotto, S.M. and Fernandes-Pedrosa, M.D.F., 2017. Medicinal Plants for the Treatment of Local Tissue Damage Induced by Snake Venoms: An Overview from Traditional Use to Pharmacological Evidence. *Evidence Based Complementary Alternative Medicine*, 2017, e1-52

Feoli, A.M.P., Macagnan, F.E., Piovesan, C.H., Bodanese, L.C. and Siqueira, I.R., 2014. Xanthine Oxidase activity is associated with risk factors for cardiovascular disease and inflammatory and oxidative status markers in metabolic syndrome: Effects of a single exercise session. *Oxidative Medicine and Cellular Longevity*, 2014, e1-8.

Ferreira, M.U., 2022. Alkaloids in future drug discovery. *Molecules*. 27(4), 1347. <https://doi.org/10.3390/molecules27041347>.

Fidy, K., Fiedorowicz, A., Strzdała, L. and Szumny, A., 2016. β -caryophyllene and β -caryophyllene oxide-natural compounds of anticancer and analgesic properties. *Cancer Medicine*, 5(10), 3007-3017.

<https://doi.org/10.1002/cam4.816>.

Floch, J.P.L., Doucet, J., Bauduceau, B. and Verny, C., 2013. Retinopathy, nephropathy, peripheral neuropathy and geriatric scale scores in elderly people with Type 2 diabetes. *Diabetic Medicine*, 31(1), 107-111.

Flora of North America, 2020. Piperaceae. Peperomia. Flora of North America, Vol 3., Available at: http://www.efloras.org/florataxon.aspx?flora_id=1andtaxon_id=200005545 Accessed:28 May 2020.

Fong, D.S., Strauber, S.F., Aiello, L.P., Beck, R.W., Callanan, D.G., Danis, R.P., Davis, M.D., Feman, S.S., Ferris, F., Friedman, S.M., Garcia, C.A., Glassman, A.R., Han, D.P., Le, D., Kollman, C., Lauer, A.K., Recchia F.M. and Solomon, S.D., 2007. Comparison of the modified Early Treatment Diabetic Retinopathy Study and mild macular grid laser photocoagulation strategies for diabetic macular edema. *Archives of Ophthalmology*, 125(4), 469-80. <https://doi.org/10.1001/archopht.125.4.469>

Fournet, M., Bonté, F. and Desmoulière, A., 2018. Glycation damage: A possible hub for major pathophysiological disorders and aging. *Aging and Disease*, 9(5), 880-900.

François, T., Lambert, S.M., Henri, A.Z.P. and Chantal, M., 2013. Composition and antifungal properties of essential oils from five plants growing in the mountainous area of the West Cameroon. *Journal of Essent Oil-Bearing Plants*, 16, 679-688.

- Frkic, R.L., Richter, K. and Bruning, J.B., 2021. The therapeutic potential of inhibiting PPAR γ phosphorylation to treat type 2 diabetes. *The Journal of Biological Chemistry*, 297(3), 101030. <https://doi.org/10.1016/j.jbc.2021.101030>.
- Fu, X., Gens, J.S., Glazier, J.A., Burns, S.A. and Gast, T.J., 2016. Progression of Diabetic Capillary Occlusion: A Model. *PLoS Computational Biology*, 12(6), e1-46.
- Gacche, R., Shaikh, R., Pund, M. and Deshmukh, R., 2011. Cyclooxygenase inhibitory, cytotoxicity and free radical scavenging activities of selected medicinal plants used in indian traditional medicine. *Pharmacognosy Journal*, 3(19), 57-64.
- Gao, H.L., Yu, X.J., Feng, Y.Q., Yang, Y., Hu, H.B., Zhao, Y.Y., Zhang, J.H., Liu, K.L., Zhang, Y., Fu, L.Y., Li, Y., Qi, J., Qiao, J.A. and Kang, Y.M., 2023. Luteolin attenuates hypertension via inhibiting NF- κ B-mediated inflammation and PI3K/Akt signaling pathway in the hypothalamic paraventricular nucleus. *Nutrients*, 15(3), 502. <https://doi.org/10.3390/nu15030502>.
- Gerhäuser, C., Klimo, K., Heiss, E., Neumann, I., Gamal-Eldeen, A., Knauff, J., Liu, G.Y., Sitthimonchai, S. and Frank, N., 2003. Mechanism-based *in vitro* screening of potential cancer chemopreventive agents. *Mutation Research - Fundamental and Molecular Mechanisms of Mutagenesis*, 523-524, 163-172.
- Ghasemi, M., Turnbull, T., Sebastian, S. and Kempson, I., 2021. The MTT assay: Utility, limitations, pitfalls, and interpretation in bulk and single-

cell analysis. *International Journal of Molecular Sciences*, 22(23), 12827.
[https://doi.org/ 10.3390/ijms222312827](https://doi.org/10.3390/ijms222312827)

Gillings, N., 2021. Quality control of radiopharmaceuticals: Basics and instrumentation. *Reference Module in Biomedical Sciences*.

Gkogkolou, P. and Böhm, M., 2012. Advanced glycation end products: Keyplayers in skin aging? *Dermato-Endocrinology*, 4(3), 259-270.

Gogoi, B. and Zaman, K., 2011. Phytochemical Constituents of Some Medicinal Plant Species Used in Recipe During " Bohag Bihu " in Assam. *Journal of Pharmacognosy and Phytochemistry*, 2(2), 30-40.

Goldberg, I. and Rokem, J.S., 2009. Organic and fatty acid production, microbial. *Microbiology (Third Edition)*, 421-442.
<https://doi.org/10.1016/B978-012373944-5.00156-5>

Goldhaber-Fiebert, J.D., Li, H., Ratanawijitrasin, S., Vidyasagar, S., Wang, X.Y., Aljunid, S., Shah, N., Wang, Z., Hirunrassamee, S., Bairy, K.L., Wang, J., Saperi, S., Nur, A.M. and Eggleston, K., 2010. Inpatient treatment of diabetic patients in Asia: evidence from India, China, Thailand and Malaysia. *Diabetic Medicine*, 27, 101-108.

Gong, J.E., Kim, J.E., Lee, S.J., Choi, Y.J., Jin, Y.J., Choi, Y.W., Choi, S.I. and Hwang, D.Y., 2022. Anti-cancer effects of α -cubebenoate derived from *Schisandra chinensis* in CT26 colon cancer cells. *Molecules*, 27(3), 737. <https://doi.org/10.3390/molecules27030737>

- Guerin-Dubourg, A., Cournot, M., Planesse, C., Debussche, X., Meilhac, O., Rondeau, P. and Bourdon, E., 2017. Association between Fluorescent Advanced Glycation End-Products and Vascular Complications in Type 2 Diabetic Patients. *BioMed Research International*, 2017, e1-10.
- Gui, F., You, Z., Fu, S., Wu, H. and Zhang, Y., 2020. Endothelial dysfunction in diabetic retinopathy. *Frontiers in Endocrinology (Lausanne)*. 11, 591. <https://doi.org/10.3389/fendo.2020.00591>.
- Gui, H., Sun, Y., Luo, Z.M., Su, D.F., Dai, S.M. and Liu, X. 2013. Cannabinoid receptor 2 protects against acute experimental sepsis in mice. *Mediators of Inflammation*, 2013, 741303. <https://doi.org/10.1155/2013/741303>
- Gullì, M., Percaccio, E., Di Giacomo, S. and Di Sotto, A., 2022. Novel insights into the immunomodulatory effects of caryophyllane sesquiterpenes: A systematic review of preclinical studies. *Applied Sciences*. 12(5), 2292. <https://doi.org/10.3390/app12052292>.
- Gushiken, L.F.S., Beserra, F.P., Hussni, M.F., Gonzaga, M.T., Ribeiro, V.P., de Souza, P.F., Campos, J.C.L., Massaro, T.N.C., Hussni, C.A., Takahira, R.K., Marcato, P.D., Bastos, J.K. and Pellizzon, C.H., 2022. Beta-caryophyllene as an antioxidant, anti-inflammatory and re-epithelialization activities in a rat skin wound excision model. *Oxidative Medicine and Cellular Longevity*, 2022, 9004014. <https://doi.org/10.1155/2022/9004014>.
- Hajimehdipoor, H., Shahrestani, R. and Shekarchi, M., 2014. Investigating

the synergistic antioxidant effects of some flavonoid and phenolic compounds. *Research Journal of Pharmacognosy*, 1(3), 35–40.

Hamdan, S., Daood, H.G., Toth-Markus, M. and Illes, V., 2008. Extraction of cardamom oil by supercritical carbon dioxide and sub-critical propane. *Journal of Supercritical Fluids*, 44(1), 25-30.

Hamidi, M. R., Jovanova, B., Panovska, T.K., 2014. Toxicological evaluation of the plant products using Brine Shrimp (*Artemia salina* L.) model. *Macedonian Pharmaceutical Bulletin*, 60(1), 9-18.

Hamzah, R.U., Odetola, A.A., Erukainure, O.L. and Oyagbemi, A.A., 2012. *Peperomia pellucida* in diets modulates hyperglycemia, oxidative stress and dyslipidemia in diabetic rats. *Journal of Acute Disease*, 1, 135-140.

Hanna, V.S. and Hafez, E.A.A., 2018. Synopsis of arachidonic acid metabolism: A review. *Journal of Advanced Research*, 11, 23-32.

Harries, L.W., 2019. RNA biology provides new therapeutic targets for human disease. *Frontiers in Genetics*, 10, 205. <https://doi.org/10.3389/fgene.2019.00205>

Hartati, S., Angelina, M., Dewiyanti, I. and Meilawati, L., 2015. Isolation and characterization compounds from hexane and ethyl acetate fractions of *Peperomia pellucida* L. *Journal of Tropical Life Sciences*, 5, 117-122.

Hartsel, J. A., Eades, J., Hickory, B. and Makriyannis, A., 2016. Cannabis sativa and Hemp in Nutraceuticals: Efficacy, Safety and Toxicity. Academic Press. 735-754. doi: 10.1016/B978-0-12-802147-7.00053-X.

- Hashiesh, H.M., Meeran, M.F.N., Azimullah, S.S.A., Adeghate, E., Saraswathiamma, D., Almarzooqi, S. and Ojha, S.K., 2023. β -caryophyllene, a CB2 receptor agonist alleviates diabetic cardiomyopathy via inhibiting AGE/RAGE-induced oxidative stress, fibrosis, and inflammasome activation. *Journal of Pharmacology and Experimental Therapeutics*, 385(3), 303.
<https://doi.org/10.1124/jpet.122.146170>
- Hashiesh, H.M., Meeran, M.F.N., Sharma, C., Sadek, B., Kaabi, J.A. and Ojha, S.K., 2020. Therapeutic potential of β -caryophyllene: A dietary cannabinoid in diabetes and associated complications. *Nutrients*. 12(10), 2963. <https://doi.org/10.3390/nu12102963>
- Hazzaa, H.H., El Shiekh, M.A.M., Abdelgawad, N., Gouda, O.M. and Kamal, N.M., 2020. Correlation of VEGF and MMP-2 levels in oral lichen planus: An *in vivo* immunohistochemical study. *Journal of Oral Biology and Craniofacial Research*, 10(4), 747-752.
<https://doi.org/10.1016/j.jobcr.2020.10.009>
- He, H., Kuriyan, A.E., Su, C., Mahabole, M., Zhang, Y., Zhu, Y., Flynn, H.W., Parel, J.M. and Tseng, S.C.G., 2017. Inhibition of proliferation and epithelial mesenchymal transition in retinal pigment epithelial cells by heavy chain-hyaluronan/pentraxin 3. *Scientific Reports*, 7, e1-15.
- Hellinen, L., Hagström, M., Knuutila, H., Ruponen, M., Urtti, A. and Reinisalo, M., 2019. Characterization of artificially re-pigmented ARPE-19 retinal pigment epithelial cell model. *Scientific Reports*, 9(1), 13761.
<https://doi.org/10.1038/s41598-019-50324-8>
- Helmenstine, A.M., 2019. Boiling points of ethanol, methanol and isopropyl

alcohol. Available at: <https://www.thoughtco.com/boiling-point-of-alcohol-608491> (Accessed: 10 April 2022).

Heming, M., Gran, S., Jauch, S.L., Fischer-Riepe, L., Russo, A., Klotz, L., Hermann, S., Schafers, M., Roth, J. and Barczyk-Kahlert, K., 2018. Peroxisome proliferator-activated receptor- γ modulates the response of macrophages to lipopolysaccharide and glucocorticoids. *Frontiers in Immunology*, 9, 893. <https://doi.org/10.3389/fimmu.2018.00893>

Hernández, C., Segura, R.M., Fonollosa, A., Carrasco, E., Francisco, G. and Simó, R., 2005. Interleukin-8, monocyte chemoattractant protein-1 and IL-10 in the vitreous fluid of patients with proliferative diabetic retinopathy. *Diabetic Medicine*, 22(6), 719-722. <https://doi.org/10.1111/j.1464-5491.2005.01538.x>

Hernandez-Quiles, M., Broekema, M.F. and Kalkhoven, E., 2021. PPAR γ in metabolism, immunity, and cancer: Unified and diverse mechanisms of action. *Frontier in Endocrinology*, 12, 624112. <https://doi.org/10.3389/fendo.2021.624112>

Ho, K.L., Tan, C.G., Yong, P.H., Wang, C.W., Lim, S.H., Kuppusamy, U.R., Ngo, C.T., Massawe, F. and Ng, Z.X., 2022a. Extraction of phytochemicals with health benefit from *Peperomia pellucida* (L.) Kunth through liquid-liquid partitioning. *Journal of Applied Research on Medicinal and Aromatic Plants*, 30(2), 100392. doi: 10.1016/j.jarmap.2022.100392

Ho, K.L., Yong, P.H., Wang, C.W., Kuppusamy, U.R., Ngo, C.T., Massawe, F. and Ng, Z.X., 2022b. *Peperomia pellucida* (L.) Kunth and eye diseases:

A review on phytochemistry, pharmacology and toxicology. *Journal of Integrative Medicine*, 20(4), 292-304.

Hosseini-pour, M., Asgari, R., Kermani, J., Goodarzi, N. and Bakhtiari, M., 2022. The antioxidant effects of hydroalcoholic extract of Ashrasi date palm on sperm parameters and DNA fragmentation in diabetic rats. *Animal Models and Experimental Medicine*. 5, 281–287. <https://doi.org/10.1002/ame2.12222>.

Hou, T., Netala, V.R., Zhang, H., Xing, Y., Li, H. and Zhang, Z., 2022. *Perilla frutescens*: A rich source of pharmacological active compounds. *Molecules*. 27(11), 3578. <https://doi.org/10.3390/molecules27113578>.

Hsu, P.C., Chen, Y.H., Cheng, C.F., Kuo, C.Y. and Sytwu, H.K., 2021. Interleukin-6 and interleukin-8 regulate STAT3 activation migration/invasion and EMT in chrysophanol-treated oral cancer cell lines. *Life (Basel)*. 11(5), 423. <https://doi.org/10.3390/life11050423>.

Htun, M., Aung, M. T., Than, N. N. and Ngwe, D. H., 2018. Investigation of some bioactivities of *Peperomia pellucida* L. (Thit-Yay-Gyi) and *Enhydra fluctuans* L. (Kana-Phaw). *Journal of the Myanmar Academy of Arts and Science*, 16(1b), 193-208.

Hu, Z., Fang, W., Liu, Y., Liang, H., Chen, W. and Wang, H., 2021. Acute glucose fluctuation promotes RAGE expression via reactive oxygen species-mediated NF- κ B activation in rat podocytes. *Molecular Medicine Reports*, 23(5), 330. <https://doi.org/10.3892/mmr.2021.11969>

Huang, J.S., Guh, J.Y., Chen, H.C., Hung, W.C., Lai, Y.H. and Chuang, L.Y., 2001. Role of receptor for advanced glycation end-product (RAGE) and the JAK/STAT-signaling pathway in AGE-induced collagen production in

NRK-49F cells. *Journal of Cellular Biochemistry*. 81(1), 102-13.
[https://doi.org/10.1002/1097-4644\(20010401\)81:1<102::aid-jcb1027>3.0.co;2-y](https://doi.org/10.1002/1097-4644(20010401)81:1<102::aid-jcb1027>3.0.co;2-y).

Huang, W.C., Liou, C.J., Shen, S.C., Hu, S., Hsiao, C.Y. and Wu, S.J., 2020. Luteolin attenuates IL-1 β -induced THP-1 adhesion to ARPE-19 cells via suppression of NF- κ B and MAPK pathways. *Mediators of Inflammation*, 2020, 9421340. <https://doi.org/10.1155/2020/9421340>.

Hung, W.C., Ling, X.H., Chang, C.C., Hsu, H.F., Wang, S.W., Lee, Y.C., Luo, C., Lee, Y. T., Hounq, J.Y., 2017. Inhibitory effects of siegesbeckia orientalis extracts on advanced glycation end product formation and key enzymes related to metabolic syndrome. *Molecules*. 22(10), 1785.

Hussain, A. and AlJabr, A.M., 2020. Potential synergy between spores of *Metarhizium anisopliae* and plant secondary metabolite, 1-Chlorooctadecane for effective natural acaricide development. *Molecules (Basel, Switzerland)*, 25(8), 1900.
<https://doi.org/10.3390/molecules25081900>

Hwang, S. H., Kim, H. Y., Quispe, Y. N. G., Wang, Z., Zuo, G. and Lim, S. S., 2019. Aldose reductase, protein glycation inhibitory and antioxidant of peruvian medicinal plants: The case of tanacetum parthenium L: The its constituents. *Molecules*, 24(10), 2010.

Ibe-Diala, J.C., Igwe, O.U., Friday, C. and Akwada, U.C., 2021. Isolation and NMR characterization of ursane-type triterpenoid from the leaves of *Peperomia pellucida*. *Journal of Applied Sciences and Environmental Management*. 25(3), 397-400.

- Ibrahim, F. and Hamzah, N., 1999. The Use of Medicinal Plant Species by the Temuan Tribe of Ayer Hitam Forest, Selangor, Peninsular Malaysia. *Pertanika Journal of Tropical Agricultural Science*, 22(2), 85-94.
- Ibrahim, S.R.M., Mohamed, G.A., Alshali, K.Z., Al-Haidari, R.A., El-Kholy, A.A. and Zayed, M.F., 2018. Lipxygenase inhibitors flavonoids from *Cyperus rotundus* aerial parts. *Revista Brasileira de Farmacognosia*, 28(3), 320-324.
- Ighodaro, O.M. and Akinloye, O.A., 2018. First line defence antioxidants-superoxide dismutase (SOD), catalase (CAT) and glutathione peroxidase (GPX): Their fundamental role in the entire antioxidant defence grid. *Alexandria Journal of Medicine*, 54(4), 287-293.
- Igwe, O.U. and Mgbemena, N.M., 2014. Chemical investigation and antibacterial activity of the leaves of *Peperomia pellucida* L. HBK (Piperaceae). *Asian Journal of Chemical and Pharmaceutical Research*. 2(1), 78-86.
- Ikeguchi, S., Izumi, Y., Kitamura, N., Kishino, S., Ogawa, J., Akaike, A. and Kume, T., 2018. Inhibitory effect of the gut microbial linoleic acid metabolites, 10-oxo-trans-11-octadecenoic acid and 10-hydroxy-cis-12-octadecenoic acid, on BV-2 microglial cell activation. *Journal of Pharmacological Sciences*, 138(1), 9-15.
<https://doi.org/10.1016/j.jphs.2018.06.015>
- Ilyasov, I.R., Beloborodov, V.L., Selivanova, I.A. and Terekhov, R.P., 2020. ABTS/PP Decolorization Assay of Antioxidant Capacity Reaction

Pathways. *International Journal of Molecular Sciences*, 21(3), 1131.

Ina, A., Hayashi, K.I., Nozaki, H. and Kamei, Y., 2007. Pheophytin a, a low molecular weight compound found in the marine brown alga *Sargassum fulvellum*, promotes the differentiation of PC12 cells. *International Journal of Developmental Neuroscience*, 25, 63-68.

International Diabetes Federation, 2022. Diabetes facts & figures: Results from the *International Diabetes Federation Diabetes Atlas 2022 Reports*, 10th edition.

Iqbal, N., Pant, M., Dubey, S., Patanjali, N. and Kambo, N., 2020. Utilization of biodiesel waste in the development of botanical-based floating tablet formulation against early stages of mosquitoes. *Waste Disposal and Sustainable Energy*, 2, 209-218.

Ismail, H., Mofarrahi, M., Echavarria, R., Harel, S., Verdin, E., Lim, H.W., Jin, Z.G., Sun, J., Zeng, H. and Hussain, S.N.A., 2012. Angiotensin-1 and vascular endothelial growth factor regulation of leukocyte adhesion to endothelial cells. *Arteriosclerosis, Thrombosis, and Vascular Biology*, 32(7), 1707-1716. <https://doi.org/10.1161/ATVBAHA.112.251546>

Ismail, N.I.M., Chua, L.S., 2021. Solvent partition for terpenoid rich fraction from crude extract of *Eurycoma longifolia*. *Advances in Engineering Research*, 200, 62-67. <https://doi.org/10.2991/aer.k.201229.009>.

Jadhav, A.P., Kareparamban, J.A., Nikam, P.H., Kadam, V.J., 2012.

Spectrophotometric estimation of ferulic acid from *Ferula asafoetida* by Folin - Ciocalteu's reagent. *Der Pharmacia Sinica*, 3(6), 680-684.

Jain, B.P., Goswami, S.K. and Pandey, S., 2021. Chapter 4 - Protein. In Jain, B.P., Goswami, S.K. and Pandey, S. (eds.) *Protocols in Biochemistry and Clinical Biochemistry*. 31-48. Academic Press. doi: 10.1016/B978-0-12-822007-8.00008-8

Jegal, J., Kim, T.Y., Park, N.J., Jo, B.G., Jo, G.A., Choi, H.S., Kim, S.N. and Yang, M.H., 2021. Inhibitory Effects of Luteolin 7-Methyl Ether Isolated from *Wikstroemia ganpi* on Tnf- α /Ifn- γ Mixture-Induced Inflammation in Human Keratinocyte. *Nutrients*. 13(12), 4387. <https://doi.org/10.3390/nu13124387>.

Jensen, L.J.N., Flyvbjerg, A. and Bjerre, M., 2015. Soluble Receptor for Advanced Glycation End Product: A Biomarker for Acute Coronary Syndrome. *BioMed Research International*. 2015, e1-7.

Jiang, C., Liu, S., Cao, Y. and Shan, H., 2018. High glucose induces autophagy through PPAR γ -dependent pathway in human nucleus pulposus cells. *PPAR Research*. 2018, 8512745. <https://doi.org/10.1155/2018/8512745>

Jing, L., Ma, H., Fan, P., Gao, R. and Jia, Z., 2015. Antioxidant potential, total phenolic and total flavonoid contents of *Rhododendron anthopogonoides* and its protective effect on hypoxia-induced injury in PC12 cells. *BMC Complementary and Alternative Medicine*, 15(287), e1-12.

- Jo, S.M., Zhang, K.A.I., Wurm, F.R. and Landfester, K., 2020. Mimic of the cellular antioxidant defense system for a sustainable regeneration of nicotinamide adenine dinucleotide (NAD). *ACS Applied Materials & Interfaces*, 12(23), 25625-25632. <https://doi.org/10.1021/acscami.0c05588>
- Johnson, K.E. and Wilgus, T.A., 2014. Vascular endothelial growth factor and angiogenesis in the regulation of cutaneous wound repair. *Advances in Wound Care (New Rochelle)*. 3(10), 647-661. <https://doi.org/10.1089/wound.2013.0517>.
- Johnston, P.A., Sen, M., Hua, Y., Camarco, D., Shun, T.Y., Lazo, J.S. and Grandis, J.R., 2014. High-content pSTAT3/1 imaging assays to screen for selective inhibitors of STAT3 pathway activation in head and neck cancer cell lines. *Assay and Drug Development Technologies*. 12(1),55-79. <https://doi.org/10.1089/adt.2013.524>
- Jousen, A. M., Poulaki, V., Le, M.L., Koizumi, K., Esser, C., Janicki, H., Schraermeyer, U., Kociok, N., Fauser, S., Kirchhof, B., Kern, T.S. and Adamis, A.P., 2004. A central role for inflammation in the pathogenesis of diabetic retinopathy. *The FASEB Journal*, 18(12), 1450-1452.
- Ju, Z., Su, M., Hong, J., Kim, E. and Jung, J.H., 2020. Anti-inflammatory effects of an optimized PPAR- γ agonist via NF- κ B pathway inhibition. *Bioorganic Chemistry*, 96, 103611. <https://doi.org/10.1016/j.bioorg.2020.103611>
- Juel, H.B., Faber, C., Udsen, M.S., Folkersen, L. and Nissen, M.H., 2012.

Chemokine expression in retinal pigment epithelial ARPE-19 cells in response to coculture with activated T cells. *Investigative Ophthalmology & Visual Science*, 53(13), 8472-80. <https://doi.org/10.1167/iovs.12-9963>

Juraneck, J.K., Daffu, G.K., Geddis, M.S., Li, H., Rosario, R., Kaplan, B.J., Kelly, L. and Schmidt, A.M., 2016. Soluble RAGE Treatment Delays Progression of Amyotrophic Lateral Sclerosis in SOD1 Mice. *Frontiers in Cellular Neuroscience*, 10(1117), e1-9.

Kačániová, M., Galovičová, L., Valková, V., Ďuranová, H., Štefániková, J., Čmiková, N., Vukic, M., Vukovic, N.L. and Kowalczewski, P.Ł., 2022. Chemical composition, antioxidant, in vitro and in situ antimicrobial, antibiofilm, and anti-insect activity of *Cedar atlantica* essential oil. *Plants (Basel, Switzerland)*, 11(3), 358. <https://doi.org/10.3390/plants11030358>

Kalita, G.J., Sarma, P., Mishra, R.K. and Rout, S., 2015. Traditionally used medicinal Plants of Bajali Sub-division, Barpeta District, Assam. *Journal of Medicinal Plants Studies*, 3(2), 8-17.

Kandasamy, R., Venkatesan, S.K., Uddin, M.I. and Ganesan, S., 2020. Anaerobic biovalorization of leather industry solid waste and production of high value-added biomolecules and biofuels. *Biovalorisation of Wastes to Renewable Chemicals and Biofuels*, 3-25.

Kanedi, M., Sutyarso, S., Busman, H., Pratami, G.D. and Mandasari, R.A., 2019. Plant extracts of Suruhan (*Peperomia pellucida* L. Kunth)

ameliorate infertility of male mice with alloxan-induced hyperglycaemia. *International Journal of Biomedical Research*, 10(2), e5039.

Kang, M.C., Ham, Y.M., Heo, S.J., Yoon, S.A., Cho, S.H., Kwon, S.H., Jeong, M.S., Jeon, Y.J., Sanjeewa, K.K.A., Yoon, W.J. and Kim, K.N., 2018. Anti-inflammation effects of 8-oxo-9-octadecenoic acid isolated from *Undaria peterseniana* in lipopolysaccharide-stimulated macrophage cells. *EXCLI Journal*, 17, 775-783. <https://doi.org/10.17179/excli2018-1422>

Kang, N.R., Pyun, B.J., Jung, D.H., Lee, I.S., Kim, C.S., Kim, Y.S. and Kim, J.S., 2019. *Pueraria lobata* Extract Protects Hydrogen Peroxide-Induced Human Retinal Pigment Epithelial Cells Death and Membrane Permeability. *Evidence-Based Complementary and Alternative Medicine*, 2019, e1-10.

Kanhar, S. and Sahoo, A.K., 2021. An insight into the bioactive compounds of genus *Homalium* with therapeutic potential in different diseases: Current applications and future prospects. *Biocatalysis and Agricultural Biotechnology*, 102173. <https://doi.org/10.1016/j.bcab.2021.102173>

Kartika, I.G.A.A., Bang, I.J., Riani, C., Insanu, M., Kwak, J.H., Chung, K.H. and Adnyana, I.K., 2020. Isolation and characterization of phenylpropanoid and lignan compounds from *Peperomia pellucida* (L.) Kunth with estrogenic activities. *Molecules*, 25(21), 4914.

Kartika, I.G.A.A., Insanu, M., Safitri, D., Putri, C.A. and Adnyana, I.K., 2016. New update: Traditional uses, phytochemical, pharmacological and toxicity review of *Peperomia pellucida* (L.) Kunth. *Pharmacology*

OnLine, 2, 30-43.

Kazeem, M.I., Adamson, J.O. and Ogunwande, I.A., 2013. Modes of inhibition of α -amylase and α -glucosidase by aqueous extract of morinda lucida benth leaf. *BioMed Research International*, 2013, e1-6.

Keane, T.J., Saldin, L.T. and Badylak, S.F., 2016. Decellularization of mammalian tissues: Preparing extracellular matrix bioscaffolds. In Tomlins, P. (ed.) *Characterisation and Design of Tissue Scaffolds*. Woodhead Publishing. 75-103. doi: 10.1016/B978-1-78242-087-3.00004-3

Keawsa-ard, S., Liawruangrath, B., Liawruangrath, S., Teerawutgulrag, A. and Pyne, S.G., 2012. Chemical constituents and antioxidant and biological activities of the essential oil from leaves of *Solanum spirale*. *Natural product communications*, 7(7), 955–958.

Kedare, S.B. and Singh, R.P., 2011. Genesis and development of DPPH method of antioxidant assay. *Journal of Food Science and Technology*, 48(4), 412-122.

Khalid, M., Petroianu, G. and Adem, A., 2022. Advanced glycation end products and diabetes mellitus: Mechanisms and perspectives. *Biomolecules*. 12(4):542. <https://doi.org/10.3390/biom12040542>.

Khan, A., Nazar, H., Sabir, S. M., Irshad, M., Awan, S. I., Abbas, R., Akram, M., Khaliq, A., Rocha, J. B. T., Ahmad, S. D. and Malik, F., 2014. Antioxidant activity and inhibitory effect of some commonly used

- medicinal plants against lipid per-oxidation in mice brain. *African Journal of Traditional, Complementary and Alternative Medicines*, 11(5), 83-90.
- Khan, A., Rahman, M. and Islam, M.S., 2008. Antipyretic activity of *Peperomia pellucida* leaves in rabbit. *Turkish Journal of Biology*, 32(1), 37-41.
- Khan, A., Rahman, M. and Islam, M.S., 2010. Neuropharmacological effects of *Peperomia pellucida* (L) leaves in mice. *DARU*, 16, 77-78.
- Kharroubi, A.T. and Darwish, H.M., 2015. Diabetes mellitus: The epidemic of the century. *World Journal of Diabetes*, 6(6), 850-867.
- Kidane, Y., Bokrezion, T., Mebrahtu, J., Mehari, M., Gebreab, Y.B., Fessehaye, N. and Achila, O.O., 2018. *In Vitro* Inhibition of α -Amylase and α -Glucosidase by Extracts from *Psiadia punctulata* and *Meriandra bengalensis*. *Evidence-based Complementary and Alternative Medicine*. 2015, e1-9.
- Kim, C., Cho, S.K., Kapoor, S., Kumar, A., Vali, S., Abbasi, T., Kim, S.H., Sethi, G. and Ahn, K.S., 2014. β -Caryophyllene oxide inhibits constitutive and inducible STAT3 signaling pathway through induction of the SHP-1 protein tyrosine phosphatase. *Molecular Carcinogenesis*, 53(10), 793-806. <https://doi.org/10.1002/mc.22035>.
- Kim, D.H., Park, M.H., Choi, Y.J., Chung, K.W., Park, C.H., Jang, E.J., An, H.J., Yu, B.P. and Chung, H.Y., 2013. Molecular study of dietary heptadecane for the anti-inflammatory modulation of NF- κ B in the aged kidney. *PloS one*, 8(3), e59316.

<https://doi.org/10.1371/journal.pone.0059316>

Kim, J., Cho, K. and Choung, S.Y., 2020. Protective effect of *Prunella vulgaris* var. L extract against blue light induced damages in ARPE-19 cells and mouse retina. *Free Radical Biology and Medicine*. 152, 622-631. <https://doi.org/10.1016/j.freeradbiomed.2019.12.003>

Kim, J.S. and Jobin, C., 2005. The flavonoid luteolin prevents lipopolysaccharide-induced NF-kappaB signalling and gene expression by blocking IkappaB kinase activity in intestinal epithelial cells and bone-marrow derived dendritic cells. *Immunology*. 115(3), 375-87. <https://doi.org/10.1111/j.1365-2567.2005.02156.x>.

Kim, M.J., Kim, H.J. and Han, J.S., 2019. Pheophorbide a from *Gelidium amansii* improves postprandial hyperglycemia in diabetic mice through α -glucosidase inhibition. *Phytotherapy Research*, 33(3), 702-707.

King, A. and Young, G., 1999. Characteristics and occurrence of phenolic phytochemicals. *Journal of the American Dietetic Association*, 99(2), 213-218.

Kipp, A.P., Frombach, J., Deubel, S. and Brigelius-Flohe, R., 2013. Chapter Five - Selenoprotein W as biomarker for the efficacy of selenium compounds to act as source for selenoprotein biosynthesis. In Cadenas, E. and Packer, L. (eds) *Methods in Enzymology*. 87-112. Academic Press. <https://doi.org/10.1016/B978-0-12-405882-8.00005-2>

Kitanovski, Z., Cuzak, A., Grgic, I. and Claeys, M., 2014. Chemical

characterization of the main products formed through aqueous-phase photonitration of guaiacol. *Atmospheric Measurement Techniques*, 7(8), 2457-2470.

Koch, M., Kehop, D.A., Kinminja, B., Sabak, M., Wavimbukie, G., Barrows, K.M., Matainaho, T.K., Barrows, L.R. and Rai, P.P., 2015. An ethnobotanical survey of medicinal plants used in the East Sepik province of Papua New Guinea. *Journal of Ethnobiology and Ethnomedicine*, 11(79), e1-26.

Kong, D.H., Kim, Y.K., Kim, M.R., Jang, J.H. and Lee, S., 2018. Emerging Roles of Vascular Cell Adhesion Molecule-1 (VCAM-1) In Immunological Disorders and Cancer. *International Journal of Molecular Sciences*, 19(4), 1-16.

Koraneeyakijkulchai, I., Phumsuay, R., Thiyajai, P., Tuntipopipat, S. and Muangnoi, C., 2023. *International Journal of Molecular Sciences*, 24(3), 2462. <https://doi.org/10.3390/ijms24032462>

Kostić, D.A., Dimitrijevic, D.S., Stojanovic, G.S., Palic, I.R., Dordevic, A.S., Ickovski, J.D., 2015. Xanthine oxidase: Isolation, assays of activity, and inhibition. *Journal of Chemistry*. 2015, e1-8.

Kowluru, R.A. and Chan, P.S., 2007. Oxidative stress and diabetic retinopathy. *Experimental Diabetes Research*, 2007, e1-12.

Kowluru, R.A. and Mishra, M., 2015. Oxidative stress, mitochondrial damage and diabetic retinopathy. *Biochimica et Biophysica Acta* -

Molecular Basis of Disease, 1852(11), 2474-2483.

Kowluru, R.A., Zhong, Q. and Santos J.M., 2012. Matrix metalloproteinases in diabetic retinopathy: Potential role of MMP-9. *Expert Opinion on Investigational Drugs*, 21(6), 797-805. doi: 10.1517/13543784.2012.681043.

Kratofil, R.M., Kubes, P. and Deniset, J., 2017. Monocyte conversion during inflammation and injury. *Arteriosclerosis, Thrombosis, and Vascular Biology*, 37(1), 35-42. <https://doi.org/10.1161/ATVBAHA.116.308198>

Krohn, S., Bohm, S., Engelmann, C., Hartmann, J., Brodzinski, A., Chatzinotas, A., Zeller, K., Prywerek, D., Fetzner, I. and Berg, T., 2014. Application of qualitative and quantitative real-time PCR, direct sequencing, and terminal restriction fragment length polymorphism analysis for detection and identification of polymicrobial 16S rRNA genes in ascites. *Journal of Clinical Microbiology*, 52(5), 1754-1757. <https://doi.org/10.1128/JCM.00552-14>

Kurien, B.T. and Scofield, R.H., 2015. Western blotting: An introduction. *Methods in Molecular Biology*, 1312, 17-30. https://doi.org/10.1007/978-1-4939-2694-7_5

Kurniawan, A., Saputri, F.C., Rissyelly, Ahmad, I. and Mun'im, A., 2016. Isolation of angiotensin converting enzyme (ACE) inhibitory activity quercetin from *Peperomia pellucida*. *International Journal of PharmTech Research*, 9, 115-121.

- Kuznetsov, D., Myagchenko, Yu. and Slobodyanyuk, O., 2014. The excitation spectra of singlet oxygen and photoluminescence of methyl pheophorbide-a. *Ukrainian Journal of Physics*, 59(3), 215-218.
- Kwon, O. S., Choi, J. S., Islam, M. N., Kim, Y. S. and Kim, H. O., 2011. Inhibition of 5-lipoxygenase and skin inflammation by the aerial parts of *Artemisia capillaris* and its constituents. *Archives of Pharmacal Research*, 34(9), 1561-1569.
- Lago, J.H.G., Oliveira, A., Guimaraes, E.F. and Kato, M.J., 2006. 3-Ishwarone and 3-ishwarol, rare sesquiterpenes in essential oil from leaves of *Peperomia oreophila* Hensch. *Journal of the Brazilian Chemical Society*, 18(3), 638-642. <https://doi.org/10.1590/S0103-50532007000300022>
- Lamson, D.W. and Plaza, S.M., 2002. Mitochondrial factors in the pathogenesis of diabetes: A hypothesis for treatment. *Alternative Medicine Review*, 7(2), 94-111.
- Lan, C.C., Wu, C.S., Huang, S.M., Wu, I.H. and Chen, G.S., 2013. High-glucose environment enhanced oxidative stress and increased interleukin-8 secretion from keratinocytes: new insights into impaired diabetic wound healing. *Diabetes*, 62(7), 2530-2538. <https://doi.org/10.2337/db12-1714>.
- Lan, Y.Q., Zhang, C., Xiao, J.H., Zhuo, Y.H., Guo, H., Peng, W. and Ge, J., 2009. Suppression of IkappaBalpha increases the expression of matrix metalloproteinase-2 in human ciliary muscle cells. *Molecular Vision*, 15,

1977-87.

Laroche, M., Perreault, V., Marciniak, A., Gravel, A., Chamberland, J. and Doyen, A., 2019. Comparison of conventional and sustainable lipid extraction methods for the production of oil and protein isolate from edible insect meal. *Foods*, 8(11), 572.

Lawrence T., 2009. The nuclear factor NF-kappaB pathway in inflammation. *Cold Spring Harbor Perspectives in Biology*, 1(6), a001651. <https://doi.org/10.1101/cshperspect.a001651>

Le, A.V., Parks, S.E., Nguyen, M.H. and Roach, P.D., 2018. Improving the vanillin-sulphuric acid method for quantifying total saponins. *Technologies*, 6(3), 84. <https://doi.org/10.3390/technologies6030084>

Lee, H., Park, H.Y. and Jeong, T.S., 2021. Pheophorbide a derivatives exert antiwrinkle effects on UVB-induced skin aging in human fibroblasts. *Life (Basel)*, 11(2), 147. <https://doi.org/10.3390/life11020147>.

Lee, I.K., Yun, B.S., Han, G., Cho, D.H., Kim, Y.H. and Yoo, I.D., 2002. Dictyoquinazols A, B, and C, new neuroprotective compounds from the mushroom *Dictyophora indusiata*. *Journal of Natural Products*, 65(12), 1769-72. <https://doi.org/10.1021/np020163w>

Lee, K.J., Oh, Y.C., Cho, W.K. and Ma, J.Y., 2015b. Antioxidant and anti-inflammatory activity determination of one hundred kinds of pure chemical compounds using offline and online screening HPLC assay. *Evidence-Based Complementary and Alternative Medicine*. 2015, 165457.

<https://doi.org/10.1155/2015/165457>

Lee, R., Wong, T.Y. and Sabanayagam, C., 2015a. Epidemiology of diabetic retinopathy, diabetic macular edema and related vision loss. *Eye and Vision. Springer Science and Business Media LLC*, 2(17), e1-25.

Lee, S.H., Sancheti, S.A., Bafna, M.R., Sancheti, S.S. and Seo, S.Y., 2011. Acetylcholinesterase inhibitory and antioxidant properties of *Rhododendron yedoense* var. *Poukhanense* bark. *Journal of Medicinal Plants Research*, 9(34), 109-113.

Li, C., Miao, X., Li, F., Wang, S., Liu, Q., Wang, Y. and Sun, J., 2017. Oxidative Stress-Related Mechanisms and Antioxidant Therapy in Diabetic Retinopathy. *Oxidative Medicine and Cellular Longevity*. 2017, e1-15.

Li, L., Pan, G., Fan, R., Li, D., Guo, L., Ma, L., Liang, H. and Qiu, J., 2022a. Luteolin alleviates inflammation and autophagy of hippocampus induced by cerebral ischemia/reperfusion by activating PPAR gamma in rats. *BMC Complementary Medicine and Therapies*, 22, 176. <https://doi.org/10.1186/s12906-022-03652-8>

Li, T., Fu, X., Liu, B., Wang, X., Li, J., Zhu, P., Niu, X., Bai, J., Liu, Y., Lu, X. and Yu ,Z.L., 2022b. Luteolin binds Src, promotes STAT3 protein ubiquitination and exerts anti-melanoma effects in cell and mouse models. *Biochemical Pharmacology*, 200, 115044. <https://doi.org/10.1016/j.bcp.2022.115044>.

- Li, W., Ling, W., Teng, X., Quan, C., Cai, S., Hu, S. and 2016. Effect of advanced glycation end products, extracellular matrix metalloproteinase inducer and matrix metalloproteinases on type-I collagen metabolism. *Biomedical Reports*, 4(6), 691-693. <https://doi.org/10.3892/br.2016.641>.
- Li, W.S., Lin, S.C., Chu, C.H., Chang, Y.K., Zhang, X., Lin, C.C. and Tung, Y.T., 2021. The gastroprotective effect of naringenin against ethanol-induced gastric ulcers in mice through inhibiting oxidative and inflammatory responses. *International Journal of Molecular Sciences*, 22(21), 11985. <https://doi.org/10.3390/ijms222111985>.
- Li, Y., Pan, J. and Gou, M., 2019. The anti-proliferation, cycle arrest and apoptotic inducing activity of Peperomin E on prostate cancer PC-3 cell line. *Molecules*, 24(8), 1472. <https://doi.org/10.3390/molecules24081472>
- Liang, G.H., Luo, Y.N., Wei, R.Z., Yin, J.Y., Qin, Z.L., Lu, L.L. and Ma, W.H., 2022. CircZNF532 knockdown protects retinal pigment epithelial cells against high glucose-induced apoptosis and pyroptosis by regulating the miR-20b-5p/STAT3 axis. *Journal of Diabetes Investigation*, 13(5), 781-795. <https://doi.org/10.1111/jdi.13722>
- Liang, N. and Kitts, D.D., 2014. Antioxidant property of coffee components: Assessment of methods that define mechanism of action. *Molecules*, 19(11), 19180-19208.
- Liau, N.P.D., Laktyushin, A., Lucet, I.S., Murphy, J.M., Yao, S., Whitlock, E., Callaghan, K., Nicola, N.A., Kershaw, N.J. and Babon, J.J., 2018. The molecular basis of JAK/STAT inhibition by SOCS1. *Nature*

Communications, 9, 1558. <https://doi.org/10.1038/s41467-018-04013-1>

Ling, S. K., Tanaka, T. and Kouno, I., 2003. Effects of iridoids on lipoxygenase and hyaluronidase activities and their activation by β -glucosidase in the presence of amino acids. *Biological and Pharmaceutical Bulletin*, 26(3), 352-356.

Liu, M., Niu, W. and Ou, L., 2021. β -Caryophyllene ameliorates the Mycoplasmal pneumonia through the inhibition of NF- κ B signal transduction in mice. *Saudi Journal of Biological Sciences*. 28(8), 4240-4246. <https://doi.org/10.1016/j.sjbs.2021.06.034>

Liu, T., Zhang, L., Joo, D. and Sun, S.C., 2017. NF- κ B signaling in inflammation. *Signal Transduction and Targeted Therapy*, 2, e17023.

Logan, S.M. and Storey, K.B., 2018. Pro-inflammatory AGE-RAGE signaling is activated during arousal from hibernation in ground squirrel adipose. *PeerJ*, 6, e4911.

Lorenzi, M., 2007. The polyol pathway as a mechanism for diabetic retinopathy: Attractive, elusive, and resilient. *Experimental Diabetes Research*. 2007, e1-10.

Louro, R. O., 2013. Introduction to biomolecular NMR and metals. *Practical Approaches to Biological Inorganic Chemistry*, 77-107.

Lubos, E., Loscalzo, J. and Handy, D.E., 2011. Glutathione peroxidase-1 in health and disease: from molecular mechanisms to therapeutic opportunities. *Antioxidants & redox signaling*, 15(7), 1957-1997.

[https://doi.org/ 10.1089/ars.2010.3586](https://doi.org/10.1089/ars.2010.3586).

Luo, L., Jia, J.J., Zhong, Q., Zhong, X., Zheng, S., Wang, G. and He, L., 2021. Synthesis and anticancer activity evaluation of naphthalene-substituted triazole spirodienones. *European Journal of Medicinal Chemistry*. 213, 113039. <https://doi.org/10.1016/j.ejmech.2020.113039>.

Lv, J., Yao, L., Li, S., Dong, J., Ye, M., Fan, D., Li, C., Tian, F., Li, Y., 2022. New aniline derivatives from the volva of *Phallus rubrovolvatus* and their anti-inflammatory activity. *Bioorganic Chemistry*. 119(2022), 105577. <https://doi.org/10.1016/j.bioorg.2021.105577>

Ma, X., Wang, Z., Li, S., Shen, Q. and Yuan, Q., 2006. Effect of CaCl₂ as activity stabilizer on purification of heparinase I from *Flavobacterium heparinum*. *Journal of Chromatography B: Analytical Technologies in the Biomedical and Life Sciences*, 843(2), 209-215.

Machiele, R., Motlagh, M. and Patel, B., 2022. Intraocular pressure. Florida: StatPearls Publishing LLC; 2023.

Mahi, T., Hariza, A., Elouissi, A., Perez-Izquierdo, C., Benguerai, A., Canelo, T. and Bonal, R., 2023. Chemical composition and toxicity of *Artemisia herba-alba* essential oil against *Cydia pomonella* L. (Lepidoptera:Tortricidae) under laboratory conditions. *Biocatalysis and Agricultural Biotechnology*, 50, 102742. <https://doi.org/10.1016/j.bcab.2023.102742>

- Mahlo, S.M. and Chauke, H., 2012. The effectiveness of polyethylene glycol (PEG) and polyvinyl polypyrrolidone (PVPP) on removal of tannins from leaf extracts of selected medicinal plants in Limpopo Province. *African Journal of Biotechnology*, 11(43), 10141-10145.
- Mahmood, T. and Yang, P.C., 2012. Western blot: Technique, theory, and trouble shooting. *North American Journal of Medical Sciences*, 4(9), 429-434. <https://doi.org/10.4103/1947-2714.100998>
- Maimulyanti, A. and Prihadi, A. R., 2016. Chemical composition of essential oil and hexane extract and antioxidant activity of various extracts of *Acmella uliginosa* (Sw.) Cass flowers from Indonesia. *Agriculture and Natural Resources*, 50(4), 264-269.
- Mallakpour, S. and Azimi, F., 2020. Spectroscopic characterization techniques for layered double hydroxide polymer nanocomposites. *Layered Double Hydroxide Polymer Nanocomposites*, 231-280.
- Majumder, P., Abraham, P. and V, S., 2012. Ethno-medicinal, Phytochemical and Pharmacological review of an amazing medicinal herb *Peperomia pellucida* (L.) HBK. *Research Journal of Pharmaceutical, Biological and Chemical Sciences*, 2(4), 358-364.
- Manaharan, T., Appleton, D., Cheng, H.M. and Palanisamy, U.D., 2012. Flavonoids isolated from *Syzygium aqueum* leaf extract as potential antihyperglycaemic agents. *Food Chemistry*, 132(4), 1802-1807.
- Mani, D., Kalpana, M.S., Patil, D.J. and Dayal, A.M. 2017. Organic matter

in gas shales. *Shale Gas*, 25-54.

Maniadakis, N., Konstantakopoulou, E., 2019. Cost Effectiveness of Treatments for Diabetic Retinopathy: A Systematic Literature Review. *Pharmacoeconomics*, 37(8), 995-1010.

Mannan, A., Garg, N., Singh, T.G. and Kang, H.K., 2021. Peroxisome proliferator-activated receptor-gamma (PPAR- γ): Molecular effects and its importance as a novel therapeutic target for cerebral ischemic injury. *Neurochemical Research*, 46(11), 2800-2831. <https://doi.org/10.1007/s11064-021-03402-1>

Manns, J.M., 2011. SDS-polyacrylamide gel electrophoresis (SDS-PAGE) of proteins. *Current Protocols in Microbiology*, 22(1), 1-13. <https://doi.org/10.1002/9780471729259.mca03ms22>

Martin, D., Galisteo, R. and Gutkind, J.S., 2009. CXCL8/IL8 stimulates vascular endothelial growth factor (VEGF) expression and the autocrine activation of VEGFR2 in endothelial cells by activating NFkappaB through the CBM (Carma3/Bcl10/Malt1) complex. *Journal of Biological Chemistry*, 284(10), 6038-42. <https://doi.org/10.1074/jbc.C800207200>.

Mateos, M.V., Tenconi, P.E., Giusto, N.M. and Salvador, G.A., 2015. Inflammation and oxidative stress in retinal diseases: The role of intracellular signaling in the retinal pigment epithelium. *International Journal of Ophthalmology and Clinical Research*. 2(3). <https://doi.org/10.23937/2378-346X/1410033>

- Mathebula, S.D., 2015. Polyol pathway: A possible mechanism of diabetes complications in the eye. *African Vision and Eye Health*. 74(1), e1-5.
- Mathieu, G. and Posada, R.C., 2006. New synonymies in the genus *Peperomia* Ruiz and Pav.(Piperaceae): an annotated checklist. *Candollea*, 61, 331-363.
- Matsumoto, T., Matsuno, M., Ikui, N., Mizushina, Y., Omiya, Y., Ishibashi, R., Ueda, T. and Mizukami, H., 2021. Identification of pheophorbide a as an inhibitor of receptor for advanced glycation end products in *Mallotus japonicus*. *Journal of Natural Medicines*. 75(3), 675-681. <https://doi.org/10.1007/s11418-021-01495-0>.
- Matsushima, K., Yang, D. and Oppenheim, J.J., 2022. Interleukin-8: An evolving chemokine. *Cytokine*, 153, 155828. <https://doi.org/10.1016/j.cyto.2022.155828>
- Mazur, P., Dumnicka, P., Tisonczyk, J., Zabek-Adamska, A. and Drozd, R., 2023. SDS electrophoresis on gradient polyacrylamide gels as a semiquantitative tool for the evaluation of proteinuria. *Diagnostics (Basel)*, 13(9), 1513. <https://doi.org/10.3390/diagnostics13091513>
- McFarland, B.C., Hong, S.W., Rajbhandari, R., Twitty Jr, G.B., Gray, G.K., Yu, H., Benveniste, E.N. and Nozell, S.E., 2013. NF- κ B-induced IL-6 ensures STAT3 activation and tumor aggressiveness in glioblastoma. *PLoS One*, 8(11), e78728. <https://doi.org/10.1371/journal.pone.0078728>

- McKenzie, B., Kay, G., Matthews, K.H., Knott, R.H. and Cairns, D., 2015. The hen's egg chorioallantoic membrane (HET-CAM) test to predict the ophthalmic irritation potential of a cysteamine-containing gel: Quantification using Photoshop® and ImageJ. *International Journal of Pharmaceutics*, 490(1-2), 1-8. <https://doi.org/10.1016/j.ijpharm.2015.05.023>
- Melo, A., Guimarães, E.F. and Alves, M., 2016. Synopsis of the genus *Peperomia* Ruiz & Pav. (Piperaceae) in Roraima State, Brazil. *Hoehnea*. 43(1), 119-134.
- Merck, 2022. IR Spectrum Table & Chart. Available at: <https://www.sigmaaldrich.com/MY/en/technical-documents/technical-article/analytical-chemistry/photometry-and-reflectometry/ir-spectrum-table> (Accessed: 15 March 2022)
- Merck, 2023. Nuclear extraction kit. Available at: https://www.merckmillipore.com/MY/en/product/Nuclear-Extraction-Kit,MM_NF-2900#documentation (Accessed: 9 August 2023)
- Mesquita, K.S.M., Feitosa, B.S., Cruz, J.N., Ferreira, O.O., Franco, C.J.P., Cascaes, M.M., Oliveira, M.S. and Andrade, E.H.A., 2021. Chemical composition and preliminary toxicity evaluation of the essential oil from *Peperomia circinnata* Link car. *circinnata*. (Piperaceae) in *Artemia salina* Leach. *Molecules*, 26(23), 7359.
- Milow, P., Malek, S., Raznan Mohd, R., 2017. Medicinal Plants of the Indigenous Tribes in Peninsular Malaysia: Current and Future Perspectives. *Active Ingredients from Aromatic and Medicinal Plants*.

- Ministry of Health Malaysia, 2017. Diabetic Retinopathy Screening: Training Module for Healthcare Providers, 2nd edition, Kuala Lumpur: Ministry of Health Malaysia.
- Miranda, E.R., Fuller, J.K.N., Perkins, R., Beisswenger, P.J., Farabi, S.S., Quinn, L.T. and Haus, J.M., 2018. Soluble RAGE Sequesters Advanced Glycation End Products following an Overnight Fast in T1DM Patients. *Diabetes*. 67(1), 275.
- Miranda, N., Gerola, A.P., Novello, C.R., Ueda-Nakamura, T., de Oliveira Silva, S., Dias-Filho, Hioka, N., de Mello, J.C.P. and Nakamura, C.V., 2017. Pheophorbide a, a compound isolated from the leaves of *Arrabidaea chica*, induces photodynamic inactivation of *Trypanosoma cruzi*. *Photodiagnosis and Photodynamic Therapy*, 19, 256-265.
- Mittal, M., Siddiqui, M.R., Tran, K., Reddy, S.P. and Malik, A.B., 2014. Reactive oxygen species in inflammation and tissue injury. *Antioxidants & Redox Signaling*, 20(7), 1126-67. <https://doi.org/10.1089/ars.2012.5149>
- Miyata, J., Fukunaga, K., Kawashima, Y., Ohara, O. and Arita, M., 2020. Cysteinyl leukotriene metabolism of human eosinophils in allergic disease. *Allergology International*, 69(1), 28-34. <https://doi.org/10.1016/j.alit.2019.06.002>
- Mohamed, E.A., Siddiqui, M.J., Ang, L.F., Sadikun, A., Chan, S.H., Tan, S.C., Asmawi, M.Z. and Yam, M.F., 2012. Potent α -glucosidase and α -amylase inhibitory activities of standardized 50% ethanolic extracts and sinensetin from *Orthosiphon stamineus* Benth as anti-diabetic

mechanism. *BMC complementary and alternative medicine*, 12, 176.
<https://doi.org/10.1186/1472-6882-12-176>

Mohammad, G., Alam, K., Nawaz, M.I., Siddiquei, M.M., Mousa, A. and El-Asrar, A.M.A., 2015. Mutual enhancement between high-mobility group box-1 and NADPH oxidase-derived reactive oxygen species mediates diabetes-induced upregulation of retinal apoptotic markers. *Journal of Physiology and Biochemistry*, 71(3), 359-372.

Mohammad, G. and Kowluru, R.A., 2010. Matrix metalloproteinase-2 in the development of diabetic retinopathy and mitochondrial dysfunction. *Laboratory Investigation*, 90(9), 1365-1372.
<https://doi.org/10.1038/labinvest.2010.89>.

Morocho, V., Hidalgo-Tapia, M., Delgado-Loyola, I., Cartuche, L., Cumbicus, N. and Valarezo, E., 2023. Chemical composition and biological activity of essential oil from leaves and fruits of Limoncillo (*Siparuna muricata* (Ruiz & Pav.) A. DC.). *Antibiotics (Basel, Switzerland)*, 12(1), 82. <https://doi.org/10.3390/antibiotics12010082>

Moshawih, S., Cheema, M.S., Ibraheem, Z.O., Tailan, N.D., Hakim, M.N., 2017. Cosmos caudatus extract/fractions reduce smooth muscle cells migration and invasion *in vitro*: A potential benefit of suppressing atherosclerosis. *Porto Biomedical Journal*, 2(6), 293-300.

Mo, Y., Wan, R., Zhang, Q., 2012. Application of reverse transcription-PCR and real-time PCR in nanotoxicity research. *Methods in Molecular Biology*, 926, 99-112. https://doi.org/10.1007/978-1-62703-002-1_7

Muhammad, I., Samoylenko, V., Machumi, F., Zaki, M., Mohammed, R.,

Hetta, M. and Gillum, V., 2013. Preparation and application of reversed phase chromatrotor™ for the isolation of natural products by centrifugal preparative chromatography. *Natural Product Communications*, 8(3), 311-314.

Mukherjee, P. K., 2019. LC-MS: A rapid technique for understanding the plant metabolite analysis. *Quality Control and Evaluation of Herbal Drugs*, 459-479.

Müller, C. and Junker, R.R., 2022. Chemical phenotype as important and dynamic niche dimension of plants. *New Phytologist*. 234(4), 1168-1174. <https://doi.org/10.1111/nph.18075>

Mulyaningsih, S., Sporer, F., Reichling, J. and Wink, M., 2011. Antibacterial activity of essential oils from *Eucalyptus* and of selected components against multidrug-resistant bacterial pathogens. *Pharmaceutical Biology*, 49(9), 893-899. <https://doi.org/10.3109/13880209.2011.553625>.

Mutee, A.F., Salhimi, S.M., Yam, M.F., Lim, C.P., Abdullah, G.Z., Ameer, O.Z., Abdulkarim, M.F., Asmawi, M.Z., 2010. In vivo anti-inflammatory and *in vitro* antioxidant activities of *Peperomia pellucida*. *International Journal of Pharmaceutics*, 6, 686-690.

Nadali, M., Lyngfelt, L., Erlandsson, M.C., Silfversward, S.T., Andersson, K.M.E., Bokarewa, M.I. and Pullerits, R., 2021. Low soluble receptor for advanced glycation end products precedes and predicts cardiometabolic events in women with rheumatoid arthritis. *Frontiers in Medicine*. 7,

594622. <https://doi.org/10.3389/fmed.2020.594622>

Nagarajan, J., Ramanan, R.N., Raghunandan, M.E., Galanakis, C.M. and Krishnamurthy, N.P., 2017. Carotenoids. In *Nutraceutical and Functional Food Components: Effects of Innovative Processing Techniques*. Elsevier, Amsterdam.

Nakamura, M., Ra, J.H., Jee, Y. and Kim, J.S., 2017. Impact of different partitioned solvents on chemical composition and bioavailability of *Sasa quepaertensis* Nakai leaf extract. *Journal of Food and Drug Analysis*, 25(2), 316-326.

Nam, M.H., Oh, J.S., Hong, C.O., Son, D.H., Hong, S.T., Seol, H.M. and Lee, K.W., 2013. Pheophorbide-a prevents vascular endothelium dysfunction and down-regulates AGEs-induced proinflammatory cytokines. *The FASEB Journal*, 27(1), 594.2. https://doi.org/10.1096/fasebj.27.1_supplement.594.2

Nam, T.G., 2011. Lipid peroxidation and its toxicological implications. *Toxicological Research*, 27(1), 1-6.

Narayanamoorthi, V., Vasantha, K. and Maruthasalam, A., 2018. *In vitro* evaluation of cytotoxic properties of *Peperomia pellucida* (L.) H.B.K. against human cancer cell lines. *Bioscience Discovery*, 9(3), 344-355.

Narayanamoorthi, V., Vasantha, K., Rency, R.C. and Maruthasalam, A., 2015. GC MS determination of bioactive components of *Peperomia pellucida* (L.) Kunth. *Bioscience Discovery*, 6(2), 83-88.

National Center for Biotechnology Information, 2022a. PubChem compound

summary for CID 152219, 2,4,5-trimethoxystyrene. Available at: https://pubchem.ncbi.nlm.nih.gov/compound/2_4_5-Trimethoxystyrene (Accessed: 2 April 2022).

National Center for Biotechnology Information, 2022b. PubChem compound summary for CID 8202, Methyl 9-octadecenoate. Available at: <https://pubchem.ncbi.nlm.nih.gov/compound/Methyl-9-octadecenoate> (Accessed: 2 April 2022).

National Center for Biotechnology Information, 2022c. PubChem compound summary for CID 135407639, Methyl pheophorbide a. Available at: <https://pubchem.ncbi.nlm.nih.gov/compound/Methyl-pheophorbide-a> (Accessed: 2 April 2022).

National Institute of Standards and Technology, 2022. Styrene, CAS Registry Number: 100-42-5. Available at: <https://webbook.nist.gov/cgi/cbook.cgi?Source=1946ROD%2FFEL896&Mask=400> (Accessed: 16 March 2022).

Nawaz, H., Shad, M. A., Rehman, N., Andaleeb, H. and Ullah, N., 2020. Effect of solvent polarity on extraction yield and antioxidant properties of phytochemicals from bean (*Phaseolus vulgaris*) seeds. *Brazilian Journal of Pharmaceutical Sciences*, 56, e1-9.

Nayaka, N. M. D. M. W., Sasalara, M.M.V., Sanjaya, D.A., Yuda, P.E.S.K., Dewi, N.L.K.A.A., Cahyaningsih, E. and Hartati, R., 2021. *Piper betle* (L): Recent review of antibacterial and antifungal properties, safety profiles, and commercial applications. *Molecules*, 26(8), 2321.

Nazir, Y., Linsaenkart, P., Khantham, C., Chaitep, T., Jantrawut, P., Chittasupho, C., Rachtanapun, P., Jantanasakulwong, K., Phimolsiripol, Y., Sommano, S.R., Tocharus, J., Mingmalairak, S., Wongsas, A., Arjin, C., Sringarm, K., Berrada, H., Barba, F.J. and Ruksiriwanich, W., 2021. High efficiency *in vitro* wound healing of *Dictyophora indusiata* extracts via anti-inflammatory and collagen stimulating (MMP-2 inhibition) mechanisms. *Journal of Fungi (Basel)*, 7(12), 1100. <https://doi.org/10.3390/jof7121100>

Nehete, J., Bhatia, M. and Narkhede, M., 2010. *In-vitro* evaluation of antioxidant activity and phenolic content of *Costus speciosus* (Koen) J.E. Sm. *Iran Journal of Pharmaceutical Research*. 9(3), 271-277.

Nentwich, M.M. and Ulbig, M.W., 2015. Diabetic retinopathy- ocular complications of diabetes mellitus. *World Journal of Diabetes*, 6(3), 489-499.

Ng, Z.X., Chua, K.H., Iqbal, T. and Kuppusamy, U.R., 2013b. Soluble receptor for advanced glycation end-product (sRAGE)/pentosidine ratio: A potential risk factor determinant for type 2 diabetic retinopathy. *International Journal of Molecular Sciences*, 14(4), 7480-7491.

Ng, Z.X., Kuppusamy, U.R., Iqbal, T. and Chua, K.H., 2013a. Receptor for advanced glycation end-product (RAGE) gene polymorphism 2245G/A is associated with pro-inflammatory, oxidative-glycation markers and sRAGE in diabetic retinopathy. *Gene*, 521(2), 227-233

Ng, Z.X., Kuppusamy, U.R., Iqbal, T., Fong, K.C.S., Koay, A.C.A. and Chua, K.H., 2012. 2245G/A polymorphism of the receptor for advanced

glycation end-products (RAGE) gene is associated with diabetic retinopathy in the Malaysian population', *British Journal of Ophthalmology*, 96(2), 289-292.

Ng, Z.X., Samsuri, S.N. and Yong, P.H., 2020. The antioxidant index and chemometric analysis of tannin, flavonoid, and total phenolic extracted from medicinal plant foods with the solvents of different polarities. *Journal of Food Processing and Preservation*. 44(9), e14680.

Ng, Z. X., Than, M. J. Y., Yong, P. H., 2021. *Peperomia pellucida* (L.) Kunth herbal tea: Effect of fermentation and drying methods on the consumer acceptance, antioxidant and anti-inflammatory activities. *Food Chemistry*, 44, e128738.

Nikolov, A. and Popovski, N., 2021. Role of gelatinases MMP-2 and MMP-9 in healthy and complicated pregnancy and their future potential as preeclampsia biomarkers. *Diagnostics (Basel)*, 11(3), 480. <https://doi.org/10.3390/diagnostics11030480>.

Noreen, H., Semmar, N., Farman, M. and McCulaagh, J. S. O., 2017. Measurement of total phenolic content and antioxidant activity of aerial parts of medicinal plant *Coronopus didymus*. *Asian Pacific Journal of Tropical Medicine*, 10(8), 792-801.

Noro, T., Oda, Y., Miyase, T., Ueno, A. and Fukushima, S., 1983. Inhibitors of Xanthine Oxidase from the Flowers and Buds of *Daphne genkwa*. *Chemical and Pharmaceutical Bulletin*, 31(11), 3984-3987.

Nowakowski, A.B., Wobig, W.J. and Petering, D.H., 2015. Native SDS-PAGE: High resolution electrophoretic separation of proteins with retention of native properties including bound metal ions. *Metallomics*, 6(5), 1068-

1078. <https://doi.org/10.1039/c4mt00033a>

Nowotny, K., Jung, T., Hohn, A., Weber, D. and Grune, T., 2015. Advanced glycation end products and oxidative stress in type 2 diabetes mellitus. *Biomolecules*, 5(1), 194-222. <https://doi.org/10.3390/biom5010194>

Nowotny, K., Schroter, D., Schreiner, M. and Grune, T., 2018. Dietary advanced glycation end products and their relevance for human health. *Ageing Research Reviews*, 47, 55-66. <https://doi.org/10.1016/j.arr.2018.06.005>

Nuutinen, T., 2018. Medicinal properties of terpenes found in *Cannabis sativa* and *Humulus lupulus*. *European Journal of Medicinal Chemistry*, 157, 198-228. <https://doi.org/10.1016/j.ejmech.2018.07.076>.

Nwokocha, C.R., Owu, D.U., Kinlocke, K., Murray, J., Delgoda, R., Thaxter, K., McCalla, G. and Young, L., 2012. Possible Mechanism of Action of the Hypotensive Effect of *Peperomia pellucida* and Interactions between Human Cytochrome P450 Enzymes. *Medicinal and Aromatic Plants*, 1(4), e1-5.

Ogawa, N., Yamaguchi, T., Yano, S., Yamauchi, M., Yamamoto, M. and Sugimoto, T., 2007. The combination of high glucose and advanced glycation end-products (AGEs) inhibits the mineralization of osteoblastic MC3T3-E1 cells through glucose-induced increase in the receptor for AGEs. *Hormone and Metabolic Research*, 39(12), 871-875. <https://doi.org/10.1055/s-2007-991157>.

Ogawa, Y. and Imamoto, N., 2021. Methods to separate nuclear soluble fractions reflecting localizations in living cells. *iScience*, 24(12), 103503. <https://doi.org/10.1016/j.isci.2021.103503>

Okoh, S.O., Okoh, S.O., Iweriebor, B.C., Okoh, O.O. and Okoh, A.I., 2017. Bioactive constituents, radical scavenging, and antibacterial properties of the leaves and stem essential oils from *Peperomia pellucida* (L.) Kunth. *Pharmacognosy Magazine*, 13(3), 392-400.

Oliveira, C.R., Paiva, M.R.B., Ribeiro, M.C.S., Andrade, G.F., Carvalho, J.L., Gomes, D.A., Nehemy, M., Fialho, S.L., Silva-Cunha, A. and Góes, A.M., 2021. Human stem cell-derived retinal pigment epithelial cells as a model for drug screening and pre-clinical assays compared to ARPE-19 cell line. *International Journal of Stem Cells*. 14(1), 74-84. <https://doi.org/10.15283/ijsc20094>.

Oliveira, G.L., Moreira, D.L., Mendes, A.D.R., Guimaraes, E.F., Figueiredo, L.S., Kaplan, M.A.C. and Martins, E.R., 2013. Growth study and essential oil analysis of *Piper aduncum* from two sites of Cerrado biome of Minas Gerais State, Brazil. *Revista Brasileira de Farmacognosia*, 23(5), 743-753. <https://doi.org/10.1590/S0102-695X2013000500005>

Oliveira, J.C.S., da Camara, C.A.G., Neves, R.C.S., Botelho, P. and Botelho, P., 2017. Chemical composition and acaricidal activity of essential oils from *Peperomia pellucida* kunth. against *Tetranychus urticae*. *Revista Virtual de Quimica*, 9(6), 2204-2213.

Oloyede, G.K. Onocha, P.A. and Olaniran, B.B., 2011. Phytochemical,

- toxicity, antimicrobial and antioxidant screening of leaf extracts of *Peperomia pellucida* from Nigeria. *Advances in Environmental Biology*, 5(12), 3700-3709.
- Ooi, D.J., Iqbal, S. and Ismail, M., 2012. Proximate composition, nutritional attributes and mineral composition of *Peperomia pellucida* L. (ketumpangan air) grown in Malaysia. *Molecules*, 17(9), 11139-11145.
- Orlova, V.V., Choi, E.Y., Xie, C., Chavakis, E., Bierhaus, A., Ihanus, E., Ballantyne, C.M., Gahmberg, C.G., Bianchi, M.E., Nawroth, P.P. and Chavakis, T., 2007. A novel pathway of HMGB1-mediated inflammatory cell recruitment that requires Mac-1-integrin. *The EMBO Journal*, 26(4), 1129-1139.
- Ortega, P.A., Guzman, M.E., Vera, L.R. and Velazquez, J.A., 2000. Dihydroeuparin as sunscreen. *Boletin de la Sociedad Chilena de Quimica*, 45(4). <https://doi.org/10.4067/S0366-16442000000400017>
- Otieno, B.A., Krause, C.E. and Rusling, J.F., 2016. Chapter seven - Bioconjugation of antibodies and enzymes labels onto magnetic beads. In Kumar, C.V. (ed.) *Methods in Enzymology*. Academic Press. 135-150. doi:10.1016/bs.mie.2015.10.005
- Ou, B., Huang, D., Hampsch-Woodill, M., Flanagan, J.A. and Deemer, E.K., 2002. Analysis of antioxidant activities of common vegetables employing oxygen radical absorbance capacity (ORAC) and ferric reducing antioxidant power (FRAP) assays: A comparative study. *Journal of Agricultural and Food Chemistry*, 50(11), 3122-3128.

- Owumi, S.E., Ijadele, A.O., Arunsi, U.O. and Odunola, O.A., 2020. Luteolin abates reproductive toxicity mediated by the oxido-inflammatory response in Doxorubicin-treated rats. *Toxicology Research and Application*, 4, 1-16. <https://doi.org/10.1177/2397847320972040>
- Oyedemi, S.O., Oyedemi, B.O., Ijeh, I.I., Ohanyerem, P.E., Coopoosamy, R.M. and Aiyegoro, O.A., 2017. Alpha-Amylase Inhibition and Antioxidative Capacity of Some Antidiabetic Plants Used by the Traditional Healers in Southeastern Nigeria. *Scientific World Journal*. 2017, e1-11
- Pal, D., Mishra, P., Sachan, N. and Ghosh, A.K., 2011. Biological activities and medicinal properties of *Cajanus cajan* (L) Millsp. *Journal of Advanced Pharmaceutical Technology & Research*, 2(4), 207-214. <https://doi.org/10.4103/2231-4040.90874>
- Panchapakesan, U., Pollock, C.A. and Chen, X.M., 2004. The effect of high glucose and PPAR-gamma agonists on PPAR-gamma expression and function in HK-2 cells. *American Journal of Physiology, Renal Physiology*. 287(3), F528-534. <https://doi.org/10.1152/ajprenal.00445.2003>
- Pandurangan, A.K., Dharmalingam, P., Sadagopan, S.K. and Ganapasam, S., 2014. Luteolin inhibits matrix metalloproteinase 9 and 2 in azoxymethane-induced colon carcinogenesis. *Human & Experimental Toxicology*, 33(11), 1176-85. <https://doi.org/10.1177/0960327114522502>.
- Papatheodorou, K., Banach, M., Bekiari, E., Rizzo, M. and Edmonds, M., 2018. Complications of Diabetes 2017. *Journal of Diabetes Research*, 2018, 1-4.

- Pappachen, L.K., 2013. Isolation and characterization of flavones glycoside vitexin from *Peperomia pellucida* Linn. *Journal of Drug Delivery Therapy*, 3, 91-92.
- Pappachen, L.K. and Chacko, A., 2013. Preliminary phytochemical screening and *in-vitro* cytotoxicity activity of *Peperomia pellucida* Linn. *Pharmacie Globale*, 4(8), 1.
- Parawansah, P., Nuralifah, N., Alam, G. and Natzir, R., 2016. Inhibition of Xanthine Oxidase Activity by Ethanolic Extract of *Piperomia pellucida* L., *Acacypha indica* L. and *Momordica charantia* L. *The Indonesian Biomedical Journal*, 8(3), 161-166.
- Parise-Filho, R., Pastrello, M., Camerlingo, C.E.P., Silva, G.J., Agostinho, L.A., Souza, T., Magri, F.M.M., Ribeiro, R.R., Brandt, C.A. and Polli, M.C., 2011. The anti-inflammatory activity of dillapiole and some semisynthetic analogues. *Pharmaceutical Biology* 49, 1173-1179.
- Park, J., Kwock, C. K. and Yang, Y. J., 2016. The effect of the sodium to potassium ratio on hypertension prevalence: A propensity score matching approach. *Nutrients*, 8(8), 482.
- Patel, D. K., Kumar, R., Kumar, M., Sairam, K. and Hemalatha, S., 2012b. Evaluation of *in vitro* aldose reductase inhibitory potential of different fraction of *Hybanthus enneaspermus* Linn F. Muell. *Asian Pacific Journal of Tropical Biomedicine*, 2(2), 134-139.
- Patel, J.K., Clifford, R.L., Deacon, K. and Knox, A.J., 2012a. Ciclesonide inhibits TNF α - and IL-1 β -induced monocyte chemotactic protein-1 (MCP-1/CCL2) secretion from human airway smooth muscle cells. *American Journal of Physiology Lung Cellular and Molecular Physiology*. 302(8),

785-792. <https://doi.org/10.1152/ajplung.00257.2011>.

Patel, R., Rinker, L., Peng, J. and Chilian, W.M., 2018. Reactive Oxygen Species: The Good and the Bad. In *Reactive Oxygen Species (ROS) in Living Cells*.

Pejin, B., Kojic, V. and Bogdanovic, G., 2014. An insight into the cytotoxic activity of phytol at *in vitro* conditions. *Natural Product Research*, 28(22), 2053-2056. <https://doi.org/10.1080/14786419.2014.921686>

Peleg, H., Naim, M., Rouseff, R. L. and Zehavi, U., 1991. Distribution of bound and free phenolic acids in oranges (*Citrus sinensis*) and Grapefruits (*Citrus paradisi*). *Journal of the Science of Food and Agriculture*, 57(3), 417-426.

Perera, H.D.S.M., Samarasekera, J.K.R.R., Handunnetti, S.M. and Weerasena, O.V.D.S.J., 2016. *In vitro* anti-inflammatory and anti-oxidant activities of Sri Lankan medicinal plants. *Industrial Crops and Products*, 94, 610-620.

Pérez Zamora, C. M., Torres, C. A. and Nuñez, M. B., 2018. Antimicrobial activity and chemical composition of essential oils from Verbenaceae species growing in South America. *Molecules (Basel, Switzerland)*, 23(3), 544. <https://doi.org/10.3390/molecules23030544>

Perkin Elmer, 2014. Obtaining optimum reproducibility for FT-IR measurements in ZnSe liquid transmission cells. Available at: https://resources.perkinelmer.com/lab-solutions/resources/docs/TCH_FTIRMeasurementsinLiquidTransmissionCells.pdf (Accessed 2 April 2022).

- Peters-Golden, M. and Brock, T.G., 2003. 5-Lipoxygenase and FLAP. *Prostaglandins Leukotrienes and Essential Fatty Acids*, 69(2003), 99-109.
- Phongtongpasuk, S. and Poadang, S., 2014. Extraction of antioxidants from *Peperomia pellucida* L. Kunth. *Thammasat International Journal of Science and Technology*, 19(3), 38-43.
- Pineda, R., Vizcaino, S., Garcia, C.M., Gil, J.H. and Durango, D., 2018. Antifungal activity of extracts, essential oil and constituents from *Petroselinum crispum* against *Colletotrichum acutatum*. *Revista Facultad Nacional de Agronomia Medellin*, 71(3), 8563-8572.
- Pinheiro, B.G., Silva, A.S.B., Souza, G.E.P., Figueiredo, J.G., Cunha, F.Q., Lahlou, S., da Silva, J.K.R., Maia, J.G.S. and Sousa, P.J.C., 2011. Chemical composition, antinociceptive and anti-inflammatory effects in rodents of the essential oil of *Peperomia serpens* (Sw.) Loud. *Journal of Ethnopharmacology*, 138(2), 479-486.
<https://doi.org/10.1016/j.jep.2011.09.037>
- Pontis, J.A., da Costa, L.A.M.A., da Silva, S.J.R. and Flach, A., 2014. Color, phenolic and flavonoid content, and antioxidant activity of honey from Roraima, Brazil. *Food Science and Technology*, 34(1), 69-73.
- Poole, C. F., 2003. General concepts in column chromatography. *The Essence of Chromatography*. 1-78.
- Prakash, M., Sun, J.K. and King, G.L., 2008. The Role of Protein Kinase C in Diabetic Retinopathy. In Duh, E.J. (ed.) *Diabetic Retinopathy*. Humana Press.

- Punthakee, Z., Goldenberg, R. and Katz, P., 2018. Definition, Classification and Diagnosis of Diabetes, Prediabetes and Metabolic Syndrome. *Canadian Journal of Diabetes*, 42, 10-15.
- Puttaraju, N.G., Venkateshaiah, S.U., Dharmesh, S.M., Urs, S.M.N. and Somasundaram, R., 2006. Antioxidant activity of indigenous edible mushrooms. *Journal of Agricultural and Food Chemistry*, 54(26), 9764-9772.
- Queiroz, R.M., Oliveira, I.A., Piva, B., Catao, F.B., Rodrigues, B.C., Pascoal, A.D.C., Diaz, B.L., Todeschini, A.R., Caarls, M.B. and Dias, W.B., 2019. Hexosamine Biosynthetic Pathway and Glycosylation Regulate Cell Migration in Melanoma Cells. *Frontiers in Oncology*, 9, 116.
- Quintero-Fabián, S., Arreola, R., Becerril-Villanueva, E., Torres-Romero, J.C., Arana-Argáez, V., Lara-Riegos, J., Ramirez-Camacho, M.A., Alvarez-Sánchez, M.E., 2019. Role of matrix metalloproteinases in angiogenesis and cancer. *Frontiers in Oncology*, 9, 1370. <https://doi.org/10.3389/fonc.2019.01370>
- Quy, T. and Xuan, T., 2019. Xanthine Oxidase Inhibitory Potential, Antioxidant and Antibacterial Activities of *Cordyceps militaris* (L.) Link Fruiting Body. *Medicines*. 6(1), 20.
- Rahayu, A.A.D., Prihantini, A.I., Krisnawati, Nugraheni, Y.M.M.A., 2022. Chemical components of different parts of *Strychnos ligustrina*, a medicinal plant from Indonesia. *IOP Conference Series: Earth and Environmental Science*, 959, 012061. <https://doi.org/10.1088/1755->

Rahmatullah, M., Mollik, A.H., Paul, A.K., Jahan, R., Khatun, A. and Seraj, S., 2010. A comparative analysis of medicinal plants used to treat gastrointestinal disorders in two sub-districts of greater Khulna division, Bangladesh. *Advances in Natural and Applied Sciences*, 4(1), 22.

Rakhee, Mishra, J., Sharma, R.K. and Misra, K. 2018. Characterization techniques for herbal products. *management of high altitude pathophysiology*, 171-202.

Raman, N., 2012. Isolation of chemical compound from methanol extract of *Peperomia pellucida*. <https://doi.org/10.13140/RG.2.1.4737.2888>

Ramasamy, R., Yan, S.F. and Schmidt, A.M., 2011. Receptor for AGE (RAGE): Signaling mechanisms in the pathogenesis of diabetes and its complications. *Annals of the New York Academy of Sciences*, 1243, 88-102.

Rasheed, Z., Akhtar, N. and Haqqi, T.M., 2011. Advanced glycation end products induce the expression of interleukin-6 and interleukin-8 by receptor for advanced glycation end product-mediated activation of mitogen-activated protein kinases and nuclear factor- κ B in human osteoarthritis chondrocytes. *Rheumatology (Oxford)*. 50(5), 838-51. <https://doi.org/10.1093/rheumatology/keq380>

Rasoanaivo, P., Wright, C.W., Willcox, M.L. and Gilbert, B., 2011. Whole plant extracts versus single compounds for the treatment of malaria:

Synergy and positive interactions. *Malaria Journal*, 10(1), 4.

Re, R., Pellegrini, N., Proteggente, A., Pannala, A., Yang, M. and Rice-Evans, C., 1999. Antioxidant activity applying an improved ABTS radical cation decolorization assay. *Free Radical Biology and Medicine*, 26(9-10), 1231-1237.

Réb , C., V gran, F., Berger, H. and Ghiringhelli, F., 2013. STAT3 activation. *JAK-STAT*. 2(1), e23010. <https://doi.org/10.4161/jkst.23010>

Reiniger, N., Lau, K., McCalla, D., Eby, B., Cheng, B., Lu, Y., Qu, W., Quadri, N., Ananthakrishnan, R., Furmansky, M., Rosario, R., Song, F., Rai, V., Weinberg, A., Friedman, R., Ramasamy, R., D'Agati, V., Schmidt, A.M., 2010. Deletion of the receptor for advanced glycation end products reduces glomerulosclerosis and preserves renal function in the diabetic OVE26 mouse. *Diabetes*, 59, 2043-2054.

Rezazi, S., Abdelmalek, S. and Hanini, S., 2017. Kinetic Study and Optimization of Extraction Process Conditions. *Energy Procedia*, 139(2017), 98-104.

Rezzola, S., Loda, A., Corsini, M., Semeraro, F., Annese, T., Presta, M. and Ribatti, D., 2020. Angiogenesis-inflammation cross talk in diabetic retinopathy: Novel insights from the chick embryo chorioallantoic membrane/human vitreous platform. *Frontiers in Immunology*, 11, 581288. <https://doi.org/10.3389/fimmu.2020.581288>.

Rhee, S.Y. and Kim, Y.S., 2018. The role of advanced glycation end products in diabetic vascular complications. *Diabetes and Metabolism Journal*, 42(3), 188-195.

Ricciotti, E. and Fitzgerald, G.A., 2011. Prostaglandins and Inflammation. *Arteriosclerosis, Thrombosis and Vascular Biology*, 31(5), 986-1000.

Riyadi, S. A., Naini, A. A. and Supratman, U., 2023. Sesquiterpenoids from Meliaceae family and their biological activities. *Molecules (Basel, Switzerland)*, 28(12), 4874.
<https://doi.org/10.3390/molecules28124874>

Robinson, M.L., Schillmiller, A.L. and Wetzel, W.C., 2022. A domestic plant differs from its wild relative along multiple axes of within-plant trait variability and diversity. *Ecology and Evolution*, 12(1), e8545.
<https://doi.org/10.1002/ece3.8545>

Rockwood, A. L., Kushnir, M. M. and Clarke, N. J., 2018. Mass spectrometry. *Principles and Applications of Clinical Mass Spectrometry: Small Molecules, Peptides, and Pathogens*, 33-65.

Rodebush, W. H. and Feldman, I., 1946. Ultraviolet absorption spectra of organic molecules. III. Mechanical interference of substituent groups with resonance configurations. *Journal of the American Chemical Society*, 68(5), 896-899.

Rojas-Martínez, R., Arrieta, J., Cruz-Antonio, L., Arrieta-Baez, D., Velázquez-Méndez, A. M. and Sánchez-Mendoza, M. E., 2013. Dillapiole, isolated from *Peperomia pellucida*, shows gastroprotector activity against ethanol-induced gastric lesions in wistar rats. *Molecules*. 18(9), 11327-37

Roman, H., Niculescu, A. G., Lazăr, V. and Mitache, M. M., 2023. Antibacterial efficiency of *Tanacetum vulgare* essential oil against

ESKAPE pathogens and synergisms with antibiotics. *Antibiotics (Basel, Switzerland)*, 12(11), 1635.
<https://doi.org/10.3390/antibiotics12111635>

Romero, H., Pott, D.M., Vallarino, J.G. and Osorio, S., 2021. Metabolomics-based evaluation of crop quality changes as a consequence of climate change. *Metabolites*, 11(461), 1-31.

Roshidi, M.A.H., Mahyuddin, H.S., Mohamad, M.A.N. and Noh, A.L., 2020. The effect of different fertilizer and extraction method on secondary metabolites of *Azolla Pinnata*. *Acta Chemica Malaysia*. 4(1), 28-32.
<https://doi.org/10.2478/acmy-2020-0005>

Roslida, A.H. and Aini, N.Z., 2009. Evaluation of Gastroprotective Effect of the Ethanolic Extract of *Peperomia pellucida* (L) Kunth. *Pharmacologyonline*, 2(2009), 678-686.

Rouzer, C.A. and Marnett, L.J., 2009. Cyclooxygenases: structural and functional insights. *Journal of Lipid Research*, 50:S29-34.
<https://doi.org/10.1194/jlr.R800042-JLR200>

Rübsam, A., Parikh, S. and Fort, P.E., 2018. Role of inflammation in diabetic retinopathy. *International Journal of Molecular Sciences*, 19(4), 942. <https://doi.org/10.3390/ijms19040942>.

Ruysschaert, S., van Andel, Tinde, Van de Putte, K. and Van Damme, P., 2009. Bathe the baby to make it strong and healthy: Plant use and child care among Saramaccan Maroons in Suriname. *Journal of Ethnopharmacology*, 121(1), 148-170.

Safi, S.Z., Qvist, R., Kumar, S., Batumalaie, K. and Ismail, I.S.B., 2014.

Molecular mechanisms of diabetic retinopathy, general preventive strategies, and novel therapeutic targets. *BioMed Research International*, 2014, e1-18.

Sahgal, G., Ramanathan, S., Sasidharan, S., Mordi, M. N., Ismail, S. and Mansor, S. M., 2010. Brine shrimp lethality and acute oral toxicity studies on *Swietenia mahagoni* (Linn.) Jacq. seed methanolic extract. *Pharmacognosy Research*, 2(4), 215-220.

Saide, A., Lauritano, C. and Ianora, A., 2020. Pheophorbide a: State of the art. *Marine Drugs*. 18(5), 257. <https://doi.org/10.3390/md18050257>

Saito, S., Numadate, N., Teraoka, H., Enami, S., Kobayashi, H. and Hama, T., 2023. Impurity contribution to ultraviolet absorption of saturated fatty acids. *Science Advances*, 9(38), eadj6438. <https://doi.org/10.1126/sciadv.adj6438>.

Sakamoto, S., Putalun, W., Vimolmangkang, S., Phoolcharoen, W., Shoyama, Y., Tanaka, H. and Morimoto, S., 2018. Enzyme-linked immunosorbent assay for the quantitative/qualitative analysis of plant secondary metabolites. *Journal of Natural Medicines*, 72(1), 32-42. <https://doi.org/10.1007/s11418-017-1144-z>

Sakti, A. S., Widyastanto, H., Maulidina, A., Mitasari, D., Eriyani, D. S. and Mun'im, A., 2020. Xanthine oxidase inhibitory activity of methanol extract fractions of various Indonesian ethnopharmacological plants. *International Journal of Applied Pharmaceutics*, 12(1), 43-46.

- Saldanha, A.A., Vieira, L., Maia, D.S.S., Oliveira, F.M., Ribeiro, R.M.A., Thome, R.G., Santos, H.B., Lopes, D.O., Carollo, C.A., Silva, D.B., Soares, A.C. and Siqueira, J.M., 2020. Anti-inflammatory and antinociceptive activities of a phenylpropanoid-enriched fraction of *Duguetia furfuracea*. *Inflammopharmacology*, 29(2), 409-422.
- Salma, N, Paendong, J., Momuat, L.I. and Togubu, S., 2013. Antihiperглиkemik ekstrak tumbuhan Suruhan (*Peperomia pellucida* [L.] Kunth terhadap tikus Wistar (*Rattus norvegicus* L.) yang diinduksi sukrosa. *Jurnal Ilmiah Sains*, 13(2), 116-123.
- Samuel, W., Jaworski, C., Postnikova, O.A., Kutty, R.K., Duncan, T., Tan, L.X., Poliakov, E., Lakkaraju A. and Redmond, T.M., 2017. Appropriately differentiated ARPE-19 cells regain phenotype and gene expression profiles similar to those of native RPE cells. *Molecular Vision*, 23, 60-89.
- Sana, T.R., Roark, J.C., Li, X.D., Waddell, K. and Fischer, S.M., 2008. Molecular Formula and METLIN Personal Metabolite Database Matching Applied to the Identification of Compounds Generated by LC/TOF-MS. *Journal of Biomolecular Techniques*, 19(4), 258-266.
- Santiago, M. and Strobel, S., 2013. Thin layer chromatography. *Methods in Enzymology*, 303-324.
- Santos, R. C., Chagas, E.A., Filho, A.A.M., Takahashi, J.A., Montero, I.F., Santos, G.F., Chagas, P.C. and Melo, A.C.G.R., 2018. Chemical characterization of oils and fats from amazonian fruits by ¹H NMR.

Chemical Engineering Transactions, 64, 235-240.

Sarah, Q.S., Anny, F.C. and Misbahuddin, M., 2017. Brine shrimp lethality assay. *Bangladesh Journal of Pharmacology*, 12, 186-189.

Schmidt, A.M., 2015. Soluble RAGEs - Prospects for treating and tracking metabolic and inflammatory disease. *Vascular Pharmacology*, 72, 1-8.

Senanayake, P.D.S., Calabro, A., Nishiyama, K., Hu, J.G., Bok, D. and Hollyfield, J.G., 2001. Glycosaminoglycan synthesis and secretion by the retinal pigment epithelium: Polarized delivery of hyaluronan from the apical surface. *Journal of Cell Science*, 114, 199-205.

Sethi, G., Chatterjee, S., Rajendran, P., Li, F., Shanmugam, M.K., Wong, K.F., Kumar, A.P., Senapati, P., Behera, A.K., Hui, K.M., Basha, J., Natesh, N., Luk, J.M. and Kundu, T.K., 2014. Inhibition of STAT3 dimerization and acetylation by garcinol suppresses the growth of human hepatocellular carcinoma *in vitro* and *in vivo*. *Molecular Cancer*. 13, 66. <https://doi.org/10.1186/1476-4598-13-66>

Shalaby, E.A. and Shanab, S.M.M., 2013. Comparison of DPPH and ABTS assays for determining antioxidant potential of water and methanol extracts of *Spirulina platensis*. *Indian Journal of Marine Sciences*, 42(5), 556-564.

Sharma, M., Chahal, K.K., Kaur, R., Singh, R. and Kataria, D., 2019. Antifungal potential and structure activity relationship of carrot seed constituents. *Journal of Food Biochemistry*, 43(9), e12971. <https://doi.org/10.1111/jfbc.12971>

- Sheikh, H., Sikder, S., Paul, S.K., Hasan, A.M.R., Rahaman, M.M., Kundu, S.P., 2013. Hypoglycaemic, anti-inflammatory and analgesic activity of *Peperomia pellucida* (L.) HBK (Piperaceae). *International Journal of Pharmaceutical Science Research*, 4, 458-463
- Shen, C.H., 2019a. Chapter 6 - Extraction and purification of nucleic acids and proteins. In Shen, C.H. (ed.) *Diagnostic Molecular Biology*. 143-166. Academic Press. doi: 10.1016/B978-0-12-802823-0.00006-7
- Shen, C.H., 2019b. Chapter 8 - Quantification and analysis of proteins. In Shen, C.H. (ed.) *Diagnostic Molecular Biology*. 187-214. Academic Press. doi: 10.1016/B978-0-12-802823-0.00008-0
- Shi, Y., Zhang, Y., Li, Y. and Tong, C., 2019. Sauchinone inhibits high glucose-induced oxidative stress and apoptosis in retinal pigment epithelial cells. *The Royal Society of Chemistry*, 9, 17068-17071. <https://doi.org/10.1039/c9ra02817j>.
- Shojaei, T. R. and Azhari, S., 2018. Fabrication, functionalization, and dispersion of carbon nanotubes. *Emerging Applications of Nanoparticles and Architectural Nanostructures: Current Prospects and Future Trends*, 501-531.
- Siddhuraju, P. and Manian, S., 2007. The antioxidant activity and free radical-scavenging capacity of dietary phenolic extracts from horse gram (*Macrotyloma uniflorum* (Lam.) Verdc.) seeds. *Food Chemistry*, 105(3), 950-958. <https://doi.org/10.1016/j.foodchem.2007.04.040>

- Silva, J. K., da Trindade, R., Alves, N.S., Figueiredo, P.L., Maia, J.G.S. and Setzer, W.N., 2017. Essential oils from neotropical *Piper* species and their biological activities. *International Journal of Molecular Sciences*, 18(12), 2571.
- Silva, L.B., Neto, A.P.d.S., Maia, S.M.A.S., Guimarães, C.d.S., Quidute, I.L., Carvalho, A.d.A.T., Júnior, S.A. and Leão, J.C., 2019. The Role of TNF- α as a Proinflammatory Cytokine in Pathological Processes. *The Open Dentistry Journal*, 13, 332-338.
- Silva, M.T., 2010. When two is better than one: macrophages and neutrophils work in concert in innate immunity as complementary and cooperative partners of a myeloid phagocyte system. *Journal of Leukocyte Biology*, 87(1), 93-106. <https://doi.org/10.1189/jlb.0809549>
- Silva, R.A.C., Mesquita, B.M., Farias, I.F., Nascimento, P.G.G., Lemos, T.L.G. and Monte, F.J.Q., 2018. Enzymatic chemical transformations of aldehydes, ketones, esters and alcohols using plant fragments as the only biocatalyst: *Ximenia americana* grains. *Molecular Catalysis*. 445(2018), 187-194. <https://doi.org/10.1016/j.mcat.2017.11.033>
- Sim, D.Y., Lee, H.J., Jung, J.H., Im, E., Hwang, J., Kim, D.S. and Kim, S.H., 2019. Suppression of STAT3 phosphorylation and RelA/p65 acetylation mediated by microRNA134 plays a pivotal role in the apoptotic effect of lambertianic acid. *International Journal of Molecular Sciences*. 20(12), 2993. <https://doi.org/10.3390/ijms20122993>.
- Singh, H. and Agrawal, D.K., 2022. Therapeutic potential of targeting the receptor for advanced glycation end products (RAGE) by small molecule inhibitors. *Drug Development Research*. 83(6), 1257-1269. <https://doi.org/10.1002/ddr.21971>.

- Singh, J.K., Simoes, B.M., Sacha, J.H., Farnie, G. and Clarke, R.B., 2013. Recent advances reveal IL-8 signaling as a potential key to targeting breast cancer stem cells. *Breast Cancer Research*, 15(4), 210. <https://doi.org/10.1186/bcr3436>
- Singh, S., Anshita, D., Ravichandiran, V., 2021. MCP-1: Function, regulation, and involvement in disease. *International Immunopharmacology*, 101, 107598. <https://doi.org/10.1016/j.intimp.2021.107598>
- Singleton, V.L. and Rossi, J.A.J., 1965. Colorimetry to total phenolics with phosphomolybdic acid reagents. *American Journal of Enology and Viniculture*, 16, 144-158.
- Soares, S., Brandão, E., Guerreiro, C., Soares, S., Mateus, N. and de Freitas, V., 2020. Tannins in food: Insights into the molecular perception of astringency and bitter taste. *Molecules*, 25(11), 2590. <https://doi.org/10.3390/molecules25112590>.
- Sobolev, V., Nesterova, A., Soboleva, A., Dvoriankova, E., Piruzyan, A., Mildzikhova, D., Korsunskaya, I. and Svitich, O., 2020. The model of PPAR γ -downregulated signaling in psoriasis. *PPAR Research*, 2020, 6529057. <https://doi.org/10.1155/2020/6529057>.
- Sofowora, A., Ogunbodede, E. and Onayade, A., 2013. The Role and Place of Medicinal Plants in the Strategies for Disease Prevention. *African Journal of Traditional, Complementary and Alternative Medicine*, 10(5), 210-229.
- Srivastava, N., Singh, A., Kumari, P., Nishad, J.H., Gautam, V.S., Yadav, M., Bharti, R., Kumar, D. and Kharwar, R.N., 2021. Advances in

extraction technologies: isolation and purification of bioactive compounds from biological materials. *Natural Bioactive Compounds*, 409-433.

Stalikas, C. D., 2007. Extraction, separation, and detection methods for phenolic acids and flavonoids. *Journal of Separation Science*, 30(18), 3268-3295.

Stark, N. M., Yelle, D. J. and Agarwal, U. P., 2016. Techniques for characterizing lignin. *Lignin in Polymer Composites*, 49-66.

Starowicz, M. and Zieliński, H., 2019. Inhibition of advanced glycation end-product formation by high antioxidant-leveled spices commonly used in European cuisine. *Antioxidants*, 8(4), 100.

Stitt, A.W., Curtis, T.M., Chen, M., Medina, R.J., McKay, G.J., Jenkins, A., Gardiner, T.A., Lyons, T.J., Hammes, H.P., Simo, R. and Lois, N., 2016. The progress in understanding and treatment of diabetic retinopathy. *Progress in retinal and eye research*, 51, 156-186.

Sulistiyani, Safithri, M. and Sari, Y.P., 2016. Inhibition of α -glucosidase activity by ethanolic extract of *Melia azedarach* L. leaves. *IOP Conference Series: Earth and Environmental Science*, 31(2016), 012025.

Sun, M., Li, Y., Bu, W., Zhao, J., Zhu, J., Gu, L., Zhang, P. and Fang, Z. 2017. DJC suppresses advanced glycation end products-induced JAK-STAT signaling and ROS in mesangial cells. *Evidence-Based Complementary and Alternative Medicine*, 2017, 2942830.

<https://doi.org/10.1155/2017/2942830>

Sun, S.C., Chang, J.H. and Jin, J., 2013. Regulation of nuclear factor- κ B in autoimmunity. *Trends in Immunology*, 34(6), 282-289.

<https://doi.org/10.1016/j.it.2013.01.004>.

Sun, W., Kim, D.H., Byon, C.H., Choi, H.I., Park, J.S., Bae, E.H., Ma, S.K. and Kim, S.W., 2022. β -elemene attenuates renal fibrosis in the unilateral ureteral obstruction model by inhibition of STAT3 and Smad3 signaling via suppressing MyD88 expression. *International Journal of Molecular Sciences*, 23(10), 5553.

<https://doi.org/10.3390/ijms23105553>

Supriatno and Lelifajri, L., 2018. Effect of sequential extraction on total phenolic content (TPC) and antioxidant activities (AA) of *Luffa acutangula* Linnaeus dried pulps. *AIP Conference Proceedings*, 2002(1), 020062.

Suryavanshi, S.V. and Kulkarni, Y.A., 2017. NF- κ B: A potential target in the management of vascular complications of diabetes. *Frontiers in Pharmacology*, 8, 798. <https://doi.org/10.3389/fphar.2017.00798>

Susilawati, Y., Nugraha, R., Krishnan, J., Muhtadi, A., Sutardjo, S. and Supratman, U., 2017. A new Antidiabetic compound 8, 9-dimethoxy ellagic acid from Sasaladaan. *Research Journal of Pharmaceutical, Biological and chemical Sciences*, 2017:269-274

Taghavi, Y., Hassanshahi, G., Kounis, N.G., Koniari, I. and Khorramdelazad,

H., 2019. Monocyte chemoattractant protein-1 (MCP-1/CCL2) in diabetic retinopathy: Latest evidence and clinical considerations. *Journal of Cell Communication and Signaling*, 13(4), 451-462. <https://doi.org/10.1007/s12079-018-00500-8>.

Tahoun, M., Gee, C.T., McCoy, V.E., Sander, P.M. and Muller, C.E., 2021. Chemistry of porphyrins in fossil plants and animals. *RSC Advances*, 11(13), 7552-7563.

Takahashi, E. and Tanihara, H., 2012. Hyaluronic Acid as a Contributing Factor to Epithelial-Mesenchymal Transition in Retinal Pigment Epithelial Cells and Angiogenesis. *Investigative Ophthalmology & Visual Science*, 53(14), 2553.

Tarr, J.M., Kaul, K., Chopra, M., Kohner, E.M. and Chibber, R., 2013. Pathophysiology of Diabetic Retinopathy. *ISRN Ophthalmology*, 2013, e1-13.

Telagari, M. and Hullatti, K., 2015. *In-vitro* α -amylase and α -glucosidase inhibitory activity of *Adiantum caudatum* Linn. and *Celosia argentea* Linn. extracts and fractions. *Indian Journal of Pharmacology*. 47(4), 425-429.

Teoh, L., Gnanasegaran, N., Adnan, A.F.M. and Taha, R.M. 2021. The comparative antimicrobial and anticancer of chemical extract from *in vitro* and *in vivo* *Peperomia pellucida* plantlet. *Journal of Applied Biology and Biotechnology*, 9(2), 115-123.

Termote, C., van Damme, P. and Djailo, B. D. a., 2010. Eating from the wild: Turumbu indigenous knowledge on noncultivated edible plants,

Tshopo district, DR Congo. *Ecology of Food and Nutrition*, 49(3), 173-207.

Thoss, V., Murphy, P.J., Marriot, R. and Wilson, T., 2012. Triacylglycerol composition of British bluebell (*Hyacinthoides non-scripta*) seed oil. *RSC Advances*, 2(12), 5314.

Tilvi, S., Majik, M. S. and Singh, K. S., 2014. Mass spectrometry for determination of bioactive compounds. *Comprehensive Analytical Chemistry*, 65, 193-218.

Ting, D.S.W., Cheung, G.C.M. and Wong, T.Y., 2016. Diabetic retinopathy: global prevalence, major risk factors, screening practices and public health challenges: a review. In *Clinical and Experimental Ophthalmology*, 44(4), 260-277.

Tóbon-Velasco, J.C., Cuevas, E. and Torres-Ramos, M.A., 2014. Receptor for AGEs (RAGE) as mediator of NF-κB pathway activation in neuroinflammation and oxidative stress. *CNS Neurological Disorders and Drug Targets*. 13(9), 1615-1626.
<https://doi.org/10.2174/1871527313666140806144831>.

Togubu. S., Momuat, L.I., Paendong, J.E. and Salma, N., 2013. Aktivitas antihiperqlikemik dari ekstrak etanol dan heksana tumbuhan suruhan (*Peperomia pellucida* [L.] Kunth) pada tikus Wistar (*Rattus norvegicus* L.) yang hiperqlikemik. *Jurnal Mipa Unsrat Online*, 2,109-114

Tokeshi, I., Yoshimoto, T., Muto, N., Nakamura, S., Ashizawa, K., Nakada, T. and Tatemoto, H., 2007. Antihyaluronidase action of ellagic acid effectively prevents polyspermy as a result of suppression of the acrosome reaction induced by sperm-zona interaction during in vitro

fertilization of porcine oocytes. *The Journal of Reproduction and Development*. 53(4), 755-64.

Toni, L.S., Garcia, A.M., Jeffrey, D.A., Jiang, X., Stauffer, B.L., Miyamoto, S.D. and Sucharov, C.C., 2018. Optimization of phenol-chloroform RNA extraction. *MethodsX*, 5(2018), 599-608. <https://doi.org/10.1016/j.mex.2018.05.011>

Tsuboi, K., Hilligsmann, C., Vandevoorde, S., Lambert, D.M. and Ueda, N., 2004. N-cyclohexanecarbonylpentadecylamine: a selective inhibitor of the acid amidase hydrolysing N-acylethanolamines, as a tool to distinguish acid amidase from fatty acid amide hydrolase. *Biochemical Journal*, 379(1), 99-106. <https://doi.org/10.1042/BJ20031695>.

Upadhyay, R., Chaurasia, J.K., Tiwari, K.N. and Singh, K., 2014. Antioxidant property of aerial parts and root of phyllanthus fraternus webster, an important medicinal plant. *The Scientific World Journal*, 2014, e1-7.

Usman, L. A. and Ismaeel, R. O., 2020. Chemical composition of root essential oil of *Peperomia pellucida* (L.) Kunth. grown in Nigeria. *Journal of Essential Oil-Bearing Plants*, 23(3), 628-632.

Uzodimma, D.E., 2013. Medico-Ethnobotanical inventory of Ogii , Okigwe Imo State , South Eastern Nigeria - I. *Global advanced research journal of medicinal plants*, 2(2), 30-44.

Valdivieso-Ugarte, M., Gomez-Llorente, C., Plaza-Diaz, J. and Gil, A., 2019. Antimicrobial, antioxidant, and immunomodulatory properties of essential oils: A systematic review. *Nutrients*. 11(11), 2786.

- Vandebroek, I., Balick, M.J., Ososki, A., Kronenberg, F., Yukes, J., Wade, C., Jimenez, F., Peguero, B. and Castillo, D., 2010. The importance of botellas and other plant mixtures in Dominican traditional medicine. *Journal of Ethnopharmacology*, 128(1), 20-41.
- Vanhooren, V., Santos, A.V., Voutetakis, K., Petropoulos, I., Libert, C., Simm, A., Gonos, E.S. and Friguet, B., 2015. Protein modification and maintenance systems as biomarkers of ageing. *Mechanisms of Ageing and Development*, 151(2015), 71-84. <https://doi.org/10.1016/j.mad.2015.03.009>.
- Velasquez, M., 2015. Oxidative Stress. In Kimmel, P.L. and Rosenberg, M.R. (ed.) *Chronic Renal Disease*. Elsevier.
- Verma, R.S., Padalia, R.C., Goswami, P. and Chauhan, A., 2015. Essential oil composition of *Peperomia pellucida* (L.) Kunth from India. *Journal of Essential Oil Research*, 27, 89-95
- Vittum, P.J., 2009. Chapter 238 - Soil habitats. In Resh, V.H. and Cardé, R.T. (eds.) *Encyclopedia of Insects (Second Edition)*. 935-939. Academic Press. <https://doi.org/10.1016/B978-0-12-374144-8.00247-2>
- Vučković, I., Stiković, S., Stesević, D., Jadranin, M. and Trifunović, S., 2021. Phytochemical investigation of *Pimpinella serbica*. *Journal of the Serbian Chemical Society*, 86(12), 1241-1247.
- Wacker, M.J. and Godard, M.P., Analysis of one-step and two-step real-time RT-PCR using SuperScript III. *Journal of Biomolecular Techniques*,

16(3), 266-271.

Wang, J., Xu, X., Elliott, M.H., Zhu, M. and Le, Y.Z., 2010. Müller cell-derived VEGF is essential for diabetes-induced retinal inflammation and vascular leakage. *Diabetes*, 59(9), 2297-2305.

Wang, P., Xing, Y., Chen, C., Chen, Z. and Qian Z., 2016. Advanced glycation end-product (AGE) induces apoptosis in human retinal ARPE-19 cells via promoting mitochondrial dysfunction and activating the Fas-FasL signaling. *Bioscience, Biotechnology, and Biochemistry*, 80(2):250-6. <https://doi.org/10.1080/09168451.2015.1095065>.

Wang, S., Ling, Y., Yao, Y., Zheng, G. and Chen, W., 2020. Luteolin inhibits respiratory syncytial virus replication by regulating the MiR-155/SOCS1/STAT1 signaling pathway. *Virology Journal*, 17(1), 187. <https://doi.org/10.1186/s12985-020-01451-6>.

Wang, S.S., Liao, X., Liu, F., Zhang, Q., Qiu, J.J. and Fu, S.H., 2021a. miR-132 mediates cell permeability and migration by targeting occludin in high-glucose-induced ARPE-19 cells. *Endocrine Journal*, 68(5), 531-541. <https://doi.org/10.1507/endocrj.EJ20-0277>

Wang, S.H., Sun, Z.L., Guo, Y.J., Yuan, Y. and Li, L., 2009. PPARgamma-mediated advanced glycation end products regulation of neural stem cells. *Molecular and Cellular Endocrinology*, 307(1-2), 176-84. <https://doi.org/10.1016/j.mce.2009.02.012>.

Wang, W. and Lo, A.C.Y., 2018. Diabetic Retinopathy: Pathophysiology and

Treatments. *International Journal of Molecular Sciences*, 19(6), 1816.

Wang, Y., Li, N., Wang, Y., Zheng, G., An, J., Liu, C., Wang, Y. and Liu, Q., 2021b. NF- κ B/p65 competes with peroxisome proliferator-activated receptor gamma for transient receptor potential channel 6 in hypoxia-induced human pulmonary arterial smooth muscle cells. *Frontiers in Cell and Developmental Biology*, 9, 656625. <https://doi.org/10.3389/fcell.2021.656625>

Wang, Y., Zhang, W., Zhao, H., Wang, Y., Lu, C., Li, X., Wang, Y., Xiao, Y., Wang, Y. and Wang, B., 2018. Fasting blood soluble RAGE may be causally implicated in impaired glucose metabolism in Chinese patients with primary hypertension. *Gene*. 639, 11-17. <https://doi.org/10.1016/j.gene.2017.09.066>

Waty, D.R., Saputri, F.C. and Mun'im, A., 2017. Secondary metabolites screening and acute toxicity test of *Peperomia pellucida* (L.) Kunth methanolic extracts. *International Journal of PharmTech Research*, 10(1), 31-38.

Wei, L.S., Wee, W., Siong, J.Y.F. and Syamsumir, D.F., 2011. Characterization of anticancer, antimicrobial, antioxidant properties and chemical compositions of *Peperomia pellucida* leaf extract. *Acta Medica Iran*, 49, 670-674.

White, D.E., Stewart, I.C., Seashore-Ludlow, B.A., Grubbs, R.H. and Stoltz, B.M., 2010. A general enantioselective route to the chamigrene natural product family. *Tetrahedron*, 66(26), 4668-4686.

<https://doi.org/10.1016/j.tet.2010.04.128>

Wibisono, K., Aisyah, S.I., Suhesti, S. and Nurcholis, W., 2019. Optimization of total flavonoids extraction and A-glucosidase inhibitory activity from *Plectranthus amboinicus* (Lour.) Spreng. leaves using the simplex-centroid design. *Molekul*, 14(2), 84-91.

Wilkinson, C.R., Bower, L.M. and Warren, C., 1996. Measurement of hyaluronidase activity in normal human serum. *Journal of Pharmaceutical and Biomedical Analysis*, 14(6), 707-712.

Winter, D. and Steen, H., 2011. Optimization of cell lysis and protein digestion protocols for the analysis of HeLa S3 cells by LC-MS/MS. *Proteomics*, 11(24), 4726-4730. <https://doi.org/10.1002/pmic.201100162>.

Wiraswati, H.L., Fauziah, N., Pradini, G.W., Kurnia, D., Kodir, R.A., Berbudi, A., Arimdayu, A.R., Laelalugina, A., Supandi and Ma'ruf I.F., 2023. *Breynia cernua*: Chemical profiling of volatile compounds in the stem extract and its antioxidant, antibacterial, antiplasmodial and anticancer activity *in vitro* and *in silico*. *Metabolites*. 13(2), 281. <https://doi.org/10.3390/metabo13020281>

Wolk, A., Hatipoglu, D., Cutler, A., Ali, M., Bell, L., Qi, J.H., Singh, R., Batoki, J., Karle, L., Bonilha, V.L., Wessely, O., Stoehr, H., Hascall, V. and Anand-Apte, B., 2020. Role of FGF and Hyaluronan in Choroidal Neovascularization in Sorsby Fundus Dystrophy. *Cells*. 9(3), 608.

- Wu, C., 2014. An important player in brine shrimp lethality bioassay: The solvent. *Journal of Advanced Pharmaceutical Technology and Research*, 5(1), 57-58.
- Widyawati, P.S., Budianta, T.D.W., Kusuma, F.A. and Wijaya, E.L., 2014. Difference of Solvent Polarity To Phytochemical Content and Antioxidant Activity of *Pluchea indica* Less Leaves Extracts. *International Journal of Pharmacognosy and Phytochemical Research*, 6(4), 850-855.
- Wisastra, R. and Dekker, F.J., 2014. Inflammation, cancer and oxidative lipooxygenase activity are intimately linked. *Cancers*. 6(3), 1500-1521.
- Xie, C., Wang, S., Cao, M., Xiong, W. and Wu, L., 2022. (E)-9-octadecenoic acid ethyl ester derived from lotus seedpod ameliorates inflammatory responses by regulating MAPKs and NF- κ B signalling pathways in LPS-induced RAW264.7 macrophages.. *Evidence-Based Complementary and Alternative Medicine*, 2022, 6731360.
- Xu, D.P., Li, Y., Meng, X., Zhou, T., Zhou, Y., Zheng, J., Zhang, J.J. and Li, H.B., 2017. Natural Antioxidants in Foods and Medicinal Plants: Extraction, Assessment and Resources. *International Journal of Molecular Sciences*, 18(1), 96.
- Xu, J., Chen, L.J., Yu, J., Wang, H.J., Zhang, F., Liu, Q. and Qu, J., 2018. Involvement of Advanced Glycation End Products in the Pathogenesis of Diabetic Retinopathy. *Cellular Physiology and Biochemistry*. 48(2), 705-717.
- Xu, S., Li, N., Ning, M. M., Zhou, C. H., Yang, Q.R., Wang, M.W., 2006. Bioactive compounds from *Peperomia pellucida*. *Journal of Natural Products*, 69, 247-250.

Yahia, Y., Benabderrahim, M.A., Tlili, N., Bagues, M. and Nagaz, K., 2020. Bioactive compounds, antioxidant and antimicrobial activities of extracts from different plant parts of two *Ziziphus* Mill. species. *PLoS ONE*, 15(5), e0232599.

Yamagishi, S., Maeda, S., Matsui, T., Ueda, S., Fukami, K. and Okuda, S., 2012. Role of advanced glycation end products (AGEs) and oxidative stress in vascular complications in diabetes. *Biochimica et Biophysica Acta (BBA) – General Subjects*, 1820(5), 663-671. <https://doi.org/10.1016/j.bbagen.2011.03.014>

Yan, L.J., 2014. Pathogenesis of chronic hyperglycaemia: From reductive stress to oxidative stress. *Journal of Diabetes Research*, 2014, e1-11

Yan, L., 2018. Redox imbalance stress in diabetes mellitus: Role of the polyol pathway. *Animal Models and Experimental Medicine*, 1(1), 7-13.

Yang, J., Zhang, L., Yu, C., Yang, X.F. and Wang, H., 2014. Monocyte and macrophage differentiation: circulation inflammatory monocyte as biomarker for inflammatory diseases. *Biomarker Research*, 2(1), 1. <https://doi.org/10.1186/2050-7771-2-1>.

Yang, R., Wang, L., Sheng, J., Huang, Q., Pan, D., Xu, Y., Yan, J., Wang, X., Dong, Z. and Yang, M., 2019. Combinatory effects of vaccinia virus VG9 and the STAT3 inhibitor Stattic on cancer therapy. *Archives of Virology*. 164, 1805–1814. <https://doi.org/10.1007/s00705-019-04257-2>

Yang, S., Zhao, J. and Sun, X., 2016. Resistance to anti-VEGF therapy in

neovascular age-related macular degeneration: A comprehensive review. *Drug Design, Development and Therapy*, 10, 1857-1867.

Yang, X., Bao, M., Fang, Y., Yu, X., Ji, J. and Ding, X., 2021. STAT3/HIF-1 α signaling activation mediates peritoneal fibrosis induced by high glucose. *Journal of Translational Medicine*, 19, 283. <https://doi.org/10.1186/s12967-021-02946-8>

Yao, D. and Brownlee, M., 2010. Hyperglycemia-induced reactive oxygen species increase expression of the receptor for advanced glycation end products (RAGE) and RAGE ligands. *Diabetes*, 59(1), 249-55. <https://doi.org/10.2337/db09-0801>.

Yao, D., Taguchi, T., Matsumura, T., Pestell, R., Edelstein, D., Giardino, I., Suske, G., RAbbani, N., Thornalley, P.J., Sarthy, V.P., Hammes, H.P. and Brownlee, M., 2007. High glucose increases angiotensin-2 transcription in microvascular endothelial cells through methylglyoxal modification of mSin3A. *Journal of Biological Chemistry*, 282(42), 31038-31045.

Yeh, W.J., Hsia, S.M., Lee, W.H. and Wu, C.H., 2017. Polyphenols with antiglycation activity and mechanisms of action: A review of recent findings. *Journal of Food and Drug Analysis*, 25(1), 84-92.

Youssef, D.A., El-Fayoumi, H.M. and Mahmoud, M.F., 2019. Beta-caryophyllene protects against diet-induced dyslipidemia and vascular inflammation in rats: Involvement of CB2 and PPAR- γ receptors. *Chemico-Biological Interactions*, 297, 16-24.

<https://doi.org/10.1016/j.cbi.2018.10.010>

Yu, X., Li, Z., Zhang, Y., Xu, M., Che, Y., Tian, X., Wang, R., Zou, K. and Zou, L., 2019. β -elemene inhibits radiation and hypoxia-induced macrophages infiltration via Prx-1/NF- κ B/HIF-1 α signaling pathway. *Onco Targets and Therapy*, 12, 4203-4211. <https://doi.org/10.2147/OTT.S196910>.

Zegeye, M.M., Lindkvist, M., Fälker, K., Kumawat, A.K., Paramel, G., Grenegård, M., Sirsjö, A. and Ljungberg, L.U., 2018. Activation of the JAK/STAT3 and PI3K/AKT pathways are crucial for IL-6 trans-signaling-mediated pro-inflammatory response in human vascular endothelial cells. *Cell Communication and Signaling*, 16, 55. <https://doi.org/10.1186/s12964-018-0268-4>.

Zhang, C., Wang, R., Zhang, G. and Gong, D., 2018. Mechanistic insights into the inhibition of quercetin on xanthine oxidase. *International Journal of Biological Macromolecules*. 112, 405-412. <https://doi.org/10.1016/j.ijbiomac.2018.01.190>

Zhang, D.Q., Wang, R., Li, T., Zhou, J.P., Chang, G.Q., Zhao, N., Yang, L.N., Zhai, H. and Yang, L., 2016c. Reduced soluble RAGE is associated with disease severity of axonal Guillain-Barré syndrome. *Scientific Reports*. 6, 21890. <https://doi.org/10.1038/srep21890>.

Zhang, H., Li, S., Bao, J., Ge, N., Hong, F. and Qian, L., 2021. β -elemene inhibits non-small cell lung cancer cell migration and invasion by inactivating the FAK-Src pathway., 2021. *Experimental and Therapeutic*

Medicine, 22(4), 1095. <https://doi.org/10.3892/etm.2021.10529>

Zhang, L.S., Wang, X. and Dong, L.L., 2011. Antioxidation and antiglycation of polysaccharides from *Misgurnus anguillicaudatus*. *Food Chemistry*. 124(1), 183-187.

Zhang, S., Gu, H. and Hu, N., 2015a. Role of peroxisome proliferator-activated receptor γ in ocular diseases. *Journal of Ophthalmology*, 2015, 275435. <https://doi.org/10.1155/2015/275435>

Zhang, S., Zhang, H., Chen, L., Xia, W. and Zhang, W., 2016a. Phytochemical profiles and antioxidant activities of different varieties of *Chimonanthus Praecox*. *Industrial Crops and Products*, 85, 11-21. <https://doi.org/10.1016/j.indcrop.2016.02.009>

Zhang, X., Retyunskiy, V., Qiao, S., Zhao, Y. and Tzeng, C.M., 2022b. Alloferon-1 ameliorates acute inflammatory responses in λ -carrageenan-induced paw edema in mice. *Scientific Reports*, 12(1), 16689. <https://doi.org/10.1038/s41598-022-20648-z>.

Zhang, Y., Huang, Q., Wang, S., Liao, Z., Jin, H., Huang, S., Hong, X., Liu, Y., Pang, J., Shen, Q., Wang, Q., Li, C. and Ji, L., 2022a. The food additive β -caryophyllene exerts its neuroprotective effects through the JAK2-STAT3-BACE1 pathway. *Frontiers in Aging Neuroscience*, 14, 814432. <https://doi.org/10.3389/fnagi.2022.814432>

Zhang, Y., Xiao, W., Ji, G., Chen, X., Han, L. and Gao, C., 2016b. Effects on physiochemical properties of black tea by mechanical superfine and general grinding. *Transactions of the Chinese Society of Agricultural Engineering*, 32(11), 295-301

Zhang, Y.J., Gan, R.Y., Li, S., Zhou, Y., Li, A.N., Xu, D.P. and Li, H.N., 2015b. Antioxidant phytochemicals for the prevention and treatment of

chronic diseases. *Molecules*. 20(12), 21138-21156.

Zhou, M., Geathers, J. S., Grillo, S. L., Weber, S. R., Wang, W., Zhao, Y. and Sundstrom, J. M., 2020a. Role of Epithelial-Mesenchymal Transition in Retinal Pigment Epithelium Dysfunction. *Frontiers in Cell and Development Biology*, 8,501.

Zhou, Y., Chen, J., Li, L.H. and Chen, L., 2020b. β -elemene down-regulates HIF-1 α , VEGF and iNOS in human retinal pigment epithelial cells under high glucose conditions. *International Journal of Ophthalmology*, 13(12), 1887-1894. <https://doi.org/10.18240/ijo.2020.12.07>.

Zong, H., Ward, M., Madden, A., Yong, P.H., Limb, G.A., Curtis, T.M. and Stitt, A.W., 2010. Hyperglycaemia-induced pro-inflammatory responses by retinal Müller glia are regulated by the receptor for advanced glycation end-products (RAGE). *Diabetologia*, 53(12), 2656-2666.

Zuccolotto, T., Bressan, J., Lourenço, A.V.F., Bruginski, E., Veiga, A., Marinho, J.V.N., Raeski, P.A., Heiden, G., Salvador, M.J., Murakami, F.S., Budel, J.M. and Campos, F.R., 2019. Chemical, antioxidant, and antimicrobial evaluation of essential oils and an anatomical study of the aerial parts from *Baccharis* species (Asteraceae). *Chemistry & biodiversity*, 16(4), e1800547. <https://doi.org/10.1002/cbdv.201800547>

Appendices

Appendix A1

Materials and reagents.

Phase of study	Materials and reagents	Brand (Manufacturing country)
Plant processing and extraction	Methanol	Merck Millipore (Massachusetts, U.S.)
	Chloroform	R & M Chemicals (London, U.K.)
	Ethyl acetate	
	Hexane	
	n-butanol	
Phase 1	COX colorimetric inhibitor screening assay kit	Cayman Chemicals (Michigan, U.S.)
	NADPH	
	Thiobarbituric acid	
	2, 4, 6-tripyridyl-s-triazine	Himedia (Maharashtra, India)
	D-glucose	
	Ferrous sulphate heptahydrate	
	Absolute EtOH	Merck Millipore (Massachusetts, U.S.)
	Folin-Ciocalteu reagent	
	Potassium persulfate	
	Sodium hydroxide	
	Calcium chloride	Nacalai Tesque (Kyoto, Japan)
	Sodium dodecyl sulphate	
	Starch	
	Brine shrimp eggs	Ocean Nutrition (Dartmouth, Canada)
	Bromocresol green	R & M Chemicals (London, U.K.)
Disodium tetraborate		

Glacial acetic acid	
Hydrochloric acid	
<i>p</i> -dimethylaminobenzaldehyde	
Potassium hydrogen phthalate	
Sodium acetate	
Sodium carbonate	
Sodium citrate	
Sulphuric acid	
ABTS diammonium salt	Roche (Basel, Switzerland)
3,5-dinitrosalicylic acid	Sigma-Aldrich (Missouri, U.S.)
4-Nitrophenyl α -D-glucoopyranoside	
Trolox	
α -amylase	
α -glucosidase	
Acetylsalicylic acid	
Ascorbic acid	
Berberine chloride	
Bovine serum albumin	
DL-glyceraldehyde	
DPPH	
Ferric chloride hexahydrate	
Gallic acid	
Girard's Reagent T	
Human recombinant AR	
Hyaluronidase	
Linoleic acid	
LOX from glycine max	
NBT	

	Potassium acetate	
	Potassium dichromate	
	Quercetin	
	Quillaja saponin	
	Sodium azide	
	Sodium formate	
	Sodium hyaluronate	
	Sodium phosphate dibasic	
	Tannic acid	
	Trichloroacetic acid	
	Tween® 20	
	Vanillin	
	Xanthine	
	XO	
	Potassium sodium tartrate tetrahydrate	System Chemicals (Selangor, Malaysia)
	Acarbose	
	Aluminium chloride	Thermo Fisher Scientific (Massachusetts, U.S.)
	Sodium phosphate monobasic	
	Aminoguanidine hydrochloride	Tokyo Chemical Industry (Tokyo, Japan)
	Glyoxal	
	Chloroform	
	n-butanol	R & M Chemicals (London, U.K.)
Phase 2	SDS	Nacalai Tesque (Kyoto, Japan)
	D-glucose	Himedia (Maharashtra, India)
	Absolute EtOH	Merck Millipore (Massachusetts, U.S.)
	ARPE-19	American Type Culture Collection (Manassas, U.S.)
	Human sRAGE ELISA kit	Finetest (Wuhan, China)
	Horseradish peroxidase conjugated secondary antibody	GeneTex (California, U.S.)

4X protein loading buffer	LI-COR Biosciences (Nebraska, U.S.)	
MTT	Merck Millipore (Massachusetts, U.S.)	
DMSO		
Nuclear protein extraction kit		
polyvinylidene difluoride membranes		
SensiFAST™ SYBR® qPCR kit	Meridian Bioscience (Ohio, U.S.)	
Chemiluminescent substrate	Nacalai Tesque (Kyoto, Japan)	
Ribonuclease-free deoxyribonuclease	Promega (Wisconsin, U.S.)	
Sodium chloride	R & M Chemicals (London, U.K.)	
Non-fat dry milk	Santa Cruz Biotechnology (Texas, U.S.)	
Acrylamide/bisacrylamide solution (40 %, 37.5:1)	Sigma-Aldrich (Missouri, U.S.)	
Ammonium persulfate		
N,N,N,N-Tetramethylethylenediamine		
Penicillin-streptomycin		
Radioimmunoprecipitation lysis buffer		
Tris(hydroxymethyl)aminomethane		
Trizol reagent		
Trypsin-ethylenediaminetetraacetic acid		
Primary antibodies		St. John's Laboratory (London, U.K.)
β-mercaptoethanol		Thermo Fisher Scientific (Massachusetts, U.S.)
High-capacity cDNA reverse transcription kit		
Pierce BCA protein assay kit		
SnakeSkin™ dialysis tubing		
Sulphuric acid	R & M Chemicals (London, U.K.)	
Bovine serum albumin	Sigma-Aldrich (Missouri, U.S.)	
Trichloroacetic acid		
Tween® 20		
Sodium phosphate monobasic	Thermo Fisher Scientific (Massachusetts, U.S.)	

Phase 3	Absolute EtOH	Merck Millipore (Massachusetts, U.S.)
	Dichloromethane	
	Diethyl ether	
	Silica gel 60 PF ₂₅₄ containing gypsum	
	TLC silica gel 60 F ₂₅₄ aluminium plates	
	CDCl ₃	Sigma-Aldrich (Missouri, U.S.)
	Hexane	R & M Chemicals (London, U.K.)

Appendix A2

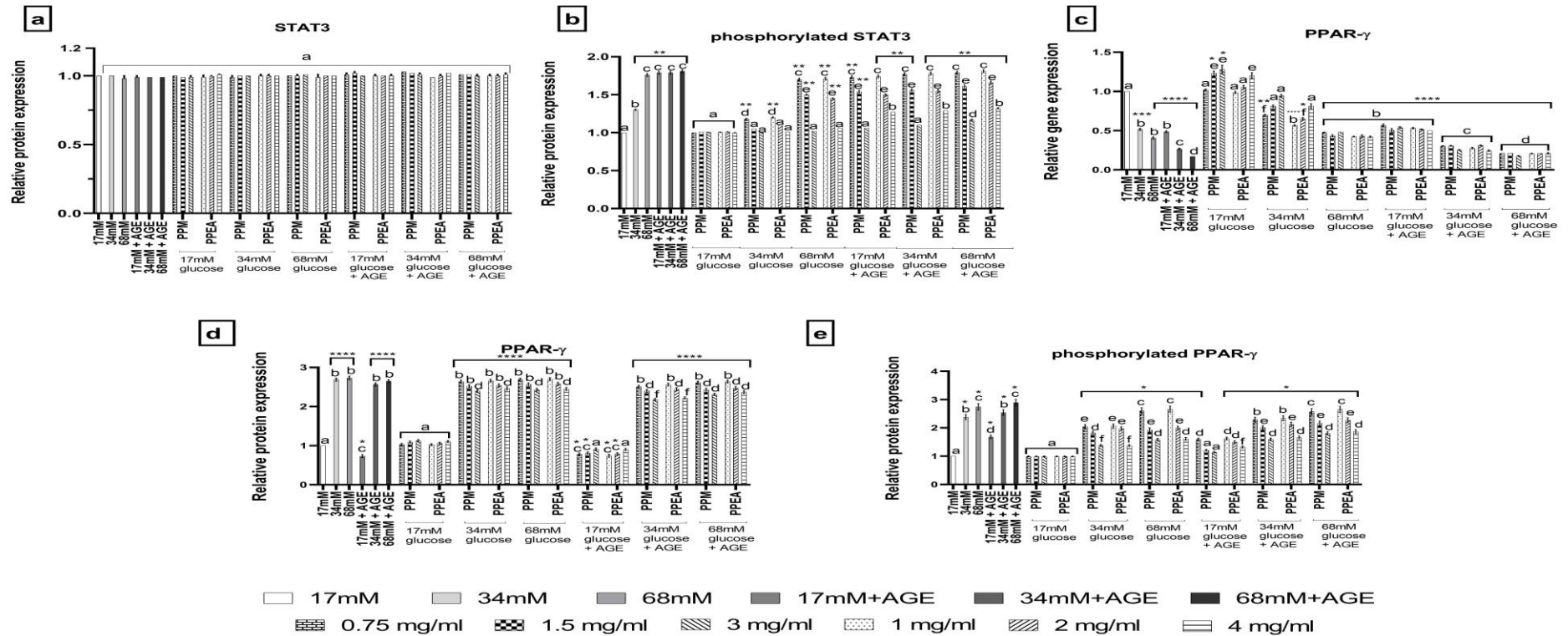
List of equipment.

Phase of study	Equipment (Model name)	Brand (Manufacturing country)
Plant processing and extraction	Analytical balance (CP225D)	Sartorius (Göttingen, Germany)
	Top-loading balance (CPA2202S)	
	Fumehood (Safeaire)	Hamilton Laboratory Solution (Wisconsin, U.S.)
	Rotary evaporator (R-100)	BUCHI (Flawil, Switzerland)
	Vacuum pump for rotary evaporator (V-700)	
	Recirculating cooler for rotary evaporator (FL1703)	Julabo (Seelbach, Germany)
	Separatory funnel (4150801)	Favorit (Selangor, Malaysia)
	Distilled water dispenser (PureLab Chorus 2)	Elga LabWater (Illinois, U.S.)
Phase 1	Microplate reader (Biotek Epoch)	Agilent Technologies (California, U.S.)
	Vortex mixer (MX-S)	DLAB Scientific (Beijing, China)
	Distilled water dispenser (PureLab Chorus 2)	Elga LabWater (Illinois, U.S.)
	Centrifuge (5418R)	Eppendorf (Hamburg, Germany)
	Micropipettors (0.5-10 µl, 10-100 µl, 100-1000 µl) (Research Plus)	
	Water Bath (TW20)	Julabo (Seelbach, Germany)
	Freezer (-20°C) (LGex 3410)	Liebherr (Bulle, Switzerland)
	Analytical balance (CP225D)	Sartorius (Göttingen, Germany)
	pH meter (PB-10)	
	Fumehood (Safeaire)	Hamilton Laboratory Solution (Wisconsin, U.S.)
	Sonicator (FB15047)	Thermo Fisher Scientific (Massachusetts, U.S.)
	Microplate fluorescence spectrophotometer (Varioskan® Flash)	

Phase 2	Microplate reader (Biotek Epoch)	Agilent Technologies (California, U.S.)
	Vertical electrophoresis tank (Azure Aqua Quad Mini Cell)	Azure Biosystems (California, U.S.)
	Western blot transfer tank (Azure Aqua Transfer Cell)	
	Gel imaging system (ChemiDoc)	Bio-Rad Laboratories (California, U.S.)
	Power supply (PowerPac)	
	Real-time thermal cycler (CFX Connect)	
	Mini shaker (MR-1)	Biosan (Riga, Latvia)
	PCR microcentrifuge (D1008)	DLAB Scientific (Beijing, China)
	Vortex mixer (MX-S)	
	Ultrapure water dispenser (PureLab Chorus 1)	Elga LabWater (Illinois, U.S.)
	Distilled water dispenser (PureLab Chorus 2)	
	Refrigerated microcentrifuge (5418R)	Eppendorf (Hamburg, Germany)
	Refrigerated centrifuge (5810R)	
	Freezer (-80°C) (Cryocube F740h)	
	Incubator shaker (New Brunswick Innova 42)	
	Micropipettors (0.5-10 µl, 10-100 µl, 100-1000 µl) (Research Plus)	
	Thermomixer (Comfort)	
	CO2 incubator (CelCulture)	Esco Lifesciences (Singapore)
	Class II biological safety cabinet (Airstream)	
	Water Bath (TW20)	Julabo (Seelbach, Germany)
	Magnetic stirrer (LMS-1003)	Labtech (Gyeonggi-do, Republic of Korea)
	Freezer (-20°C) (LGex 3410)	Liebherr (Bulle, Switzerland)
	Freeze dryer (Christ Alpha 1-2LC Plus)	Martin Christ (Osterode, Germany)
	Sterile polyethersulfone 0.22 µM syringe filter	Microlab Scientific (Shanghai, China)
	Inverted microscope (Eclipse TS100)	Nikon (Tokyo, Japan)
	Analytical balance (CP225D)	Sartorius (Göttingen, Germany)
	pH meter (PB-10)	

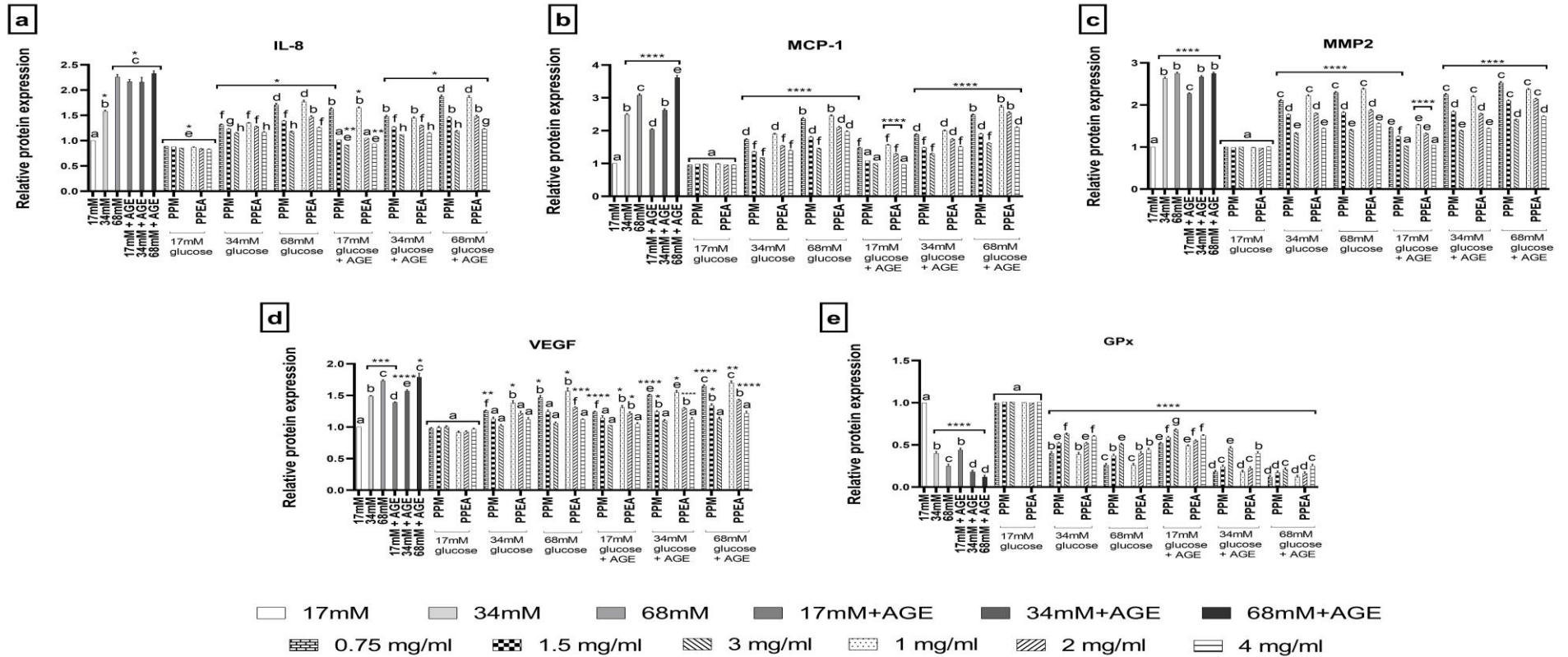
	NanoDrop spectrophotometer (NanoDrop One C)	Thermo Fisher Scientific ((Massachusetts, U.S.)
	Sonicator (FB15047)	
	Cooled incubator (FOC 120i)	Velp Scientifica (Monza and Brianza, Italy)
Phase 3	Liquid chromatograph system (1260 Infinity)	Agilent Technologies (California, U.S.)
	Mass spectrometer triple quadrupole (6410 Triple Quad)	
	Mass spectrometer quadrupole time-of-flight (6520 Accurate Mass)	
	NMR spectrometer (Ascend 400 MHz)	Bruker (Massachusetts, U.S.)
	Rotary evaporator (R-100)	BUCHI (Flawil, Switzerland)
	Vacuum pump for rotary evaporator and column chromatography (V-700)	
	Freezer (-20°C) (RF373SLDW1)	Fisher & Paykel (Auckland, New Zealand)
	Fumehood (Safeaire)	Hamilton Laboratory Solution (Wisconsin, U.S.)
	FTIR spectrometer (L1280127)	PerkinElmer (Massachusetts, U.S.)
	Analytical balance (CP225D)	Sartorius (Göttingen, Germany)
	Gas chromatograph-mass spectrometer (GCMS-QP 2010 Plus)	Shimadzu (Kyoto, Japan)
	UV-Vis spectrophotometer (UV-1650PC)	
	Portable ultraviolet backlight (ENF-240C)	Spectro-UV (New York, U.S.)
	Sonicator (FB15047)	Thermo Fisher Scientific (Massachusetts, U.S.)

Appendix B1



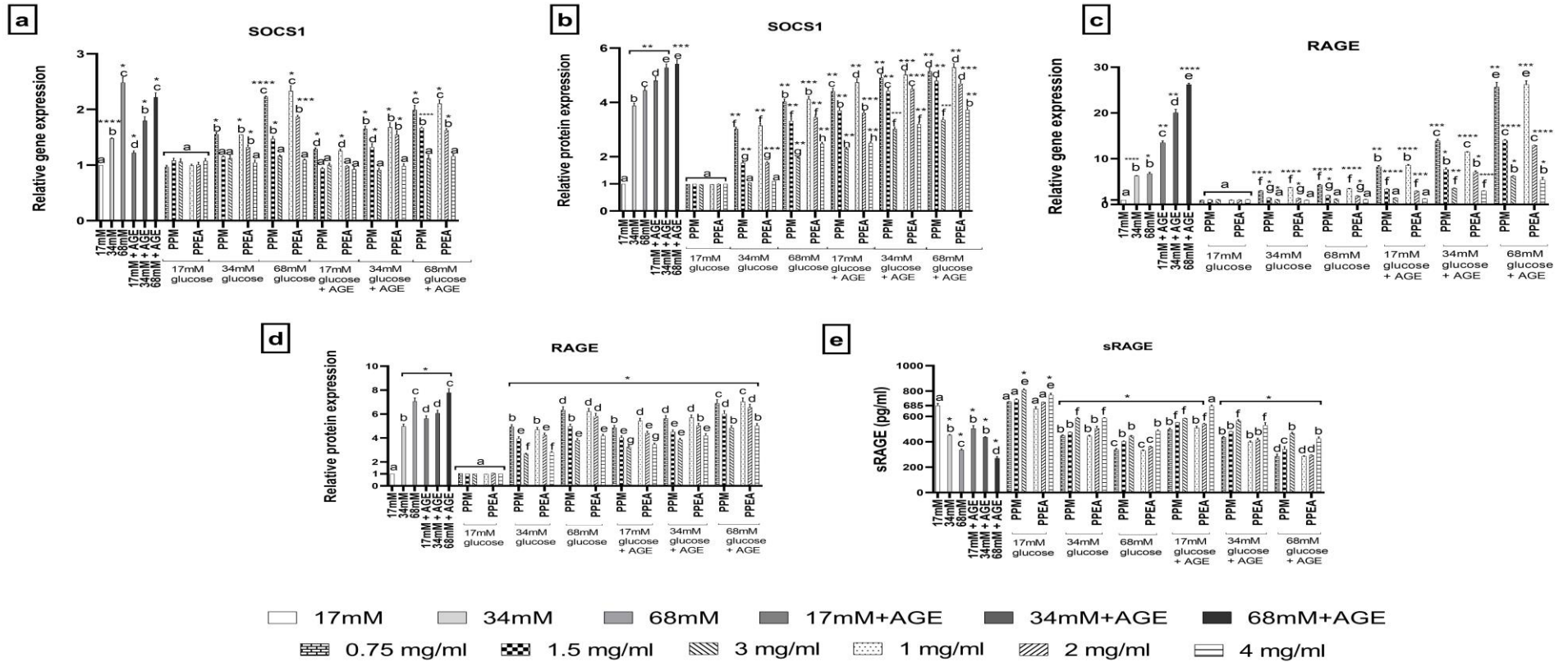
The expression of transcription factors in ARPE-19. (a) STAT3 protein. (b) Phosphorylated STAT3 protein. (c) PPAR- γ gene. (d) PPAR- γ protein. (e) Phosphorylated PPAR- γ protein. Data are expressed as mean \pm standard deviation of three independent determinations. Different alphabetical letters indicate significant ($p < 0.05$) differences of means among the treatment groups. AGE, advanced glycation end-product; PPAR- γ , peroxisome proliferator activated receptor gamma; PPEA, *P. pellucida* ethyl acetate; PPM, *P. pellucida* methanolic extract; STAT3, signal transducer and activator of transcription 3.

Appendix B3



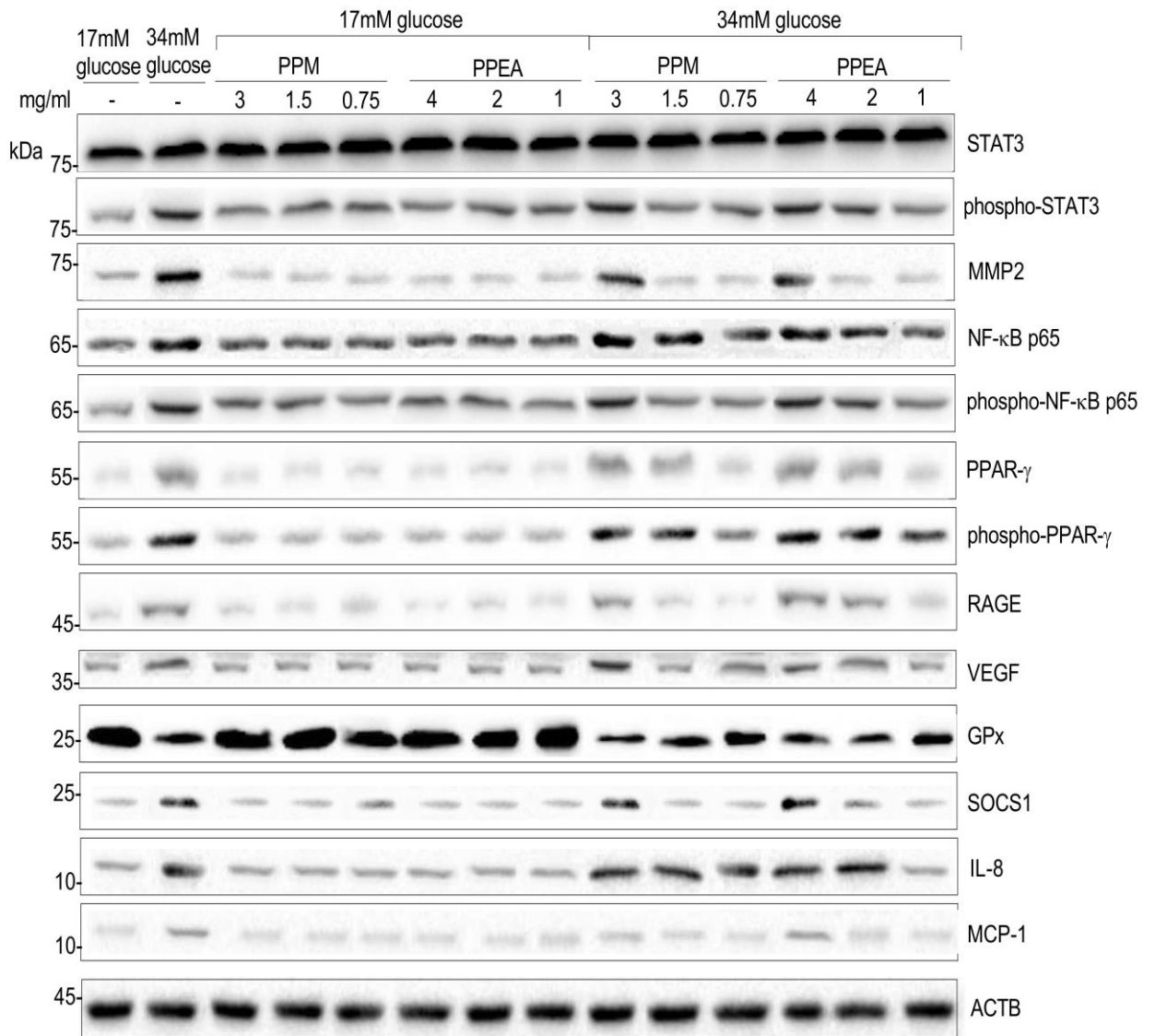
The relative protein expression of antioxidant, pro-inflammatory and angiogenic markers in ARPE-19. (a) IL-8. (b) MCP-1. (c) MMP2. (d) VEGF. (e) GPx. Data are expressed as mean \pm standard deviation of three independent determinations. Different alphabetical letters indicate significant ($p < 0.05$) differences of means among the treatment groups. AGE, advanced glycation end-product; GPx, glutathione peroxidase; PPEA, *P. pellucida* ethyl acetate fraction; IL-8, interleukin 8; PPM, *P. pellucida* methanolic extract; MCP-1, monocyte chemoattractant protein 1; MMP2, matrix metalloproteinase 2; VEGF, vascular endothelial growth factor.

Appendix B4



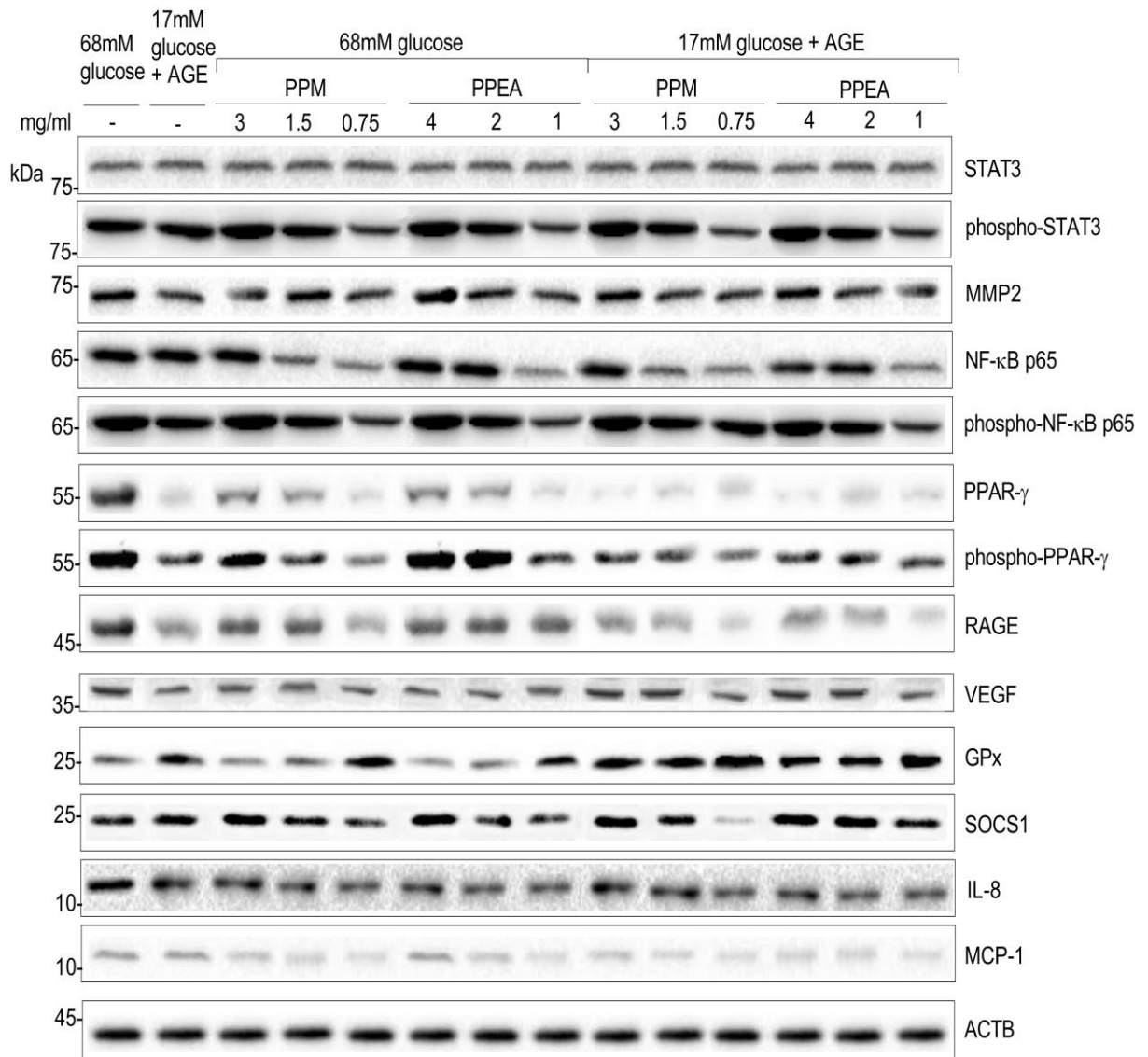
The expression of pro-inflammatory and anti-inflammatory markers involved in cytokine signalling in ARPE-19. (a) SOCS1 gene. (b) SOCS1 protein. (c) RAGE gene. (d) RAGE protein. (e) sRAGE protein. Data are expressed as mean \pm standard deviation of three independent determinations. Different alphabetical letters indicate significant ($p < 0.05$) differences of means among the treatment groups. AGE, advanced glycation end-product; PPEA, *P. pellucida* ethyl acetate fraction; PPM, *P. pellucida* methanolic extract; RAGE, receptor for advanced glycation end product; SOCS1, suppressor of cytokine signalling 1; sRAGE, soluble receptor for advanced glycation end product.

Appendix B5



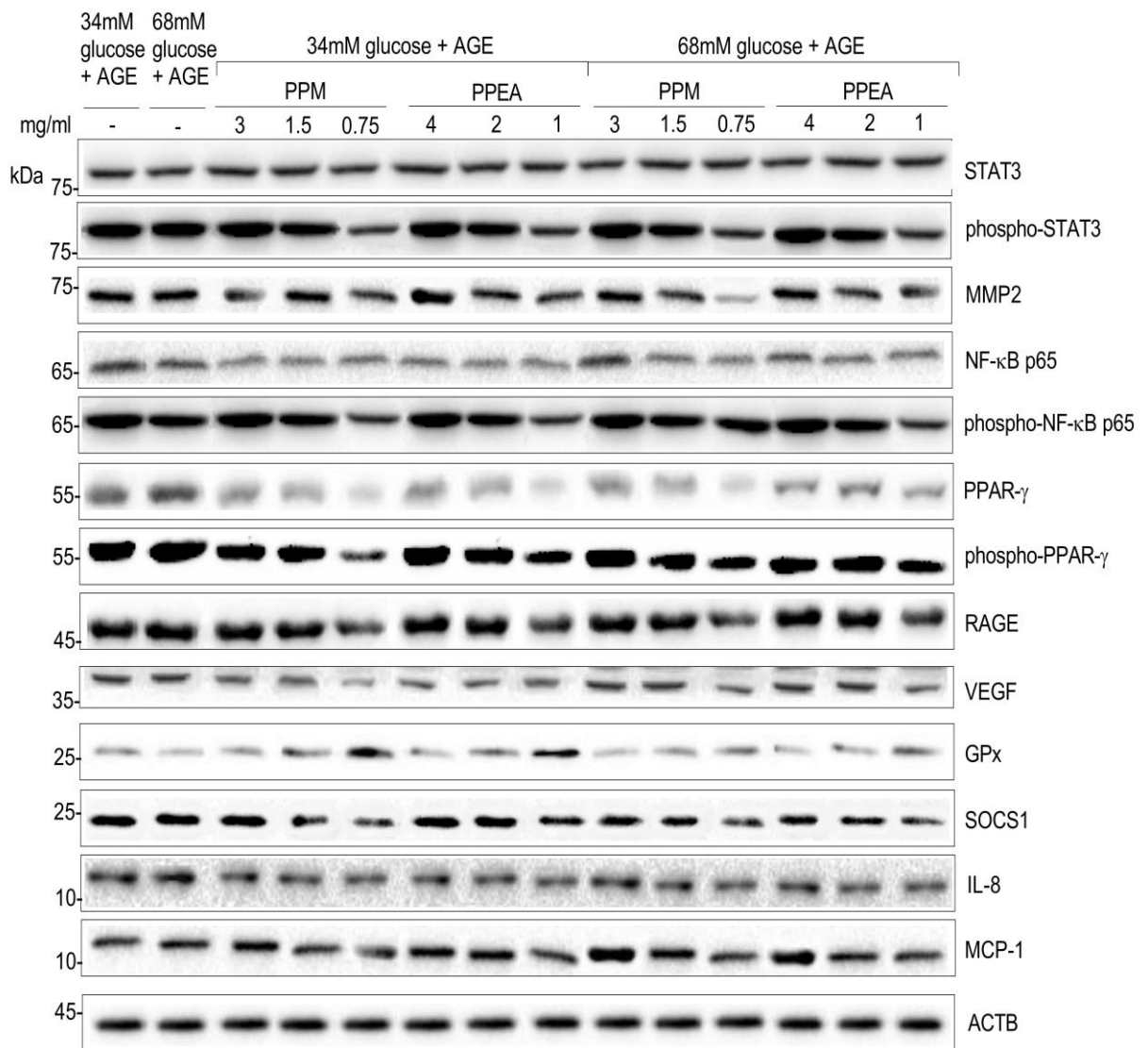
The western blot bands of antioxidant, anti-inflammatory and pro-inflammatory biomarkers in ARPE-19 under normal glucose (17 mM) and moderately high glucose (34 mM) conditions. ACTB, beta-actin; GPx, glutathione peroxidase; IL-8, interleukin 8; MCP-1, monocyte chemoattract protein 1; MMP2, matrix metalloproteinase 2; NF-κB, nuclear factor kappa B; PPAR-γ, peroxisome proliferator activated receptor gamma; PPEA, *P. pellucida* ethyl acetate; PPM, *P. pellucida* methanolic extract; RAGE, receptor of advanced glycation end product; SOCS1, suppressor of cytokine signalling 3; STAT3, signal transducer and activator of transcription 3; VEGF, vascular endothelial growth factor.

Appendix B6



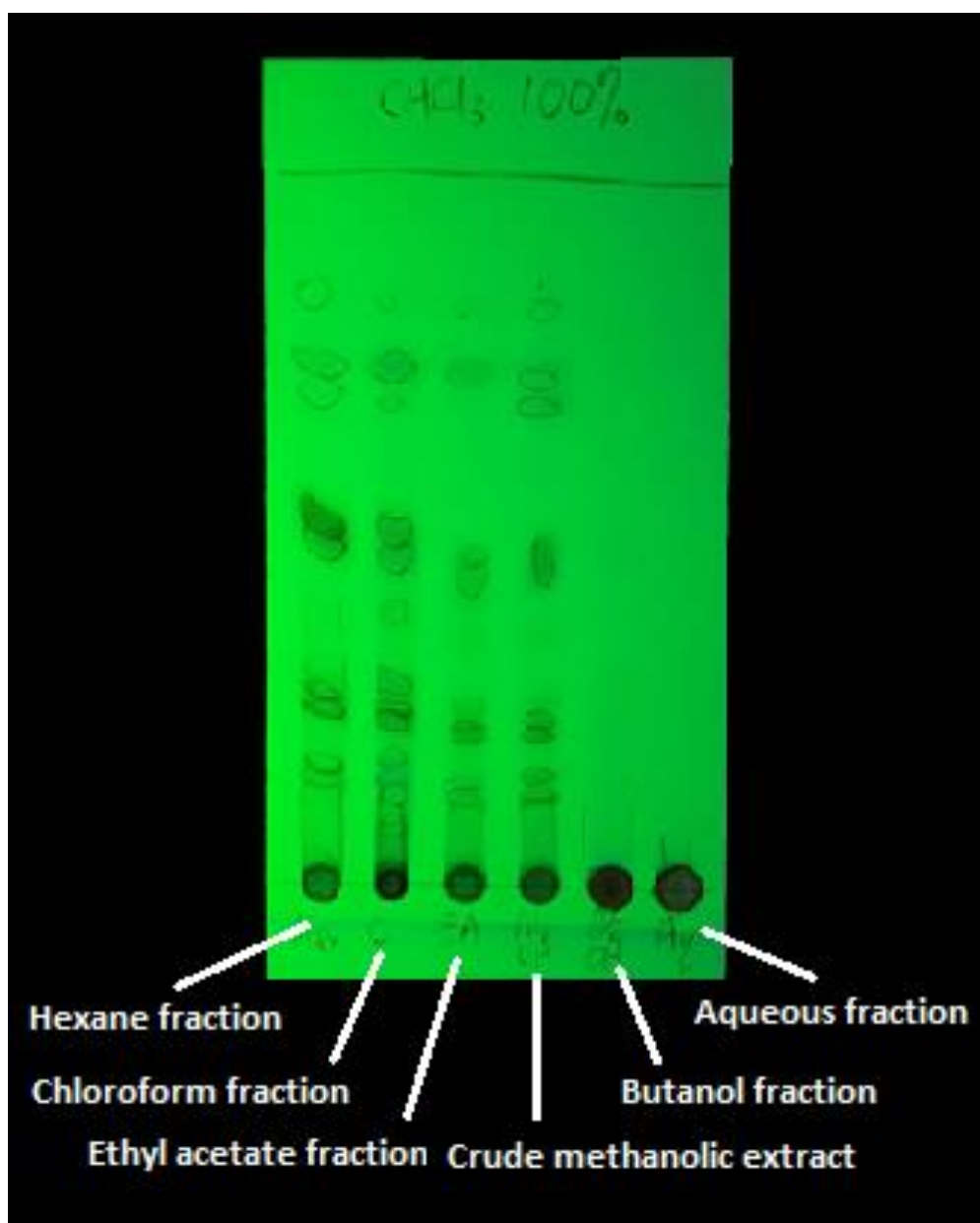
The western blot bands of antioxidant, anti-inflammatory and pro-inflammatory biomarkers in ARPE-19 under high glucose (68 mM) condition and normal glucose (17 mM) AGE-treated condition. ACTB, beta-actin; AGE, advanced glycation end-product; GPx, glutathione peroxidase; IL-8, interleukin 8; MCP-1, monocyte chemoattract protein 1; MMP2, matrix metalloproteinase 2; NF-κB, nuclear factor kappa B; PPAR-γ, peroxisome proliferator activated receptor gamma; PPEA, *P. pellucida* ethyl acetate; PPM, *P. pellucida* methanolic extract; RAGE, receptor of advanced glycation end product; SOCS1, suppressor of cytokine signalling 3; STAT3, signal transducer and activator of transcription 3; VEGF, vascular endothelial growth factor.

Appendix B7



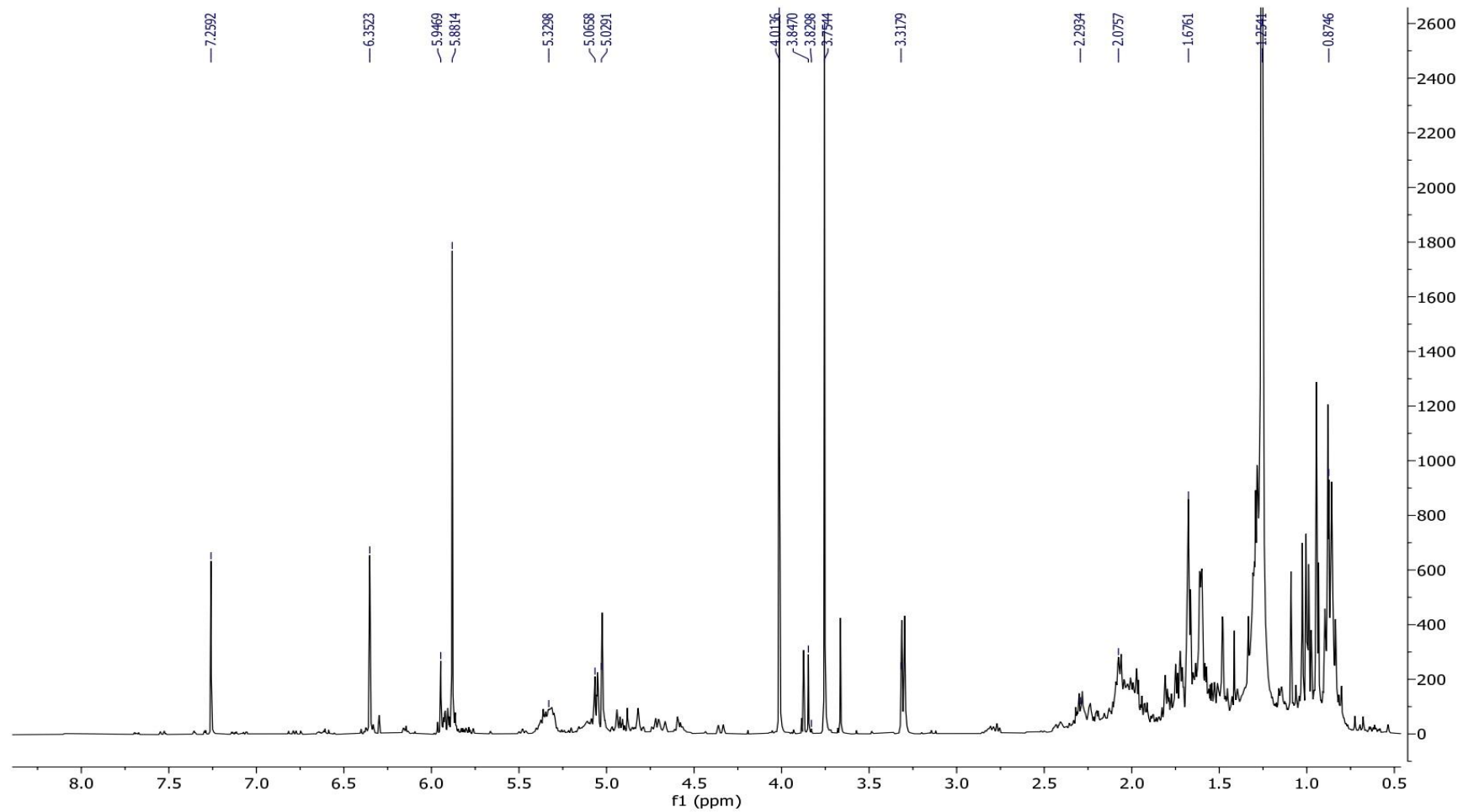
The western blot bands of antioxidant, anti-inflammatory and pro-inflammatory biomarkers in ARPE-19 under moderately high glucose (34 mM) and high glucose (68 mM) AGE-treated conditions. ACTB, beta-actin; AGE, advanced glycation end-product; GPx, glutathione peroxidase; IL-8, interleukin 8; MCP-1, monocyte chemoattract protein 1; MMP2, matrix metalloproteinase 2; NF-κB, nuclear factor kappa B; PPAR-γ, peroxisome proliferator activated receptor gamma; PPEA, *P. pellucida* ethyl acetate; PPM, *P. pellucida* methanolic extract; RAGE, receptor of advanced glycation end product; SOCS1, suppressor of cytokine signalling 3; STAT3, signal transducer and activator of transcription 3; VEGF, vascular endothelial growth factor.

Appendix C1



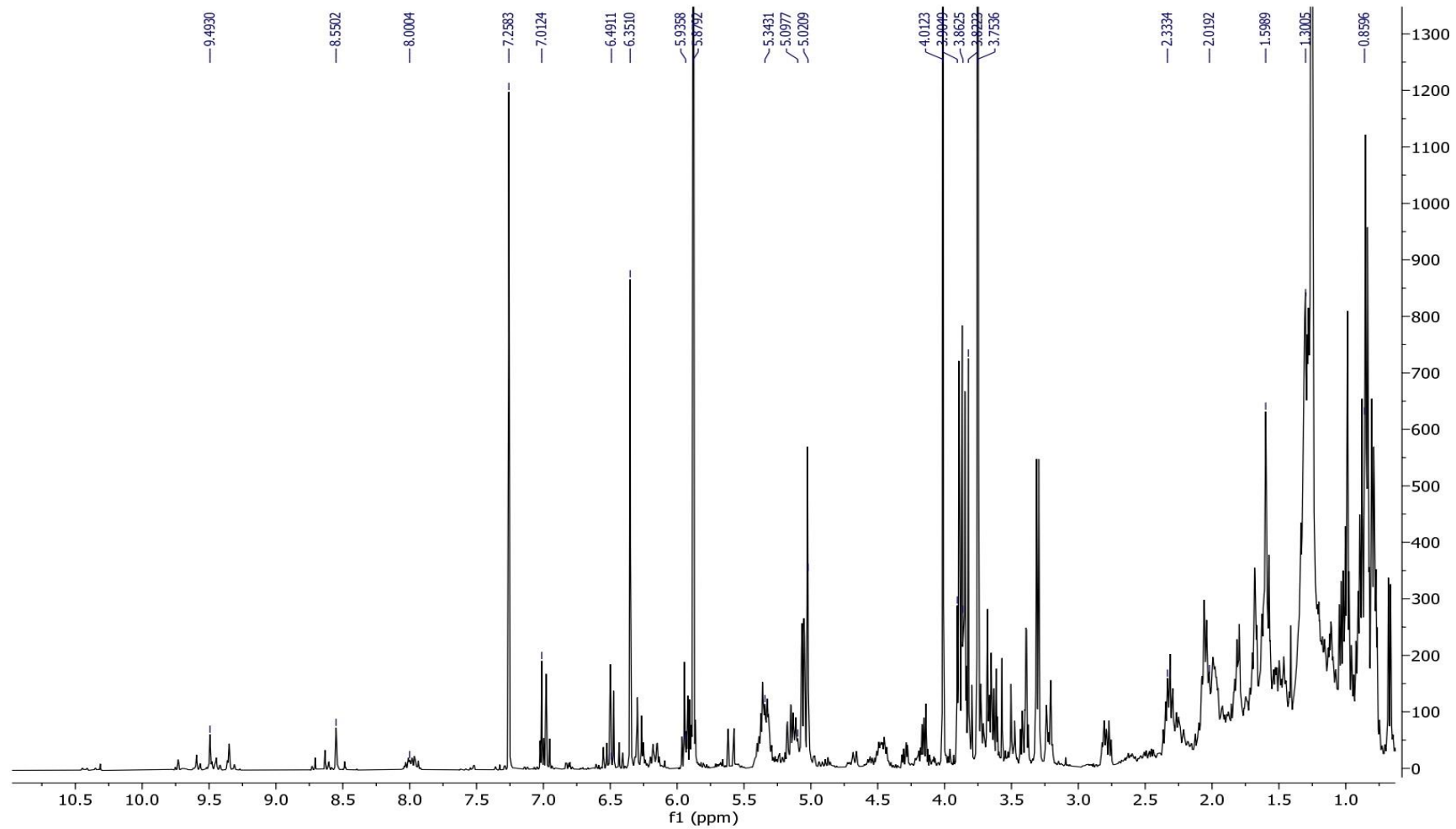
TLC profiles of *P. pellucida* crude methanolic extract and solvent fractions.

Appendix C2



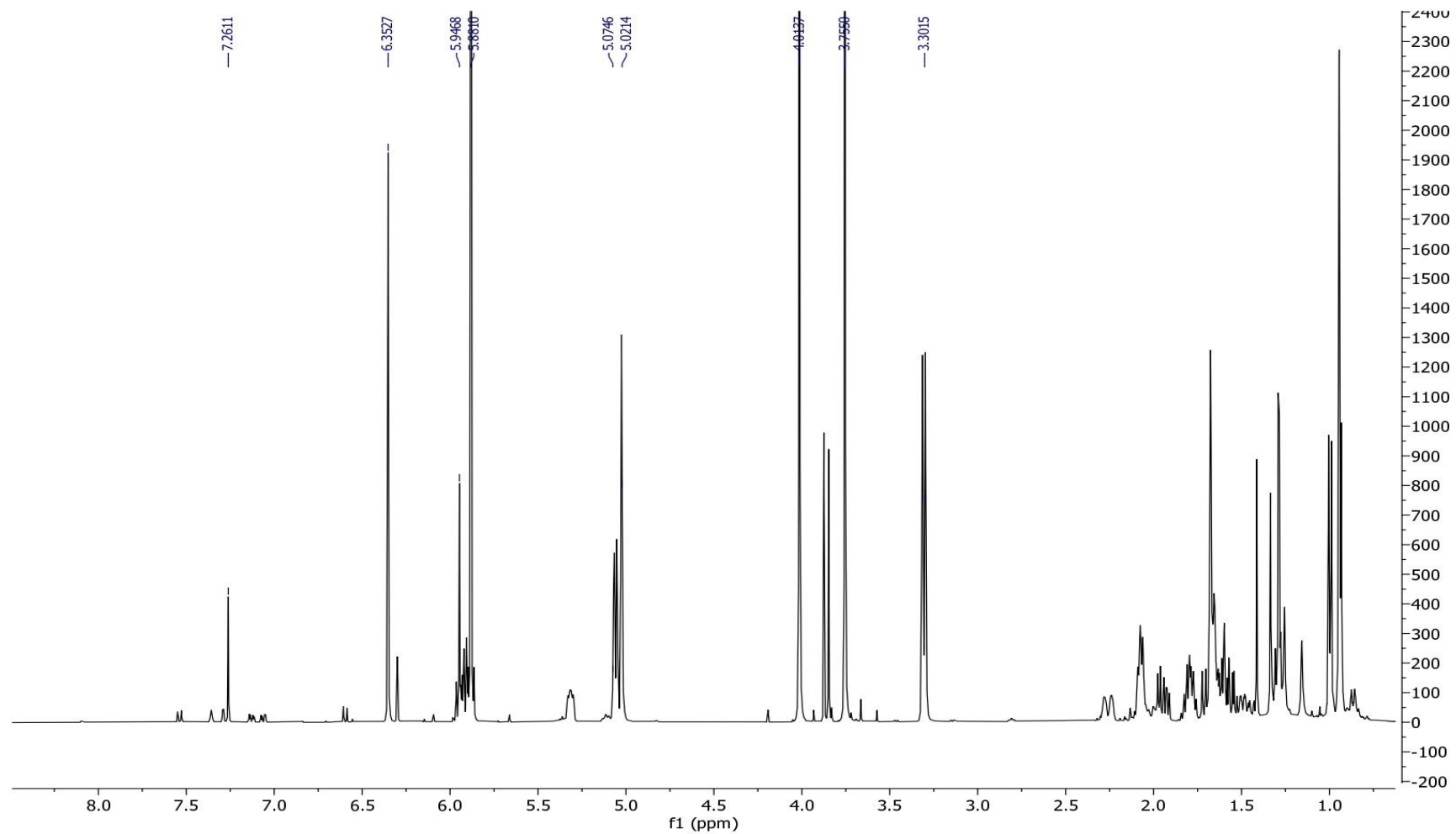
¹H NMR spectrum (CDCl₃, 400 MHz) of fraction PPM/A.

Appendix C3



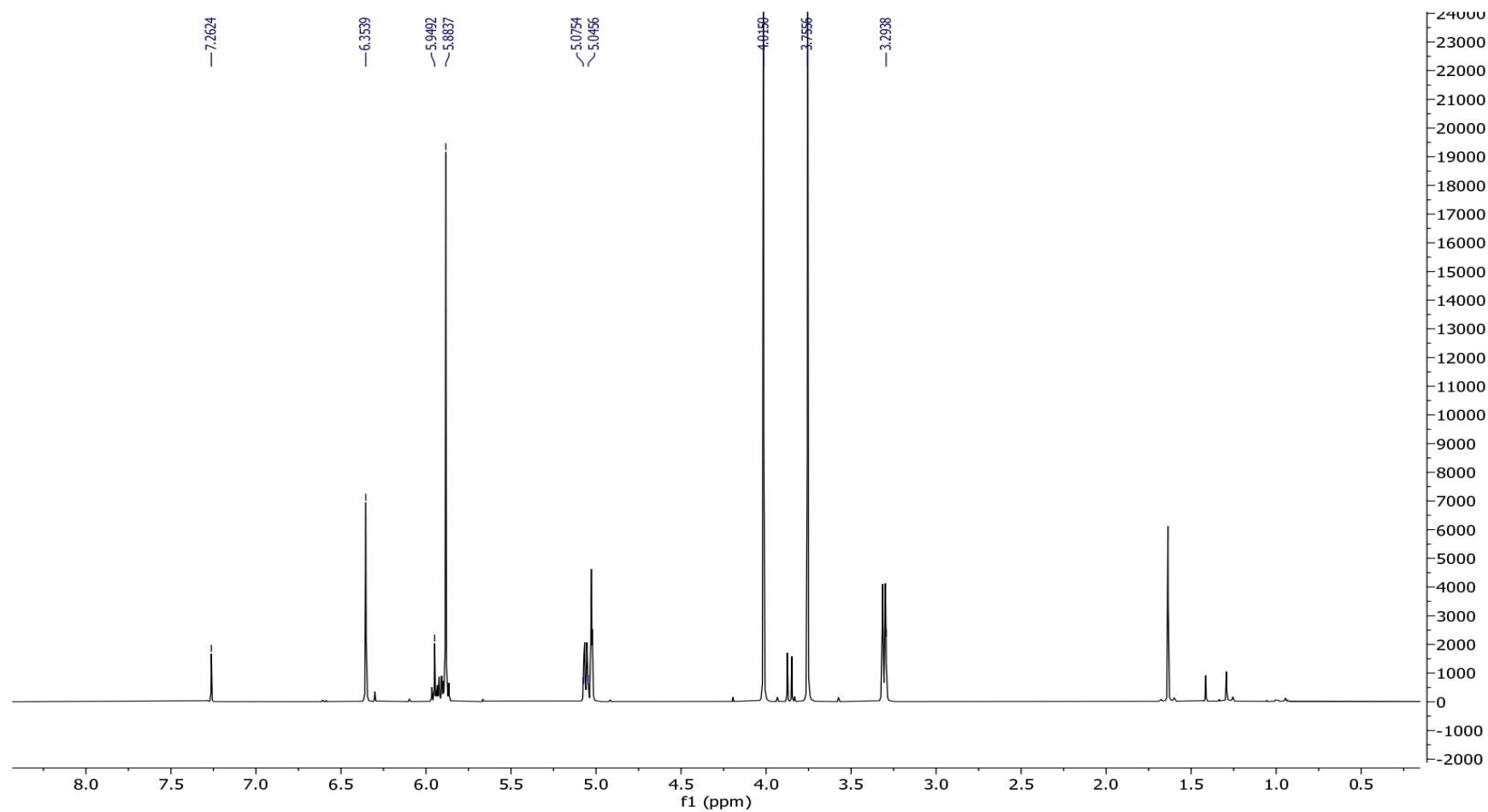
^1H NMR spectrum (CDCl_3 , 400 MHz) of fraction PPM/B.

Appendix C4



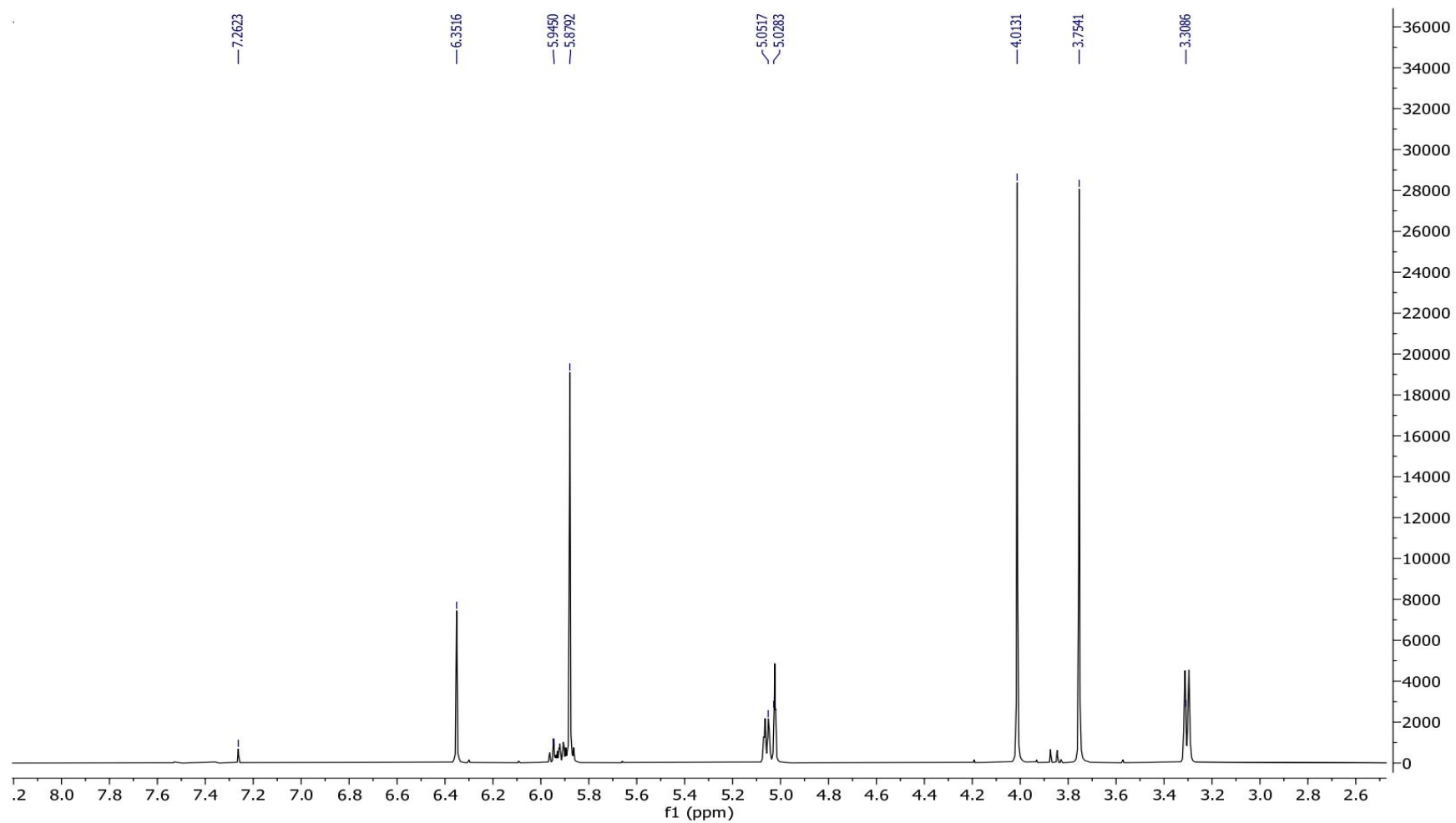
¹H NMR spectrum (CDCl₃, 400 MHz) of fraction PPM/A/5-7/2-4.

Appendix C5



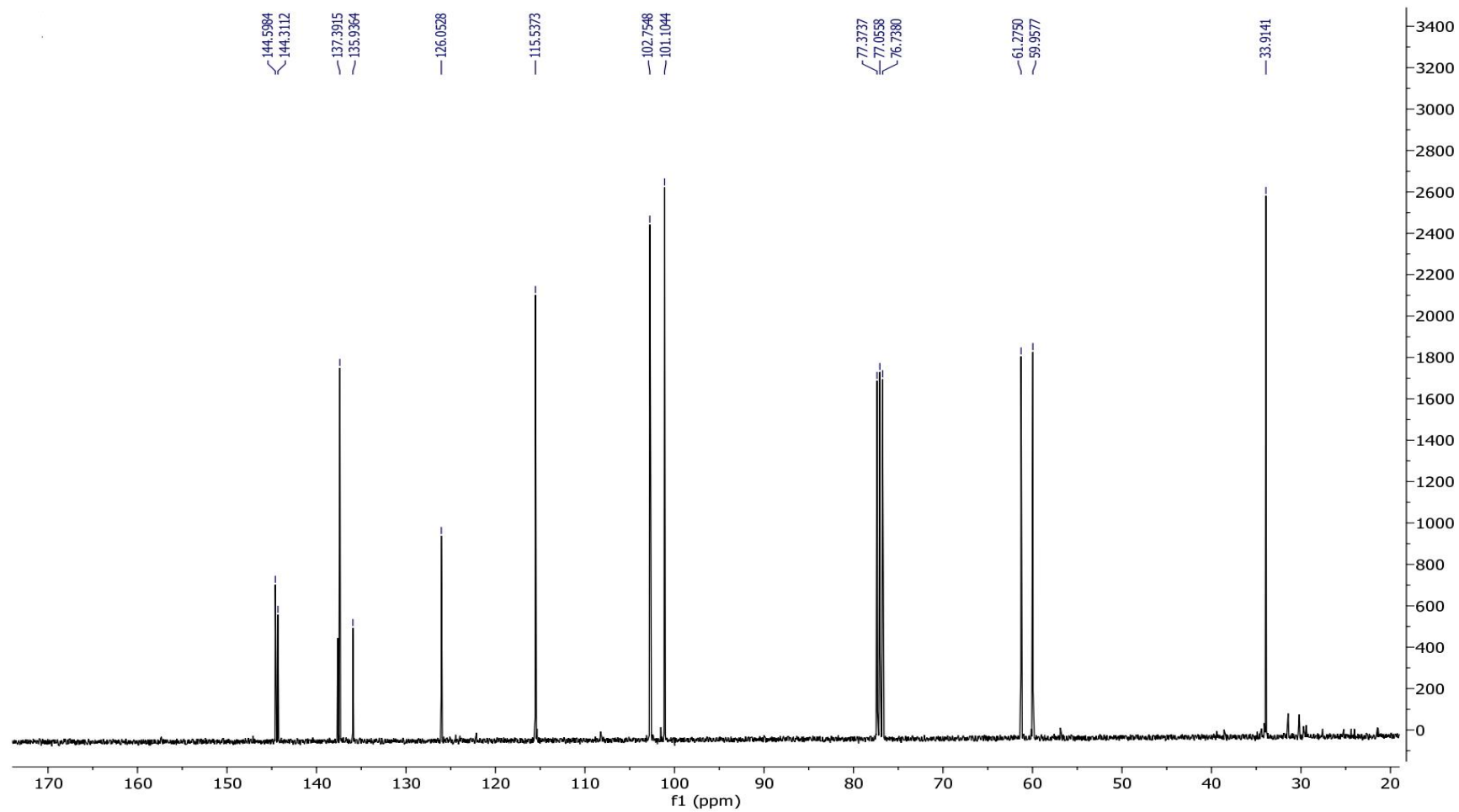
¹H NMR spectrum (CDCl₃, 400 MHz) of fraction PPM/B/2-4/7.

Appendix D1



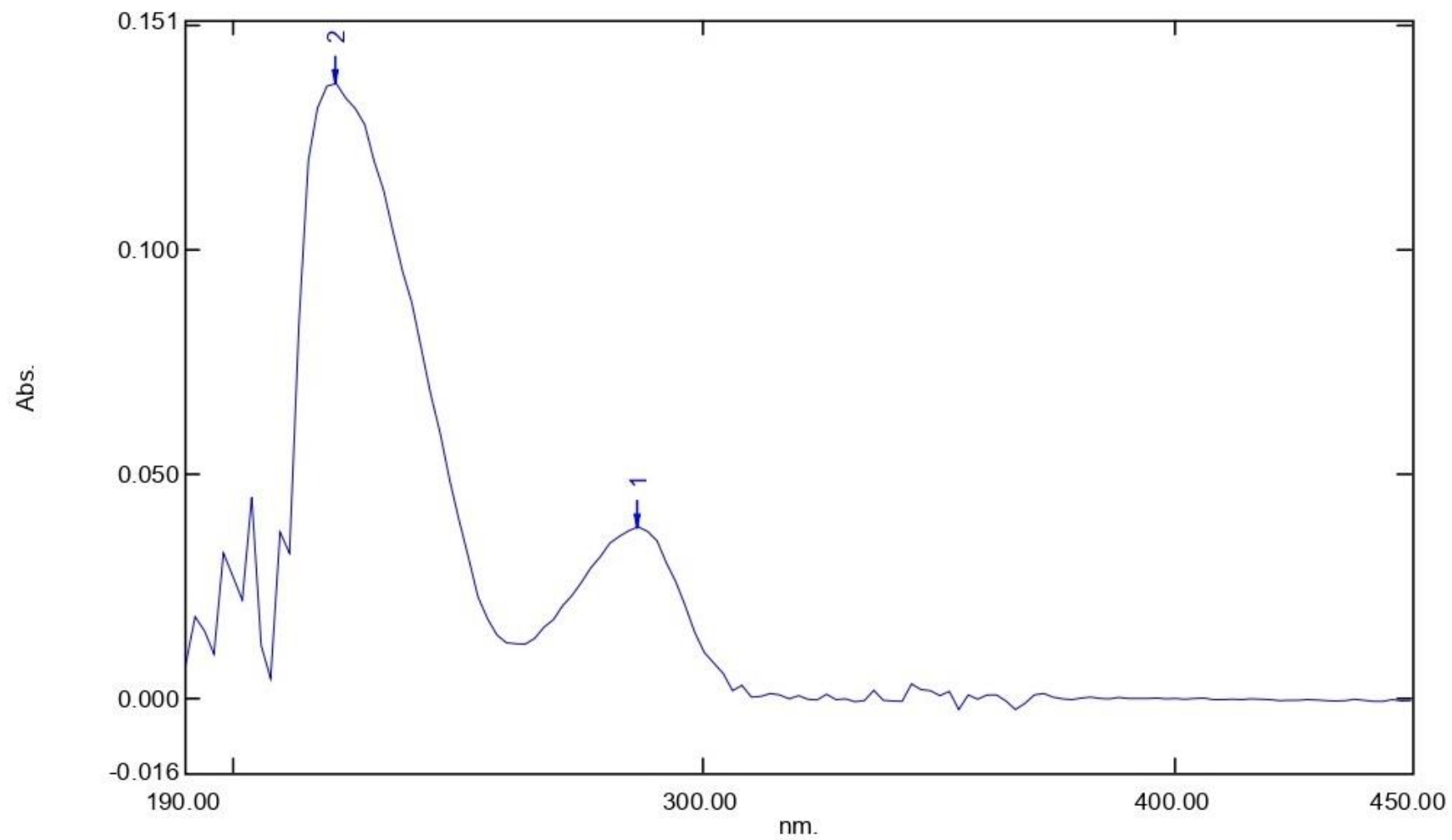
¹H NMR spectrum (CDCl₃, 400 MHz) of fraction 1.

Appendix D2



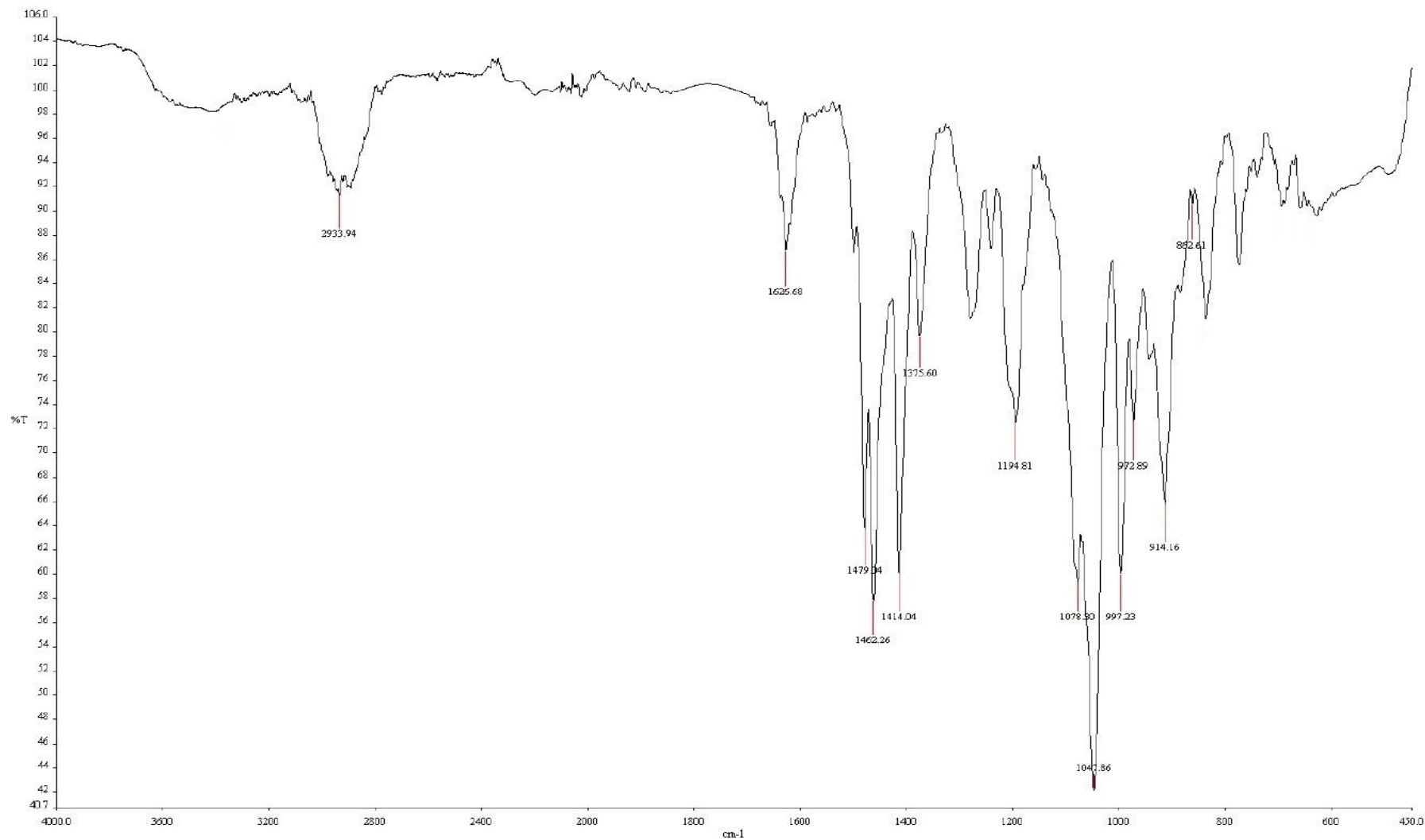
¹³C NMR spectrum (CDCl₃, 100 MHz) of fraction 1.

Appendix D3



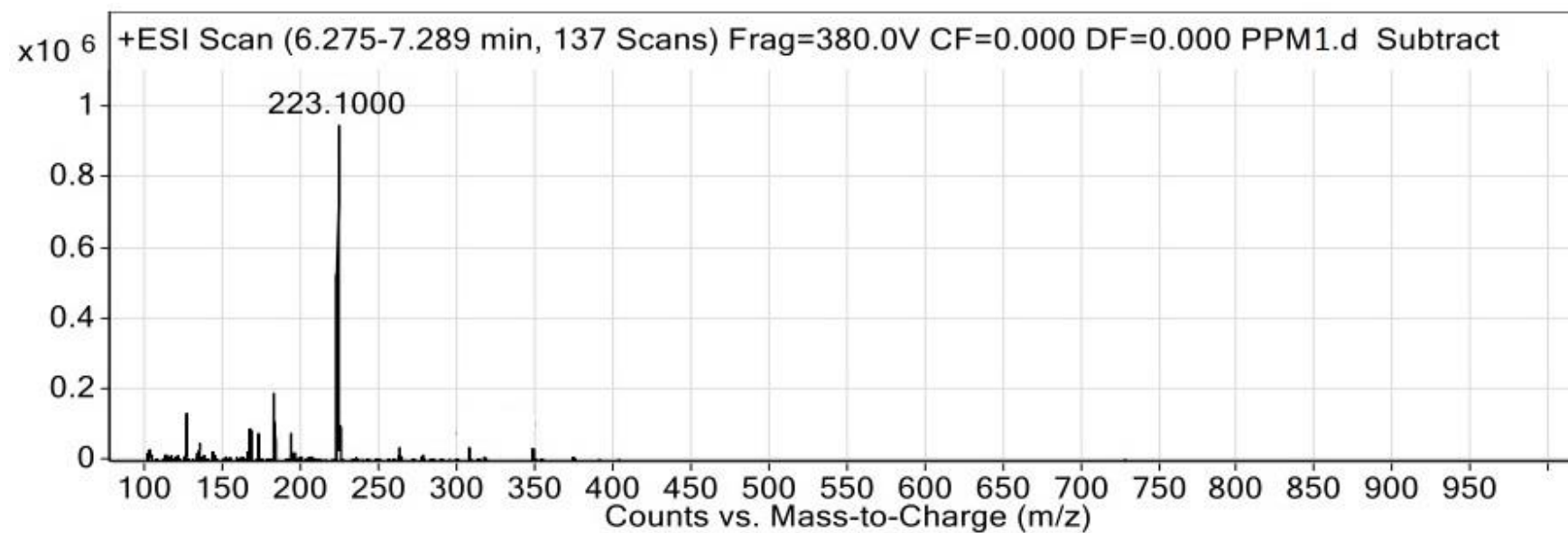
UV-Vis spectrum of fraction 1.

Appendix D4



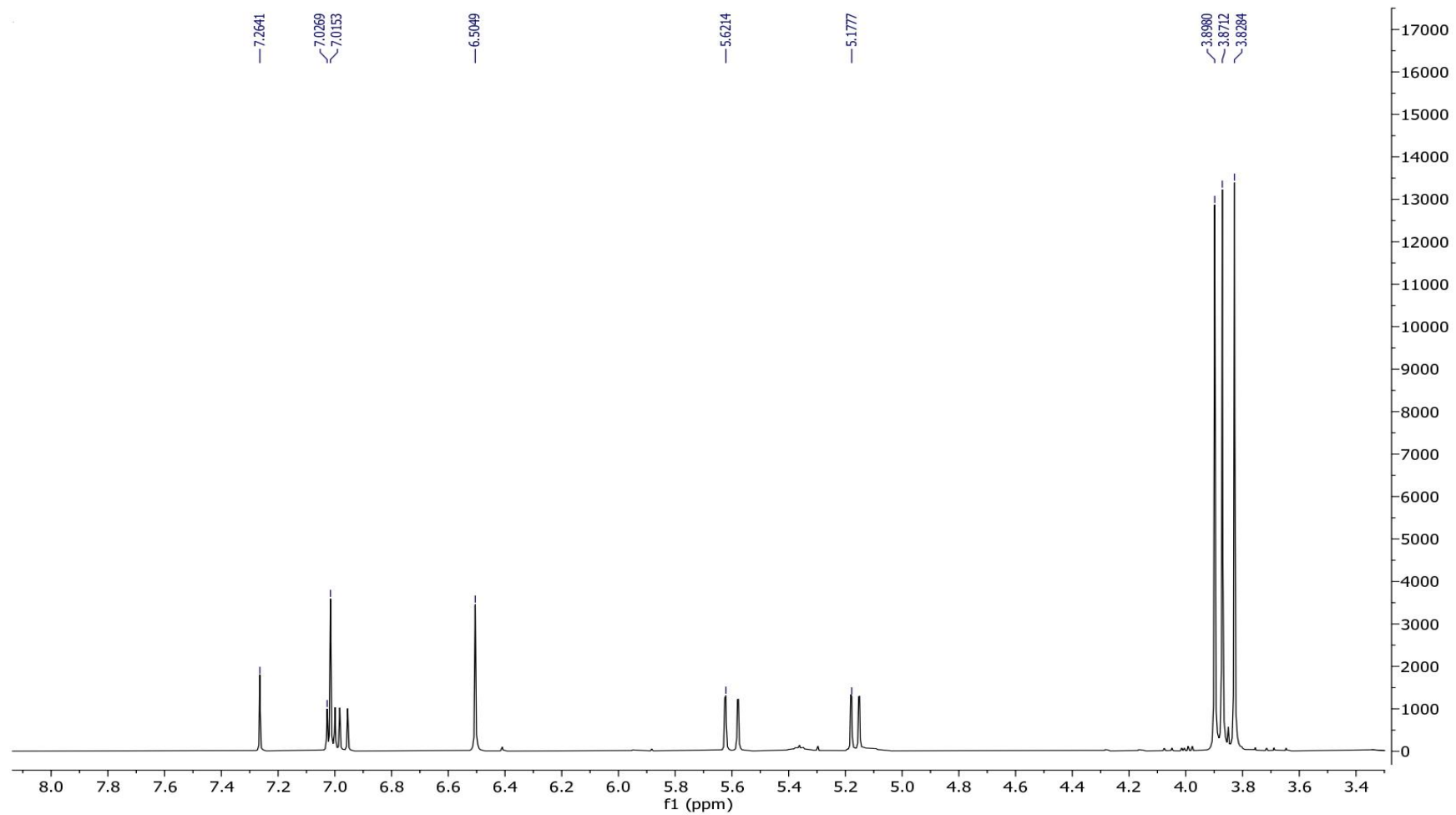
FTIR spectrum of fraction 1.

Appendix D5



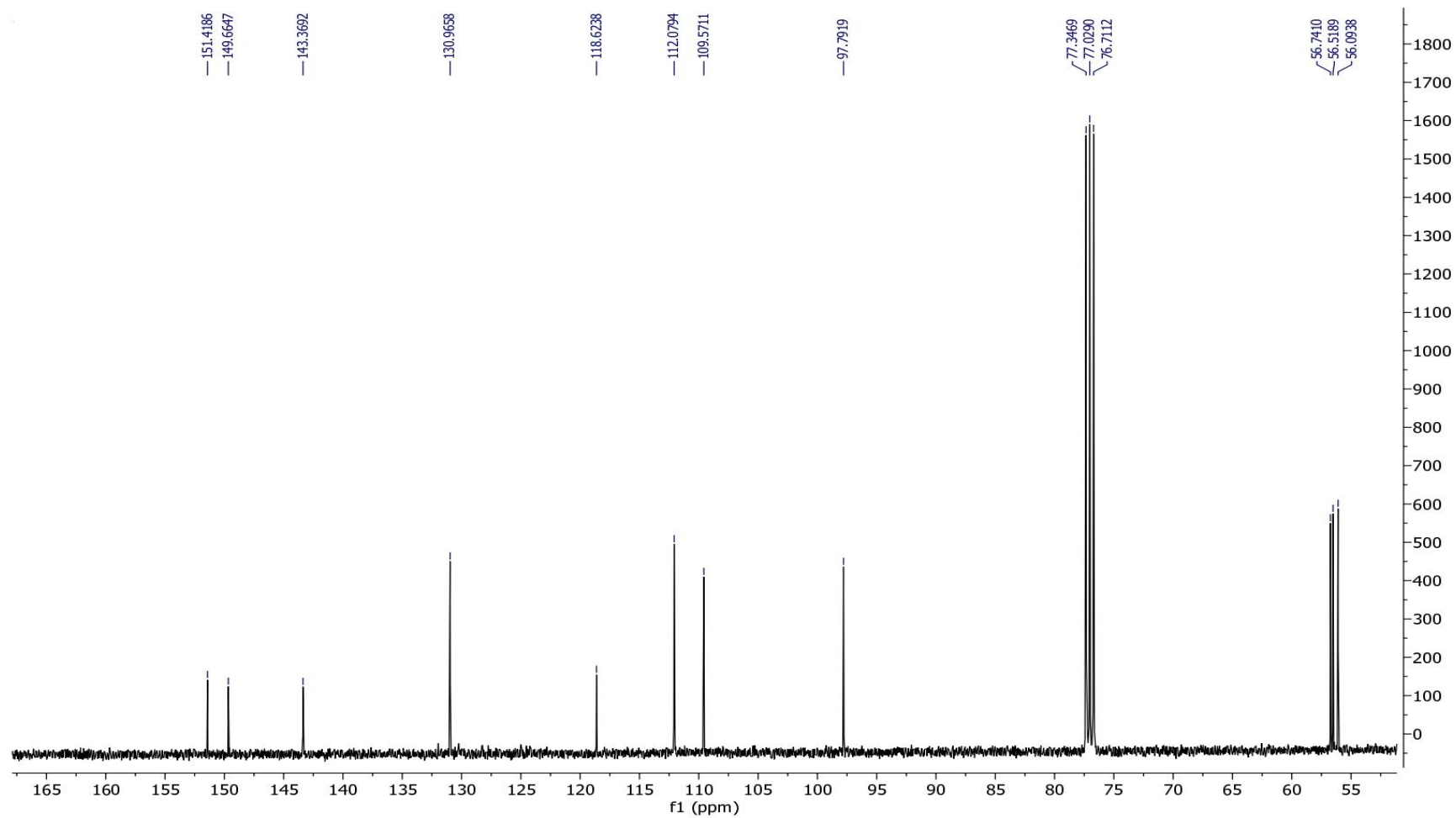
ESIMS spectrum of fraction 1.

Appendix E1



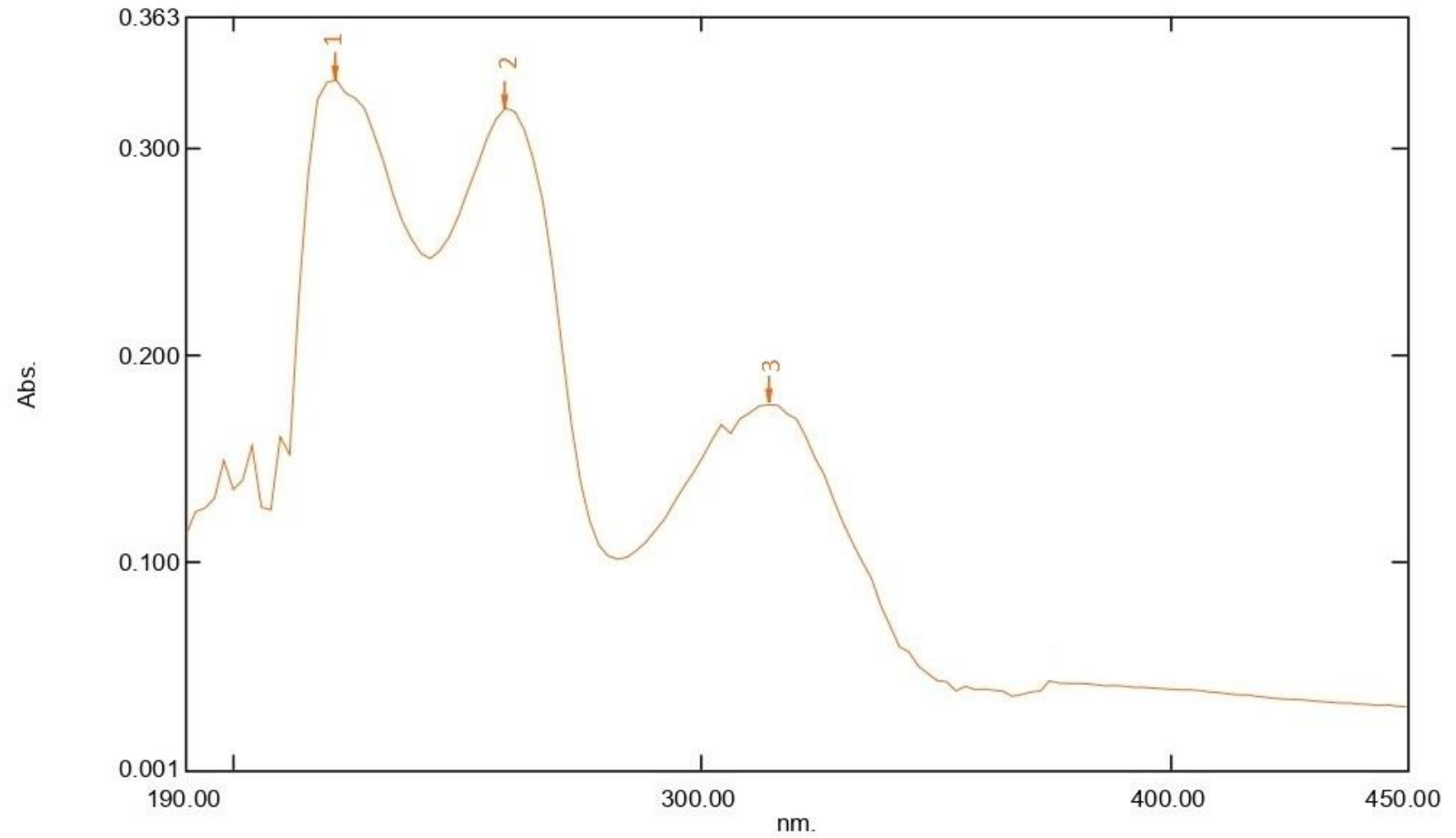
¹H NMR spectrum (CDCl₃, 400 MHz) of fraction 2.

Appendix E2



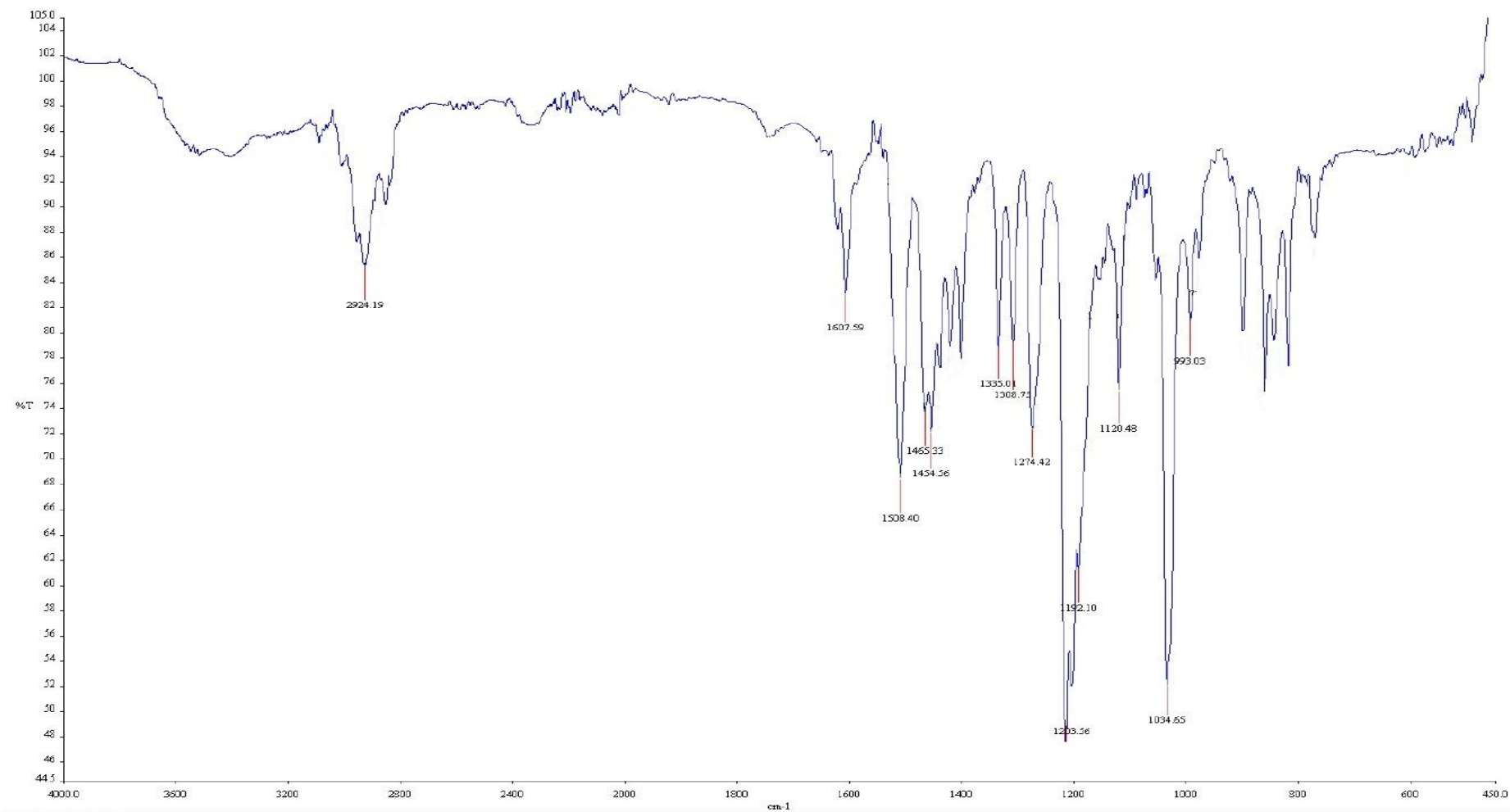
^{13}C NMR spectrum (CDCl_3 , 100 MHz) of fraction 2.

Appendix E3



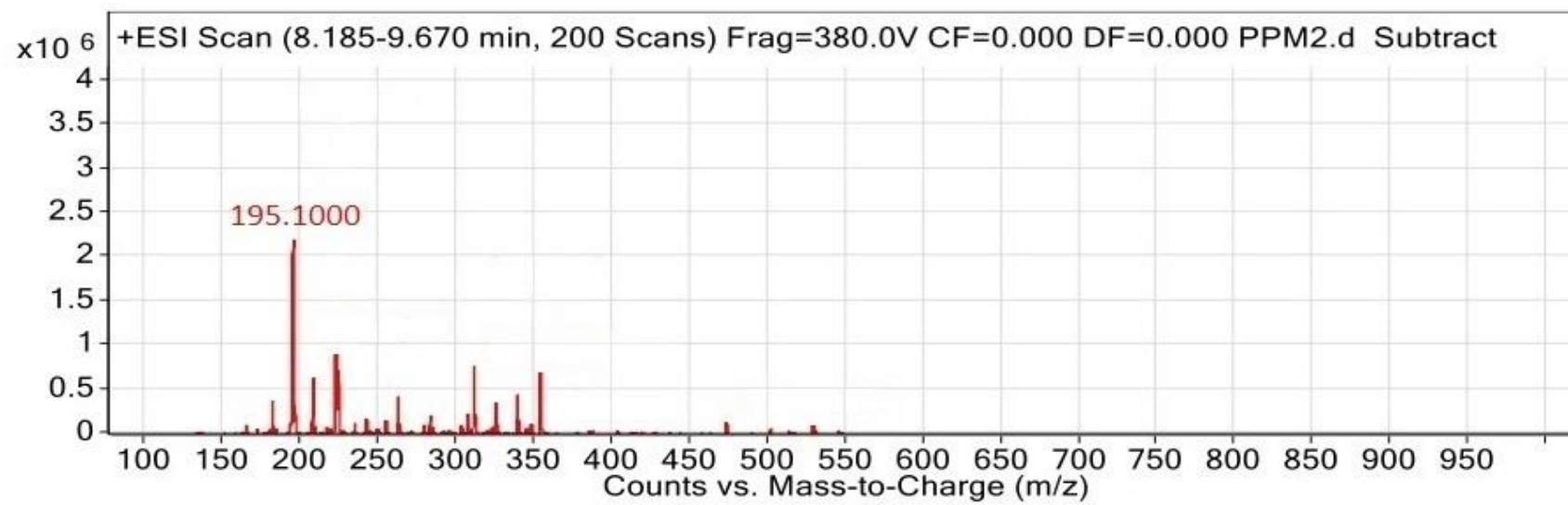
UV-Vis spectrum of fraction 2.

Appendix E4



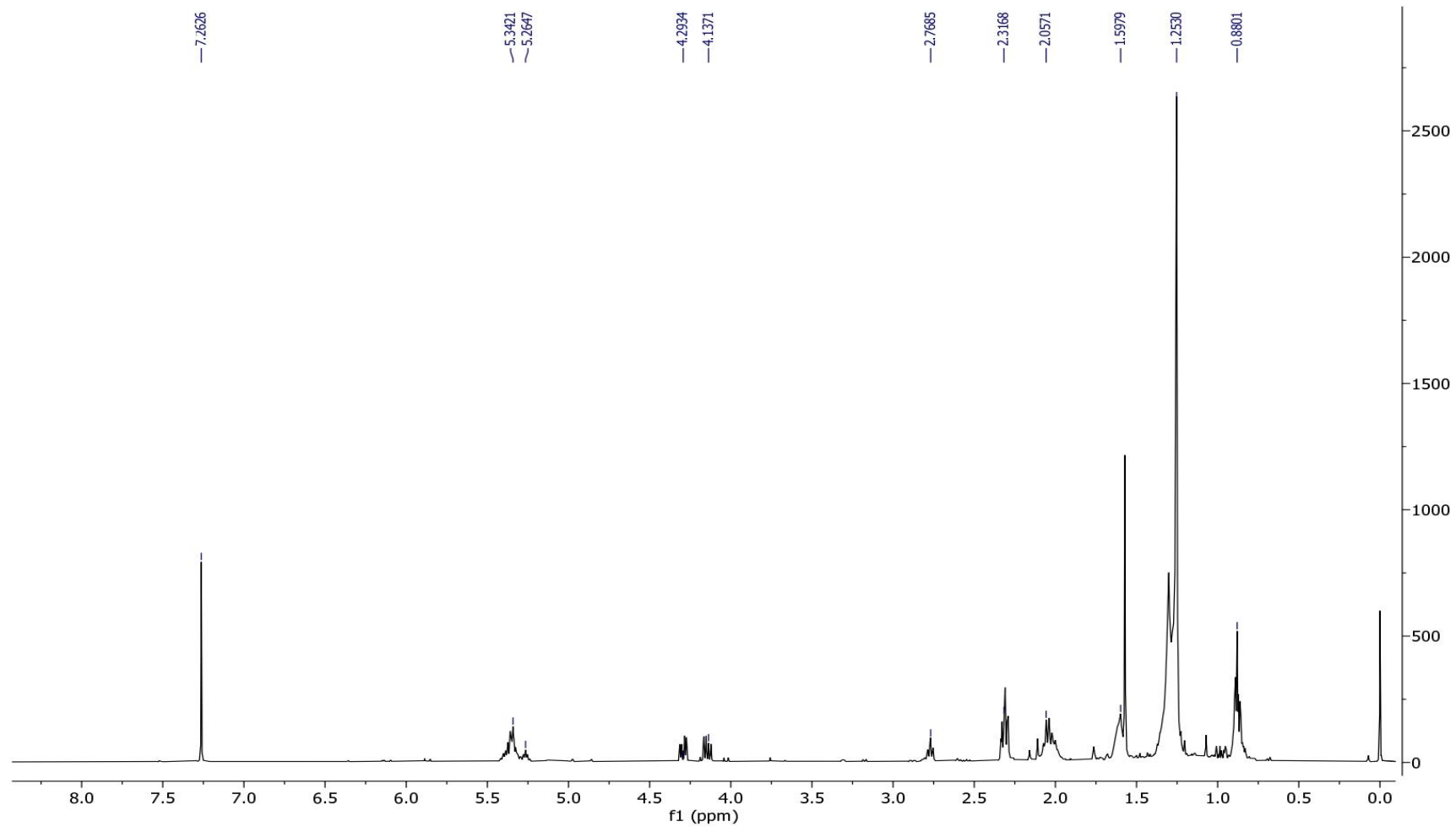
FTIR spectrum of fraction 2.

Appendix E5



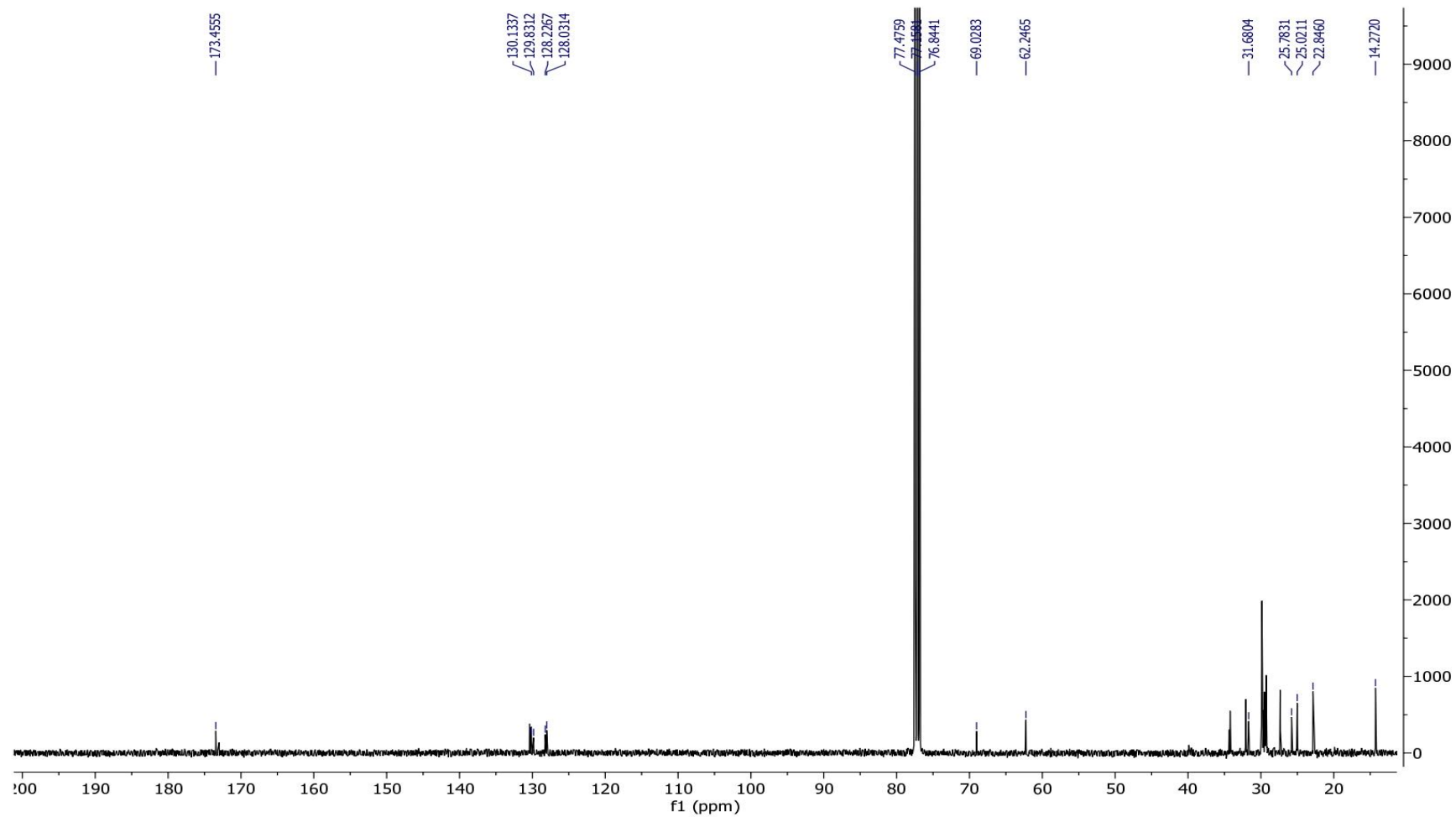
ESIMS spectrum of fraction 2.

Appendix F1



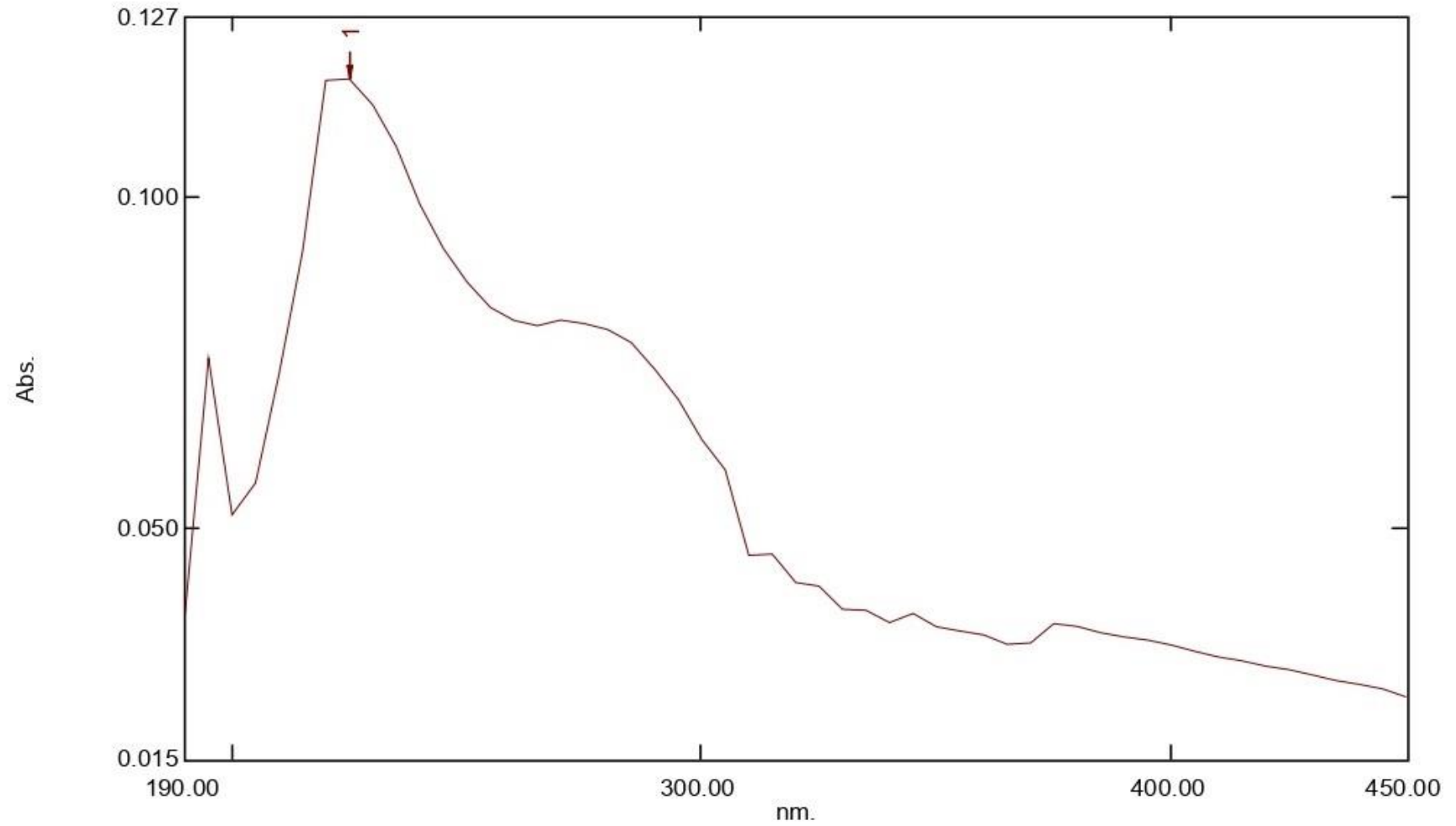
¹H NMR spectrum (CDCl₃, 400 MHz) of fraction 3.

Appendix F2



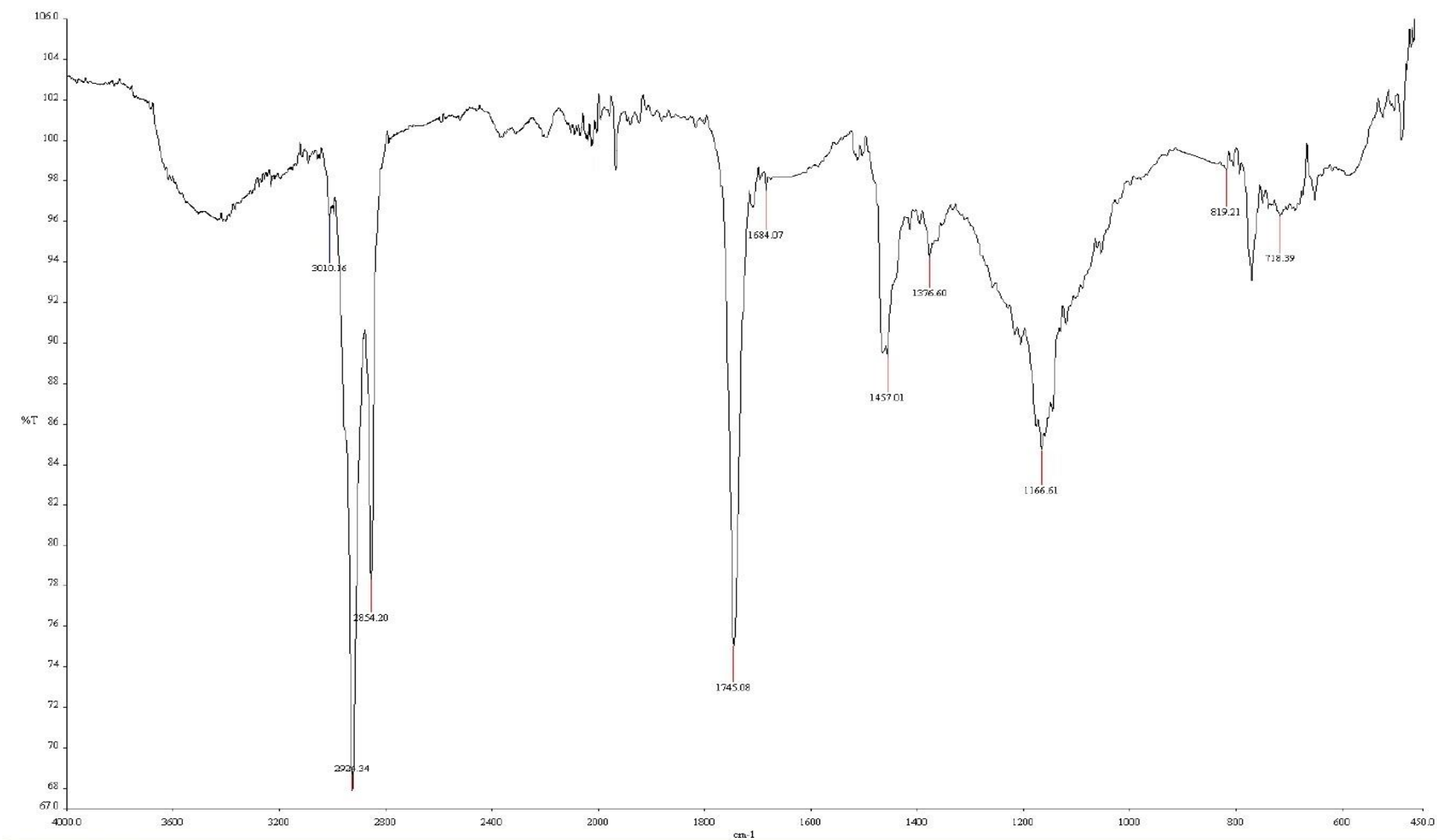
¹³C NMR spectrum (CDCl₃, 100 MHz) of fraction 3.

Appendix F3



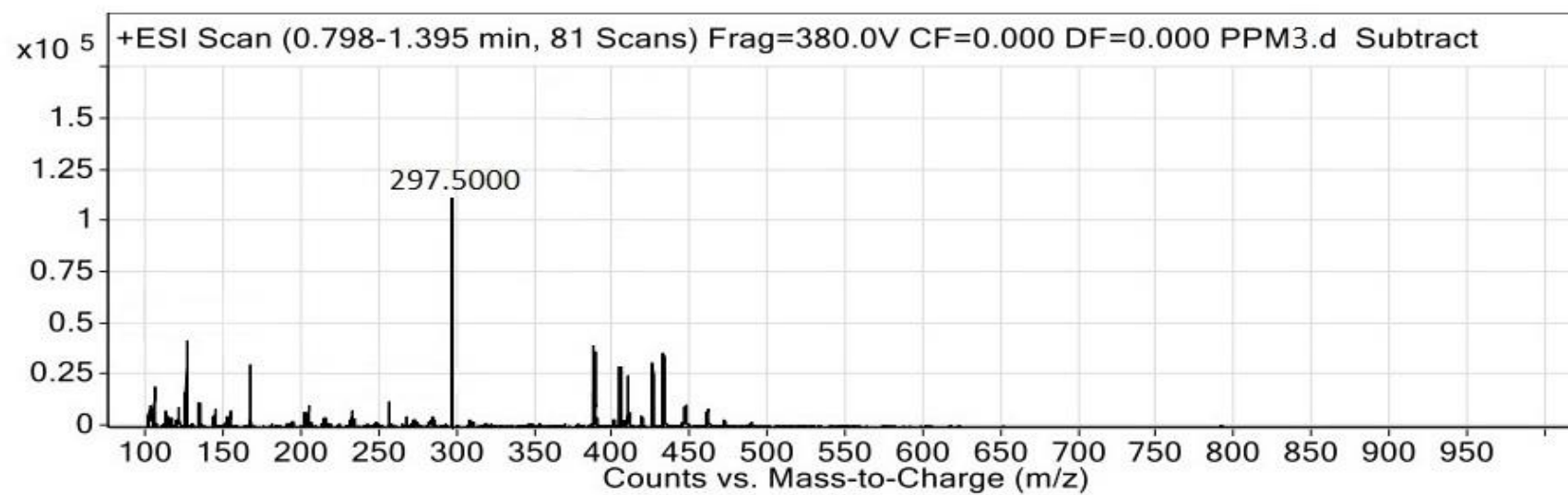
UV-Vis spectrum of fraction 3.

Appendix F4



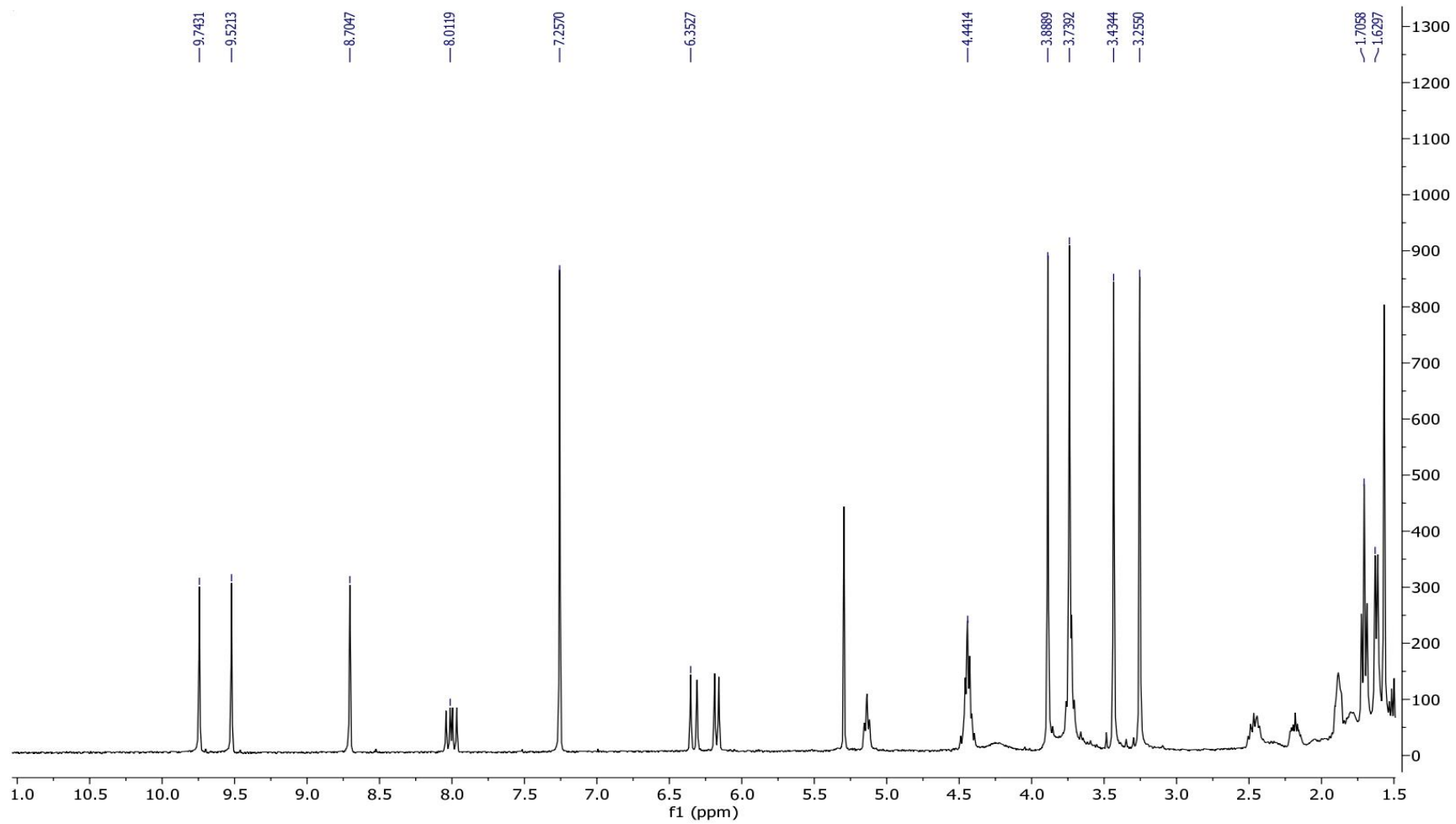
FTIR spectrum of fraction 3.

Appendix F5



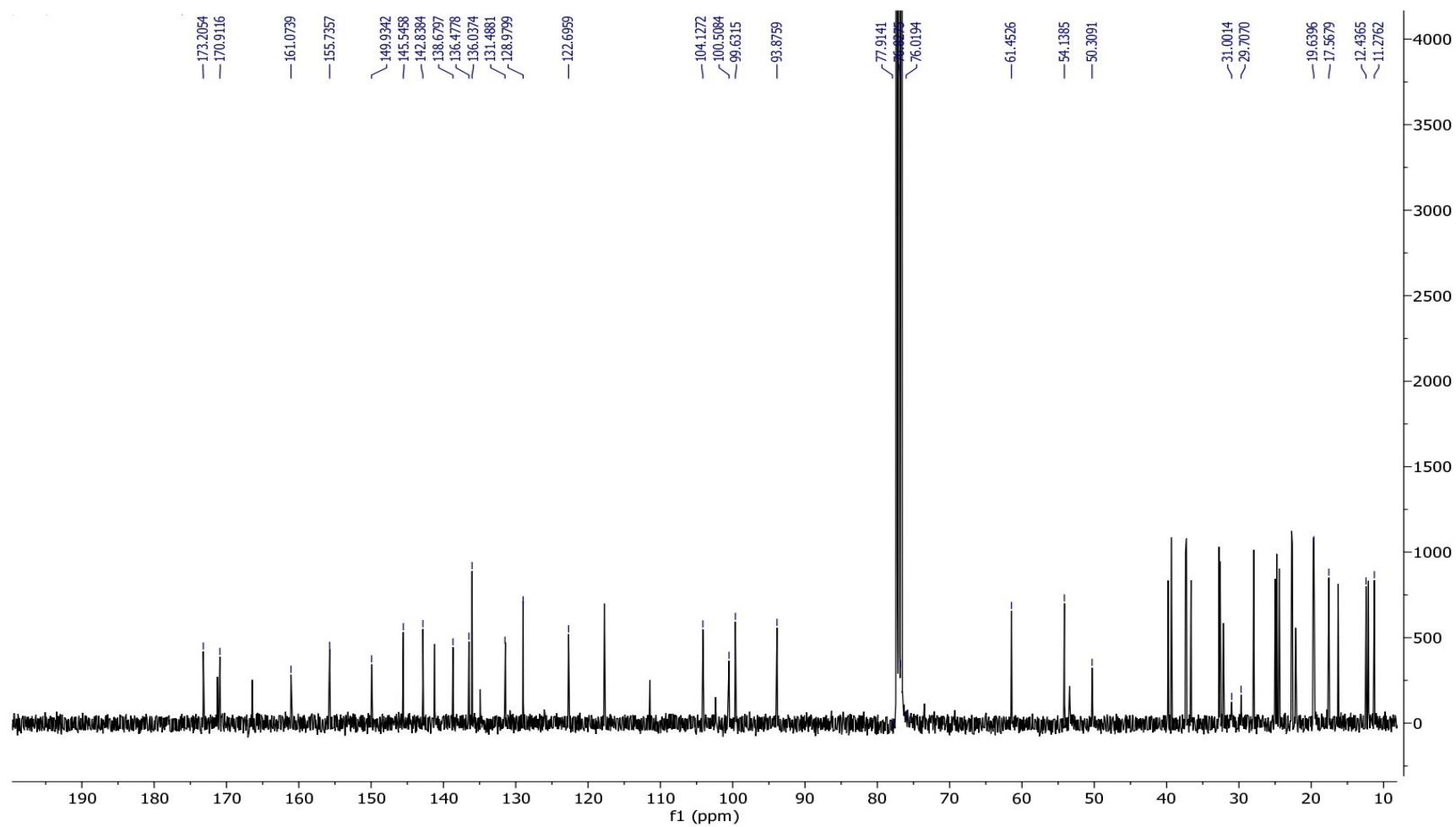
ESIMS spectrum of fraction 3.

Appendix G1



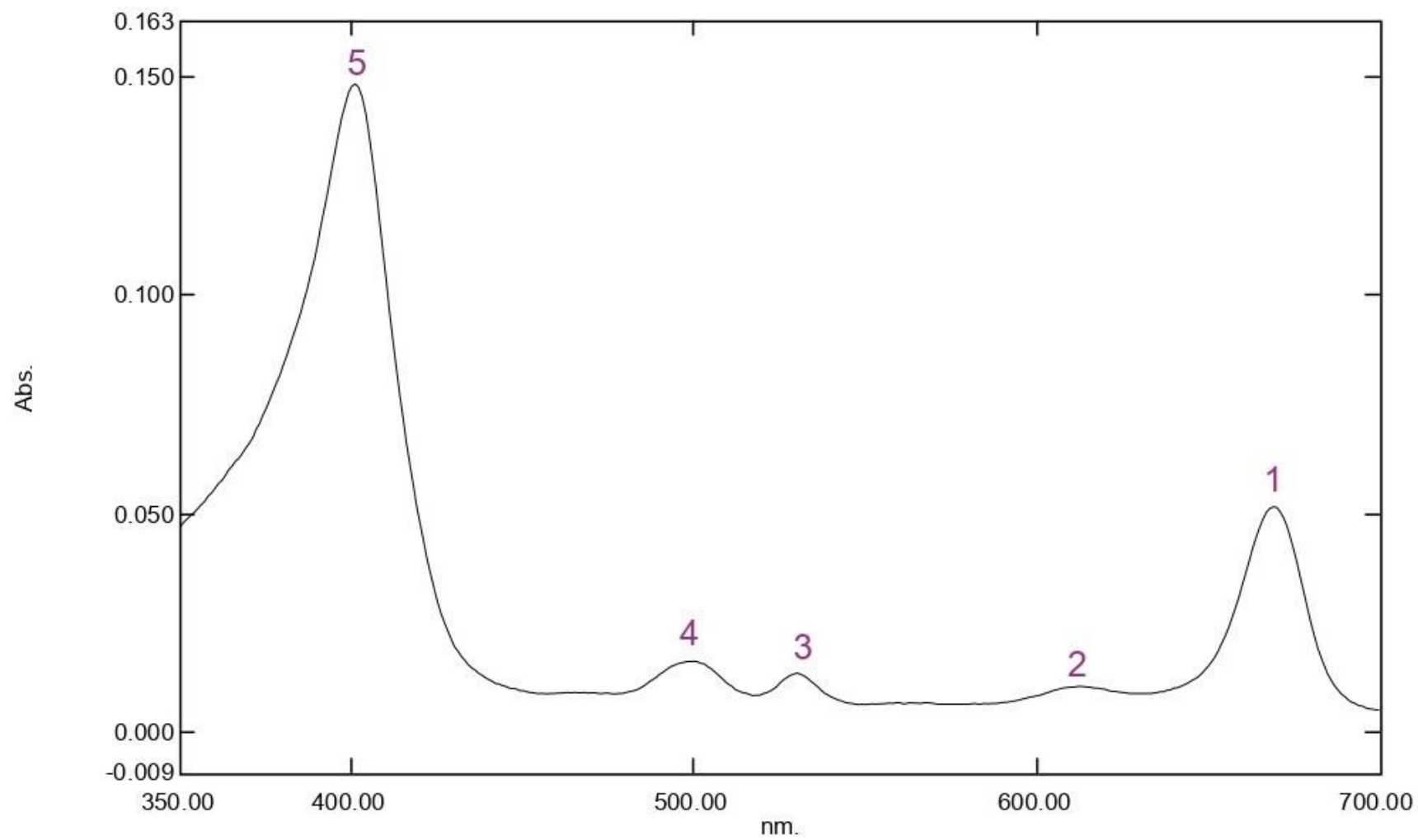
¹H NMR spectrum (CDCl₃, 400 MHz) of fraction 4.

Appendix G2



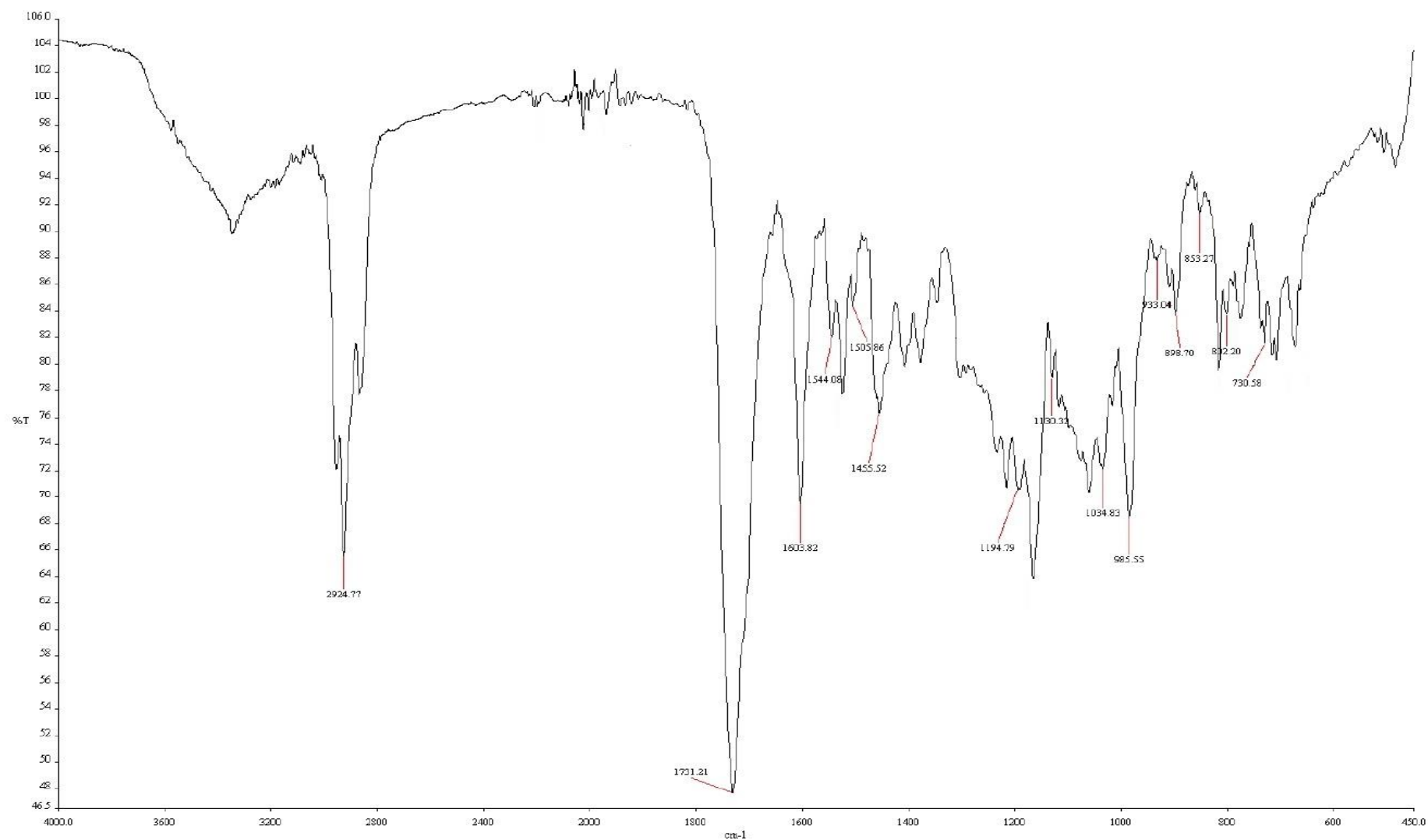
¹³C NMR spectrum (CDCl₃, 100 MHz) of fraction 4.

Appendix G3



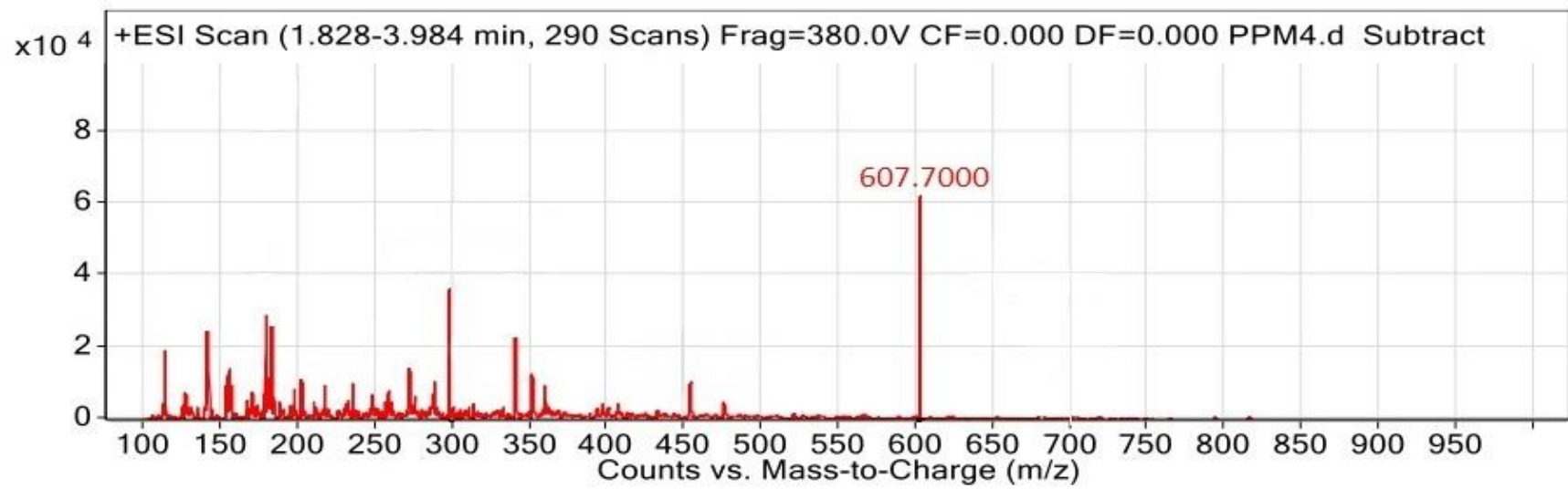
UV-Vis spectrum of fraction 4.

Appendix G4



FTIR spectrum of fraction 4.

Appendix G5



ESIMS spectrum of fraction 4.